NOVA SCHOOL OF SCIENCE & TECHNOLOGY

DEPARTAMENT OF CHEMISTRY

BEATRIZ PEREIRA MACHADO

BSc in Applied Chemistry

WELL DEFINED COPPER(I) CATALYSTS FOR THE CHEMOSELECTIVE OXIDATION REACTION OF ALCOHOLS TO ALDEHYDES

MASTER IN BIOORGANIC CHEMISTRY

NOVA University Lisbon

november, 2023

DEPARTAMENT OF CHEMISTRY

WELL DEFINED COPPER(I) CATALYSTS FOR THE CHEMOSELECTIVE OXIDATION REACTION OF ALCOHOLS TO ALDEHYDES

BEATRIZ PEREIRA MACHADO

BSc in Applied Chemistry

Adviser: Vitor Rosa
Researcher, FCT- NOVA

Co-advisers: João Carlos Lima
Associate Professor, FCT-NOVA

Examination Committee:

Chair: Luísa P. Ferreira,
Assistant Professor, FCT-NOVA

Rapporteurs: Paulo N. Martinho,
Auxiliary Researcher, Faculdade de Ciências, Universidade de Lisboa

Adviser: Vitor Rosa
Researcher, FCT-NOVA

MASTER IN BIOORGANIC CHEMISTRY

NOVA University Lisbon
november, 2023

Well defined copper(I) catalysts for the chemoselective oxidation reaction of alcohols to aldehydes

To my mum,

Acknowledgments

First of all, I wish to express my sincere gratitude to those who provided invaluable support and contributed to the completing this thesis:

I am immensely thankful to Dr Vitor Rosa, my advisor, and co-advisor Dr Professor João Carlos Lima for their guidance, expertise, and unwavering support throughout this research journey, even when I was tardy in delivering the reports. The study's direction was shaped by insightful feedback, dedication, and encouragement. I would also like to acknowledge Dr Clara Gomes for her contributions to this project, despite not being my official advisor. Her level of professionalism and dedication was commendable.

My family and Vicente deserve heartfelt appreciation for their endless love, understanding, and encouragement. Their unwavering belief in my capabilities has been a constant source of motivation.

I extend my gratitude to friends and colleagues, particularly Diogo Costa, who has endured my company for the whole year, and provided me with motivation and a patient ear throughout the challenging stages of this research. Thank you for your friendship and support.

This dissertation would not have been possible without the collective support of these individuals. I hope that this research contributes in some small way to the advancement of knowledge in our field.

Beatriz Pereira Machado

September, 2023

Abstract

One of the key concerns in contemporary chemistry is the development of sustainable processes that adhere as closely as possible to the principles of Green Chemistry without compromising the activity of involved processes. Several principles can be applied in the development of this work, including the catalysis and the atomic economy, among others. The harsh conditions and the disposal of subproducts that characterize typical oxidation reactions pose significant challenges for the chemoselective oxidation of alcohols to benzaldehydes. To tackle these issues, the use of copper(I) complexes comprising diimine ligands, usually bipyridine and phenanthroline shown promising outcomes. Furthermore, new studies by our research group, suggests that bis-aryldiiminoacenaphthene ligands may also be effective, and even increase catalyst activity of such systems. However, such complexes regularly incorporate halogens as counterions. The impact of the diimine backbone on the catalytic activity and stability was investigated in the newly synthesised compounds. Additionally, the effects of the counterion and chelating solvent on the activity and stability were examined. Characterization of all compounds included mono and heteronuclear 1D and 2D-NMR, IR, EA, UV/Vis, and, when possible, X-ray diffraction. The efficiency of all compounds was tested in the oxidation reaction, and they all revealed to be active. Various conditions of the catalytic system were studied to optimize it, and subsequently, the catalytic system was tested with benzyl, allylic, and aliphatic alcohols for efficiency.

Keywords: DAB, DAD, BIAN, copper(I), benzylic alcohol, allylic alcohol, aliphatic alcohol, chemoselective oxidation.

RESUMO

Uma das principais preocupações da química contemporânea é o desenvolvimento de processos sustentáveis que se aproximem o mais possível dos princípios da Química Verde sem comprometer a atividade em processos envolvidos. Diversos princípios podem ser aplicados no decorrer deste trabalho, nomeadamente a catálise e economia atómica, entre outros. As condições adversas e a eliminação dos subprodutos que caracterizam reações de oxidação representam desafios significativos para a oxidação quimioselectiva de álcoois a aldeídos. Para resolver estas questões, foram utilizados complexos de cobre(I) que incluem ligandos diimina, geralmente bipiridina e fenantrolina. Além disso, novos estudos do nosso grupo de investigação sugerem que os ligandos bis-arildiiminoacenafteno também podem ser eficazes e até aumentar a atividade catalítica deste tipo de sistemas. No entanto, esses complexos incorporam regularmente halogéneos como contra-iões. O impacto da estrutura da diimina na atividade e estabilidade do complexo foi investigado nos compostos recentemente sintetizados. Adicionalmente, foram examinados os efeitos do contra-ião e do solvente quelante na atividade e estabilidade do catalisador. A caracterização de todos os compostos incluiu 1D e 2D-RMN mono e heteronuclear, IV, AE, UV/Vis e, quando possível, difração de raios-X. A eficiência de todos os compostos foi testada na reação de oxidação, e todos eles se relaram ser ativos. Foram estudadas várias condições do sistema catalítico para o otimizar e, subsequentemente, este foi testado com álcoois benzílicos, alílicos e alifáticos para verificar a sua eficiência.

Palavras chave: DAB, DAD, BIAN, cobre(I), álcoois benzílicos, álcoois alílicos, álcoois alifáticos, oxidação quimioselectiva.

CONTENTS

LIST OF FIGURES

LIST OF TABLES

List of Annexes

SYMBOLS AND ABBREVIATIONS

ε	Molar extinction coefficient
ABNO	9-Azabicyclo[3.3.1]nonane N-Oxyl
AcOEt	Ethyl acetate
ATR	Attenuated total reflectance
BIAN	Bis(imino)acenaphthene
BIAN^{diip}	2, 2', 6, 6'-Diisopropyl bis(imino)acenaphthene
bpy	2,2'-bipyridine
C1	[Cu(DAB^{diip})(PhCN)$_2$]BF$_4$
C2	[Cu(DAD^{diip})(PhCN)$_2$]BF$_4$
C3	[Cu(BIAN^{diip})(PhCN)$_2$]SO$_3$CF$_3$
C4	[Cu(DAB^{diip})(MeCN)$_2$] SO$_3$CF$_3$
C5	[Cu(DAD^{diip})(MeCN)$_2$] SO$_3$CF$_3$
C6	[Cu(DAB^{diip})(MeCN)$_2$] BF$_4$
C7	[Cu(DAD^{diip})(MeCN)$_2$] BF$_4$
C8	[Cu(DAB^{Me})$_2$] SO$_3$CF$_3$
C9	[Cu(DAB^{iPr})$_2$] SO$_3$CF$_3$

ca.	*Circa* (latin), approximately
COSY	Homonuclear correlation spectroscopy
CuAAC	Copper-catalyzed Azide-alkyne cycloaddition
DAB	Diazabutadiene
DAB^{diip}	2, 2', 6, 6'-Diispropyl diazabutadiene
DAB^{iPr}	4,4'-Diisopropyl diazabutadiene
DAB^{Me}	4,4'-Dimethyl diazabutadiene
DAD	Diazadiene
DAD^{diip}	2, 2', 6, 6'-Diispropyl diazadiene
DBAB	Dibenzo-fused 1,4-azaborine
DBADH2	Di-tert-butyl hydrazine dicarboxylate
DCM	Dichloromethane
DEAD	Diethyl azocarboxylate
DFT	Density functional theory
DMAP	4-Dimethylaminopyridine
DMF	Dimethylformamide
DMSO	Dimethyl sulfoxide
DNA	Deoxyribonucleic Acid
e.g.	For example
EA	Elemental analysis
EPR	Electron paramagnetic resonance
eq	Equivalent
FTIR	Fourier-transform infrared spectroscopy
HMBC	Heteronuclear multiple bond correlation

HSQC	Heteronuclear single quantum coherence spectroscopy
i.e.	*Id est* (latin), what that means is
IR	Infrared
MeCN	Acetonitrile
MeOH	Methanol
MLCT	Metal-to-ligand charge-transfer
NMI	1-Methylimidazole
NMR	Nuclear magnetic resonance spectroscopy
NOESY	Nuclear Overhauser effect spectroscopy
^{OMe}bpy	4-4'-Dimethoxy-2-2-bipyridine
OTf	Triflate (trifluoromethanesulfonate)
PCC	Pyridinium chlorochromate
PhCN	Benzonitrile
phen	1,10-phenanthroline
r.t.	Room temperature
R1	2, 2', 6, 6'-Diispropyl diazabutadiene
R2	2, 2', 6, 6'-Diispropyl diazadiene
R3	2, 2', 6, 6'-Diisopropyl bis(imino)acenaphthene
R4	4,4'-Dimethyl diazabutadiene
R5	4,4'-Diisopropyl diazabutadiene
R6	Tetrakis(benzonitrile)copper(I) tetrafluoroborate
R7	Tetrakis(acetonitrile)copper(I) triflate
R8	Tetrakis(acetonitrile)copper(I) tetrafluoroborate
^{t}BuDEAD	Di-tert-butyl azodicarboxylate

^{t}BuOK	Potassium tert-butoxide
TD-DFT	Time-dependent density functional theory
TEMPO	2,2,6,6-Tetramethylpiperidinyloxy
THF	Tetrahydrofuran
TLC	Thin layer chromatography
UV/Vis	Ultraviolet-visible spectroscopy
δ	Chemical shift
η	yield (expressed in %)
φ	Represents the angle that formed by the aryl group's plane and the diimine backbone's plane
λ	Wavelength
ν	Wavenumber
θ	Represents the angle formed by the diimine backbone's plane and the chelating solvent's plane
ω	Represents the angle formed by the two aryls group

1

INTRODUCTION

Oxidation reactions are among the most frequent types of industrial reactions.[1,2] Therefore, they hold significance in several industries.[3,4] Combustion, a type of oxidation, is employed in energy production as fossil fuels are burned to release energy through oxidation. Redox reactions also find their role in electrochemical procedures, such as batteries and fuel cells.[5,6] The food and beverage industry are also impacted by oxidation reactions, mainly in terms of the quality and shelf life of food products. The spoilage of food caused by oxidation can be prevented with antioxidants. Fermentation processes, which are used to produce various beverages and dairy products, are also impacted by these reactions.[7] Metallurgy and Materials Science is impacted by oxidation reactions, for example, corrosion is a major concern in industries that deal with metals and alloys. Therefore, understanding how to prevent these oxidation processes is crucial to avoid the material degradation and increase the lifespan of products such as automobiles, infrastructure, and machinery.[8] Moreover, these reactions find application in various industries such as environmental applications, and industries of polymers and plastics,[9] textile,[10] pulp and paper[11] and cosmetics and personal care. For instance, these reactions can be used for oxidising hair dyes and the stabilizing of skincare products.[12] Finally, these reactions play a crucial role in chemical and pharmaceutical industries for synthesising diverse chemical compounds that add value to raw materials. For instance, these reactions can convert alcohols into aldehydes or fully oxidise them into acids.[13]

1.1 Alcohol oxidation reactions

The common idea of an oxidation and reduction reaction is that when a compound or atom is oxidized it loses electrons, and when it is reduced it gains electrons. An example of a substrate is the alcohols, these compounds can be primary, secondary or tertiary. The primary alcohols usually can be oxidised to aldehydes or carboxylic acids and the secondary to ketones. The tertiary alcohols usually are not affected by oxidation due to the impediment to form a double bond. These carbonyl containing compounds are important groups due to being important precursors and intermediates for many drugs, vitamins and fragrances, among others.

These reactions are particularly important in the field of organic chemistry for several reasons, such as their selectivity, i.e. they do not suffer from overoxidation and the oxidation process stops at the aldehyde or the ketone, which is an important intermediate in the synthesis of several organic compounds; they are also important for their reactivity, this type of alcohol tends to be oxidized more easily than others. The versatility of this reaction is also an important factor, as it can be performed using different reagents, such as chromium oxide (VI), the pyridinium chlorochromate (PCC) and the Jones reagent, among many others. This versatility in reagents provides many options for controlling the reaction outcome and product characteristics (**Figure 1.1**).[14]

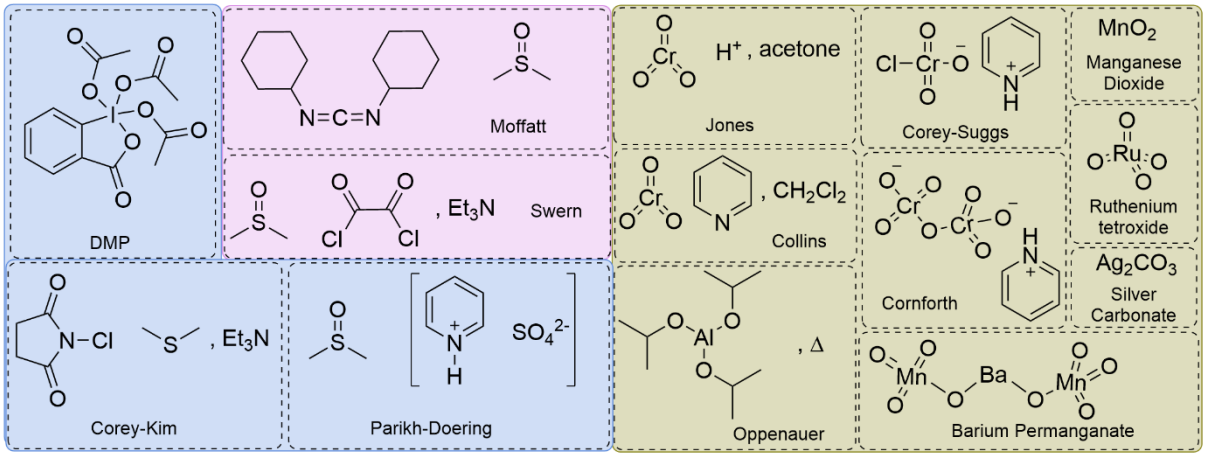

Figure 1.1. Common reagents used for the oxidation of primary and secondary alcohols.

As it was previously mentioned, the ketones and aldehydes are important intermediates and precursors of other reactions. This occurs because these compounds can react to produce many others with a higher market value than the precursors. An example of a reaction

that uses ketones or aldehydes is the hydration and hemiacetal formation, which occurs when a ketone or an aldehyde reacts with an alcohol. The next step in this process is the formation of the acetal or ketal depending on the use of aldehyde or ketone, respectively. The formation of imines and related compounds, also known as Schiff bases, is also an application of the products of alcohol oxidation. These compounds are most relevant as intermediates for the synthesis of nitrogen heterocycles. Depending on the conditions the enamine formation can also be obtained by favouring the equilibrium to this compound by a basic-catalysed reaction.[15] Another reaction is the cyanohydrin formation, these compounds are biologically active and can be useful in the synthesis of β-aminoalcohols, α-hydroxyketones and α-hydroxyacids, which are important intermediates for fine chemicals, pharmaceuticals and agrochemicals. All the previous uses of the products of the alcohol oxidation were reversible addition reactions, but there are also the irreversible ones that corresponds to the reduction of these compounds using metal hydrides, the Wolff-Kishner reaction and the Clemmensen one (**Figure 1.2**).

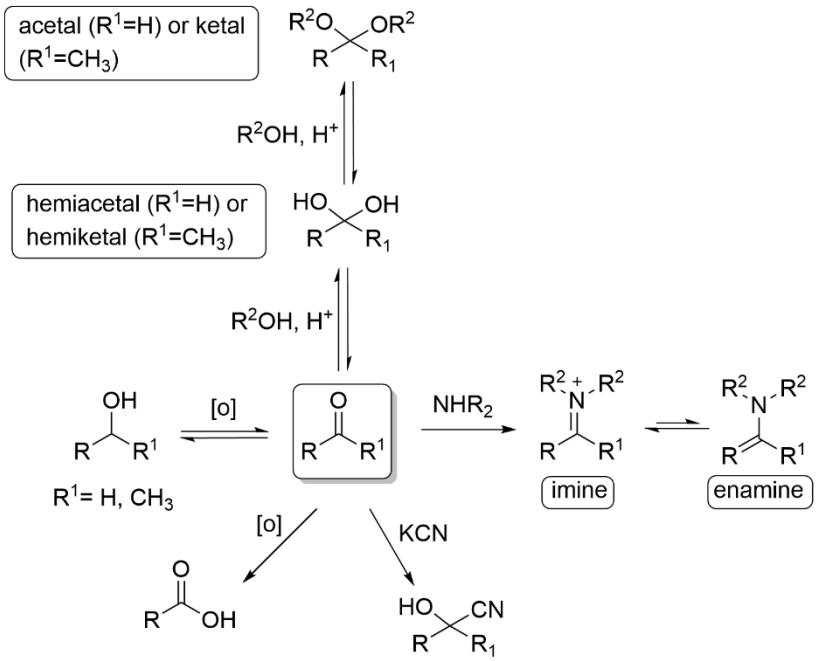

Figure 1.2. Scheme showing the different reactions that the aldehydes and ketones are precursors.

1.1.1 Oxidation reactions in Pharmaceutical Industry

Oxidation reactions represent only 3% of the reactions used in the pharmaceutical industry. The major effort in this area is to find pathways that induce functionality in the correct oxidation state and without the use of a protecting group.[13]

The oxidants commonly used produce by-products that can be relatively sustainable, but most selective oxidants produce by-products that are undesirable and not so sustainable. In large scale processes the main concern is safety, this because, the use of flammable organic solvents and the risk of static electrical discharge in the solvent line or in the reactor is significant. In other reactions that are not oxidations, the risk of fire is avoided by not using oxidants in solvents and reagents, but in oxidations these compounds are needed so there is a safety risk.[13]

Despite the risks mentioned above, these reactions are regularly used in the production of commercial reagents or in the synthesis of various drugs, although some classes of drugs involve a high number of oxidation reactions in their total synthesis, such as steroids and prostaglandins. An example of this is the conversion of deoxycholic acid into cortisone acetate (**Figure 1.3**), a process developed by Merck in the 1950s and 1960s involving eleven different oxidations.[13,16]

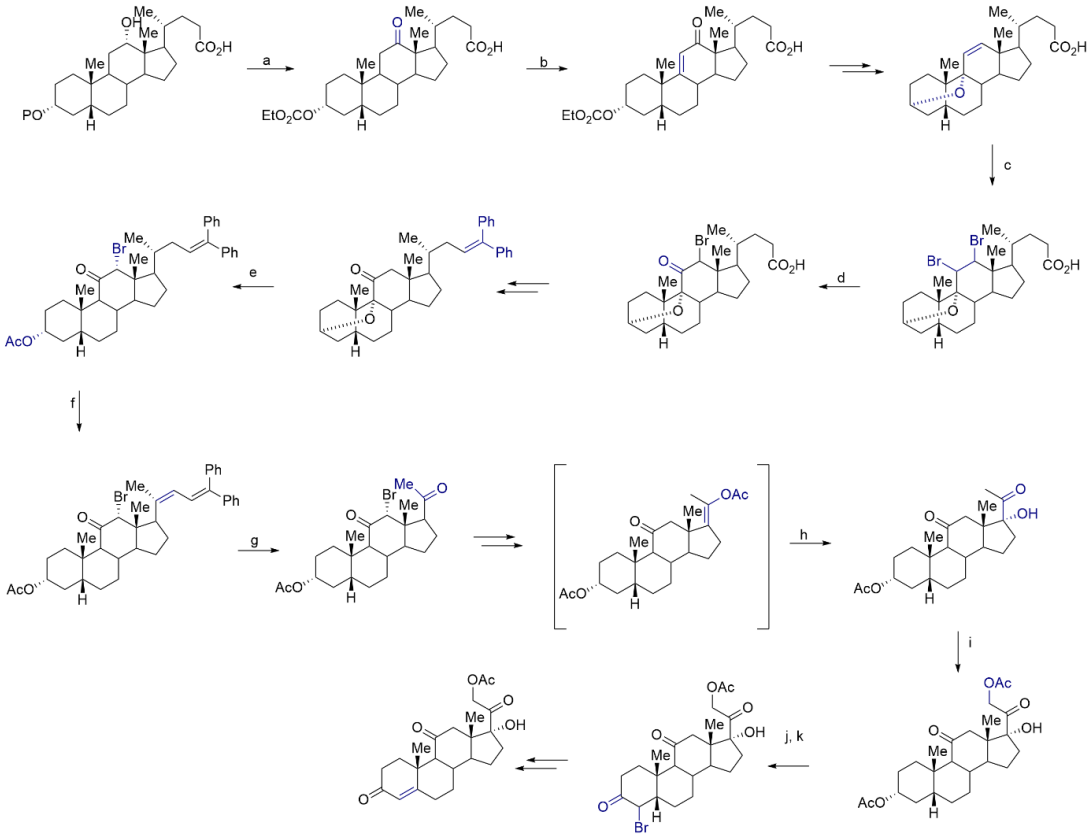

Figure 1.3. Total synthesis of cortisone acetate with the different synthetic steps that use oxidation processes. Figure adapted from ref[13].

1.1.1.1 Moffat processes and derivates of Moffat to the oxidation of primary alcohols into aldehydes

The Moffat oxidation, presented in 1965, has become the preferred method for the preparation of aldehydes from primary alcohols. This procedure offers the advantage of forming the oxosulfenic ion, which is deprotonated under mild conditions. Currently, the Swern modification is the most used procedure for this type of reaction in the pharmaceutical industry (**Figure 1.4**).[17–20]

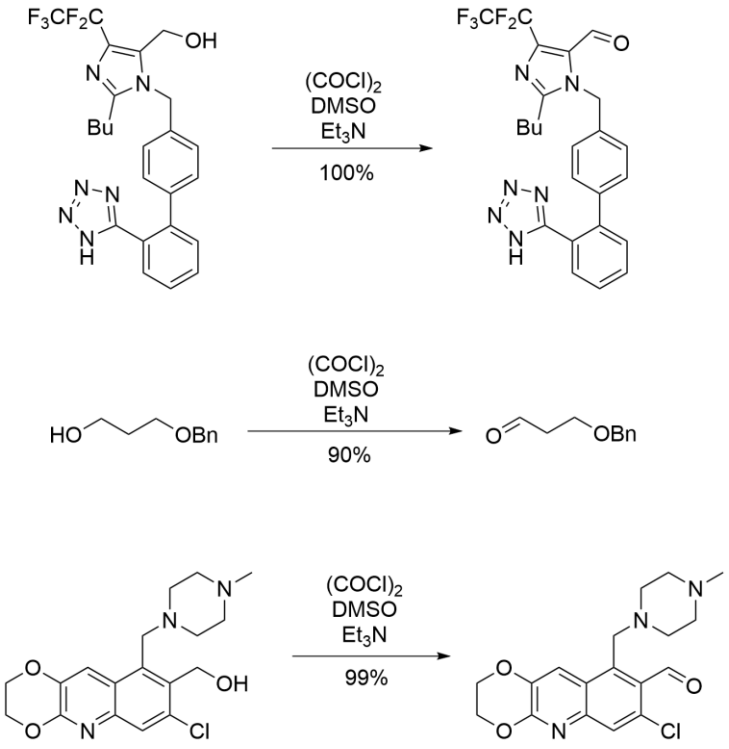

Figure 1.4. Synthetic steps of different pharmaceutical relevant molecules using oxidation steps (adapted from ref [18–20]).

One of the main drawbacks of the Swern oxidation process on a large scale is the significant production of CO_2 and CO in the reaction consequential from the $(COCl)_2$ compound. A relevant oxidant in the industry is the SO_3.pyridine complex. This reagent possesses the practicality of being a solid and the reaction can be used at or near room temperature, in contrast to the cryogenic conditions usually necessary when oxalyl chloride is employed in the reaction. This promotes reagent addition in case the reaction is incomplete.[21] For example, the phenyl alaninol is oxidized to its corresponding aldehyde on a scale of 190 kg without losing its chiral purity. This step serves as a component of the synthesis of an HIV protease inhibitor (**Figure 1.5**).[22]

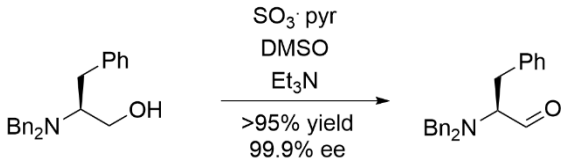

Figure 1.5. Synthetic step corresponding to the oxidation of an aminoacid derivate using the Swern conditions. Figure adapted from ref[13].

1.1.1.2 Oxidation processes of aldehydes from primary alcohols mediated by TEMPO

The (2,2,6,6-tetramethylpiperidin-1-yl)oxidanyl, also known as TEMPO, has been established as the go-to catalyst for oxidising primary alcohols. This is largely due to the hydroxyl radical catalyst's efficacy at modest conditions, such as room temperature, and with affordable co-oxidants such as bleach (NaOCl) (**Figure 1.6**). Under appropriate conditions, TEMPO can also exhibit chemoselectivity towards primary alcohols without experiencing total oxidation to the carboxylic acid. This reaction is commonly utilised in biphasic conditions with dichloromethane as the solvent and works well with reactive substrates, such as prostaglandins.[23,24]

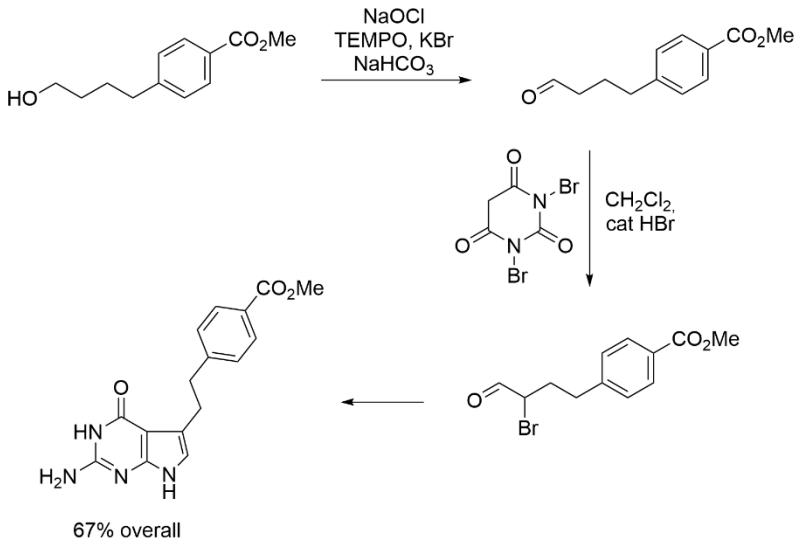

Figure 1.6. Synthesis of Antifolate using the TEMPO as the oxidant. Figure adapted from ref [13].

1.2 Copper as a catalyst

A range of metals, including manganese, palladium and ruthenium, have the ability to oxidise alcohols. However, copper stands out as a promising option for use as a building block in catalytic systems due to its advantageous properties. Its low cost and toxicity, high availability and capability to be recycled make it an ideal candidate for sustainable processes.

Copper's versatility and reactivity have made it a common metal in catalysis. It is particularly useful in hydrogenation reactions, where it aids the addition of hydrogen to unsaturated compounds, enabling the synthesis of various chemicals, as alcohols, alkanes, and fatty acids.[25] It can also be crucial in the production of methanol via the methanol synthesis reaction, which involves the conversion of carbon monoxide and hydrogen into methanol. This reaction holds significant importance in the chemical industry, since its products have the potential to become a green fuel.[26] In the reverse reaction of hydrogenation, the dehydrogenation, copper can also play an important role in it, whereby a hydrogen atom is removed from a compound resulting in the formation of unsaturated products. This is particularly relevant in the production of olefins and aromatics.[27]

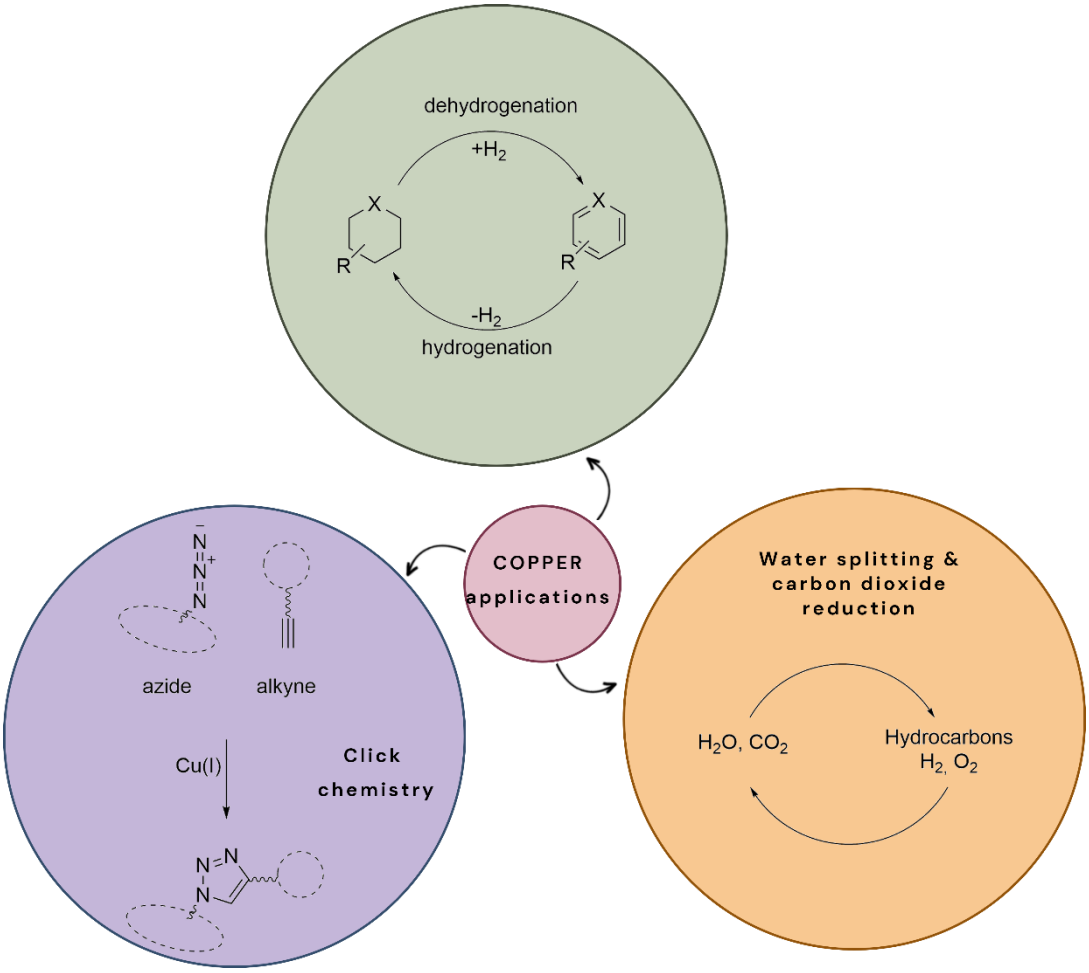

Figure 1.7. Scheme showing some copper applications.

The Nobel Prize-winning field of click chemistry also requires the presence of copper(I) for the copper catalysed azide-alkyne cycloaddition (CuAAC), a powerful and versatile reaction used in the synthesis of complex molecules and polymers.[28] The electrochemical applications of copper are significant in sustainable energy conversion and storage through water splitting and CO_2 reduction.[29] Copper catalysts play a crucial role in the Haber-Bosch process, which produces ammonia for fertilizer production.[30] Additionally, copper's affinity to certain compounds that promotes their oxidation makes it useful in wastewater treatment for removing pollutants from industrial wastewater, thus aiding in mitigating environmental impacts (**Figure 1.7**).[31]

While copper can be a useful tool in various reactions, it also poses hazards and considerations, such as its toxicity, which can be harmful to both humans and aquatic organisms, especially in an industrial scale. However, comparing to the toxicity of other metals that

undergo these reactions, copper exhibits low toxicity. Exposure to high levels of copper can result in severe health issues, such as gastrointestinal disturbances, liver and kidney damage and skin irritation. As noted earlier, the environmental impact must also be taken into account, as high levels of copper concentration in industrial discharge can contaminate water bodies and harm aquatic life if not properly managed.[32] Additionally, these catalysts can undergo deactivation over time due to processes such as sintering or poisoning by impurities, ultimately reducing their catalytic activity and efficiency. In certain applications where copper is involved, it may corrode or leach copper ions into the reaction mixture, resulting in unwanted side reactions or product contamination.[33] Finally, appropriate safety measures must be followed during the handling, storage, and disposal of copper and copper-based catalysts to minimize risks and prevent accidents.

In brief, copper has a crucial role as a catalyst in numerous reactions and industrial processes, allowing for the efficient generation of valuable chemicals and materials, due to its reactivity and abundant availability. Nevertheless, it is necessary to contemplate and tackle the possible hazards associated with this metal to guarantee its secure and sustainable application. To promote cautious management and rigorous compliance with safety protocols can aid in reducing the risks mentioned and maximising the benefits of using copper.

1.3 State of the art on the chemoselective oxidation of alcohols to aldehydes

1.3.1 Brackman and Gaasbeek's research

The research of Brackman and Gaasbeek, in 1966, led to the use of copper in catalytic oxidation systems. They found that these systems were effective in oxidizing a variety of substrates, including alcohols, amines and imines, and could operate within a temperature range of 0-50 °C. Additionally, the use of co-catalysts or promoters, created an autocatalytic system. Their work was significant for comprehending the promoter effect of the removal of a proton with the aid of cupric complex assistance from a substrate AH, which cannot be oxidised through the two-step alternative mechanism (**Figure 1.8**).[34]

Figure 1.8. Representation of a two-step mechanism that the authors concluded that could not be the reaction mechanism.

For this study, a (phenanthroline)Cu^{II}/di-tertbutyl nitroxide was utilised (**Figure 1.9**). This radical was selected based on its behaviour during the reaction, as it can be easily tracked through UV spectra and NMR techniques, despite not being the most reactive. Nonetheless, we have given limited attention to these findings as the circumstances have advanced in the subsequent catalytic systems, but they were important as a starting point for future work.[34]

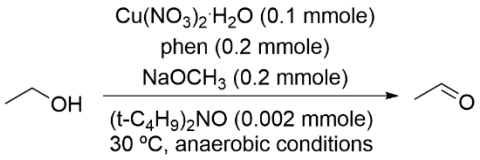

Figure 1.9. Scheme representing the reaction conditions of Brackmaan and Gaasbeek's reaction, using a catalyst constituted by 2 equivalents of phen to 1 equivalent of $Cu(NO_3)_2$.

1.3.2 Semmelhack's research

In 1984, Semmelhack published a catalytic system that facilitated alcohol and amine oxidation through electrolysis. This system was mediated by TEMPO and resulted in the formation of the nitrosonium ion, allowing oxidation to occur without the overoxidation to the carboxylic acid. Semmelhack's system, which has grown greater relevance than the previously mentioned research, provides a valuable tool for the oxidation of alcohols and amines.[35]

The study focused on allylic and benzylic alcohols, was conducted at room temperature with an oxygen atmosphere, utilizing a mixture of cuprous chloride and TEMPO. The catalytic mechanism presented in this study comprises of five steps (**Figure 1.10**). Firstly, the nitrosonium radical is oxidized while the Cu^{II} complex is simultaneously reduced to Cu^{I}. Following that, the alcohol is oxidized by the TEMPO radical resulting in the formation of the aldehyde, where a hydroxylamine is also generated. The fast proportion of hydroxylamine syn in combination with the TEMPO radical oxidized forms a radical. In the final step, Cu^{I} is regenerated by the oxygen. This process consumes protons and the results in the formation of Cu^{II} and water (**Figure 1.10**).[35]

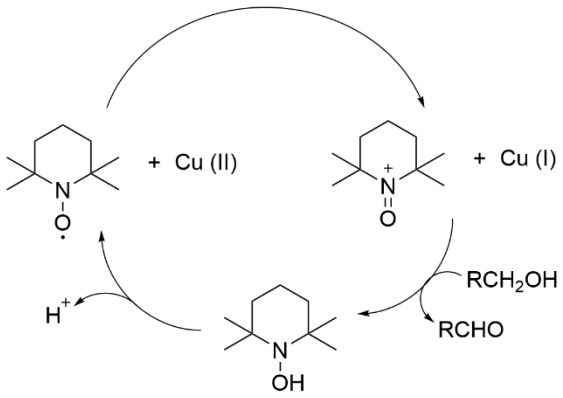

Figure 1.10. Proposed steps in the of oxidation of Semmelhack's catalytic system.

In this catalytic system, an alcohol was combined with TEMPO (10 mol%) and CuCl (10 mol%) were added, in 25 mL of DMF, within an oxygen atmosphere at 25 °C (**Figure 1.11**). While these conditions proved unsuitable for aliphatic alcohols, benzylic and allylic alcohols resulted in high yields. For converting benzyl alcohol to benzaldehyde, a 94% yield was achieved within four hours using 5 mol% of CuCl and TEMPO.[35]

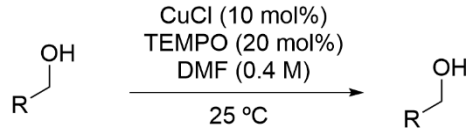

Figure 1.11. General conditions for the oxidation reaction of Semmelhack's catalytic system.

It was also noted that secondary alcohols are oxidized very slowly compared to primary alcohols. An experiment to study the selectivity of this catalytic system, which involved a mixture of 1-hexanol and cyclohexanol was performed and after 2h, the catalytic system shows 60% conversion of the primary alcohol and 0% of the secondary.

Beyond that, a range of substrates were examined. It was concluded that benzylic alcohols with electron-withdrawing groups in the aryl ring tend to slow down the reaction. Additionally, the cupric salts with non-coordinating counterions are more efficient, but $CuCl_2$ and $CuBr_2$ salts exhibit decreased activity suggesting a stoichiometric amount of chloride is needed.[35]

1.3.3 Markò's research

In 1996, Markò conducted a study based on a seminar led by Jallabert and Rivière. In their work, CuCl (5 mol%), phen (5 mol%) and $DBADH_2$ (5 mol%) were used alongside 2 equivalents of K_2CO_3 in an oxygen atmosphere (**Figure 1.12**). It should be noted that this reaction can also be carried out in an air atmosphere but required a longer amount of time. Toluene was selected as the solvent and the reaction was performed at 70-90 °C. The *p*-chlorobenzyl alcohol is oxidized to its corresponding aldehyde in 90 min with a conversion of 100% and yielding 83%, meanwhile the cinnamyl alcohol is oxidized to its corresponding aldehyde in 60 min, yielding 89% and with a 100% conversion. It was also noted that no trace of carboxylic acid was shown.[36]

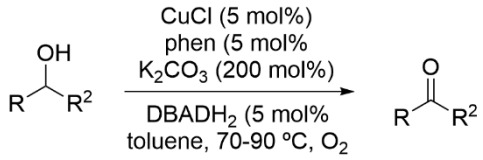

Figure 1.12. General conditions for the oxidation reaction of Markò's catalytic system.

Supplementary investigations were undertaken to explore the impact of additives, counterion nature, and solvent selection. Regarding this matter, it has been determined that azo ligands, such as DEAD, ^{t}BuDEAD or the DBAB, improve reaction turnover, catalyst lifespan, and the reaction rate. Concerning the counterion, chlorides, acetates and triflates are found to be highly efficient, as are diimines, such as phenanthroline. Finally, it was concluded that polar solvents, such as acetonitrile, inhibit the reaction, while apolar solvents, like benzene tend to favour it. However, due to practicality, toluene and trifluoromethylbenzene are preferable options.[36,37]

A drawback of this Markò catalytic system is the need for 2 equivalents of potassium carbonate. With further research, it was found that 1 equivalent of the base was sufficient if the solvent was changed to fluorobenzene.[37]

1.3.4 Sheldon's research

In 2003, new research emerges with the use of $CuBr_2$ and bipyridine (bpy). This system differs from the ones mentioned before because of the use of Cu^{II} as the starting material. In

Sheldon's mechanistic studies, he concluded that the mechanism involves a copper-mediated dehydrogenation of the alcohol substrate rather than an oxoammonium-based mechanism as it was thought to be before. This mechanism is similar to the one Galactose Oxidase performs, which is supported by the feasibility of re-oxidizing Cu^{I} to Cu^{II} by TEMPO.[38,39]

This catalytic system uses 5 mol% of $CuBr_2$ and bpy to form the catalyst in situ, 5 mol% of TEMPO and 5 mol% of ^{t}BuOK as base (**Figure 1.13**). Sheldon's research allowed to understand that when a diimine was not added the reaction was barely done possibly due to poor solubility of the copper catalyst without the diimine ligand and the absence of the beneficial electronic effects caused by the pyridine rings. In this catalytic system is used a mixture of

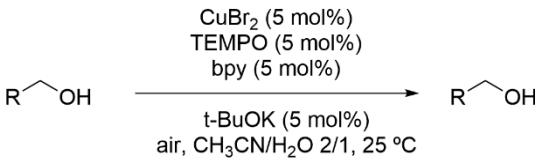

Figure 1.13. General conditions for the oxidation reaction of Sheldon's catalytic system.

solvents (acetonitrile/water 2:1) and the reaction is performed at room temperature using the oxygen of the air as the oxidant.[38,39]

The main advantage of this method is that has mild conditions, and it is efficient with high conversions and selectivity to the corresponding aldehydes when using benzylic, allylic, and aliphatic alcohols. The benzyl alcohol was oxidized to its corresponding aldehyde in 2.5h with a conversion of 100% and for the entire substrate scope the selectivity was always superior to 99%. A substrate scope competition experiment was performed with benzyl alcohol and octan-2-ol in which it was shown a 67 % of benzaldehyde and no presence of the corresponding aldehyde from octan-2-ol.[38,39]

1.3.5 Stahl's research

In 2013, Stahl devised a system to enhance the one published by Sheldon using copper in its oxidation state of one. He recognized that oxidizing the copper was a crucial initial step in initiating the reaction. So, he developed a system that would simplify the reaction conditions and be accessible for every chemistry laboratory to utilize. Therefore, his initial

conditions were to include the copper salt, bpy, NMI and TEMPO (10 mol% each) in acetone at room temperature and open-air.[40] Upon further investigation, Stahl managed to refine his conditions to only 5 mol% of $[Cu(MeCN)_4](OTf)$, 5 mol% of bpy and TEMPO and 10 mol% of NMI, in MeCN at room temperature and in open-air conditions (**Figure 1.14**).[14,41] The benzyl alcohol was oxidized to its corresponding aldehyde in 3h yielding 95%. Studies were conducted to determine the scope and functional group tolerance of this system, which showed its efficiency in oxidizing alcohols containing alkynes, heterocycles, ethers and thioethers to yield good-to-excellent products. It was also concluded that the alkenes and alkynes are not subject to oxidation.[42]

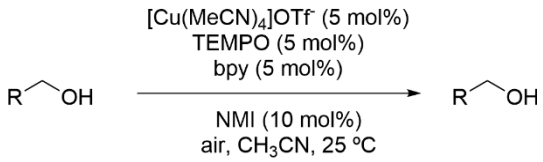

Figure 1.14. General conditions for the oxidation reaction of Stahl's catalytic system.

In a separate report, Stahl started his studies by comparing the reaction rates, yields, and substrate scope of the different catalytic systems, and complemented his results with UV/Vis and EPR spectroscopic to gain insight into the nature of the active catalyst species present during the reaction.[43] A study investigating the mechanism of alcohol oxidation utilizing copper(II) and nitroxyl catalysts revealed the involvement of a bimolecular pathway through which hydrogen-atom transfer occurs from a copper(II)-alkoxide species to the nitroxyl radical. The observed reactivity and chemoselectivity were in agreement with the results from experimental and computational studies. This research was significant for gaining a better understanding of the reactivity variances among various nitroxyl cocatalysts, which entail distinct mechanisms.[44]

In another study, a suggested mechanism for the aerobic oxidation of alcohol is presented. It is believed to involve two distinct half-reactions. In the first reaction, the reduced catalyst (Cu^{I} and TEMPOH) undergoes oxidation by the O_2 in the air. In the second reaction, the alcohol is oxidized via Cu^{II} and TEMPO mediation. This compound has a critical role as a co-catalyst in the reaction, working alongside Cu^{I} to achieve the net two-electron alcohol-to-aldehyde catalyst. The NMI is believed to function as a ligand in the Cu^{I} complex.[45]

A subsequent study by Stahl observed the impact of changing the TEMPO compound on the catalyst's reactivity. It was concluded that bicyclic nitroxyl derivates with less steric hindrance, such as ABNO (9-azabicyclo[3.3.1]nona N-oxyl), have a higher rate of alcohol oxidation than more sterically hindered TEMPO derivates. This conclusion was supported by kinetic studies conducted during the study. Relating to the previous section, this system demonstrates efficiency in the aerobic oxidation of sterically unhindered primary alcohols and electronically activated substrates. It overcomes the steric and electronic limitations of the previous system, leading to a broader range of substrate scope and increased reactivity. It also utilises the oxygen of the air as the source of oxidiser, thereby obviating the necessity of expensive and potentially hazardous oxidants, such as molecular oxygen and peroxides. Additionally, it is readily available and easily accessible. Lastly, it simplifies the reaction setup and reduces the overall cost of the process.[46]

Stahl also studied the utilization of continuous-flow processing for the aerobic oxidation of primary alcohols compared to a batch process, which enables scalability and efficiency enhancements. This process provides various advantages, such as improved regulation of reaction conditions, heightened safety, and the capacity to conduct reactions on a larger scale. It is significant because it is a greener and more effective approach to producing pharmaceutical intermediates.[47]

Stahl's subsequent paper details the advancements made in the development of a superior Cu/nitroxyl catalyst system for the oxidation of alcohols using aerobic conditions. These modifications comprise replacing $[Cu(MeCN)_4]OTf$ with the more affordable Cu^{I}, reducing ABNO loading to 0.05-0.3 mol% and employing NMI as the sole ligand/additive. The cinnamyl alcohol was able to be oxidized to its corresponding aldehyde in 1h with 95% yield, while with the previous system this reaction takes 2h yielding 92%. This eliminates the necessity for ^{MeO}bpy, allowing for a more compatible integration in batch and flow processes (**Figure 1.15**).[48–50] This optimized system demonstrated excellent performance in oxidising various alcohols with a broad substrate scope, high selectivity for primary alcohols, and fast reaction rates for both primary and secondary alcohols.[49,51,52] Additionally, the solvent found to be most useful was acetonitrile due to its good performance, excellent solubility of reaction components, and high potential operating temperature, allowing for effective and reproducible gas-liquid mixing. Furthermore, it was safe to use in flow reactions with a slug flow reactor, even under elevated pressures of dilute O_2 and organic solvents.[49]

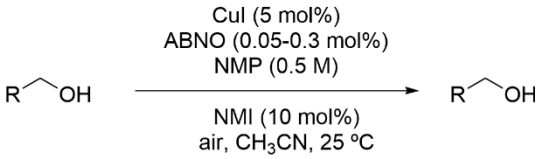

Figure 1.15. Proposed modifications in the Stahl's first catalytic system.

After optimizing the system, Stahl identified other applications for this reaction. In a subsequent article, he found that Cu/nitroxyl catalysts can efficiently and selectively promote the aerobic oxidative lactonization of diols. This occurs under mild reaction conditions using the oxygen present in the air as the oxidant. Moreover, it was discovered that the chemo- and regioselectivity of the reaction can be adjusted by changing the identity of the nitroxyl cocatalyst. This being, the Cu/ABNO system demonstrates exceptional reactivity with symmetrical diols and hindered unsymmetrical diols, whereas the Cu/TEMPO system yields superior results for oxidising less hindered unsymmetrical diols while also favouring primary alcohols over secondary alcohols. The selectivity observed in the reaction of oxidative lactonization can be explained by the anticipated acidity of the alcohol, indicating that electronic effects can be just as influential as steric effects in governing the selectivity of the reaction. This system is compatible with all classes of alcohols (benzylic, allylic, aliphatic), enables efficient lactonization of 1,4-, 1,5- and some 1,6-diols, and can tolerate diverse functional groups, including alkenes, heterocycles, and other heteroatom-containing groups. In the meantime, the Cu/ABNO system demonstrates substantial activity and selectivity in the aerobic oxidative lactonization of symmetrical diols, like diethylene glycol, a critical precursor for biodegradable polyesters extensively used in biomedical applications.[53,54]

Another work of Stahl that involves the system being studied is the oxidative coupling of alcohols and amines to form amide bonds using aerobic copper/nitroxyl catalysis. The main advantage of this system is its practical application and functional group compatibility, which enables the synthesis of diverse α-heteroatom substituted amides that are essential in pharmaceuticals and bioactive compounds. The reaction tolerates more than 20 distinct functional groups, can be executed on a large scale under mild conditions, and the catalyst components are commercially obtainable, easily accessible synthetic procedures. The comprehensive substrate scope and functional group tolerance of this catalytic system render it appropriate for the synthesis of drug-like molecules.[55,56] For instance, the procedure was employed in the

synthesis of alogliptin, saxagliptin, and oseltamivir, resulting in the required amides with over 90%.[52,57–60]

Table 1.1. Summary of catalytic conditions for the different catalytic system presented.

Catalyst System	[Cu] source	ligand	Base	Solvent	Temperature
Brackman and Gaasbeek	$Cu(NO_3)_2.H_2O$	phen	$NaOCH_3$	MeOH	30 °C
Semmelhack	$Cu^{I}Cl$	-	-	DMF	25 °C
Sheldon	$Cu^{II}Br_2$	bpy	$KO^{t}Bu$	2:1 MeCN/H_2O	25 °C
Markò	CuCl	$DBADH_2$/ phen	K_2CO_3	Toluene	70 °C-90 °C
Stahl	$Cu^{I}OTf$	bpy/ ^{OMe}bpy	NMI	MeCN	25 °C

1.4 Work objectives & strategy

1.4.1 Diimines as ligands

In the field of coordination chemistry, designing and manipulating metal complexes with custom properties has piqued considerable interest for maximizing functional potential. Within the gamut of ligands used, diimines stand out due to their structural and electronic attributes. As a bidentate chelating agent comprising two nitrogen atoms as binding sites, diimines offer diverse interaction possibilities with metal centres. Thus, they are a valuable resource in complex design.[61]

Diimines, including bipyridine (bpy) and phenanthroline (phen) derivatives, are becoming increasingly popular ligands for copper complexes due to their chelating abilities to promote the formation of stable complexes.[62] Among the most extensively studied diimines is 2,2'-bipyridine (bpy), known for its well-defined coordination geometry and rich photophysical properties. Copper(I) and copper(II) complexes with bpy may display varied geometries, ranging from mononuclear to multinuclear species. These species can exhibit fascinating light-emitting characteristics, which may prove beneficial for sensors and illumination systems.[63]

Copper(I) complexes that contain diimine ligands have demonstrated excellent efficiency in several catalytic reactions, including C-C and C-N bond formation. It should be noted that selectivity and effectiveness of these reactions can be influenced by the electronic and steric effects of the ligand. This is particularly relevant in Ullmann and Sonogashira reactions, where copper-diimine catalysts are commonly used.[64]

The application of diimine ligands extends to biological and medicinal research, with the study of copper complexes and diimine ligands as potential anticancer agents being an example. These complexes have the ability to interact with DNA, which disrupts its structure and inhibits replication. Certain copper-diimine complexes show selective cytotoxicity towards cancer cells, sparking interest in their development as targeted chemotherapy agents.[65]

Among the first non-innocent ligands that enabled new chemical reactivities trough their facile redox activities were the α-diimines[66], diazabutadiene (DAB) and diazadiene (DAD), which are the most relevant types of ligands for this study. These ligands possess the necessary properties to form stable complexes due to their multidentate coordination nature, proving multiple sites for coordination, leading to well-defined geometries. These ligands possess both σ–donor (electron-donating) and π-acceptor (electron-accepting) properties. The nitrogen atoms in the ligands can donate electron density to the copper centre through σ–bonding, which influences the redox properties and reactivity of the complex. Moreover, the π-systems in the ligands interact with the metal's d-orbitals, thereby affecting the electronic structure of the complex. The ligands' capacity to donate and accept electrons permits regulating the complexes of electronic properties, thereby affecting redox potential, electron transfer processes, and catalytic behaviour. The substituents' steric bulk in the ligand may influence adjacent functional groups and coordination geometry, potentially altering the complex's reactivity and selectivity in a given application.[67–70] These ligands can demonstrate intriguing luminescence depending on the substituents, enabling their application in sensors, light-emitting devices, and photovoltaics.[71] In addition to chelating metallic centres, they can bridge multiple metal centres, resulting in the formation of multinuclear complexes that can affect the electronic communication between the metal centres.[72] The redox activity of these ligands is also significant in catalysis and electron transfer processes. Finally, the many applications in medicinal chemistry arise from their ability interact with biomolecules and exhibit cytotoxic properties, important in potential anticancer agents.[72]

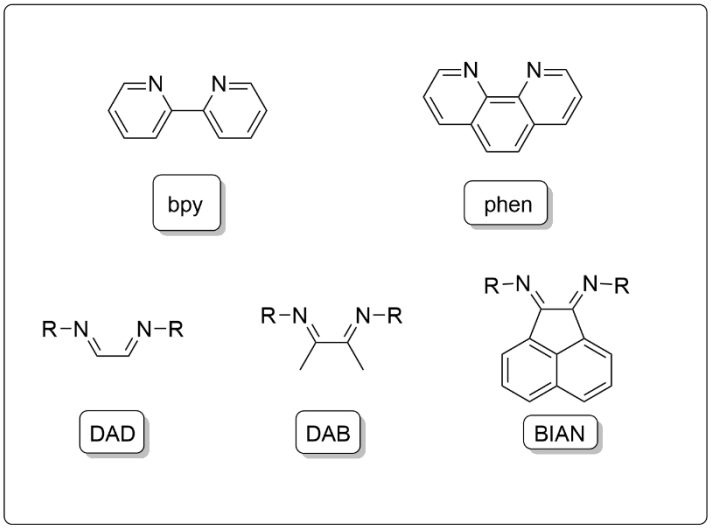

Figure 1.16. Most common types of diimines. Typical diimines of previous published catalytic systems (top) and synthesised diimines for this dissertation (bottom).

Another type of ligand that has gained a lot of interest is the BIAN ligand (bis(imino)acenaphthene), which is a diimine similar to DAB or DAD but has an acenaphthene in its backbone. This ligand has characteristics like those mentioned above but imposes a centre, which can be related to the complex stability. It is less affected by the surrounding effects. Due to their strong σ–donor properties, these ligands have the potential to activate the copper centre and impact the reactivity and selectivity in catalytic processes.[73]

1.4.2 Objectives

Following the previous catalytic system published by the group, which was formed by the BIAN complex but with different counterions (Br, I and Cl) so the main objective is to synthesize complexes that could optimize the catalytic conditions.[74] For that the use of BIAN, DAB and DAD ligands to form copper(I) complexes is proposed. Two counterions, BF_4^- and OTf^-, were chosen due to the expected stability of the BF_4^- and reactivity and effect on the solubility properties of OTf^-. These were combined with two different chelating solvents, MeCN and PhCN, to investigate their effect on the compound's stability. To investigate their potential activity in oxidising benzylic alcohol into benzaldehydes, the efficiency of the

designed system was studied, comparing the effect of the different counterions and determining the most suitable combination of ligand, chelating solvent and counterion for this reaction.

This dissertation comprises three main sections. One section is dedicated to ligands, with subsections discussing the synthesis, structural characterization, and the synthesis of the copper starting materials. Another section focuses on the complexes synthesised, discussing their synthesis, structural characterization and the obtained X-ray structures. The final section, describes the catalysis process, including the catalyst scope, the catalyst loading, the additives loading, the system concentration and substrate scope. In the following section, conclusions and future perspectives will be presented, along with the obtained results. The detailed procedures performed in this work will be described in the next section.

2

RESULTS AND DISCUSSION

Bis(imino)acenaphthene (BIAN), diazabutadiene (DAB) and diazadiene (DAD) ligands were synthesised. The ligands were then coordinated with various copper salts including ($[Cu(MeCN)_4]X$ and $[Cu(PhCN)_4]BF_4$. A more detailed discussion of the synthesis and characterization of each ligand and complex synthesised will be presented in the relevant section. These synthesised compounds were subsequently assessed for their potential as catalysts for the oxidation of benzyl alcohol to benzaldehyde. The study examined the activity, concentration of catalyst and additive, concentration of system, solvent and substrate scope.

2.1 Ligands

2.1.1 Synthesis of the ligands

Five distinct ligands were synthesised under varying conditions, following literature methods[72,75,76] but with changes in the solvent used (methanol or isopropyl alcohol), temperature (0 °C, 25 °C and 65 °C) and the acid catalyst (formic acid or *p*-toluenesulfonic acid) (**Figure 2.1**).

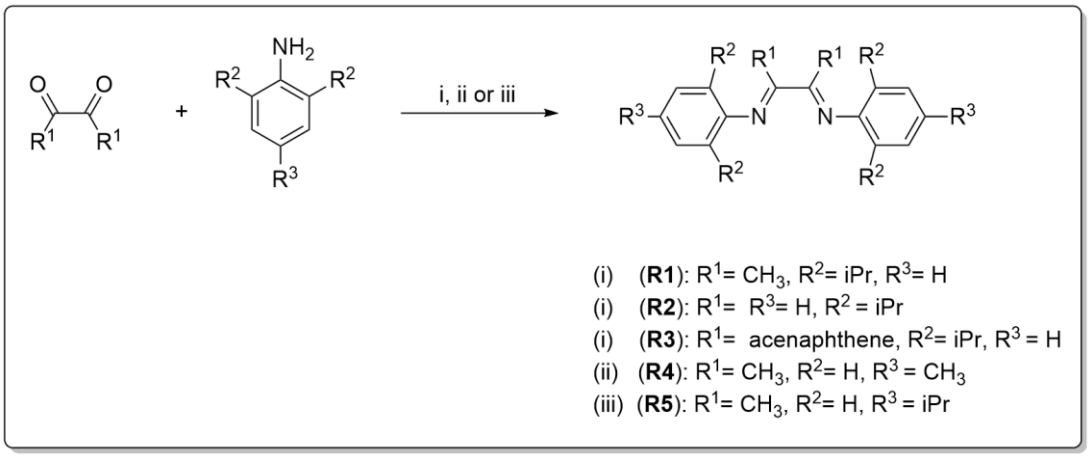

Figure 2.1. Scheme of the synthesis used for the ligands. **i)** - 2,3 - butanedione (1 eq), aniline (2 eq), formic acid (0.1 eq), MeOH, 16h, reflux. **ii)** - 2,3 - butanedione (1 eq), aniline (2 eq), p-TsOH (0.1 eq), MeOH, 24h, r.t. **iii)** - aniline (2 eq), formic acid (0.1 eq), 2,3 -butanedione (1 eq), ^{i}PrOH, 2.5h, 0 °C.

For the DAD^{dipp} (**R2**), BIAN^{dipp} (**R3**) and DAB^{Me} (**R4**) (see **Figure 2.2**), Nolan's procedure[76] was employed by adding butadione or glyoxal and aniline to a methanol mixture at room temperature and stirring for 16h-24 hours (see **Figure 2.1**). The low yields resulted from the formation of byproducts, particularly a polymeric compound that gives rise to a dark brown oil (see **Figure A.1** in the **Annexes**).

For the synthesis of DAB^{dipp} (**R1**), it was followed the method by Pepas.[72] Here, we added the butadione and the aniline to a solution of methanol at reflux temperature and stirred it for 16 hours (**Figure 2.1**). Similar to the previous procedure, the formation of a dark brown oil affected the yield.

For the preparation of DAB^{iPr} (**R5**), it was used an adapted procedure from Day's method.[75] In this case, it was added aniline to a solution of butadione and isopropanol, followed by the addition of *p*-toluenosulfonic acid to catalyse the condensation reaction (**Figure 2.1**). Under these conditions, we obtained a dark brown oil.

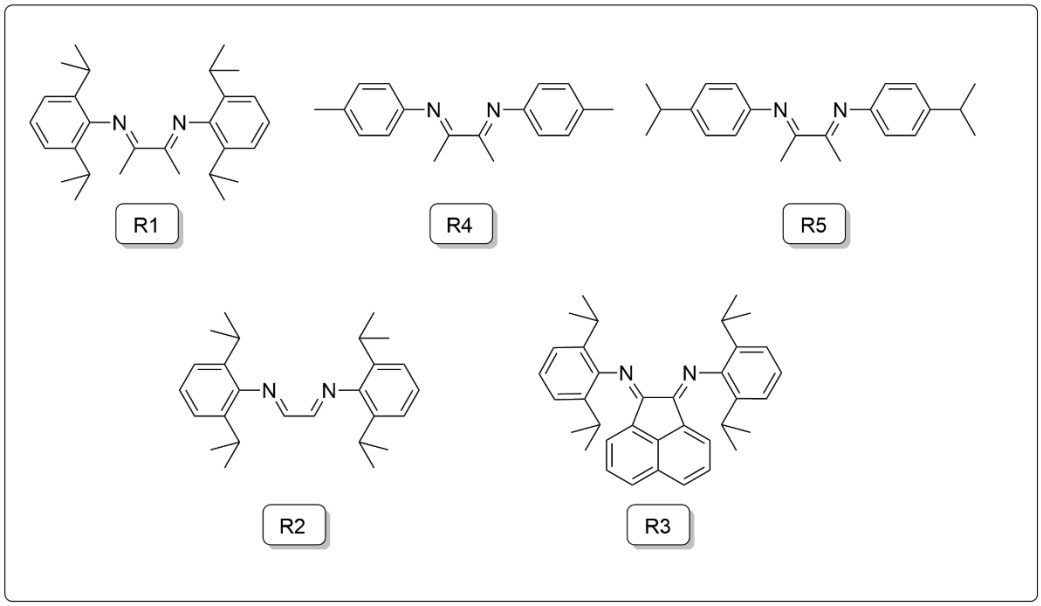

Figure 2.2. Synthesised ligands.

Two additional ligands (see **Figure 2.3**) were intended for synthesis but all attempts to produce a pure product in substantial quantities failed due to the significant formation of the polymer under the present conditions. We hypothesize that is caused by the use of glyoxal starting material in an aqueous solution, whereby the presence of water appears to impede reaction.

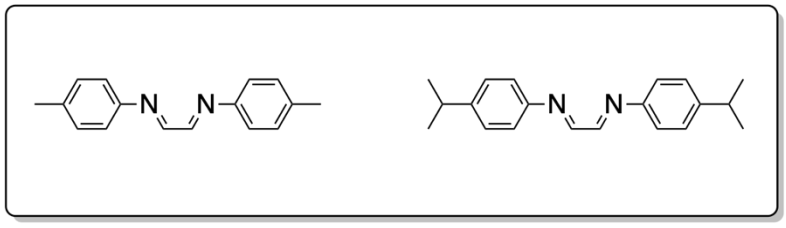

Figure 2.3. Ligands that were not able to be synthesised.

2.1.2 Structure characterisation of the ligands

2.1.2.1 NMR analysis of the ligands

The ^{1}H NMR spectrum of the various ligands provides a structural representation of the obtained compounds and their purity. In the case of the DAB ligands (**R1**, **R4** and **R5)**, the corresponding spectra are illustrated in **Figure 2.4**. For compound **R1** (**Figure A.2** in **Annexes**), the anticipated signals were fivefold, including a triplet. However, the NMR data display a

duplet of duplets at 7.10 ppm, integrating for two protons, which corresponds to the *para* proton from the aryl. Additionally, there is a duplet, integrating for four protons at 7.17 ppm representing the *meta* protons from the aryl, a septet integrating for four protons at 2.72 ppm representing the C-H from the isopropyl substituent, a duplet of duplets, integrating 24 protons at 1.19 ppm, is present due to rotation bond impediment arising from the different chemical environment of each methyl groups from the isopropyl. This results in two signals, but the shift in this case is weak, thereby leading to the observed multiplicity. Finally, a singlet, integrating 6 protons at 2.07 ppm, are assigned to the methyls attached to the iminic carbon.

It is anticipated that the two other DAB ligands will produce the same backbone signal, with only the signals for the distinct aryl substituents being differentiated. As for **R4** (**Figure A.5** in **Annexes**), only one integration for six protons is expected. Determining which signal corresponds to the methyl from the iminic carbon cannot be ascertained with certainty, but it may be speculated that it is the signal at 2.36 ppm, as it is more unshielded than the aryl methyl signal which may be the signal at 2.15 ppm. Two distinct duplets, each integrating four protons, signify the four *ortho* protons. As in the preceding case, it can be inferred that the

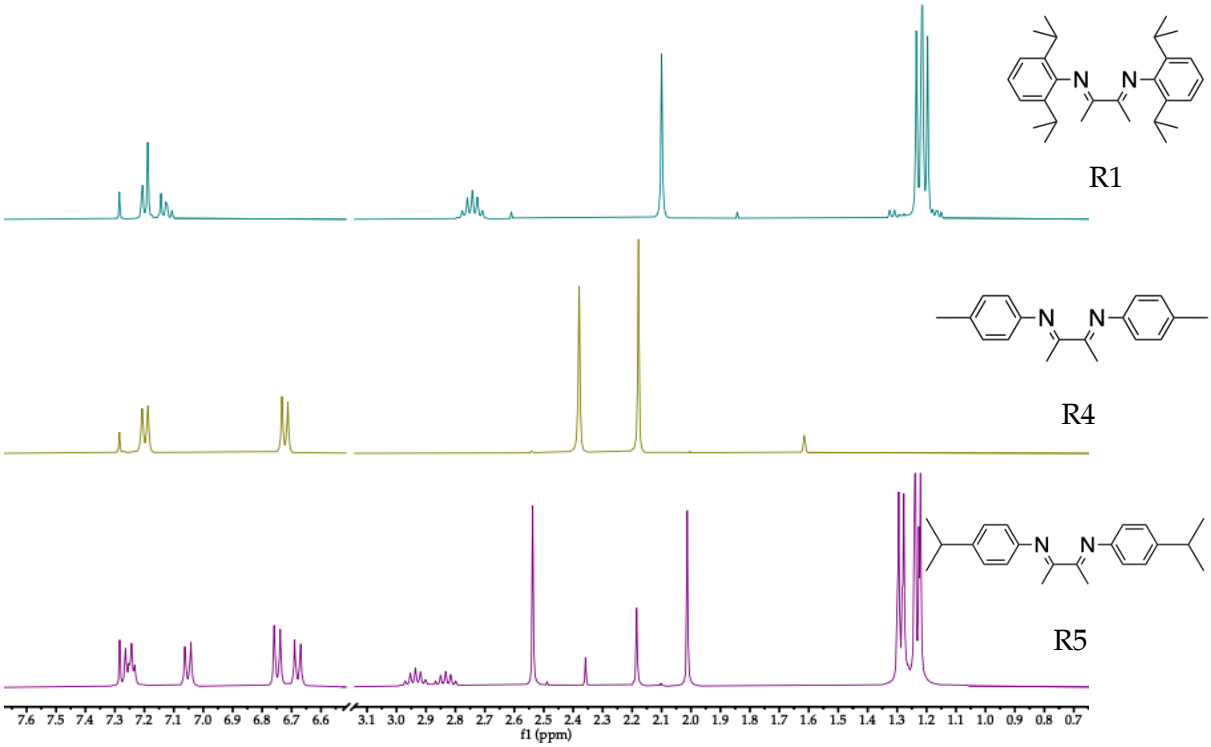

Figure 2.4. ^{1}H NMR ($CDCl_3$) obtained for the DAB ligands. The blue spectrum corresponds to the **R1** compound, the yellow one to the **R4** compound and the purple to the **R5** compound.

signal at 7.17 ppm indicates the *ortho* position, which has relatively unshielded protons. Similarly, the signal at 6.70 ppm is expected to represent the four *meta* protons. For **R5** (**Figure A.6** in **Annexes**), the expected signals for the aromatic compound are 7.23 ppm for the *ortho* protons and 6.72 ppm for the *meta* protons. Additionally, there is a septet integrating at 2.90 ppm that represents the C-H of the isopropyl and a duplet integrating for 12 protons at 1.27 ppm representing the methyl of the isopropyl.

For the DAD^{dipp} (**R2**) compound (**Figure A.3** in **Annexes**), as depicted in **Figure 2.5**, five signals ought to be detected are expected, one singlet at 8.11 ppm integrating for 2 protons corresponding to the protons from the iminic carbon, one duplet integrating for 4 protons corresponding to the *meta* protons from the aryl substituent, one triplet integrating for 2 protons corresponding to the *para* protons from the aryl substituent but what the spectrum show is a multiplet superimposed with the deuterated solvent ($CDCl_3$) at 7.18 ppm integrating for 6 protons but also the protons from the solvent, it is also expected a septet at 2.94 ppm corresponding to the C-H of the isopropyl and a duplet at 1.14 ppm from the CH_3 of the isopropyl.

For the $BIAN^{dipp}$ (**R3**) (**Figure A.4** in **Annexes**), as illustrated in **Figure 2.5**, additional signals from the ligand are anticipated. The most unshielded signal corresponds to a duplet at 7.86 ppm integrating for two protons, which is attributed to the *para* proton from the acenaphthene backbone. The subsequent signal will correspond to the triplet at 7.36 ppm characteristic of the *meta* proton from the acenaphthene backbone. The following multiplet corresponds to the aryl *meta* and *para* protons at 7.26 ppm and integrates for 6 protons. However, due to being superimposed with the deuterated solvent ($CDCl_3$) the integration is slightly higher. The following signal corresponds to the C-H from the aryl group, a septet at 3.01 ppm integrating to 4 protons. It was anticipated that a duplet integrating for 24 protons related to the methyl groups of the isopropyl group, but two duplets at 1.13 ppm and 0.96 ppm integrating to 12 protons each are shown instead. This phenomenon may be attributed to the absence of group rotation, which leads to two different chemical shifts due to steric hindrance and distinct chemical environment. This is analogous to the case of **R1**, but the presence of the acenaphthene leads to an even more hindered bond rotation.

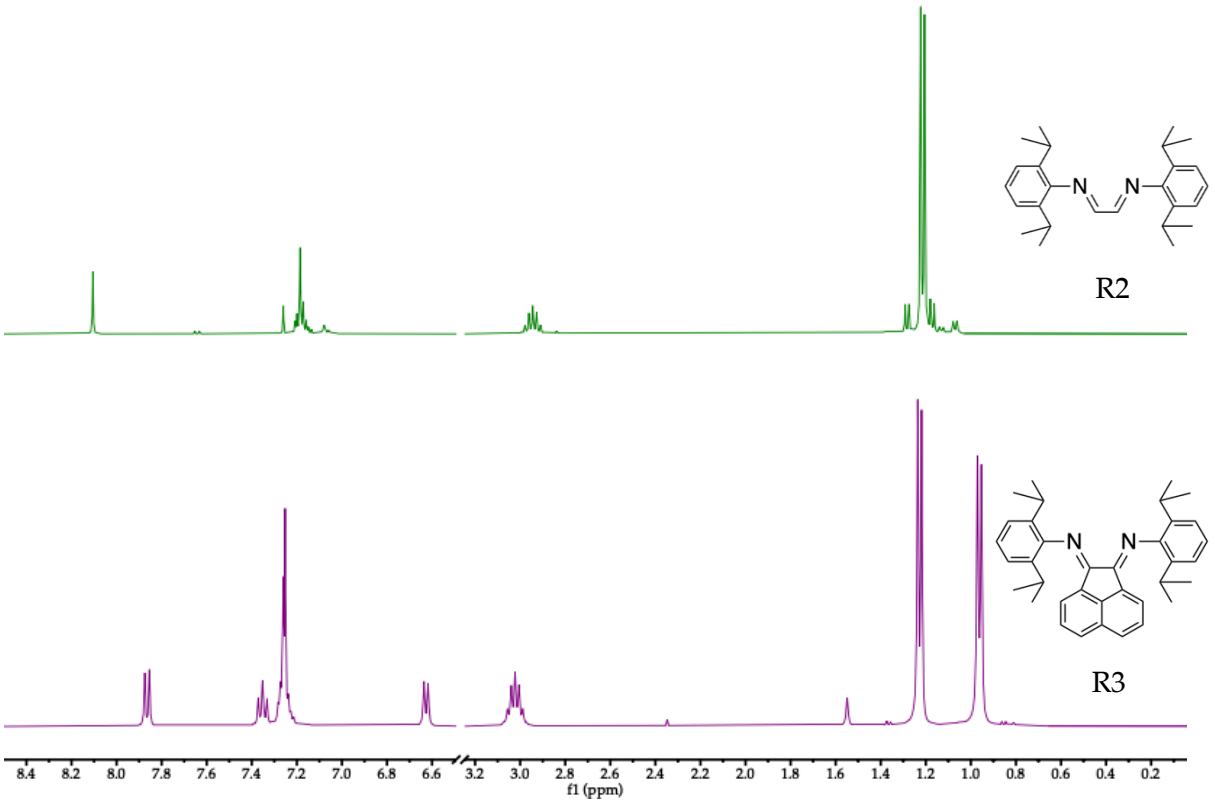

Figure 2.5. ^{1}H NMR of the DAD ligand and BIAN ligand synthesised. In the green spectrum is represented the **R2** compound and in the purple spectrum the **R3** compound.

2.1.2.2 UV/Vis analysis of ligands

The UV/Vis spectroscopy is a valuable tool to better understand the electronic properties and coordination behaviour of the ligands in study. The diazabutadiene ligands are conjugated organic molecules, and so their lower energy electronic transitions can be observed in a UV/Vis spectrum at ca 340 nm (348 (**R1, Figure A.7** in **Annexes**) and 342 nm (**R4, Figure A.10** in **Annexes**) and (**R5, Figure A.11** in **Annexes**)) with low molar absorptivity, with additional transitions at shorter wavelengths, 233 nm and 267 (**R1**), 228 nm and 284 (**R4**) and 229 nm and 287 (**R5**), represented in **Figure 2.6**. In the three spectra the transitions appear to be very similar, but a small deviation appears when the aryl substitution changes from the *ortho* to the *para* position.

To precisely determine which type of orbitals are involved in the transitions would require additional experimental studies and computational methods, such as density functional theory (DFT) or time-dependent DFT (TD-DFT).

The similarity between the **R1** and **R2 (Figure A.8** in **Annexes)**, in contrast to **R4** and **R5** could originate from the two isopropyl in the *ortho* positions, which do not allow for the rotation of the bonds specially between the two imines (see **Figure 2.7**).

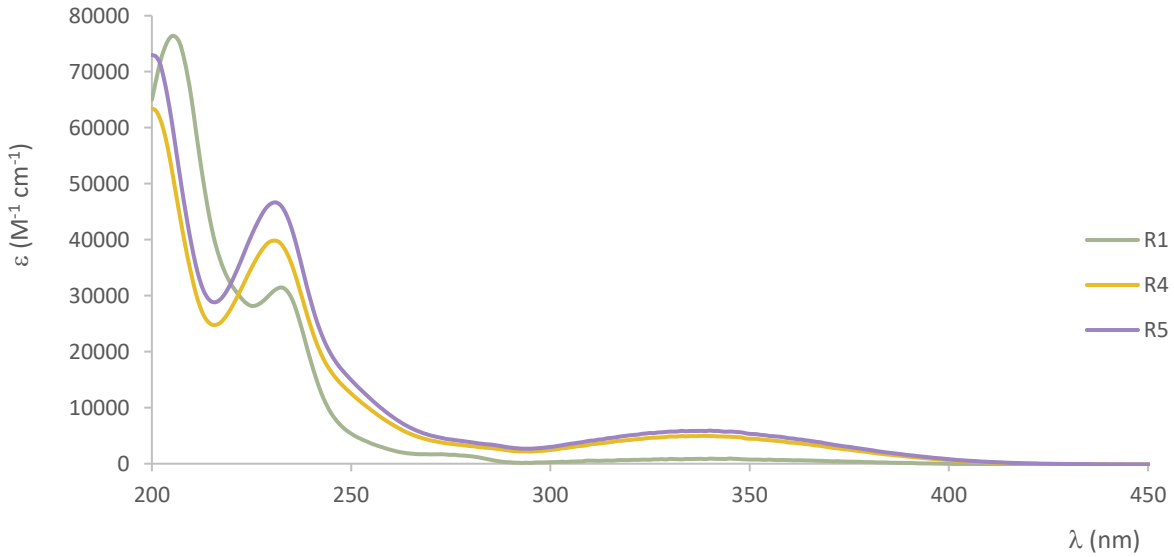

Figure 2.6. UV/Vis spectra obtained in MeCN of the DAB ligands.

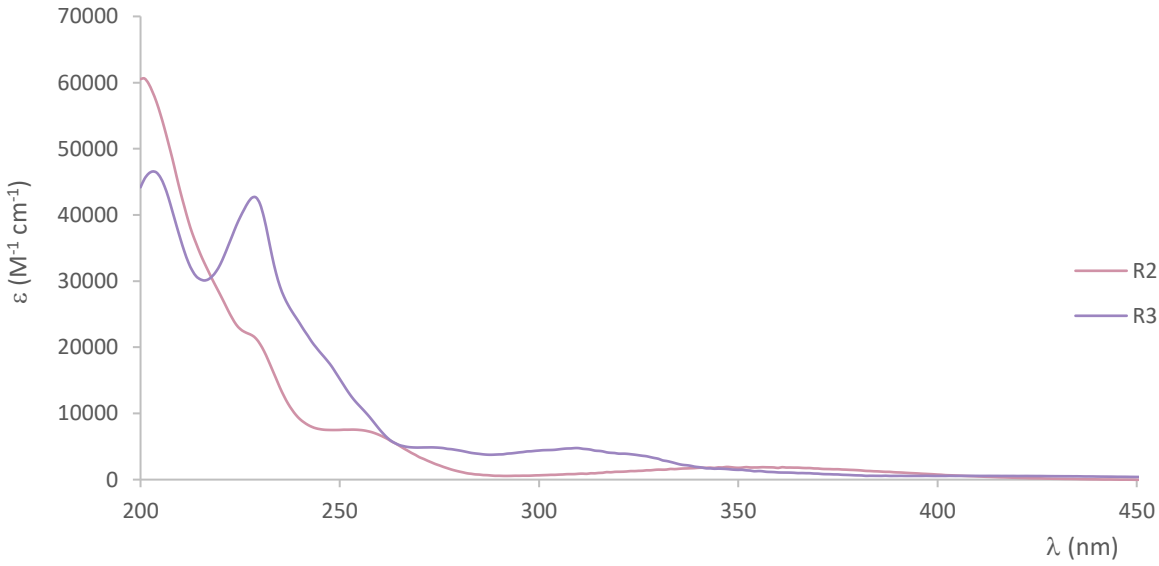

Figure 2.7. UV/Vis spectra of the DAD ligand (in MeCN) and the BIAN ligand synthesised.

2.1.2.3 IR analysis of the ligands

The infrared technique is valuable in the compound characterization as a complementary method as it detects the impact of various functional groups through the vibrations produced. The most prevalent and crucial vibrations are the stretching, a continuous alteration in the interatomic distance along the axis of the bond between two atoms, while the modification in the angle is called bending. Another piece of information that can be obtained from the infrared analysis is the alteration in bond strength. When a band shifts towards a higher wavelength number, the bond is stronger.

Based on the structures of the synthesised molecules, the main bands of importance are the C=N bands. These bands appear at 1630 cm^{-1} (**R1, Figure A.12** in **Annexes**), 1625 cm^{-1} (**R2, Figure A.13** in **Annexes,** and **R4, Figure A.15** in **Annexes**), 1668 cm^{-1} (**R3, Figure A.14** in **Annexes**) and finally at 1633 cm^{-1} (**R5, Figure A.16** in **Annexes**), as presented in **Figure 2.8**.

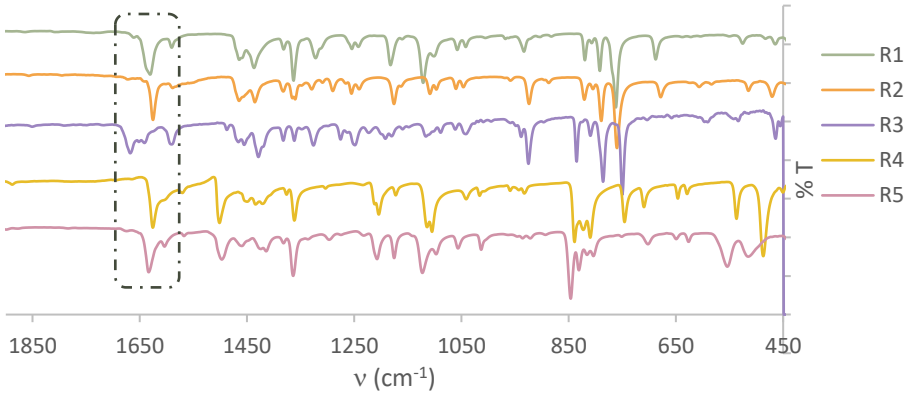

Figure 2.8. IR spectra obtained for all synthesised ligands.

2.1.3 Copper starting materials

Three distinct copper starting materials were synthesised, all of which were previously published in the literature, shown in **Figure 2.9**. The preparation of these compounds involved the use of a copper(II) complex with the corresponding counterion and an excess of metallic copper, which was refluxed with either acetonitrile or benzonitrile depending on the target

complex. The obtained complexes were sensitive to air and humidity which leads, to their oxidation; thus, they were stored in Schlenk flasks under argon at -18°C.

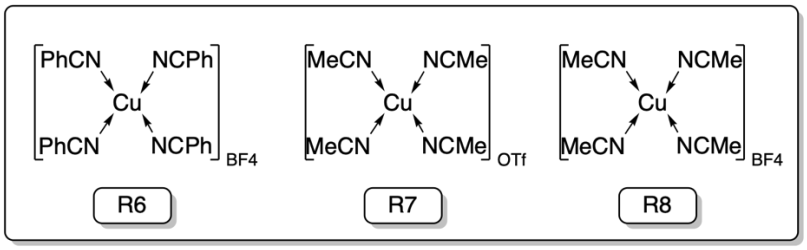

Figure 2.9. Synthesised copper starting materials.

2.2 Complexes

2.2.1 Synthesis of the complexes

Seven complexes were synthesised, with five being new and two previously reported in the literature. The synthesis of the complexes involved the ligands **R1**-**R5** described earlier, as well as various copper starting materials and counterions, showcased in **Figure 2.2**, **2.4** and **2.9**. These complexes were obtained with high yields and purity through the reaction presented in **Figure 2.10**.

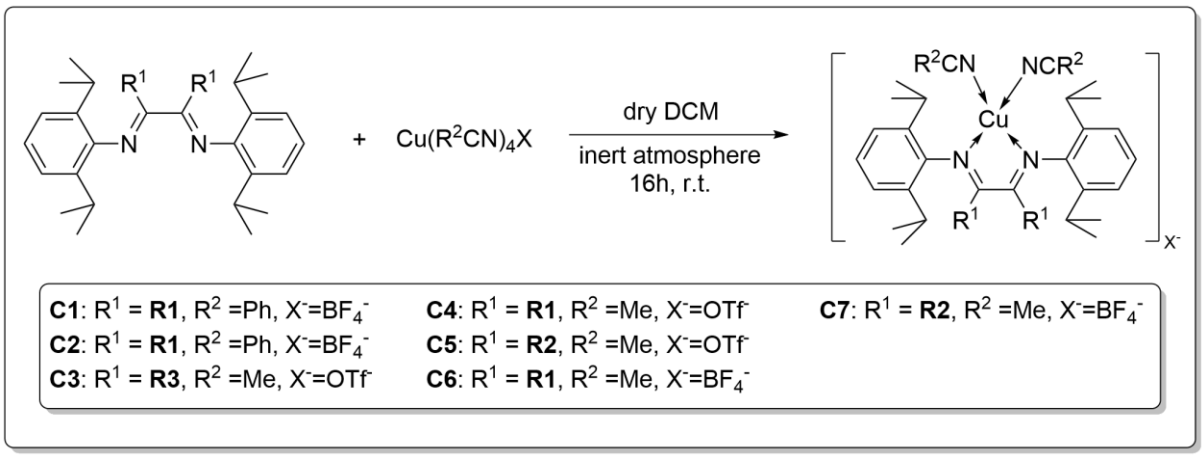

Figure 2.10. Scheme of the synthesis of complexes **C1**-**C7**.

The reaction of copper salts with ligands **R1-R3** resulted in the formation of these complexes, using 1:1 stoichiometric ratio, in dried dichloromethane under an argon atmosphere, employing Schlenk techniques. The reaction proceeded for 16 hours at room temperature. Eventually, the compounds underwent filtration and were subjected to the liquid-liquid diffusion method, using pentane as a counter solvent. The compounds precipitated as brown crystals, and filtering was repeated, as shown in **Figure 2.11**. Certain complexes, particularly those containing the smaller groups, such as the acetonitrile and DAB or DAD ligands, proved difficult to precipitate and tended to form oils. Obtaining the solid compound, required breaking the oil with liquid nitrogen and diethyl ether under vacuum.

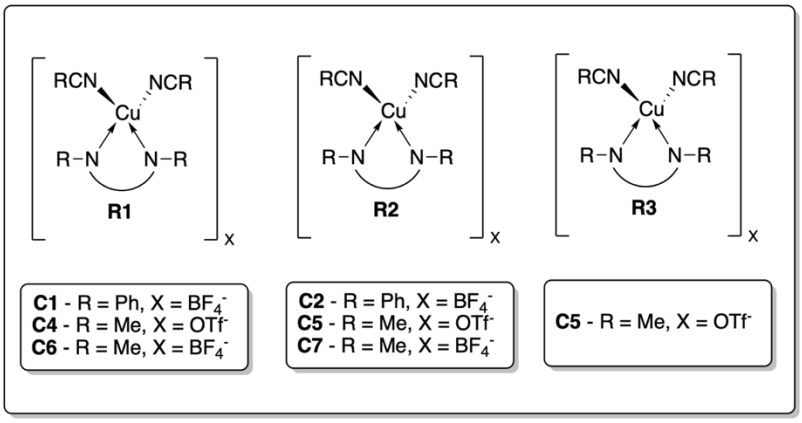

Figure 2.11. Complexes synthesised.

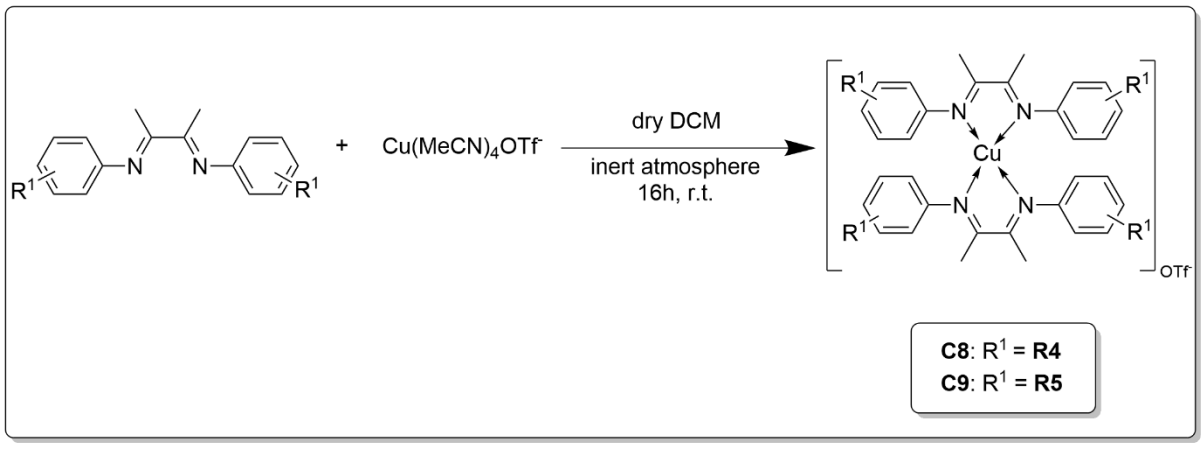

Figure 2.12. Scheme of the synthesis of complexes **C8** and **C9**.

Bischelates **C8** and **C9** (**Figure 2.13**) are a newly synthesised complex family without published information. These molecules were synthesised as previously described (**Figure 2.12**), producing a dark rose compound when in solution and a dark brown solid with high yields and purity. Treatment with liquid nitrogen and diethyl ether under vacuum is required due to the formation of an oily compound.

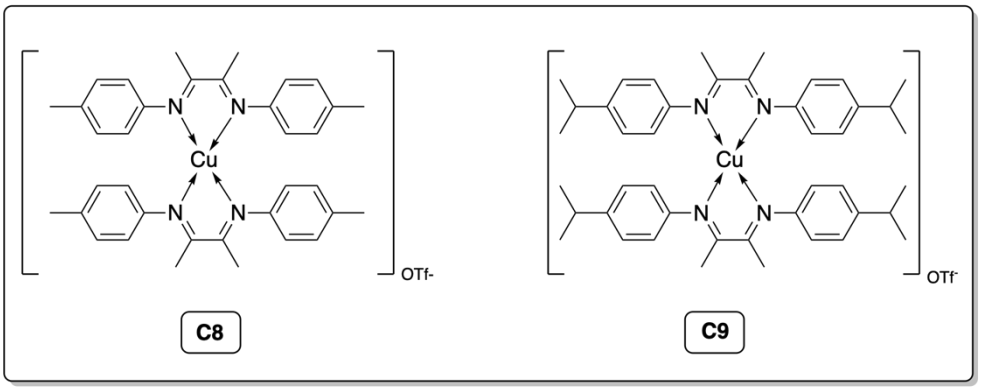

Figure 2.13. Synthesised complexes.

2.2.2 Structural characterization

Various characterization techniques were employed in the confirmation of the desired compound during the complex synthesis. Spectroscopic methods, including NMR, UV/Vis and IR spectroscopies, as well as X-ray crystallography, when possible, were utilized.

2.2.2.1 NMR analysis of the complexes

Comparing with the free ligand facilitated assignment of the chemical shift as it did not deviate significantly from the free ligand. This aided in identification of chelating solvent's signal. The ^{1}H NMR spectrum show significance across all the complexes, with the most notable change occurring due to the deviation of the hydrogen adjacent to the iminic carbon deviating towards a lower magnetic field when compared to the free ligand.

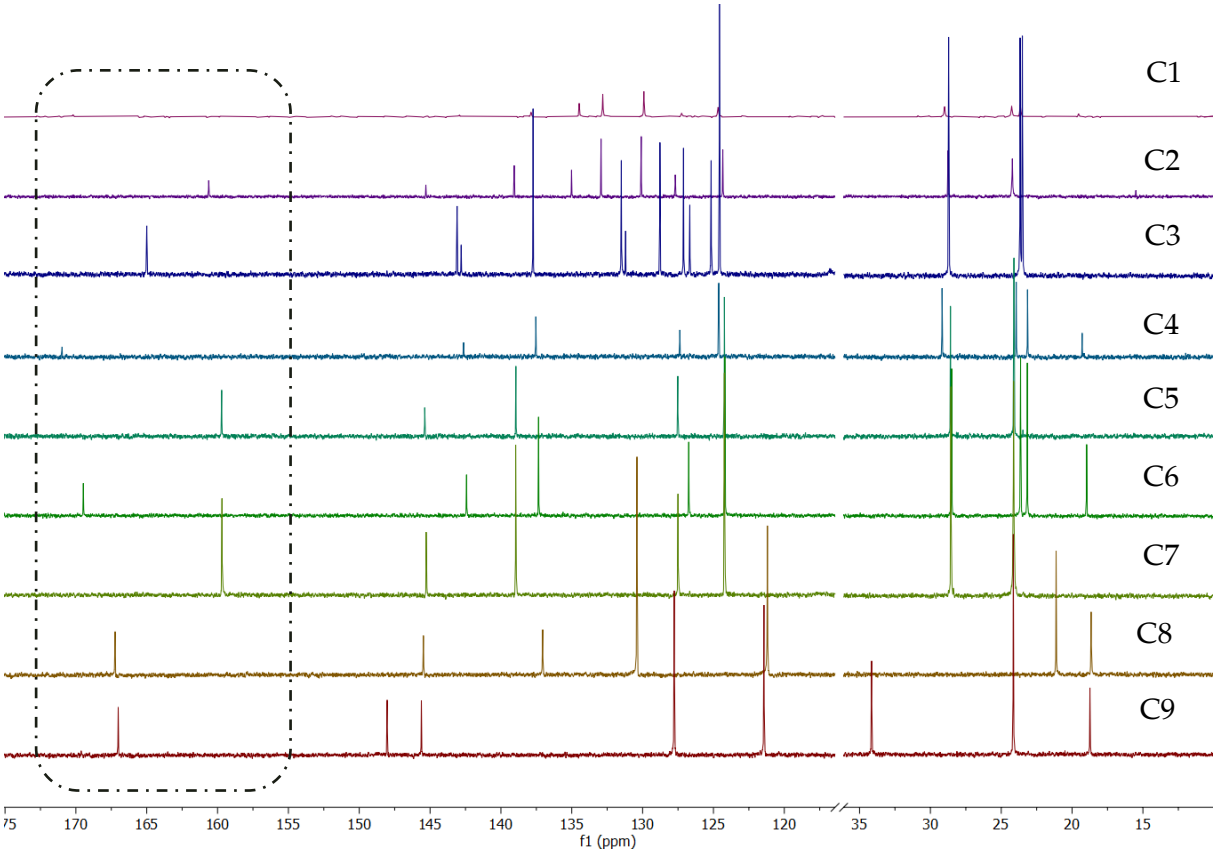

Figure 2.14. Stacked ^{13}C NMR spectra of all the synthesised complexes.

The iminic carbon in the various complexes displays the impact of resonance in the diimine backbone. **Figure 2.14** illustrates how the signal shifts to a lower field, indication of a stronger unshielding effect, when methyl groups constitute the diimine backbone. Conversely, when there is no substitution, the signal appears at a higher field, indicating greater shielding. The BIAN complex lies in between these two. There are two distinct effects at play. The electron-donating groups (methyl) activate the iminic bond by increasing the electron density surrounding the copper atom. Another effect at play is resonance, involving the delocalization of electrons in the aromatic groups or in conjunction with the aryl groups. This process leads to an increase in electron density at the position where partial negative charges are present. As a result, the signal is observed at a higher field and so is more shielded compared to the case of methyl substitution.

The coordination of the metal in the adjacent methyl to the iminic carbon was compared in the ^{1}H NMR of the complexes, resulting in a deviation to a lower magnetic field in all complexes, as shown in **Figure 2.15**. The benzonitrile assignment in compound **C2 (Figure A.24** in

Annexes) was easily identified by comparing it to the ^{1}H NMR spectrum of the free ligand, which corresponded to the three-signals missing in the reagent spectrum. For the compound **C4**, the signal of the MeCN is very broad and short, necessitating a zoom to make it visible. The complete spectrum with the appropriate zoom can be viewed in **Figure A.38** in **Annexes.** No effect of the different counterions is visible in the ^{1}H NMR.

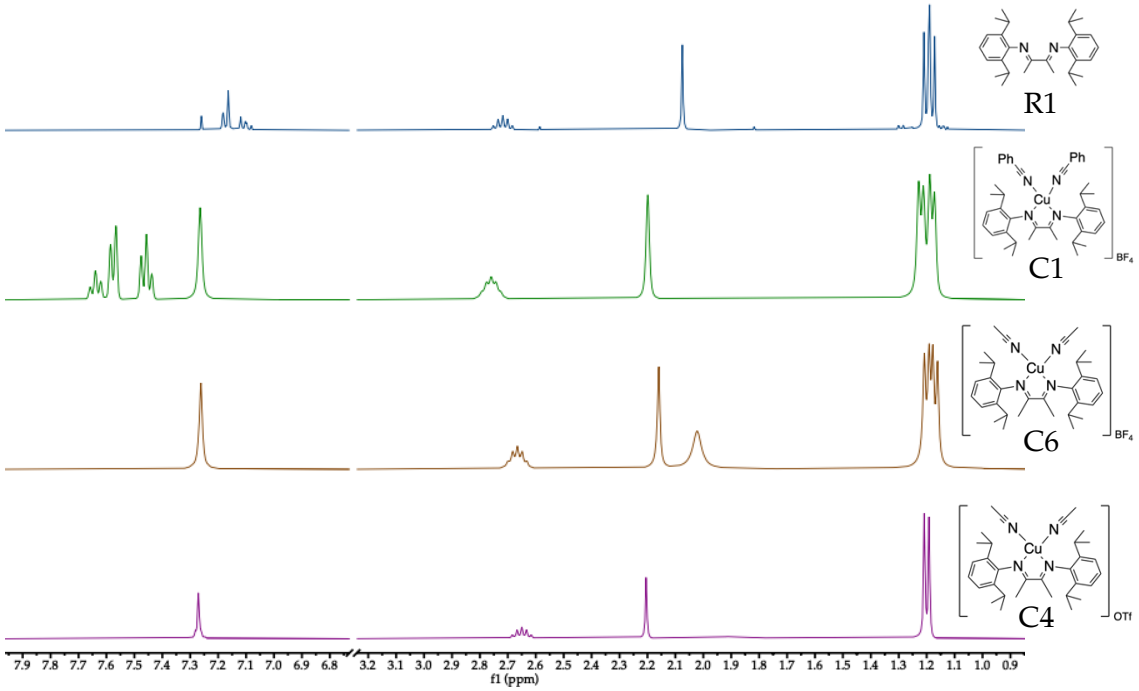

Figure 2.15. ^{1}H NMR of the free ligand **R1** and the complexes **C1**, **C4**, **C6**.

Through comparing the free ligand with the different ^{1}H NMR spectrum obtained for the complexes, it can be concluded that the iminic hydrogens have been shifted toward a lower magnetic field. This is consistent with a change in the chemical environment of these protons, specifically the presence of the copper coordination (8.11 ppm (**R2**), 8.33 ppm (**C2**), 8.20 ppm (**C5**), 8.19 ppm (**C7**)). The *meta* and *para* protons of the aryl in these complexes can be identified by two signals that are overlapping at 7.25-7.02 ppm (**R2**), 7.32 ppm (**C2**), 7.36-7.24 ppm (**C5**), 7.28 ppm (**C7**). The remaining signals in the case of **C2** correspond to the benzonitrile present as a chelating solvent. **Figure 2.16** displays these findings.

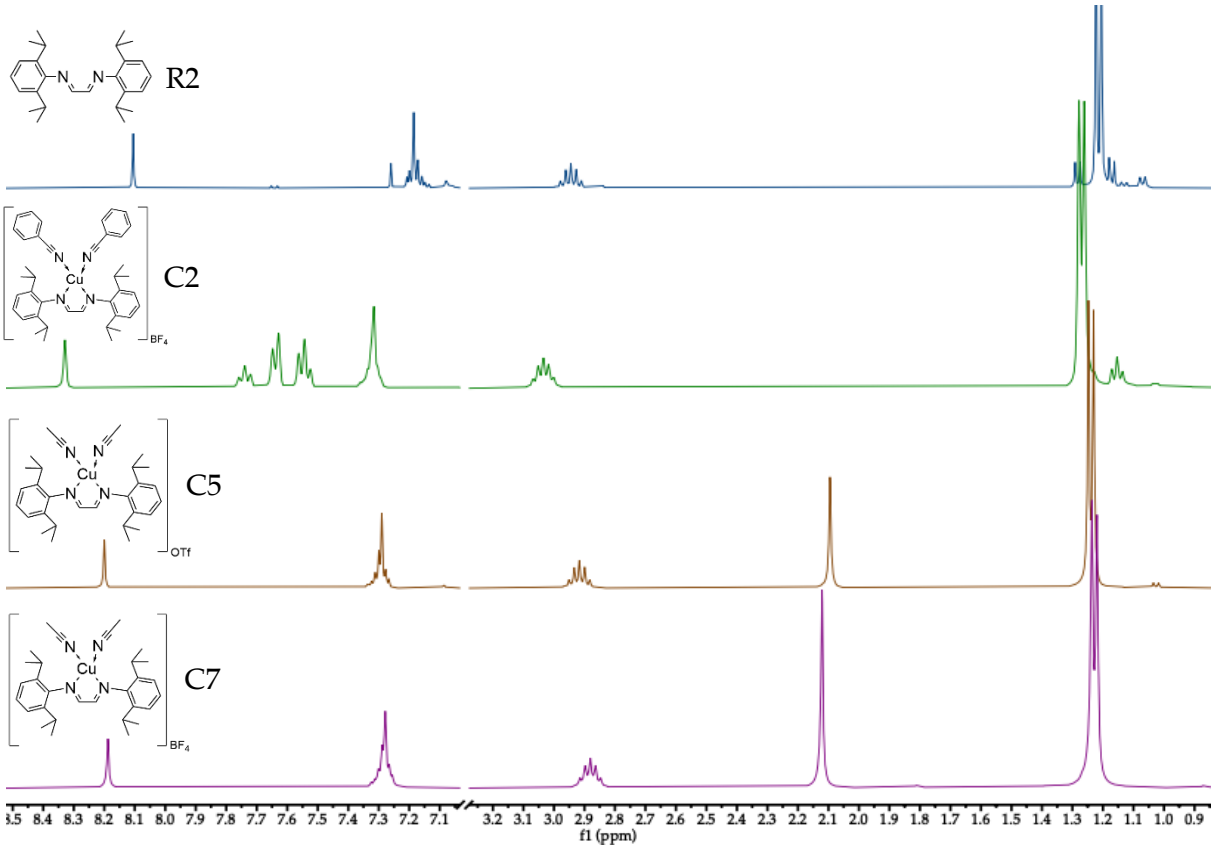

Figure 2.16. ^{1}H NMR of the free ligand **R2** and the complexes **C2**, **C5**, **C7**.

The shifts in signals when coordinating to copper were compared in the case of the **C3** complex. The acenaphthene backbone's proton signals underwent the most significant change, with *para* protons shifting from 7.87 ppm (**R3**) to 8.12 ppm (**C3**), in the *ortho* protons from 7.36 ppm (**R3**) to 7.52 ppm (**C3**), and *meta* protons shift from 6.64 ppm (**R3**) to 6.75 ppm (**C3**). The remaining signals, which correspond to the aromatic and aliphatic signals from the aryl's substitution, showed no considerable change in their chemical shift upon coordination to the metal. Another indication of the coordination is the presence of a signal at 2.15 ppm corresponding to the acetonitrile, the chelating solvent present in this complex. These results are shown in **Figure 2.17.**

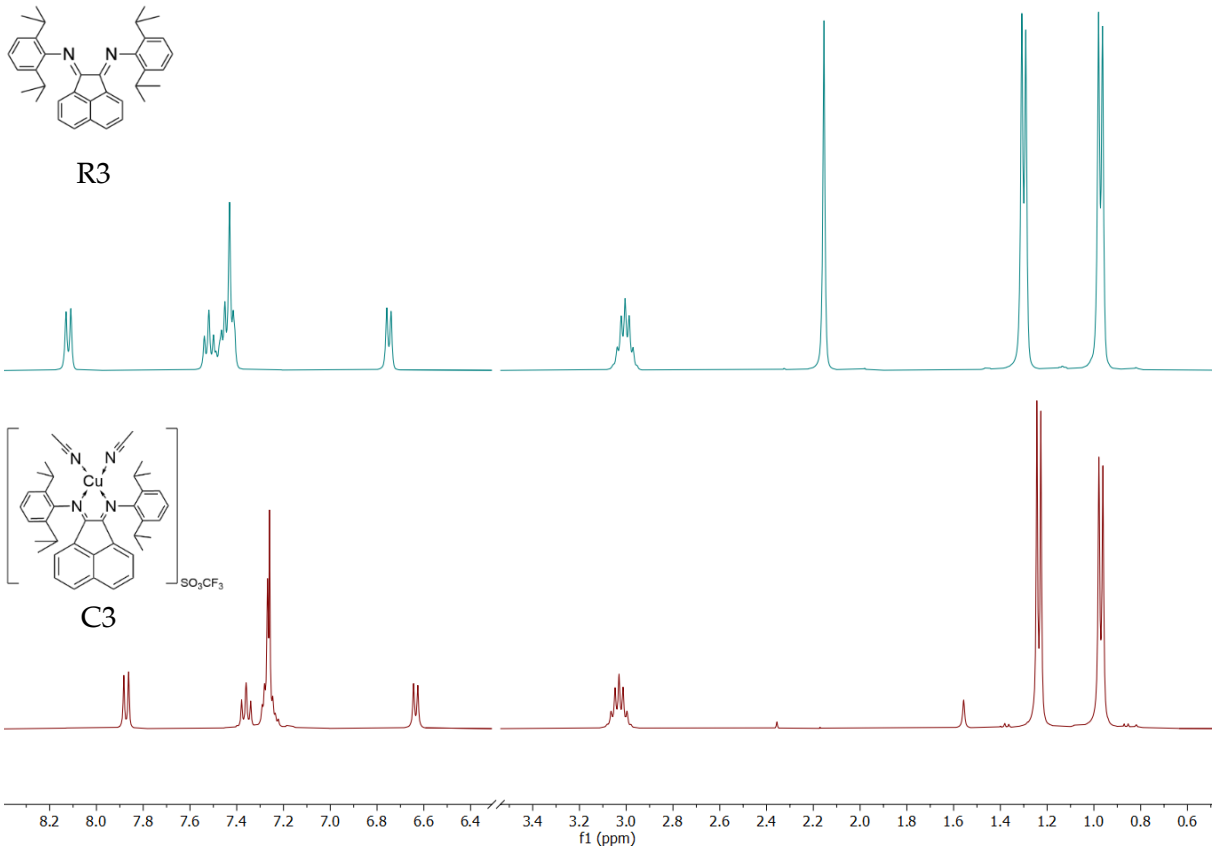

Figure 2.17. ^{1}H NMR of the BIAN free ligand **R3** (blue) and the **C3** complex (brown).

For compounds **C8** and **C9**, bischelate formation of the bischelate is expected, due to the absence of steric hindrance in *ortho* positions. To confirm this hypothesis, the presence of the MeCN signal in the ^{1}H NMR of these compounds, corresponding to the chelating solvent, was taken into consideration but not found. Instead, only a common signal with the free ligand was observed, with a slight deviation towards lower magnetic field. For instance, the adjacent iminic carbon signal in **C8** and **R4** displays a 2.36 ppm deviation in the free ligand compared to 2.39 ppm in the complexed form. In the case of the **C9**, a notable observation is made. The ^{1}H NMR of the free ligand shows a mixture of two compounds, which we presume to be the enantiomer of the cis compound that coordinates with the metal. The molecule seems to alter its conformation in order to coordinate with the metal, leaving only one species in the ^{1}H NMR of the complex. Additionally, a small deviation is observed in the general signals of this complex towards a lower magnetic field, which confirms the coordination of the copper to these molecules. The stacked spectra are shown in **Figure 2.18**.

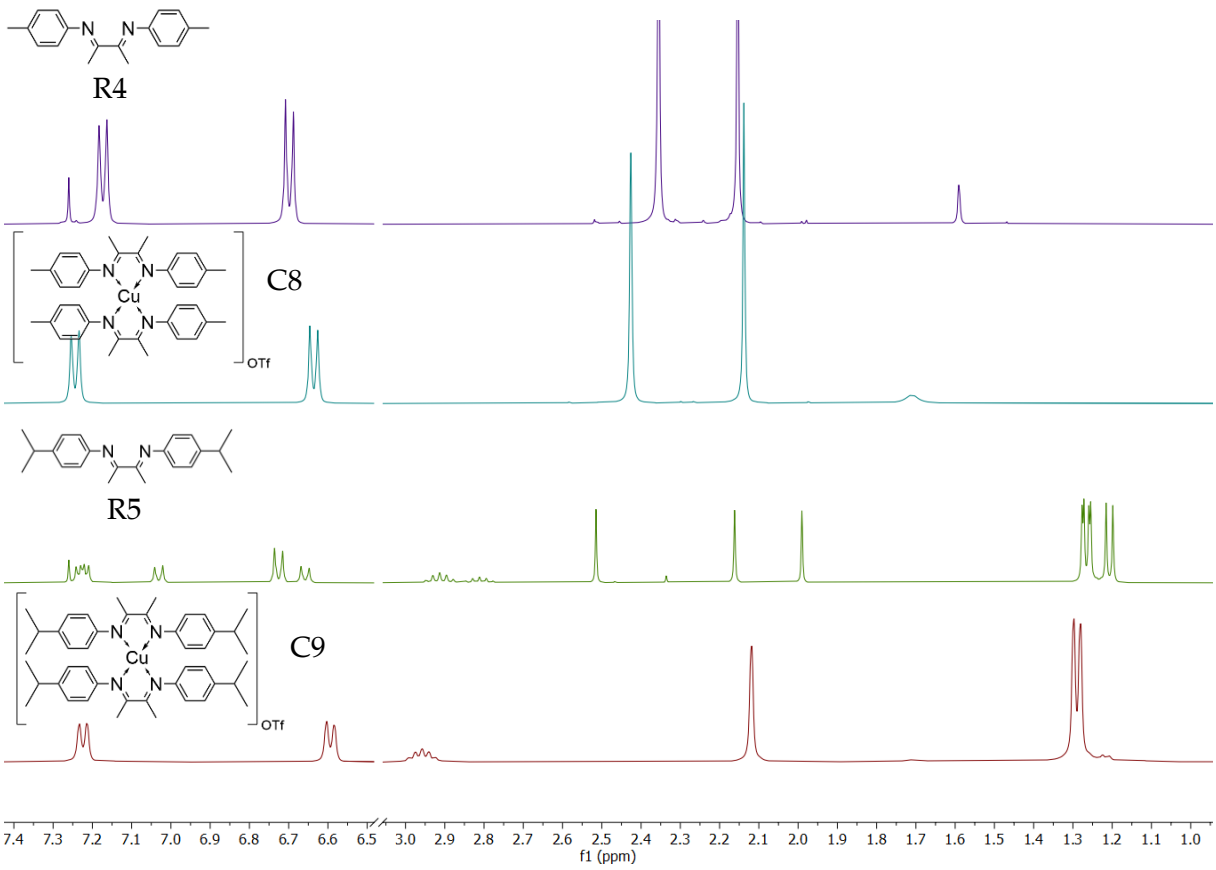

Figure 2.18. ^{1}H NMR spectrum of the ligands **R4** and **R5** and complexes **C8** and **C9**.

To verify the assigned signals, additional COSY, HSQC, HMBC, and NOESY experiments were conducted. The COSY spectrum enabled the correlation of neighbouring protons and identification of the corresponding proton signals based on the presumed molecules. The HSQC spectrum were then utilized to correlate non-quaternary carbons with their respective protons. Upon completing this assignment, the HMBC spectrum proved crucial in detecting the signals associated with quaternary carbons. This spectrum has the capability to exhibit signals with J^2 and J^3 coupling constants, confirming their presence, thereby enabling the identification of all ^{13}C spectrum signals. It was crucial to determine the spatial arrangement of the molecule, and this was achieved through the use of NOESY. This method provided information on the proximity of protons in space, rather than just in adjacent positions. Additionally, it is noteworthy that the counterions employed, BF_4 and SO_3CF_3 (OTf), contain fluorine in their composition. The ^{19}F spectrum will confirm the presence of these species. The fluor signal

for the BF_4 ion appears at -153.52 ppm (**C1**), -153.29 ppm (**C2**), -153.12 ppm (**C6**), -152.99 ppm (**C7**) and for the SO_3CF_3 ion at -78.85 ppm (**C3**), -77.90 (**C4**), -78.75 ppm (**C5**), -78.88 ppm (**C8**), -76.24 ppm (**C9**). The shift obtained for the triflates anions seems to indicate that in any case there is coordination to the metal centre.

2.2.2.2 UV/Vis analysis of the complexes

For the different complexes the UV/Vis was also performed as a characterization technique. For that, dry MeCN was used to conduct the analyses. For the DAB complexes (compounds **C1**, **C4** and **C6**) it is possible to observe that the spectra are similar to the ligand (**R1**) expect for compound **C1 (Figure A.80** in **Annexes)**, which corresponds to the complex with the benzonitrile as the chelating solvent. The results are shown in **Figure 2.19**.

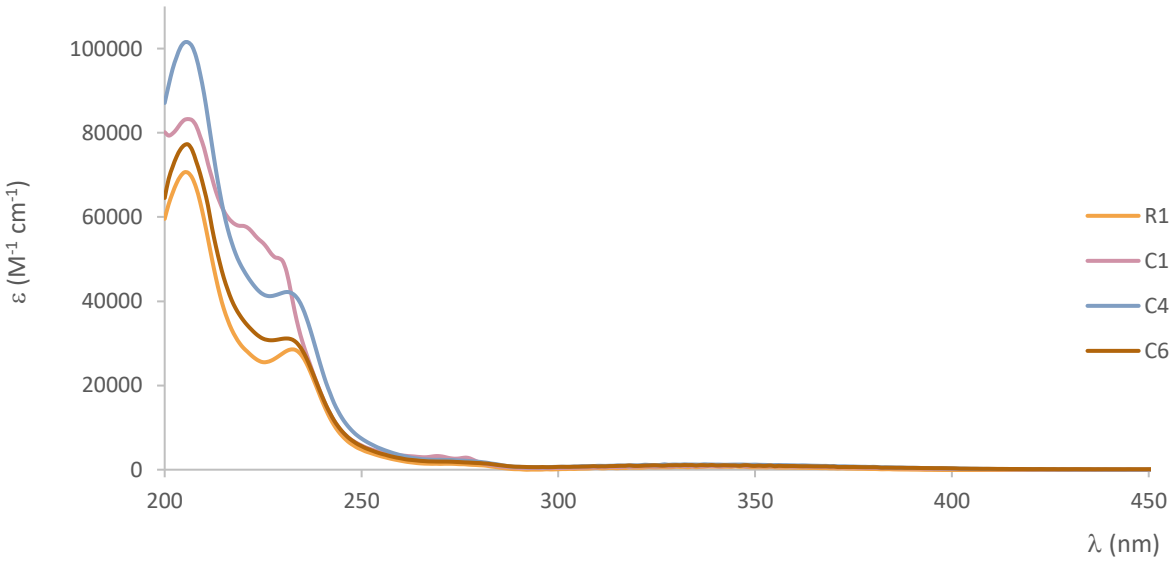

Figure 2.19. UV/Vis spectrum of the DAB ligand **R1** and the complexes **C1**, **C4**, **C6** in MeCN.

Regarding the DAD complexes, including **C2 (Figure A.81** in **Annexes)**, **C5 (Figure A.84** in **Annexes)** and **C7** (**Figure 2.19, Figure A.86** in **Annexes**), the same behaviour occurs as the benzonitrile complex appears with more transitions than the other compounds with almost superimposable spectra. A transition metal-to-ligand charge transfer (MLCT) is expected when a metal is in its low oxidation state and the ligands are composed with low-lying empty orbitals but couldn't be observed, this can be due to the lack of the sumperimposed HOMO

and LUMO orbitals resulting in low absorptivity and thus the MLCT transition is not observed.

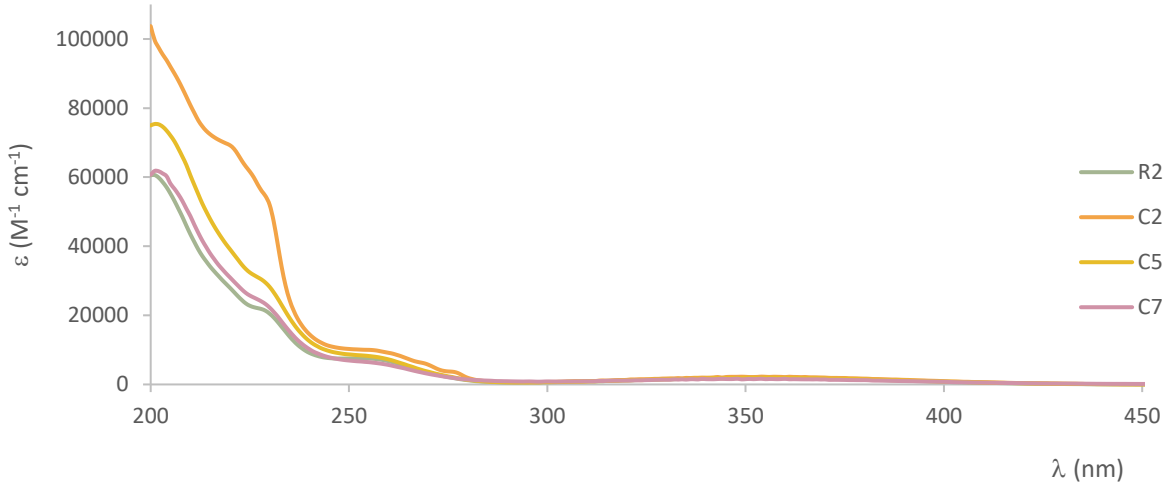

Figure 2.20. UV/Vis spectrum of the free ligand **R2** and the complexes **C2**, **C5** and **C7** in MeCN.

The **R3** and **C3** (**Figure A.82** in **Annexes**) spectra (**Figure 2.21**) seem to be practically superimposable, which indicates low influence when coordinated to the metal. For both compounds transitions at 312 nm, 230 nm and 274 nm are observed.

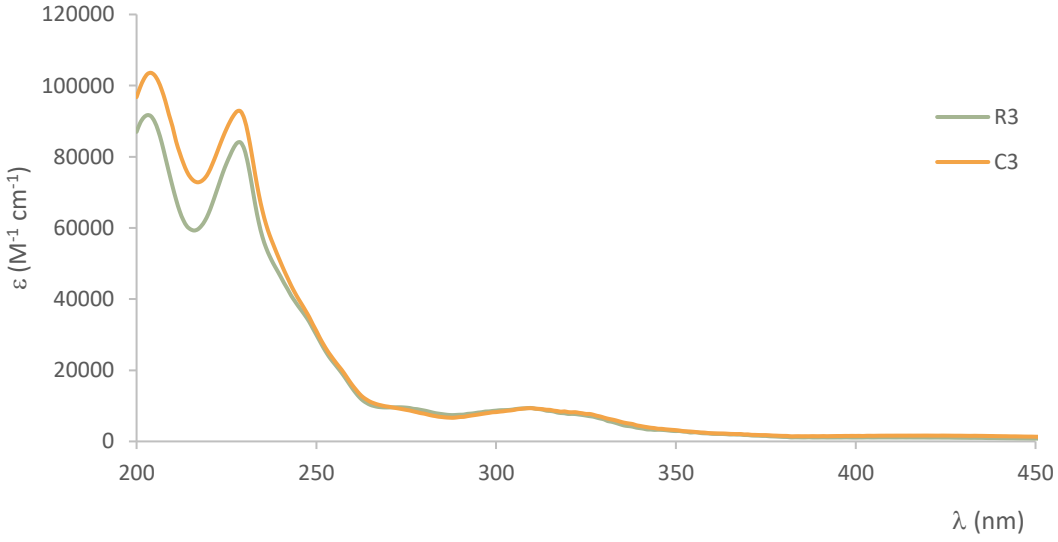

Figure 2.21. UV/Vis spectrum of the free ligand **R3** (green) and the **C3** complex (orange) in dry MeCN.

Finally, the last compounds **C8** (**Figure A.87** in **Annexes**) and **C9** (**Figure A.89** in **Annexes**), show a very similar almost superimposable behaviour with the free ligand revealing two transitions at *ca* 350 nm and 230 nm, as of the other compounds studied (**Figure 2.22**). These compounds also show the higher molar extinction coefficient, which correlates with the number of chromophore units that absorb light at the same wavelength.

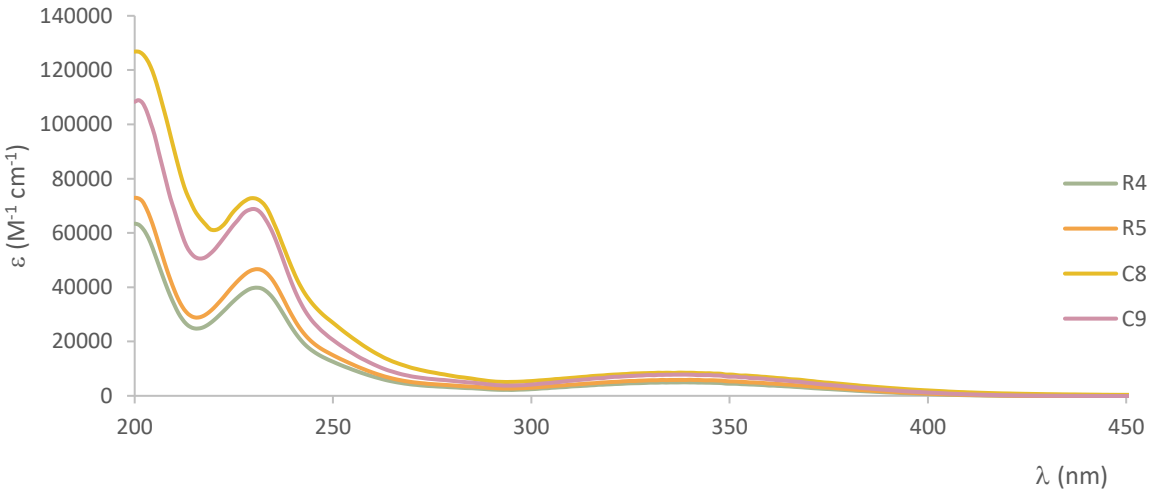

Figure 2.22. UV/Vis spectrum of the free ligands **R4** and **R5** and the complexes **C8** and **C9** in MeCN.

2.2.2.3 IR analysis of the complexes

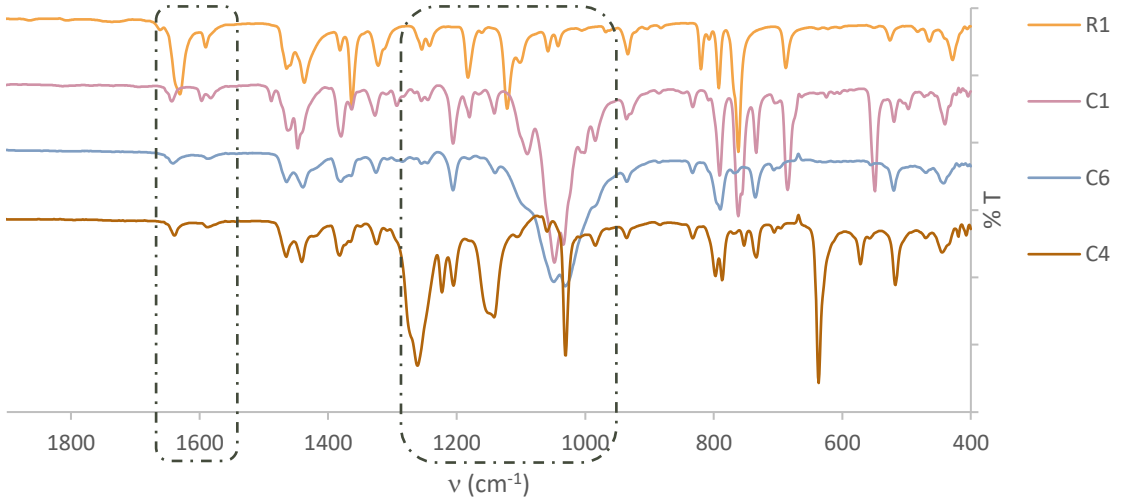

Figure 2.23. IR spectrum of the free ligand **R1** and the complexes **C1**, **C4** and **C6**.

The IR analysis mainly confirmed that the functional groups present in the molecules

under study were reflected in the corresponding functional groups. Consequently, vibration specific to B-F, S=O and C-F were sought in various complexes. These bands typically appear between 1200-1000 cm^{-1}. Another significant zone is around 2280-2215 cm^{-1}, wherein the bands -CN from the benzonitrile and acetonitrile will appear. Lastly, the band from the imines will appear around 1600 cm^{-1}.

When comparing the free ligand with the complexes, new bands are observed and a shift is noted in the C=N band at 1643 cm^{-1} (**C1**), 1641 cm^{-1} (**C6**) and 1639 cm^{-1}(**C4**). In the case of the **C1** complex (**Figure A.89** in **Annexes)**, which is composed of benzonitrile, the corresponding band to this vibration band was found at 2226 cm^{-1}, while the BF_4 vibrations were noted at 1050 cm^{-1} and 1047 cm^{-1}. As for the **C6** complex (**Figure A.93** in **Annexes)**, a band characteristic of the acetonitrile group was expected and found at 2277 cm^{-1}, along with BF_4 vibrations at 1048 cm^{-1} and 1030 cm^{-1}. A vibration at 2273 cm^{-1} corresponding to the MeCN vibrations was detected for the **C4** complex (**Figure A91** in **Annexes)**. The CF_3 vibrations were also observed, with bands at 1261 cm^{-1} and 637 cm^{-1}, as well as a band at 1142 cm^{-1} characteristic of S=O. Furthermore, a band at 1030 cm-1 characteristic of the C-F vibration was identified. These results are shown in **Figure 2.23**.

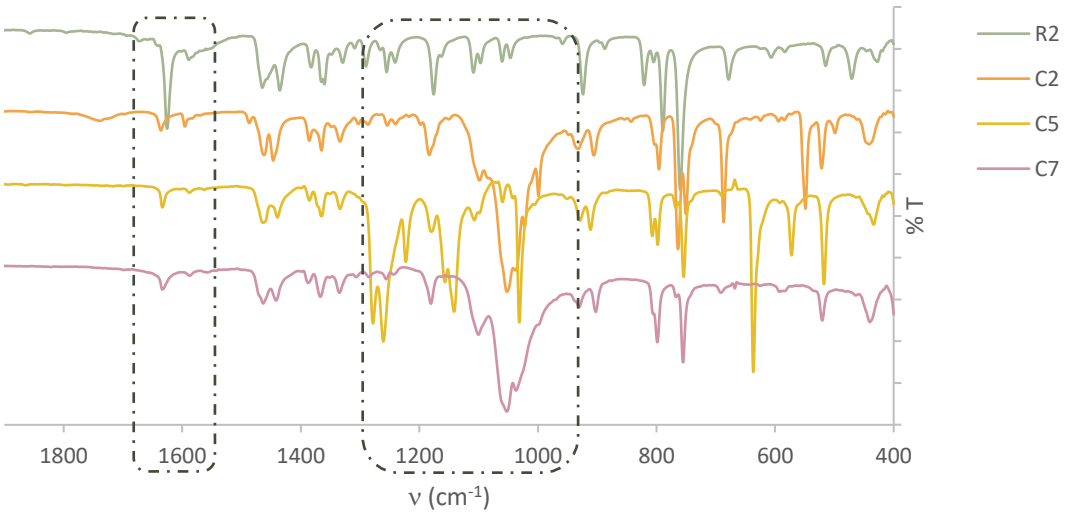

Figure 2.24. IR spectrum of the free ligand **R2** and the complexes **C2**, **C5** and **C7**.

As with the previous example, an increase in wavelength number is noticed in the imine bond at 1635 cm^{-1} (**C2**), 1633 cm^{-1} (**C7** and **C5**). Counterions vibrations were also detected. A vibration of BF_4 at 1052 cm^{-1} was established for the **C2** (**Figure A.90** in **Annexes**) and **C7** complexes (**Figure A.94** in **Annexes)**. The **C5** complex (**Figure A.92** in **Annexes)** contains and

exhibits a range of vibrations. CF_3 vibrations were identified at 1260 cm^{-1} and 636 cm^{-1}, the S=O vibrations were found at 1141 cm^{-1}, and C-F vibrations were detected at 1031 cm^{-1}. Additionally, the **C2** complex exhibit benzonitrile vibrations at 2241 cm^{-1}, while the **C5** and **C7** complexes displayed acetonitrile vibrations at 2272 cm^{-1} and 2275 cm^{-1}, respectively. These results are shown in **Figure 2.24**.

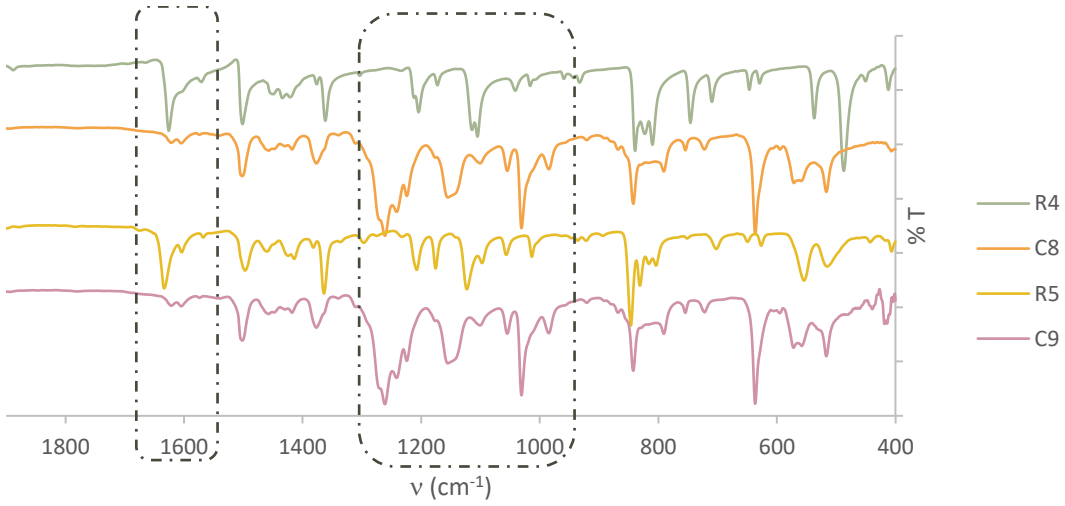

Figure 2.25. IR of the free ligands **R4** and **R5** and the complexes **C8** and **C9**.

Contrary to the other complexes, the imine bands are more prominent in the free ligand than in the complexed state. However, they still occur, at 1623 cm^{-1} and 1620 cm^{-1} for the **C8 (Figure A.95** in **Annexes)** and **C9 (Figure A.96** in **Annexes)**, respectively, and appear to shift to a lower wavelength number, which contrasts with the remaining complexes. Another way to confirm that the bischelate is the species that formed is the lack of the acetonitrile vibration at c.a. 2270 cm^{-1}. The CF_3 vibrations appear at 1261 cm^{-1} and 636 cm^{-1} for both complexes. Additionally, the S=O vibration is observed in both complexes at 1154 cm^{-1} and the C-F vibration is evident in both compounds at 1030 cm^{-1}, providing evidence of the counterion's presence. These results are presented in **Figure 2.25**.

2.2.2.4 X-ray crystallography analysis

With the objective to characterize the new complexes through X-ray crystallography, to better understand the geometry that the complexes adopted in solid state and their tridimensional properties, it was required to obtain crystals. For that, a technique known as liquid-liquid diffusion, where a second solvent is "layered" carefully on top of the solution containing the compound was used. The compound must be insoluble (or have very low solubility) in the second solvent, so when the two solvents mix, the compound starts to crystallize, usually at the layers interface. The solvents used were dichloromethane for solubilising the sample, and pentane as the counter solvent. It was possible to obtain good crystals for the analysis of complexes **C3**, **C4** and **C7**.

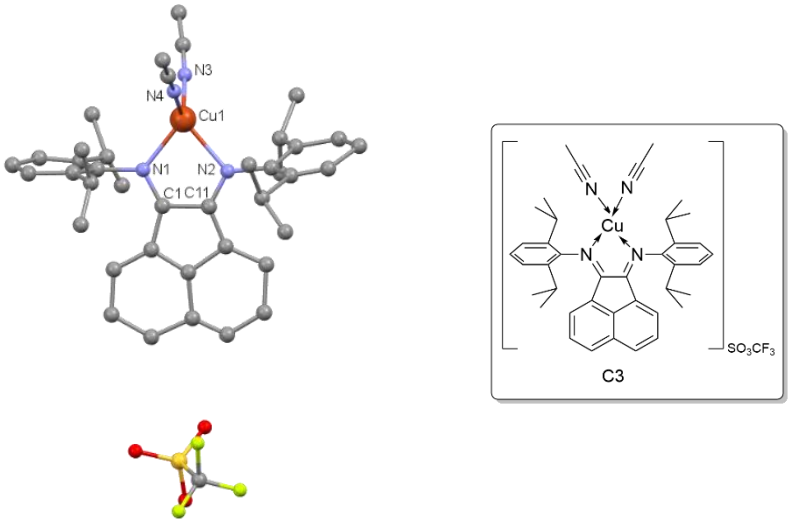

Figure 2.26. Mercury representation of the complex **C3**, with hydrogens and a dichloromethane solvent molecule omitted for clarity (left) and its structural representation (right).

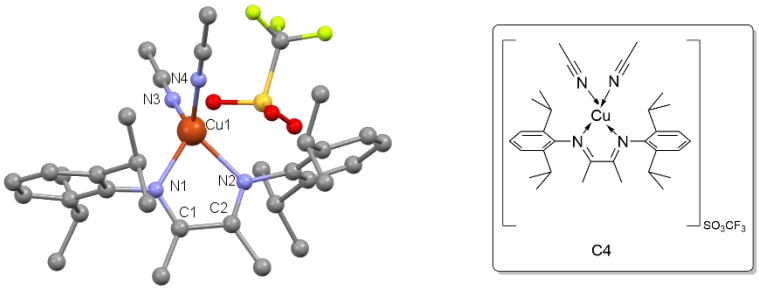

Figure 2.27. Mercury representation of the complex **C4**, with hydrogens and a dichloromethane solvent molecule omitted for clarity (left) and its structural representation (right).

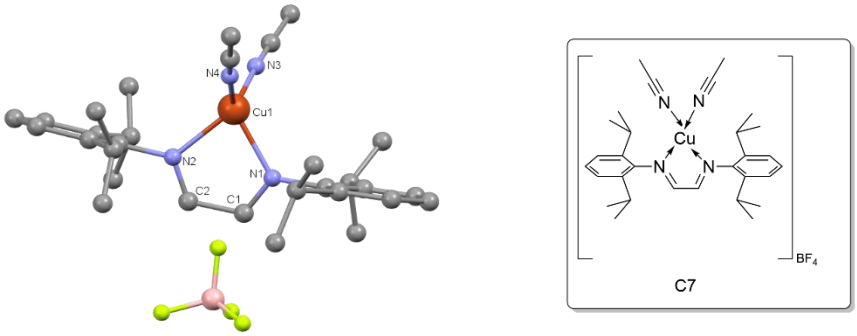

Figure 2.28. Mercury representation of the complex **C7**, with hydrogens and a dichloromethane solvent molecule omitted for clarity (left) and its structural representation (right).

In complexes **C3**, **C4** and **C7**, the asymmetric unit shows only one molecule of the cationic complex, the respective counterion and one molecule of cocrystallized solvent molecule, which in all the cases was dichloromethane. **Figure 2.26, Figure 2.27 and Figure 2.28** shown the cationic moiety of the metal complex, highlighting the metallic centre with the iminic

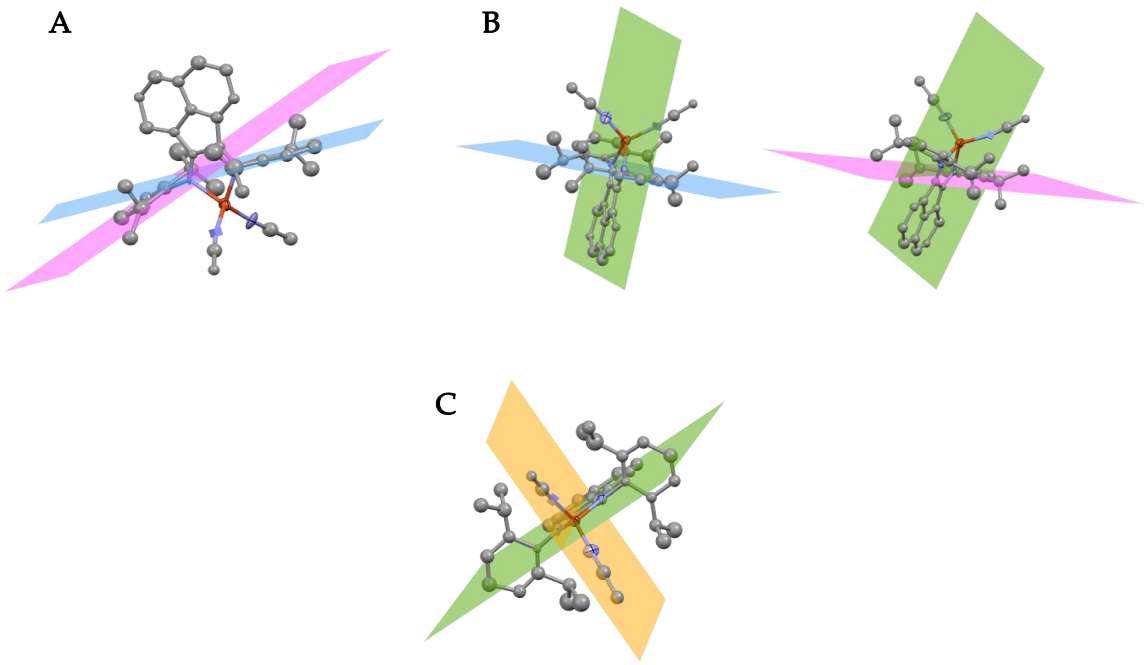

Figure 2.29. Representation of the planes studied for the characterization of the complexes **C3**. **A** - shows the ω angle relating the two planes formed by the aryl's groups. **B** - shows the two φ angles, formed by the aryl's plane and the backbone's plane. **C** - shows the θ angle, formed by the backbone's plane and the chelating solvent's plane.

Table 2.1. Selected the bond lengths, bond angles and dihedral angles (ω,φ and θ) of the **C3**, **C4** and **C7** complexes.

	C-N [Å]	*Cu-N¹ [Å]* *Cu-N² [Å]*	*Cu-N³ [Å]* *Cu-N⁴ [Å]*	*N¹-Cu-N²* *[°]*	*N³-Cu-N⁴* *[°]*	*ω[°]*	*φ₁ [°]* *φ₂ [°]*	***θ [°]***
C3	1.30 (3) 1.28 (2)	2.068 (17) 2.169 (14)	1.89 (2) 2.004 (18)	79.2 (6)	106.8 (8)	20.6 (7)	73.8 (6) 86.2 (6)	**88.3 (5)**
C4	1.275 (7) 1.276 (6)	2.057 (4) 2.057 (6)	1.962 (5) 1.939 (6)	78.42 (18)	106.3 (2)	20.2 (2)	86.03 (16) 81.46 (18)	**89.92 (14)**
C7	1.273 (3) 1.275 (3)	2.0829 (17) 2.0816 (16)	1.9396 (18) 1.945 (2)	78.76 (6)	114.69 (9)	6.96 (8)	80.04 (6) 79.05 (7)	**91.90 (6)**

carbons and in all the cases was dichloromethane, it is also highlighted the nitrogen atoms of the organic ligand, and the nitrogen atoms of the coordinated acetonitrile labelled. Next to the X-ray structure is the simplified representation of the molecules for easier understanding. The **C3** complex crystallized in the monoclinic system, space group $P2_1/n$; The **C4** complex crystallized in the triclinic system, space group $P\text{-}1$; And finally, the **C7** complex crystallized in the monoclinic system, space group $P2_1/c$.

Figure 2.29. shows a representation of the planes defined to calculate the dihedral angles.[1]

Upon analysis of the results obtained from the X-ray crystallography technique, the first conclusion to consider is the geometry of the complexes, what they appear to be tetrahedral due to the analysis of the highlighted angles obtained in **Table 2.1.** For a perfect tetrahedral geometry is required that the compound shows a dihedral angle θ of 90°, which means that the synthesised compounds have a slightly distorted tetrahedral geometry, since their dihedral angle θ are 88.3° (**C3**), 89.92° (**C4**) and 91.90° (**C7**).

The dihedral angle ω consists in the angle between the two aryls. Comparing the three complexes, discrepancies can be observed, since the two complexes that have a more hindered backbone either, with acenaphthene or methyl groups (**C3** and **C4**) show a 20.6° and 20.2°, respectively, while the derivative with a less hindered backbone (**C7**) allows for a more aligned position of the aryls, which shows an angle of 6.96 °.

The dihedral angles φ, defined between the ligand's aryls and the complex's backbone are all very similar. In fact, the main difference between the two angles is obtained with the complex **C3**, which is consistent with the statement above that the steric hindrance of the bulky backbone will interfere with the position that these aryls will adopt. This conclusion is supported by the decrease of the difference between the two angles when decreasing the bulkiness of the backbone.

Finally, the diimine ligand's bite angles show very similar results, all around 79°. All remaining bond distances are similar within the three structures and in agreement with other derivatives already reported in the literature.[77]

[1] A dihedral angle is defined as the angle when two planes intersect, i.e. in the plane's intersection. These complexes are characterized by three different angles: φ (which involves each aryl plane and the backbone's plane; ω (which involves the angle formed by each aryl's plane); and finally, θ (which involves the two planes crossing the metallic centre) this angle allows for the determination of the complex's geometry.

2.3 Catalytic studies

Various parameters were studied in order to assess the possible activity of the synthesised complexes in catalysing the oxidation reaction of benzyl alcohol to benzaldehyde. Initially, the Stahl conditions were applied to identify the most suitable complex for catalysing this reaction. The catalytic activity of the Cu^{I} complexes was then analysed using acetonitrile as the solvent and 1 mol % of the Cu^{I} complex at room temperature. 4-Dimethylaminopyridine (DMAP) was utilized as the base due to its ability to facilitate the formation of Cu^{II}–OH species that can react directly with the alcohol to produce the intermediate Cu^{II} – alkoxide without requiring an organic base. 10 mol% of DMAP was employed. Another additive utilized was the 2,2,6,6 – tetramethylpiperidinyloxy (TEMPO). This compound acts as a cocatalyst, working as a one-electron oxidant to enable the net two-electron oxidation reaction of alcohol-to-aldehyde. Hence, oxidation of both the Cu^{I} complex and TEMPOH occurs via O_2. The completion of the reaction is signalled by a change in the solution's colour. The oxidation process concludes when only Cu^{II} is present, identifiable by the green hue of the solution. This mechanism is depicted in a simplified manner in **Figure 2.30**.

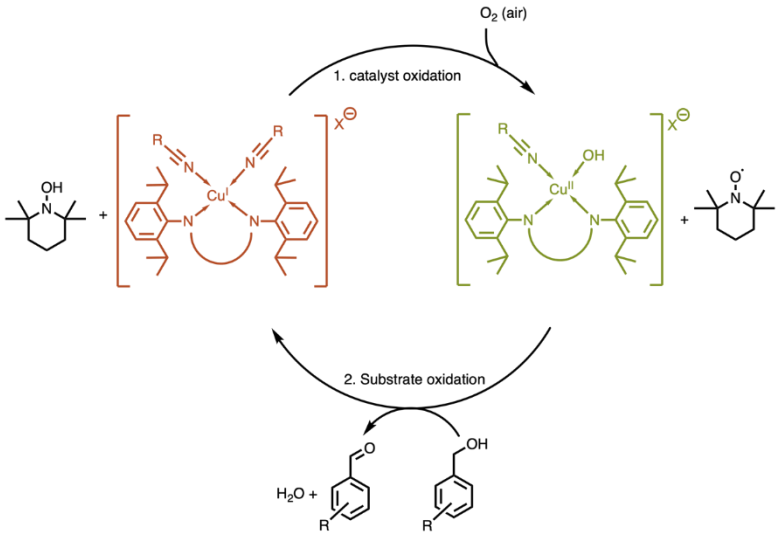

Figure 2.30. Simplified representation of the catalytic mechanism involving the oxidation of the benzyl alcohol via Cu^{I} complexes.

The experimental conditions remained constant, and only the reaction time was modified to determine which catalyst produces the aldehyde in the shortest time. The results are presented in **Table 2.2**.

All synthesised complexes exhibit activity in oxidizing this type of alcohols. However, in order to optimize the catalytic system's conditions, it was necessary to identify the most active compound. To do so, three separate experiments were carried out, each with the same quantity of additives and catalyst loading. The reactions were performed in 2h, 1h and 0.5h. The ideal complex would have the least impact on its activity. These results are shown in **Table 2.2.** By analysing the highlighted entries (**1**, **2**, **10**, **11**, **13** and **14**) it becomes apparent that all the complexes were able to complete the oxidation at the 2-hour mark. At 1-hour mark, differences between the complexes were observed, and it can be concluded that **C1**, **C3**, **C4** and **C5** exhibit higher activity. However, at the 0.5-hour mark, it is evident that complex **C3** experiences a more rapid decrease in activity compared to the other three complexes.

The most effective compound for this reaction is **C4** due to its higher activity in comparison to the other three complexes (entry **10**, **11** and **12** in **Table 2.2.**, respectively). Consequently, all studies on the catalytic system were conducted solely with this compound. The data analysis highlights that the reaction favours the OTf^- counter-ion as opposed to the BF_4^- (entry **10** and **16**, respectively, and entry **13** and **19**, respectively). A more adaptable backbone is preferable to a BIAN backbone as it restricts ligand adjustment around the metal centre due to its inflexible conformation (entries **3** and **10**). **C3**, **C4** and **C5** exhibit higher activity. However, at the 0.5-hour mark, it is evident that complex **C3** experiences a more rapid decrease in activity compared to the other three complexes.

The most effective compound for this reaction is **C4** due to its higher activity in comparison to the other three complexes (entry **10**, **11** and **12** in **Table 2.2.**, respectively). Consequently, all studies on the catalytic system were conducted solely with this compound. The data analysis highlights that the reaction favours the OTf^- counter-ion as opposed to the BF_4^- (entry **10** and **16**, respectively, and entry **13** and **19**, respectively). A more adaptable backbone is preferable to a BIAN backbone as it restricts ligand adjustment around the metal centre due to its inflexible conformation (entries **3** and **10**).

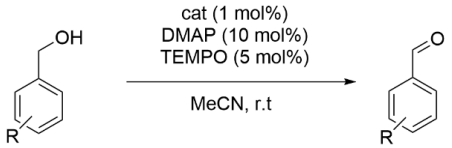

Table 2.2. Catalytic activities of complexes **C1-C9** in the oxidation reaction of benzyl alcohol into benzaldehyde and catalysts screening.

Entry	Cat.	Cat. Loading (mol %)	Time (h)	Conversion (%)
1	C1	1	0.5	79.5
2	C1	1	1	95.0
3	C1	1	2	>99
4	C2	1	0.5	66.5
5	C2	1	1	83.5
6	C2	1	2	>99
7	C3	1	0.5	52.0
8	C3	1	1	99.3
9	C3	1	2	>99
10	C4	1	0.5	89.5
11	C4	1	1	>99
12	C4	1	2	>99
13	C5	1	0.5	78.5
14	C5	1	1	>99
15	C5	1	2	>99
16	C6	1	0.5	63.3
17	C6	1	1	94.3
18	C6	1	2	>99
19	C7	1	0.5	50.4
20	C7	1	1	70.2
21	C7	1	2	82.9
22	C8	1	0.5	38.1
23	C8	1	1	52.9
24	C8	1	2	95.7
25	C9	1	0.5	30.7
26	C9	1	1	60.4
27	C9	1	2	92.2

General reaction conditions: benzylic alcohol (1.00 eq), DMAP (0.10 eq), TEMPO (0.05 eq) in 2 mL dry MeCN.

The reaction is favoured by the presence of an electron-withdrawing group, as evidenced by the superior results obtained with DAB results compared to DAD (entries **10** and **13**). **Table 2.2** highlights the impact of chelating solvents and indicates that acetonitrile promotes the reaction more effectively than benzonitrile (entries **1** and **10**, respectively, and entries **4** and **13**, respectively). Excess of acetonitrile present as the reaction solvent can justify this outcome. A further justification is that acetonitrile occupies less space, enabling the complex to adopt a better conformation during the reaction.

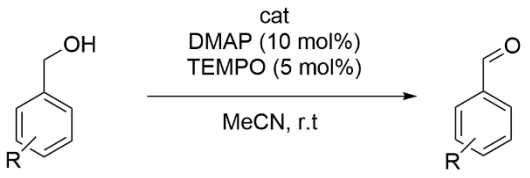

Table 2.3. Catalyst loading study of complexes **C1**, **C4** and **C5** in the oxidation reaction of benzyl alcohol into benzaldehyde.

Entry	Cat.	Cat. Loading (mol %)	Time (h)	Conversion (%)
28	C1	0.5	1	49.0
29	C1	0.5	2	83.8
30	C4	0.5	1	60.5
31	C4	0.5	2	91.3
32	C5	0.5	1	47.7
33	C5	0.5	2	89.0
34	C4	0.1	6	15.6
35	C4	0.1	16	30.8
36	C4	0.1	24	43.4

General procedure: benzylic alcohol (1.00 eq), DMAP (0.10 eq), TEMPO (0.05 eq) in 2 mL dry MeCN.

After testing several catalysts with 1 mol %, we decreased the loading to find the most effective one. The three best catalysts were studied at 0.5 mol % and the complex that maintained the highest conversion was further examined at 0.1 mol %. However, this resulted in a

significant decrease in conversion, leading us to the conclusion that the optimal catalyst loading for this reaction is 0.5 mol % in 2 hours. The results can be found in **Table 2.3**.

The solvent effect on the catalytic system was evaluated via multiple studies, testing THF, acetone, MeOH, AcOEt, toluene, DCM and acetonitrile. By maintaining uniform conditions, with only one observed solvent change between experiments, it was found that non-polar solvents (e.g. toluene) did not facilitate the desired reaction. Polar protic and aprotic solvents were also analysed to ascertain their effect on the outcome of the reaction. It was concluded that aprotic solvents promote the reaction more effectively than protic solvents such as MeOH. This rationale can be attributed to the by-product produced in the reaction (H_2O), which acts as a harmful agent to the reaction at higher concentrations. This was witnessed when dry MeCN was compared to bottled MeCN, resulting in a minor growth in conversion being noted in dry MeCN. The conversion rates show similarity among the aprotic solvents, except for MeCN. It is possible that the coordinating ability of MeCN affects the stability and activity of the catalytic active species, as illustrated in **Figure 2.31**.

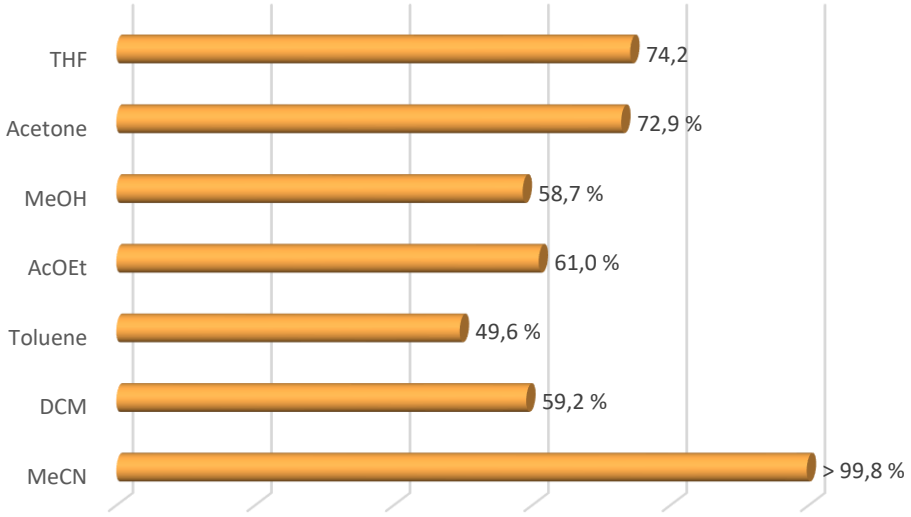

Figure 2.31. Scheme representing the results obtained for the oxidation reaction. **General Conditions**: benzyl alcohol (1 eq), **C4** (0.01 eq), DMAP (0.10 eq), TEMPO (0.05 eq), 1h, 1 mL of solvent at room temperature.

Regarding the use of solvent, the required volume was examined, i.e., the concentration of the catalytic system. Volumes of 2 mL, 1 mL, 0.5 mL and neat conditions (without solvent) were used for this purpose. Results are presented in **Table 2.4**. The optimal volume of

solvent was found to be 1mL due to the low solubility of the catalyst under neat conditions and the catalyst becoming too diluted at 2mL. Between 0.5 mL and 1 mL, there is no significant increase in activity, and the probability of the reactants not solubilizing is reduced.

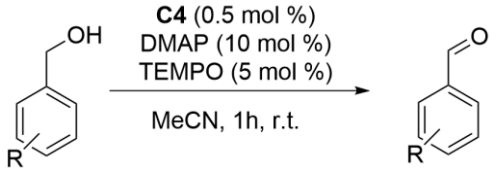

Table 2.4. Study regarding the influence of the concentration of the catalytic system in the conversion of benzyl alcohol to aldehyde.

Entry	Cat.	Cat Loading (mol %)	Volume (mL)	Conversion (%)
37	C4	0.5	0	55.7
38	C4	0.5	0.5	96.6
39	C4	0.5	1	94.2
40	C4	0.5	2	60.5

General Conditions: benzylic alcohol (1.00 eq), DMAP (0.10 eq), TEMPO (0.05 eq) in dry MeCN for 1h.

The study examines the impact of various quantities of base and co-catalyst. Specifically, tests were conducted on the base with no additive, at 1 mol% and at 10 mol%, and on the co-catalyst with no additive, and at 5 mol%, 7.5 mol%, and 10 mol%. This study was able to identify the minimum quantity necessary for a successful reaction under mild conditions, which consists of catalyst (1 mol%), TEMPO (5 mol%) and DMAP (10 mol%) in 1 mL of dry acetonitrile, to ensure total solubility of the catalyst. Our tests have determined the necessity of using each compound.

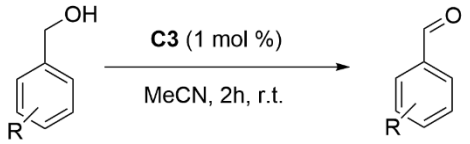

Table 2.5. Study of the required loading of the additives (TEMPO and DMAP) in the oxidation reaction of benzyl alcohol into benzaldehyde.

Entry	Cat.	TEMPO (mol %)	DMAP (mol %)	Conversion (%)
37	C3	0	10	49
38	C3	5	10	83.8
39	C3	7.5	10	60.5
40	C3	10	10	91.3
41	C3	5	0	47.7
42	C3	5	10	89

General conditions: benzylic alcohol (1.00 eq), **C3** (0.01 eq) in 2 mL dry MeCN for 2h.

The substrate scope of this reaction was expanded to include variously substituted benzylic, allylic and aliphatic alcohols (**Figure 2.32**). All alcohols were selectively oxidized to their corresponding aldehydes, demonstrating the chemoselective nature of the catalyst. Moreover, different substituents in the benzylic alcohols were found to affect the reaction development. It was determined that electron-withdrawing groups favour this chemical reaction, whereas electron-donating groups take longer to complete.

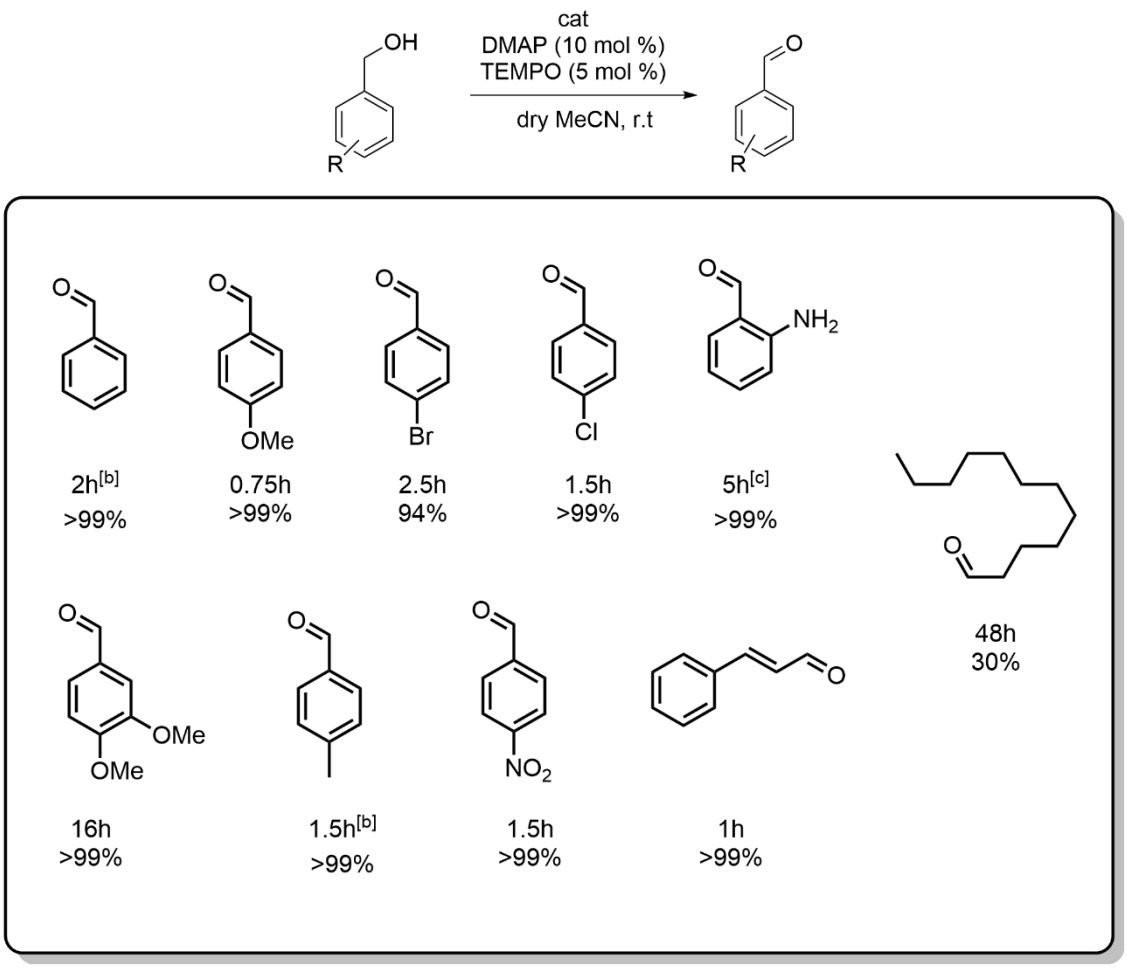

Figure 2.32. Substrate scope performed for the optimized catalytic system, representation with the respective reaction duration and conversion obtained. **General Conditions:** alcohol (1.00 eq), **C4** (1 mol %), DMAP (0.10 eq), TEMPO (0.05 eq) in dry 1 mL dry MeCN. **[b]**: alcohol (1.00 eq), **C4** (0.005 eq), DMAP (0.10 eq), TEMPO (0.05 eq) in dry 1 mL dry MeCN. **[c]**: alcohol (1.00 eq), **C4** (0.02 eq), DMAP (0.10 eq), TEMPO (0.05 eq) in dry 1 mL dry MeCN.

3

Conclusion and Future Perspectives

Two new families of copper(I) complexes given by $[Cu(RCN)_2DAB]X$ and $[Cu(RCN)_2DAD]X$ were successfully synthesised and characterized by known methodologies for the synthesis of this type of reaction and also Schlenk techniques. Most complexes were obtained by an equimolar quantity of the ligand and the copper salt, but two of the new complexes were obtained with two equivalents of the ligand and only one of the copper source. These complexes were obtained in good yields (70%-80%) and very pure. Some complexes were more difficult to obtain in the solid state due to the formation of an oil when the complexes were precipitated with dichloromethane and pentane to obtain crystals. Five different DAB complexes that differ in the counterion, the chelating solvent and the aryl's substitution were prepared. Three different DAD complexes (with different counterions and the chelating solvent), and one BIAN complex were also synthesised. All complexes were characterized by NMR, FTIR, UV/Vis and EA, and, when possible, by single-crystal X-ray crystallography.

All complexes were then tested to see their potential activity in the catalytic oxidation of benzyl alcohol to benzaldehyde, for which all of them were active. At any point on all the tests and analysis of the catalytic tests results, it found any evidence of the overoxidation of the alcohol function to acid. After a catalyst screening, it was concluded that the DAB complexes were in general more active than the others, that acetonitrile seems to favour more the reaction than benzonitrile and also that the triflate counterion increases the catalytic activity of the complex when compared to BF_4. The reason why is still not fully understood, but the study of

some hypothesis, higher solubility, ability of the counterion to coordinate and stabilize the reactional intermediate, are being currently undertaken. It was also studied the quantity of the additives (DMAP and TEMPO) and their necessity in the reaction. Different solvents were also studied, where the acetonitrile seem to be the one that mostly favoured the reaction. Curiously, the reaction can also be carried out in a MeOH medium, even though water is one of the reaction's by-products, and that the water concentration in MeOH is not irrelevant. This is in contrast with a previous Stahl study that showed that water can be an inhibitor depending on its concentration. It was also performed the substrate scope that allowed to see how the electron-withdrawing groups favoured the reaction more than the electron-donating ones.

For the future perspectives it is expected to increase the DAD and DAB complexes families and study how the changes in the aryl substituents would affect the catalytic system. It is also expected to study different nitroxyls or another radical initiators and bases that could turn the catalytic conditions more sustainable and maintain the activity. It is also expected to increase the substrate scope specially with pharmaceutical relevant aldehydes.

Finally, it would be important to carry out mechanistic studies to get a better idea of the electronic effects of the substituents on the substrates, i.e. the alcohols, but also to get a better idea of how the additives are favouring the reaction.

4

EXPERIMENTAL PROCEDURES

4.1 Chemicals and Solvents

All the alcohols used in the catalytic studies were commercially obtained from TCI, Alfa Aesar or Sigma Aldrich. The alcohols used were specifically benzyl alcohol, which was obtained through the Sigma Aldrich; 4-methylbenzyl alcohol, 4-chlorobenzyl alcohol, 4-methoxybenzyl alcohol, 4-bromobenzyl alcohol and 2-bromobenzyl alcohol, which were bought at Aldrich, and the 4-nitrobenzyl alcohol was obtained through TCI. When Schlenk techniques were performed, dry solvents were used through a distillation setup with the corresponding drying agent: sodium for diethyl ether and pentane; calcium hydride for acetonitrile and dichloromethane.

4.2 General experimental conditions

Thin-layer chromatography (TLC) was carried out using pre-coated aluminium sheets ALUGRAM® Xtra silica gel 60 with fluorescent indicator UV_{254} and were observed with 254 nm light.

The ^{13}C {^{1}H} NMR and 2D mononuclear and heteronuclear spectra were acquired using a Bruker Avance III 500, the ^{19}F {^{1}H} NMR spectra were acquired with a Bruker Avance III 400 spectrophotometer and the ^{1}H NMR spectra were acquired with both at 25 °C using either $CDCl_3$ or CD_2Cl_2 as deuterated solvent. Chemical shifts were reported in ppm at low field relative to TMS using the 7.26 ppm signal of $CDCl_3$ or 5.30 ppm signal of CD_2Cl_2 for the ^{1}H NMR spectra and 53.84 ppm signal of CD_2Cl_2 for the ^{13}C {^{1}H} NMR spectra. The signal multiplicities have been abbreviated as s (singlet), d (duplet), t (triplet), qt (quintuplet), sx (sextet), sept (septet), m (multiplet) and dd (duplet of duplet). The coupling constants given in the ^{1}H NMR spectra are $^{3}J_{HH}$. Signal assignments were confirmed by COSY, HSQC and HMBC. The

^{1}H NMR characterisation is shown as: chemical shift (multiplicity, [coupling constant], integration, attribution) in the ^{1}H NMR spectrum, and chemical shift (attribution) for the remaining spectra.

The FT-IR Spectrum Two (Perkin-Elmer) was used to acquire using the IR spectra in ATR mode without prior sample preparation. The intensity of the IR bands is classified as weak (w), medium (m) and strong (s).

The Varian Cary Bio spectrophotometer was used to acquire the UV/Vis spectra. Prior solutions of each compound were prepared with a concentration of 1 x 10^{-3} M in acetonitrile. The calibration line necessary for calculating the molar extinction coefficient is shown in **Figure A.7** to **A.11** and **Figure A.80** to **A.88** in **Annexes**. The characterization is described as: wavelength of the absorption maximum (molar extinction coefficient).

The crystal structures were determined using the X-ray crystallography service of small molecules provided by LAQV-REQUIMTE (DQ). The single crystals were chosen, coated with Fomblin oil, and arranged in a nylon loop. The data were obtained at a temperature of 110 (2) K using a Bruker D8 Venture diffractometer and a Photon II detector, equipped with an Oxford Cryosystems. The monochromatic radiation used was Mo-Kα (λ = 0,71073 Å). Crystal data and structure refinement for complexes **C3**, **C4** and **C7** are presented in **Table 4.1**. The crystals of **C3** were twinned and with low diffracting power. This led to low quality data and, consequently, a high R1.

Table 4.1. Crystal data and structure refinement for complexes **C3**, **C4** and **C7.**

	C3	**C4**	**C7**
Formula	$C_{42}H_{42}Cl_2CuF_3N_4O_3S$	$C_{34}H_{48}Cl_2CuF_3N_4O_3S$	$C_{31}H_{44}BCl_2CuF_4N_4$
M	874.29	784.26	693.95
λ (Å)	0.71073	0.71073	0.71073
T (K)	110(2)	110(2)	150(2)
crystal system	Monoclinic	Triclinic	Monoclinic
space group	$P2_1/c$	$P\bar{1}$	$P2_1/c$

Crystal description	Prism	Block	Prism
Crystal color	Bronze	Red	Black
a (Å)	16.948(6)	12.8820(16)	12.1217(14)
b (Å)	14.697(5)	12.8966(16)	16.7634(17)
c (Å)	19.107(7)	14.0920(17)	18.810(2)
α (deg)	90	64.205(4)	90
β (deg)	93.165(12)	84.955(4)	108.112(4)
γ (deg)	90	85.172(4)	90
V (Å3)	4752(3)	2097.0(5)	3632.9(7)
Z	4	2	4
ρ_{calc} (g cm^{-3})	1.222	1.242	1.269
μ (mm^{-1})	0.666	0.746	0.794
θ_{max} (deg)	22.781	25.681	25.681
total data	122339	81523	232851
unique data	6115	7943	6890
R_{int}	0.2542	0.2438	0.0740
R [I>3σ(I)]	0.2810	0.0937	0.0422
wR2	0.6896	0.2014	0.1263
Goodness of fit	0.949	1.040	1.085
ρ_{min}	-4.548	-0.780	-0.814
ρ_{max}	2.044	1.137	0.852

Synthesis and Characterization

4.2.1 General conditions for the ligands

General procedure A: To a solution of MeOH, it was added the 2,3-butanedione (1 eq) and the corresponding aniline (2 eq), after solubilization of the compounds, formic acid (2 mL) was added. The reaction was refluxed and stirred for 16h. At the end of the reaction, the solution was filtered under vacuum and washed with cold methanol. A yellow solid was obtained.

General procedure B: The 2,3-butanedione (1 eq), the corresponding aniline (2 eq) and *p*-toluenesulfonic acid (0.1 eq) were added to a solution of MeOH. The reaction was carried out for 24 hours at room temperature. At the end of the reaction, it was filtered with cold MeOH and the mother liquor was concentrated and hexane was added to precipitate a yellow compound corresponding to the desired diimine.

General procedure C: The corresponding aniline (2 eq) and formic acid were added to a solution of ^{i}PrOH. After cooling the reaction to 0 °C the 2,3-butanedione was added dropwise with vigorous stirring. The reaction was carried out at 0 °C and for 2.5 hours. The mixture was then filtered and washed with cold ^{i}PrOH. Giving a yellow solid, the mother liquor was stored at -18 °C to precipitate the remaining compound.

4.2.1.1 Synthesis and characterization of R1

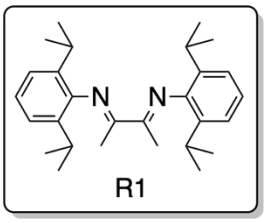

Following the **general procedure A**, the 2,3-butanedione (2.50 mL, 27.89 mmol, 1 eq), the 2,6-diisopropylaniline (12.44 mL, 59.34 mmol, 2 eq) and the formic acid (2 mL) were added to a solution of MeOH (46 mL). A yellow solid was obtained (7.59 g, η= 62%). The characterization agrees with the previously reported. [78]

^{1}H NMR (400 MHz, $CDCl_3$) δ (ppm): 7.21 – 7.06 (m, 6H), 2.72 (hept, *J* = 6.9 Hz, 4H), 2.07 (s, 6H), 1.32 – 1.10 (m, 24H).

IR ATR ν max (cm^{-1}): 1643 (C-N).

UV/Vis (MeCN) λ_{max} (nm) [ε (x 10^4 $M^{-1}.cm^{-1}$)]: 233 (2.38), 267 (1.27), 348 (0.60).

4.2.1.2 Synthesis and characterization of R2

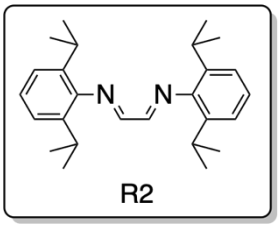

According to **general procedure A**, the diisopropylaniline (94.00 g, 530 mmol, 2 eq) was added to a solution of glyoxal 40 w/w% (30.29 mL, 265.11 mmol, 1 eq) and formic acid (244.3 mg, 5.30 mmol). The ligand was obtained after 48h stirring as a yellow powder (150g, η= 75 %). The NMR characterization agrees with the previously reported.[76]

^{1}H NMR (400 MHz, $CDCl_3$) δ (ppm): 8.11 (s, 2H), 7.25 – 7.02 (m, 6H), 2.94 (hept, *J* = 6.9 Hz, 4H), 1.25 – 1.04 (d, 24H).

IR ATR ν max (cm^{-1}): 1625 (C-N).

UV/Vis (MeCN) λ_{max} (nm) [ε (x 10^4 $M^{-1}.cm^{-1}$)]: 228 (1.67), 258 (5.51), 354 (1.42).

4.2.1.3 Synthesis and characterization of R3

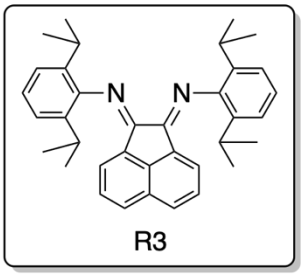

According to **general procedure A**, the acenaphthenequinone (2.7 g, 15.10 mmol, 1 eq) was added to methanol (120 mL), then the 2,6-diisopropylaniline (7.2 mL, 38.17 mmol, 2 eq), the formic acid (0.5 mL) and water (150 mL), and the ligand **R3** was obtained as an orange powder (5.71 g, η= 76 %) after being washed with diethyl ether. The NMR characterization agrees with the previously reported. [79]

^{1}H NMR (500 MHz, $CDCl_3$) δ (ppm): 7,87 (d, *J* = 8,3 Hz, 2H); 7,36 (t, *J* = 7,8 Hz, 2H); 7,31 – 7,22 (m, 6H); 6,64 (d, *J* = 7,2 Hz, 2H); 3,03 (sept, *J* = 7,0 Hz, 4H); 1,24 (d, *J* = 6,9 Hz, 12H); 0,97 (d, *J* = 6,9 Hz, 12H).

IR ATR ν max (cm^{-1}): 1667 (C-N)

UV/Vis (MeCN) λ_{max} (nm) [ε (x 10^4 $M^{-1}.cm^{-1}$)]: 229 (8.51), 253 (2.49), 278 (0.90), 312 (0.91).

4.2.1.4 Synthesis and characterization of R4

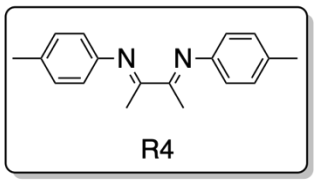

According to **general procedure B**, the 2,3-butanedione (0.41 mL, 4.51 mmol, 1 eq), the *p*-methylaniline (0.99 mL, 9.01 mmol, 2 eq) and the *p*-toluenosulfonic acid (77.61 mg, 0.45 mmol, 0.1 eq)

were added to a solution of MeOH (5 mL). The reaction was allowed to proceed for 24 hours at room temperature. A yellow solid was obtained (0.42 g, η= 70%). The characterization agrees with the previously reported.[78]

^{1}H NMR (400 MHz, $CDCl_3$) δ (ppm): 7.17 (d, *J* = 7.9 Hz, 2H), 6.74 – 6.66 (m, 2H), 2.36 (s, 3H), 2.15 (s, 3H).

IR ATR ν max (cm^{-1}): 1625 (C-N).

UV/Vis (MeCN) λ_{max} (nm) [ε (x 10^4 $M^{-1}.cm^{-1}$)]: 228 (3.06), 284 (0.22), 342 (0.39).

4.2.1.5 Synthesis and characterization of R5

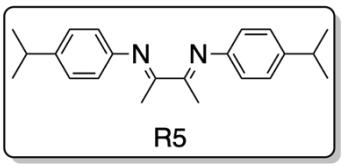

Following the **general procedure C**, it was added *p*-iso-propylaniline (1.54 mL, 11.05 mmol, 2 eq), the formic acid (0.15 mL) in a solution of ^{i}PrOH (6 mL) and the 2,3-butanedione (0.50 mL, 5.53 mmol, 1 eq) was added dropwise. A yellow compound was obtained (1.42 g, η= 80%).

^{1}H NMR (400 MHz, $CDCl_3$) δ (ppm): 7.23 (m, 4H), 6.72 (m, 4H), 2.99 – 2.84 (m, *J* = 6.7 Hz, 4H), 2.90 (m, 2H), 2.16 (s, 6H), 1.27 (dd, *J* = 7.0, 1.9 Hz, 12H).

IR ATR ν max (cm^{-1}): 1633 (C-N).

UV/Vis (MeCN) λ_{max} (nm) [ε (x 10^4 $M^{-1}.cm^{-1}$)]: 229 (3.42), 342 (0.43).

4.2.2 General Conditions for the salts

In this procedure, $Cu(X)_2$, where X corresponds to the counterions OTf^- or BF_4^-, and an excess of metallic copper, Cu^0, were added to a 100 mL round-bottomed flask and then approximately 20 mL of dried acetonitrile was added. The reaction was refluxed and stirred for 2-4 hours. The reaction has the peculiarity of changing colour, first blue, then green and finally is colourless. While the reaction remained hot, it was filtered into a Schlenk with a porous plate funnel containing silica and purged with argon. The reaction was then concentrated to half volume at 60 °C and stored at -18 °C where the compounds precipitated as white solids.

4.2.2.1 Synthesis of R6

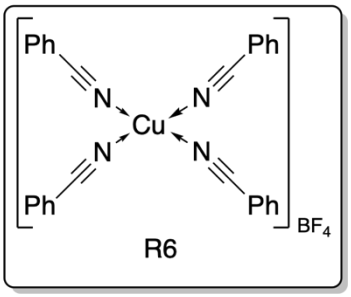

R6

Following the general procedure, $Cu(BF_4)_2$ (500.00 mg, 2.07 mmol, 1 eq) and Cu^0 (346.6 mg, 5.45 mmol, 2 eq) were added in about 20 mL of dried acetonitrile. The reaction was refluxed and stirred for 2 hours. A white powder was obtained yielding (1.32 g, η= 56%). [80]

4.2.2.2 Synthesis of R7

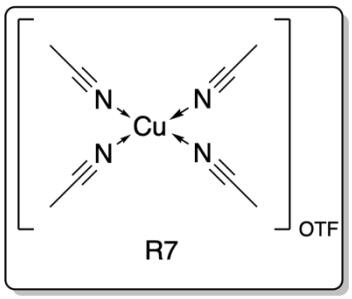

R7

Following the general procedure, $Cu(OTf)_2$ (201.60 mg, 0.948 mmol, 1 eq) and Cu^0 (124.60 mg, 1.96 mmol, 2 eq) were added, in about 5 mL of dried acetonitrile. The reaction was refluxed and stirred for 2 hours. The compound precipitated as a white powder (0.186 g, η= 52%). The compound obtained agrees with the previously described in the literature. [80]

4.2.2.3 Synthesis of R8

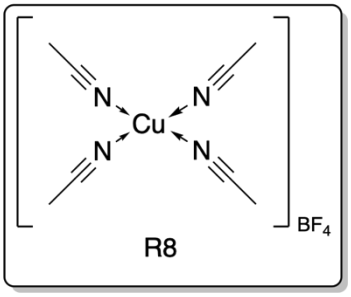

R8

Following the general procedure, $Cu(BF_4)_2$ (500.40 mg, 2.11 mmol, 1 eq) and Cu^0 (267.30, 4.21 mmol, 2 eq) were added to approximately 15 mL of dried acetonitrile. The reaction was refluxed and stirred for 4 hours. The compound precipitated as a white powder (0.325 g, η= 49 %). The compound obtained agrees with the previously described in literature. [80]

4.2.3 General Conditions for the complexes

To carry out this reaction the ligand **R1-R3** (1 eq or 2 eq when indicated) and the corresponding copper salt R4-R6 (1 eq), were prepared using Schlenk techniques and an argon atmosphere. Approximately 20 mL of previously dried dichloromethane was added, and the

reaction was stirred at room temperature for 16 hours. After filtrating to another Schlenk, pentane was added to obtain the precipitated compound.

4.2.3.1 Synthesis and characterization of C1

The ligand **R1** (302.00 mg, 0.75 mmol, 1 eq) and the copper salt **R4** (418.40, 0.75 mmol, 1 eq) were added to ca. 20 mL of dry dichloromethane and stirred for 16 hours. When pentane was added, the compound did not precipitate, so the solvent was evaporated, and the compound was left to dry under vacuum. A yield of 81% (460.00mg) was obtained.

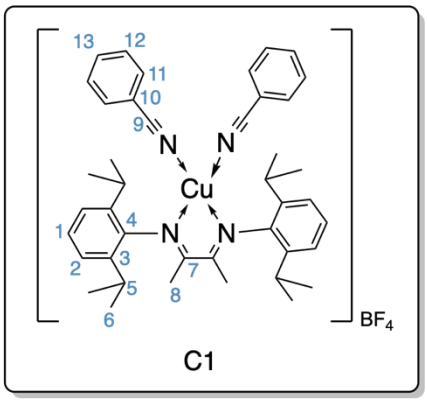

C1

^{1}H NMR (400 MHz, CD_2Cl_2) δ (ppm): 7.70 (t, *J* = 7.6 Hz, 2H, H13), 7.64 (d, *J* = 7.7 Hz, 4H, H11), 7.52 (dd, *J* = 7.7 Hz, 4H, H12), 7.33 (s, 6H; H1-H2), 2.82 (p, *J* = 6.8 Hz, 4H, H5), 2.26 (s, 6H, H8), 1.26 (dd, *J* = 16.0, 6.8 Hz, 24H, H6).

^{13}C {^{1}H} NMR (101 MHz, CD_2Cl_2) δ (ppm): 170.21, 142.92, 137.88, 134.48, 129.91, 127.24, 124.67, 117.29, 110.94, 29.00, 24.26, 23.65, 19.54.

^{19}F {^{1}H} NMR (376 MHz, CD_2Cl_2) δ (ppm): -153.52.

IR ATR ν max (cm^{-1}): 1643 (C-N), 1047 (BF_4).

Elemental Analysis (%) calculated for $C_{42}H_{50}BCuF_4N_4$: C, 66.27; H, 6.62; N, 7.36. Found: C, 66.79; H, 6.02, N, 7.68.

LC/MS (MeCN/H_2O) *m/z*: Positive mode: 508.3 [**R1**+CuMeCN]$^+$ (90%); 405.3 [**R1**+H]$^+$ (100%). Negative mode: 87.2 (100 %) [BF_4]$^-$.

UV/Vis (MeCN) λ_{max} (nm) [ε (x 10^4 $M^{-1}.cm^{-1}$)]: 231 (3.92), 268 (0.25), 276 (0.23), 347 (0.07).

4.2.3.2 Synthesis and characterization of C2

R2 (300.00 mg, 0.80 mmol, 1 eq) and **R4** (448.38 mg, 0.80 mmol, 1 eq) were added to ca. 20 mL of dried dichloromethane and stirred for 16 hours. When the solution was ready, it was transferred to a round-bottomed flask and was evaporated in a rotary evaporator, to give a brown oil was obtained which was washed with diethyl ether and stirred (3x), then filtrated in a porous-plate funnel. A reddish-brown compound was obtained, which was dried under vacuum to give 95% (496.00mg) yield.

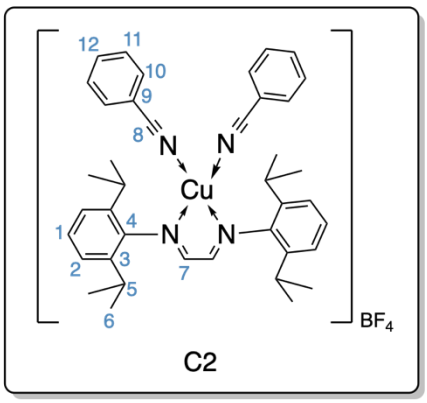

C2

^{1}H NMR (400 MHz, CD_2Cl_2) δ (ppm): 8.33 (s, 2H, H7), 7.74 (t, *J* = 7.6 Hz, 2H, H12), 7.64 (d, *J* = 7.7 Hz, 4H, H10), 7.54 (t, *J* = 7.8 Hz, 4H, H11), 7.32 (q, *J* = 5.1 Hz, 6H, H1-H2), 3.03 (h, *J* = 7.0 Hz, 4H, H5), 1.27 (d, *J* = 6.8 Hz, 24H, H6).

^{13}C {^{1}H} NMR (101 MHz, CD_2Cl_2) δ (ppm): 160.63 (C7), 145.30 (C3), 139.06 (C4), 135.02 (C12), 132.93 (C10), 130.10 (C11), 127.70 (C1), 124.34 (C2), 110.10 (C9), 28.75 (C5), 24.22 (C6).

^{19}F {^{1}H} NMR (376 MHz, CD_2Cl_2) δ (ppm): -153.29.

IR ATR ν max (cm^{-1}): 1635 (C-N), 1052 (BF_4).

Elemental Analysis (%) calculated for $C_{40}H_{46}BCuF_4N_4$,1/6CH_2Cl_2: C, 64.55; H, 6.25; N, 7.50. Found: C, 64.54; H, 6.30; N, 7.36.

LC/MS (MeCN/H_2O) *m/z*: Positive mode: 480.3 [**R2**+CuMeCN]$^+$ (90%); 377.3 [**R2**+H]$^+$ (25%). Negative mode: 87.1 (100 %) $[BF_4]^-$.

UV/Vis (MeCN) λ_{max} (nm) [ε (x 10^4 $M^{-1}.cm^{-1}$)]: 224 (5.83), 259 (0.85), 356 (0.19).

4.2.3.3 Synthesis and characterization of C3

The ligand **R3** (222.00 mg, 0.44 mmol, 1eq) and the copper salt **R5** (154.30 mg, 0.41 mmol, 1 eq) were added to ca. 20 mL of dried dichloromethane and stirred for 16 hours. When the reaction was complete, the reaction was filtrated, and pentane was added to precipitate the complex. Yield of 72% (206.70 mg).

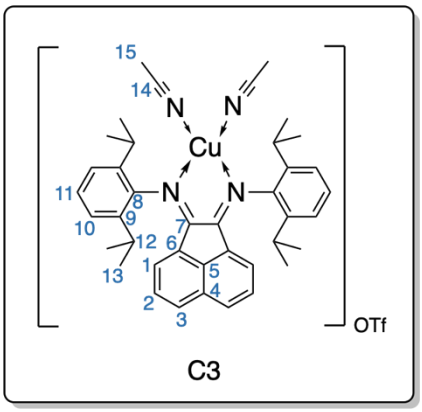

C3

^{1}H NMR (400 MHz, CD_2Cl_2) δ (ppm): 8.12 (d, *J* = 8.3 Hz, 2H), 7.56 – 7.39 (m, 2H), 6.75 (d, *J* = 7.3 Hz, 2H), 3.00 (m, *J* = 6.8 Hz, 4H), 2.15 (s, 6H), 1.30 (d, *J* = 7.0 Hz, 12H), 0.97 (d, *J* = 7.0 Hz, 12H).

^{13}C {^{1}H} NMR (101 MHz, CD_2Cl_2) δ (ppm): 165.00, 143.09, 142.80, 137.73, 131.50, 131.20, 128.78, 127.11, 126.67, 125.16, 124.57, 28.71, 23.67, 23.51, 2.30.

^{19}F {^{1}H} NMR (376 MHz, CD_2Cl_2) δ (ppm): -78.85.

Elemental Analysis (%) calculated for $C_{41}H_{46}CuF_3N_4O_3S$: C, 61.92; H, 5.83; N, 7.04; S, 4.03. Found: C, 61.92; H, 5.82; N, 6.99; S, 3.7

UV/Vis (MeCN) λ_{max} (nm) [ε (x 10^4 $M^{-1}.cm^{-1}$)]: 227 (6.73), 276 (0.63), 313 (0.65).

MALDI-TOF-MS (*m/z*, positive mode): 501.2 (100%) [*o,o'*-$iPr_2C_6H_3$-BIAN$^+$H]$^+$, 604.2 (52%) [Cu(*o,o'*- $iPr_2C_6H_3$-BIAN)(MeCN)]$^+$.

4.2.3.4 Synthesis and characterization of C4

The ligand **R1** (202.90 mg, 0.50 mmol, 1 eq) and the copper salt **R5** (186.25, 0.49 mmol, 1 eq) were stirred for 16 hours in about 20 mL of dried dichloromethane. At the end of the reaction, the mixture was filtered, and pentane was added. The complex precipitated as a brown solid. Yield 70% (196.00mg).

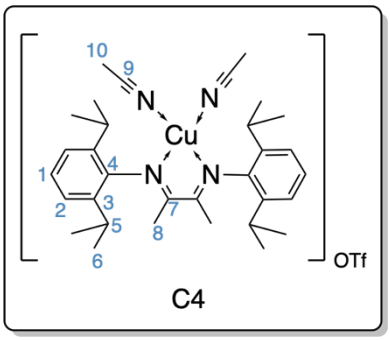

C4

^{1}H NMR (400 MHz, CD_2Cl_2) δ (ppm): 7.30 (s, 5H, H1-H2), 2.70 (hept, *J* = 7.0 Hz, 4H, H5), 2.21 (s, 6H, H8), 2.06 (s, 6H, H10), 1.23 (dd, *J* = 8.9, 6.9 Hz, 24H, H6).

^{13}C NMR (101 MHz, CD_2Cl_2) δ (ppm): 169.67 (C7), 142.41 (C4), 137.24 (C3), 126.78 (C2), 124.19 (C1), 29.58 (C5), 23.59 (C6), 23.04 (C9), 18.95 (C8), 2.23 (C10).

^{19}F {^{1}H} NMR (376 MHz, CD_2Cl_2) δ (ppm): -77.90.

IR ATR ν max (cm^{-1}): 2273 (MeCN), 1639 (CN), 1261 (CF_3), 1142 (S=O), 1030 (C-F), 637 (CF_3).

UV/Vis (MeCN) λ_{max} (nm) [ε (x 10^4 $M^{-1}.cm^{-1}$)]: 230 (3.51), 273 (0.19), 343 (0.10).

4.2.3.5 Synthesis and characterization of C5

The ligand **R2** (256.00 mg, 0,68 mmol, 1eq) and the copper salt **R5** (194.60 mg, 0.52 mmol, 1 eq), were stirred for 16 hours in about 20 mL of dried dichloromethane. At the end of the reaction, pentane was added, but the compound did not precipitate so it was stored at -18 °C and, after the complex precipitated a filtration was performed. A brown solid was obtained as the complex, yielding 70% (250.00 mg).

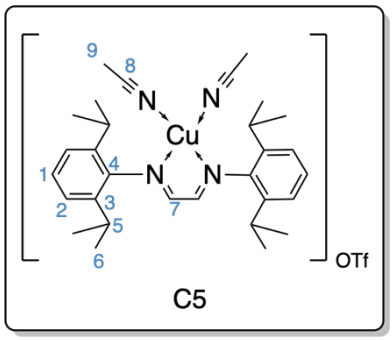

C5

^{1}H NMR (400 MHz, CD_2Cl_2) δ (ppm): 8.20 (s, 2H, H7), 7.36 – 7.24 (m, 6H, H1-H2), 2.92 (hept, *J* = 6.8 Hz, 4H, H5), 2.09 (s, 6H, H9), 1.24 (d, *J* = 6.8 Hz, 24H, H6).

^{13}C NMR (101 MHz, CD_2Cl_2) δ (ppm): 159.71 (C7), 145.38 (C4), 138.94 (C3), 127.51 (C1), 124.23 (C2), 28.58 (C5), 24.10 (C6), 2.63 (C9).

^{19}F {^{1}H} NMR (376 MHz, CD_2Cl_2) δ (ppm): -78.75.

IR ATR ν max (cm^{-1}): 2272 (MeCN), 1633 (C-N), 1260 (CF_3), 1141 (S=O), 1031 (C-F), 636 (CF_3).

UV/Vis (MeCN) λ_{max} (nm) [ε (x 10^4 $M^{-1}.cm^{-1}$)]: 232 (2.49), 257 (0.79), 359 (0.19).

4.2.3.6 Synthesis and characterization of C6

After adding the ligand **R1** (102.00 mg, 0.32 mmol, 1 eq) and the copper salt **R8** (129.1 mg, 0.32 mmol, 1 eq), they were stirred together in nearly 20 mL of anhydrous dichloromethane for 16 hours. The reaction was completed by adding pentane at the end, and the complex precipitated as a brown solid, producing a yield of 78% (138.60 mg).

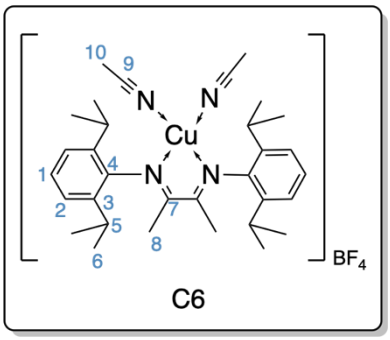

C6

^{1}H NMR (400 MHz, CD_2Cl_2) δ (ppm): 7.30 (s, 6H, H1-H2), 2.71 (hept, *J* = 7.0 Hz, 4H, H5), 2.20 (s, 6H, H8), 2.06 (s, 6H, H10), 1.22 (dd, *J* = 12.2, 6.8 Hz, 24H, H6).

^{13}C NMR (101 MHz, CD_2Cl_2) δ (ppm): 169.87 (C7), 142.83 (C4), 137.74 (C3), 127.14 (C1), 124.59 (C2), 28.90 (C5), 24.03, 23.56 (C6), 19.37 (C8), 2.88 (C10).

^{19}F {^{1}H} NMR (376 MHz, CD_2Cl_2) δ (ppm): -153.12.

IR ATR ν max (cm^{-1}): 1641 (C-N), 1030 (BF_4).

Elemental Analysis (%) calculated for $C_{32}H_{46}BCuF_4N_4.1/4CH_2Cl_2$: C, 58.84; H, 7.12;; N, 8.51. Found: C, 58.72; H, 7.17; N, 8.06.

LC/MS (MeCN/H_2O) *m/z*: Positive mode: 508.3 [**R1**+CuMeCN]$^+$ (90%); 405.3 [**R1**+H]$^+$ (100%). Negative mode: 87.2 (100 %) $[BF_4]^-$.

UV/Vis (MeCN) λ_{max} (nm) [ε (x 10^4 $M^{-1}.cm^{-1}$)]: 236 (2.20), 273 (1.56), 339 (0.91).

4.2.3.7 Synthesis and characterization of C7

The ligand **R2** (171.40 mg, 0.54 mmol, 1 eq) and the copper salt **R8** (203.70 mg, 0.54 mmol, 1 eq) were combined and stirred in ca 20 mL of anhydrous dichloromethane for 16 hours. Pentane was added at the completion of the reaction, and the complex was precipitated as a brown solid with a yield of 75% (250.00 mg).

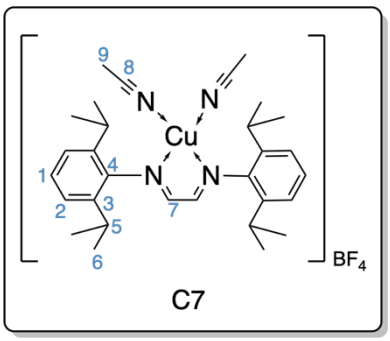

C7

^{1}H NMR (400 MHz, CD_2Cl_2) δ (ppm): 8.19 (s, 2H, H7), 7.28 (q, *J* = 5.1 Hz, 6H, H1-H2), 2.88 (hept, *J* = 6.9 Hz, 4H, H5), 2.12 (s, 6H, H9), 1.23 (d, *J* = 6.8 Hz, 24H, H6).

^{13}C NMR (101 MHz, CD_2Cl_2) δ (ppm): 159.69 (C7), 145.28 (C4), 138.96 (C3), 127.50 (C1), 124.23 (C2), 28.55 (C5), 24.13 (C6), 2.56 (C9).

^{19}F {^{1}H} NMR (376 MHz, CD_2Cl_2) δ (ppm): -152.99.

IR ATR ν max (cm^{-1}): 2275 (MeCN), 1633 (C-N), 1052 (BF_4).

UV/Vis (MeCN) λ_{max} (nm) [ε (x 10^4 $M^{-1}.cm^{-1}$)]: 233 (1.84), 255 (0.65), 358 (0.15).

4.2.3.8 Synthesis and characterization of C8

The ligand **R4** (200.00 mg, 0.76 mmol, 2 eq) and the copper salt **R5** (142.53 mg, 0.38 mmol, 1 eq) were combined and stirred in ca 20 mL of anhydrous dichloromethane for 16 hours. Pentane was added at the completion of the reaction, and the complex was precipitated as a dark rose oil, which was treated with diethyl ether and liquid nitrogen to obtain a dark brown solid with a yield of 75% (210.60 mg).

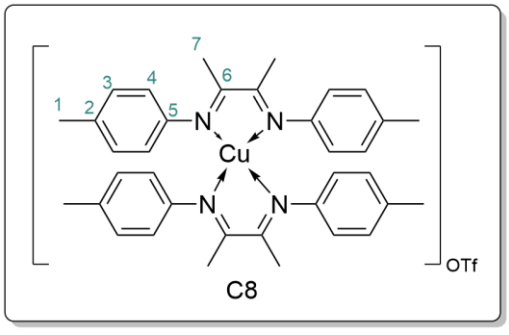

C8

^{1}H NMR (400 MHz, CD_2Cl_2) δ (ppm): 7.21 (d, *J* = 8.0 Hz, 4H, H4), 6.64 – 6.57 (m, 4H, H3), 2.39 (s, 6H, H1), 2.10 (s, 6H, H7).

^{13}C NMR (101 MHz, CD_2Cl_2) δ (ppm): 167.23 (C6), 145.47 (C2), 137.05 (C5), 130.40 (C4), 121.19 (C3), 21.13 (C1), 18.66 (C7).

^{19}F {^{1}H} NMR (376 MHz, CD_2Cl_2) δ (ppm): -78.88.

IR ATR ν max (cm^{-1}): 1623 (C=N), 1261 (CF_3, s), 1154 (S=O), 1030 (C-F), 636 (CF_3, b).

Elemental Analysis calculated for $C_{37}H_{40}CuF_3N_4O_3S$: C, 59.95; H, 5.44; Cu, 8.57; F, 7.69; N, 7.56; O, 6.47; S, 4.32. Found: C, 60.09; H, 5.50; N, 7.68; S, 4.07.

LC/MS (MeCN/H_2O) *m/z*: Positive mode: 591.2 [**C8**-OTf]$^+$ (100%); 368.0 [**R4**+$CuCH_3CN$]$^+$ (14%); 265.1 [**R4**+H]$^+$ (75%). Negative mode: 148.9 (100 %) [CF_3SO_3]$^-$.

UV/Vis (MeCN) λ_{max} (nm) [ε (x 10^4 $M^{-1}.cm^{-1}$)]: 229 (6.8), 284 (0.5), 340 (0.8).

4.2.3.9 Synthesis and characterization of C9

The ligand **R2** (200.00 mg, 0.62 mmol, 2 eq) and the copper salt **R5** (117.58 mg, 0.31 mmol, 1 eq) were combined and stirred in ca 20 mL of anhydrous dichloromethane for 16 hours. Pentane was added at the completion of the reaction, and the complex was precipitated as a black oil which was treated with diethyl ether and liquid nitrogen and the compound precipitated as a brown solid with a yield of 75% (204.10 mg).

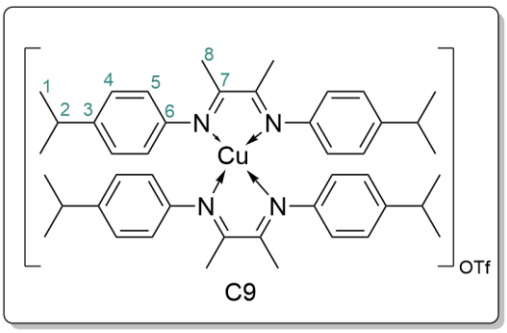

C9

^{1}H NMR (400 MHz, CD_2Cl_2) δ (ppm): 7.26 – 7.19 (m, 4H, H5), 6.59 (dd, *J* = 8.2, 1.9 Hz, 4H, H4), 2.96 (p, *J* = 6.9 Hz, 2H, H2), 2.12 (d, *J* = 1.8 Hz, 6H, H8), 1.29 (dd, *J* = 6.9, 1.8 Hz, 12H, H1).

^{13}C NMR (101 MHz, CD_2Cl_2) δ (ppm): -167.01 (C7), 148.03 (C1), 145.62 (C4), 127.77 (C2), 121.43 (C3), 34.15 (C5), 24.15 (C6), 18.74 (C8).

^{19}F {^{1}H} NMR (376 MHz, CD_2Cl_2) δ (ppm): -76.24.

IR ATR ν max (cm^{-1}): 1620 (C=N), 1261 (CF_3, s), 1154 (S=O), 1030 (C-F), 636 (CF_3, b).

Elemental Analysis (%) calculated for $C_{45}H_{56}CuF_3N_4O_3S.2/3CH_2Cl_2$: C, 60.26; H, 6.35; N, 6.16; S, 3.52. Found: C, 60.09; H, 5.50; N, 7.68; S, 4.07.

LC/MS (MeCN/H_2O) *m/z*: Positive mode: 703.3 [**C9**-OTf]$^+$ (100%); 424.1 [**R5**+$CuCH_3CN$]$^+$ (20%); 321.2 [**R5**+H]$^+$ (62%). Negative mode: 149.0 (100 %) [CF_3SO_3]$^-$.

UV/Vis (MeCN) λ_{max} (nm) [ε (x 10^4 $M^{-1}.cm^{-1}$)]: 231 (7.2), 336 (0.8).

4.3 Catalytic studies

General procedure: The flask was charged with alcohol, TEMPO (5 mol%), catalyst (1 mol%) and MeCN (1 mL) as the solvent. The reaction was initiated by adding DMAP (10 mol%) and a colour change was observed (yellow to orange or brown to red for the BIAN complex case). When the reaction was complete the solution presented a green colour. After the reaction time has elapsed, the procedure involved two different work ups. One involved filtering through silica gel with an eluent mixture of pentane/ diethyl ether (1:1), followed by drying the compound under vacuum (**option A**). The other possible work up involved a liquid-liquid extraction with water and pentanes, then washing with a brine solution and drying the organic layers with Na_2SO_4, and drying the solvents under vacuum (**option B**).

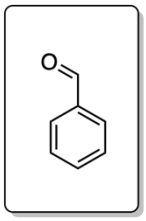

The alcohol (0.1 mL, 0.96 mmol, 1 eq), the **C4** (3.36 mg, 0.004 mmol, 0.005 eq), the TEMPO (7.56 mg, 0.048 mmol, 0.05 eq) were added to a solution of 1 mL of dry MeCN, then it was added the DMAP (11.75 mg, 0.096 mmol, 0.10 eq). The mixture was treated according to **option B**, and a yellow oil was obtained with quantitative yield.

^{1}H NMR (400 MHz, $CDCl_3$) δ (ppm): 10.04 (s, 1H), 7.90 (d, 2H), 7.64 (t, 1H), 7.55 (dd, *J* = 8.3, 6.9 Hz, 2H).

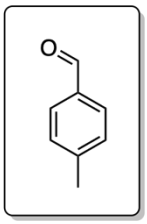

The alcohol (100 mg, 0.82 mmol, 1 eq), the **C4** (2.85 mg, 0.004 mmol, 0.005 eq), the TEMPO (6.44 mg, 0.041 mmol, 0.05 eq) were added to a solution of 1 mL of dry MeCN, then it was added the DMAP (10.00 mg, 0.082 mmol, 0.10 eq). The mixture was treated according to **option A**, and a yellow oil was obtained with quantitative yield.

^{1}H NMR (400 MHz, $CDCl_3$) δ (ppm): 9.98 (s, 1H), 7.80 (d, 2H), 7.35 (d, *J* = 7.8 Hz, 2H), 2.46 (s, 3H).

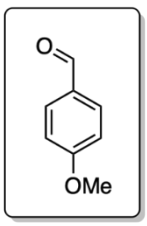

The alcohol (100 mg, 0.72 mmol, 1 eq), the **C4** (5.06 mg, 0.007 mmol, 0.01 eq), the TEMPO (5.69 mg, 0.036 mmol, 0.05 eq) were added to a solution of 1 mL of dry MeCN, then it was added the DMAP (8.84 mg, 0.072 mmol, 0.10 eq). The mixture was treated according to **option A**, and a yellow oil was obtained yielding 87%.

^{1}H NMR (400 MHz, $CDCl_3$) δ (ppm): 9.90 (s, 1H), 7.86 (d, 2H), 7.02 (d, 2H), 3.91 (s, 3H).

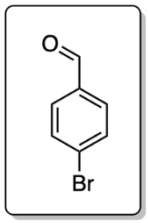

The alcohol (100 mg, 0.53 mmol, 1 eq), the **C4** (3.74 mg, 0.005 mmol, 0.01 eq), the TEMPO (4.20 mg, 0.026 mmol, 0.05 eq) were added to a solution of 1 mL of dry MeCN, then it was added the DMAP (6.53 mg, 0.053 mmol, 0.10 eq). The mixture was treated according to **option B**, and a white powder was obtained yielding 94%.

^{1}H NMR (400 MHz, $CDCl_3$) δ (ppm): 9.99 (s, 1H), 7.77 (d, 2H), 7.70 (d, *J* = 8.5 Hz, 2H).

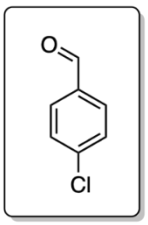

The alcohol (100 mg, 0.70 mmol, 1 eq), the **C3** (5.58 mg, 0.007 mmol, 0.01 eq), the TEMPO (5.51 mg, 0.035 mmol, 0.05 eq) were added to a solution of 1 mL of dry MeCN, then it was added the DMAP (8.57 mg, 0.070 mmol, 0.10 eq). The mixture was treated according to **option A**, and a yellow powder was obtained yielding 87%.

^{1}H NMR (400 MHz, $CDCl_3$) δ (ppm): 9.99 (s, 1H), 7.83 (d, 2H), 7.53 (d, 2H).

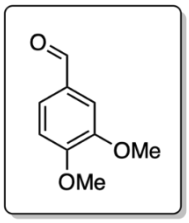

The alcohol (0.1 mL, 0.68 mmol, 1 eq), the **C4** (4.81 mg, 0.007 mmol, 0.01 eq), the TEMPO (5.41 mg, 0.034 mmol, 0.05 eq) were added to a solution of 1 mL of dry MeCN, then it was added the DMAP (8.40 mg, 0.069 mmol, 0.10 eq). The mixture was treated according to **option A**, and a yellow solid was obtained with a quantitative yield.

^{1}H NMR (400 MHz, $CDCl_3$) δ (ppm): 9.87 (s, 1H), 7.47 (dd, *J* = 8.2, 1.9 Hz, 1H), 7.43 (d, *J* = 1.9 Hz, 1H), 6.99 (d, *J* = 8.2 Hz, 1H), 3.97 (d, *J* = 9.2 Hz, 6H).

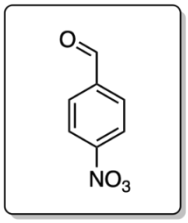

The alcohol (100.40 mg, 0.59 mmol, 1 eq), the **C4** (4.70 mg, 0.006 mmol, 0.01 eq), the TEMPO (5.20 mg, 0.033 mmol, 0.05 eq) were added to a solution of 1 mL of dry MeCN, then it was added the DMAP (7.90 mg, 0.065 mmol, 0.10 eq). The mixture was treated according to **option A**, and a yellow solid was obtained with a quantitative yield.

^{1}H NMR (400 MHz, $CDCl_3$) δ (ppm): 10.17 (s, 1H), 8.41 (d, 2H), 8.08 (d, 2H).

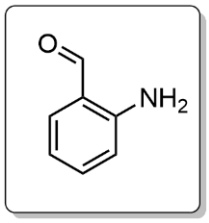

The alcohol (100.00 mg, 0.81 mmol, 1 eq), the **C4** (11.36 mg, 0.016 mmol, 0.02 eq), the TEMPO (6.38 mg, 0.041 mmol, 0.05 eq) were added to a solution of 1 mL of dry MeCN, then it was added the DMAP (9.92 mg, 0.081 mmol, 0.10 eq). The mixture was treated according to **option A**, and a yellow solid was obtained with a quantitative yield.

^{1}H NMR (400 MHz, $CDCl_3$) δ (ppm): 9.89 (s, 1H), 7.50 (dd, *J* = 7.7, 1.6 Hz, 1H), 7.33 (ddd, *J* = 8.5, 7.1, 1.6 Hz, 1H), 6.81 – 6.71 (m, 1H), 6.66 (d, *J* = 8.3 Hz, 1H).

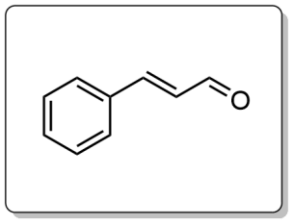

The alcohol (100.00 mg, 0.75 mmol, 1 eq), the **C4** (5.21 mg, 0.007 mmol, 0.01 eq), the TEMPO (5.86 mg, 0.037 mmol, 0.05 eq) were added to a solution of 1 mL of dry MeCN, then it was added the DMAP (9.11 mg, 0.074 mmol, 0.10 eq). The mixture was treated according to **option A**, and a yellow oil was obtained with a 99% yield.

^{1}H NMR (400 MHz, $CDCl_3$) δ (ppm): 9.73 (d, *J* = 7.7 Hz, 1H), 7.62 – 7.55 (m, 2H), 7.52 (s, 1H), 7.49 – 7.42 (m, 2H), 6.74 (dd, *J* = 16.0, 7.7 Hz, 1H).

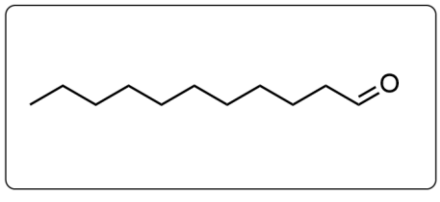

The alcohol (100.00 mg, 0.53 mmol, 1 eq), the **C4** (7.48 mg, 0.011 mmol, 0.01 eq), the TEMPO (4.20 mg, 0.027 mmol, 0.05 eq) were added to a solution of 1 mL of dry MeCN, then it was added the DMAP (6.53 mg, 0.053 mmol, 0.10 eq). The mixture was treated according to **option A**, and a yellow oil was obtained with a quantitative yield.

^{1}H NMR (400 MHz, $CDCl_3$) δ (ppm): 9.77 (q, J = 2.0 Hz, 1H), 3.64 (t, J = 6.6 Hz, 5H), 2.42 (td, J = 7.4, 1.9 Hz, 2H), 1.69 – 1.51 (m, 8H), 1.39 – 1.26 (m, 72H), 0.88 (t, J = 6.7 Hz, 11H).

BIBLIOGRAPHY

[1] G. Tojo, M. Fernández, Oxidation of Alcohols to Aldehydes and Ketones, USA, 2006.

[2] T. Mallat, A. Baiker, Oxidation of alcohols with molecular oxygen on solid catalysts, Chem. Rev. 104 (2004) 3037–3058. https://doi.org/10.1021/cr0200116.

[3] R.A. Sheldon, I.W.C.E. Arends, A. Dijksman, New developments in catalytic alcohol oxidations for fine chemicals synthesis, Catal. Today. 57 (2000) 157–166. https://doi.org/10.1016/S0920-5861(99)00317-X

[4] S.E. Allen, R.R. Walvoord, R. Padilla-Salinas, Aerobic copper-catalyzed organic reactions, Chem. Rev. 113 (2013) 6234–6458. https://doi.org/10.1021/cr300527g.

[5] M. Trincado, D. Banerjee, H. Grützmacher, Molecular catalysts for hydrogen production from alcohols, Energy Environ. Sci. 7 (2014) 2464–2503. https://doi.org/10.1039/c4ee00389f.

[6] A.M. Bonastre, Catalysts for alcohol-fuelled direct oxidation fuel cells, Platin Met. Rev. 57 (2013) 297–301. https://doi.org/10.1595/147106713X671871.

[7] J.M. Lü, P.H. Lin, Q. Yao, Chemical and molecular mechanisms of antioxidants: Experimental approaches and model systems, J. Cell. Mol. Med. 14 (2010) 840–860. https://doi.org/10.1111/j.1582-4934.2009.00897.x.

[8] G.Y. Lai, High-temperature corrosion and materials applications, ASM International, 2007.

[9] T.M. Aminabhavi, R.H. Balundgi, P.E. Cassidy, A reviewed on biodegradable plastics, Polym. Plast. Technol. Eng. 29 (1990) 235–262. https://doi.org/10.1080/03602559008049843.

[10] K. V. Radha, V. Sridevi, K. Kalaivani, Electrochemical oxidation for the treatment of textile industry wastewater, Bioresour. Technol. 100 (2009) 987–990. https://doi.org/10.1016/j.biortech.2008.06.048.

[11] D. Hermosilla, N. Merayo, A. Gascó, The application of advanced oxidation technologies to the treatment of effluents from the pulp and paper industry: A review, Environmental Science and Pollution Research. 22 (2014) 168–191. https://doi.org/10.1007/s11356-014-3516-1.

[12] J.F. Corbett, An historical review of the use of dye precursors in the formulation of commercial oxidation hair dyes, Dyes and Pigments. 41 (1998) 127–136. https://doi.org/10.1016/S0143-7208(98)00075-8.

[13] S. Caron, R.W. Dugger, S.G. Ruggeri, Large-scale oxidations in the pharmaceutical industry, Chem Rev. 106 (2006) 2943–2989. https://doi.org/10.1021/cr040679f.

[14] J.M. Hoover, J.E. Steves, S.S. Stahl, Copper(I)/tempo-catalyzed aerobic oxidation of primary alcohols to aldehydes with ambient air, Nat. Protoc. 7 (2012) 1161–1166. https://doi.org/10.1038/nprot.2012.057.

[15] S.F. Martin, Recent applications of imines as key intermediates in the synthesis of alkaloids and novel nitrogen heterocycles, Pure and Applied Chemistry. 81 (2009) 195–204. https://doi.org/10.1351/PAC-CON-08-07-03.

[16] S.H. Pines, The merck bile acid cortisone process: The next-to-last word, Org. Process Res. Dev. 8 (2004) 708–724. https://doi.org/10.1021/op030050z.

[17] A.J. Mancuso, S.-L. Huang, Oxidation of Long-chain and Related Alcohols to Carbonyls by Dimethyl Sulfoxide "Activated" by Oxalyl Chloride, J. Org. Chem. 43 (1978) 2480–2482. https://doi.org/10.1021/jo00406a041

[18] F.G. Fang, D.D. Bankston, Convergent Catalytic Asymmetric Synthesis of Camptothecin Analog GI147211C1, Tetrahedron. 53 (1997) 10953–10970. https://doi.org/10.1016/S0040-4020(97)00357-8

[19] S.J. Wittenberger, A. Tasker, 2-butyl-4-iodoimidazole-5-carboxaldehyde: A versatile intermediate for the synthesis of highly functionalized 1midazoles, Synth. Commun. 23 (1993) 3231–3248. https://doi.org/10.1080/00397919308011184.

[20] M.J. Martinelli, Asymmetric Diels-Alder Reactions with y-Functionalized α,β-Unsaturated Chiral N-Acyloxazolidinones: Synthesis of (+) -EL145, J. Org. Chem. 55 (1990) 5065–5073. https://doi.org/10.1021/jo00304a019

[21] J.R. Parikh, W. von E. Doering, Sulfur Trioxide in the Oxidation of Alcohols by Dimethyl Sulfoxide, J. Am. Chem. Soc. 89 (1967) 5505–5507. https://doi.org/10.1021/ja00997a067.

[22] C. Liu, J.S. Ng, J.R. Behling, C.H. Yen, Development of a Large-Scale Process for an HIV Protease Inhibitor, Org. Process. Res. Dev. 1 (1997) 45–54. https://doi.org/10.1021/op960040g.

[23] A.E.J. de Nooy, A.C. Besemer, H. van Bekkum, On the Use of Stable Organic Nitroxyl Radicals for the Oxidation of Primary and Secondary Alcohols, Synthesis. (1996) 1153–1174.

[24] M. F. Semmelhack, C. S. Chou, D. A. Cortes, Nitroxyl-mediated electrooxidation of alcohols to aldehydes and ketones, J. Am. Chem. Soc. 105 (2002) 4492–4494. https://doi.org/10.1021/ja00351a070.

[25] Y. Lu, R. Zhang, B. Cao, Elucidating the Copper-Hägg Iron Carbide Synergistic Interactions for Selective CO Hydrogenation to Higher Alcohols, ACS Catal. 7 (2017) 5500–5512. https://doi.org/10.1021/acscatal.7b01469.

[26] E.C. Blanco, A. Sánchez, M. Martín, Methanol and ammonia as emerging green fuels: Evaluation of a new power generation paradigm, Renew. Sustain. Energy Revs. 175 (2023). https://doi.org/10.1016/j.rser.2023.113195.

[27] A. Conde, L. Vilella, D. Balcells, Introducing copper as catalyst for oxidative alkane dehydrogenation, J. Am. Chem. Soc. 135 (2013) 3887–3896. https://doi.org/10.1021/ja310866k.

[28] S.G. Agalave, S.R. Maujan, V.S. Pore, Click chemistry: 1,2,3-triazoles as pharmacophores, Chem. Asian J. 6 (2011) 2696–2718. https://doi.org/10.1002/asia.201100432.

[29] Y. Chen, Y. Liu, F. Wang, Toward practical photoelectrochemical water splitting and CO2 reduction using earth-abundant materials, J. Energy Chem. 61 (2021) 469–488. https://doi.org/10.1016/j.jechem.2021.02.003.

[30] J. Humphreys, R. Lan, S. Tao, Development and Recent Progress on Ammonia Synthesis Catalysts for Haber–Bosch Process, Adv. Energy Sustainability Res. 2 (2021) 2000043. https://doi.org/10.1002/aesr.202000043.

[31] S.A. Al-Saydeh, M.H. El-Naas, S.J. Zaidi, Copper removal from industrial wastewater: A comprehensive review, J. Ind. Eng. Chem. 56 (2017) 35–44. https://doi.org/10.1016/j.jiec.2017.07.026.

[32] E.J. Van Genderen, A.C. Ryan, J.R. Tomasso, S.J. Klaine, Evaluation of Acute Copper Toxicity to Fathead Minnows (Pimephales Promelas) in Soft Surface Waters, Environ. Toxicol. Chem. 24 (2005) 408–414. http://www.epa.gov/.

[33] P. Szakálos, G. Hultquist, G. Wikmark, Corrosion of copper by water, Electrochem. Solid-State Lett. 10 (2007) 63–67. https://doi.org/10.1149/1.2772085.

[34] W. Brackman, C.J. Gaasbeek, Studies in Homogeneous Catalysis, RECUEL. 85 (1966) 221–241.

[35] M.F. Semmelhack, C.R. Schmid, D.A. Cortés, C.S. Chou, Oxidation of Alcohols to Aldehydes with Oxygen and Cupric Ion, Mediated by Nitrosonium Ion, J. Am. Chem. Soc. 106 (1984) 3374–3376. https://doi.org/10.1021/ja00323a064.

[36] I.E. Markó, P.R. Giles, M. Tsukazaki, S.M. Brown, C.J. Urch, Copper-Catalyzed Oxidation of Alcohols to Aldehydes and Ketones: An Efficient, Aerobic Alternative, Science (1979). 274 (1992) 2044–2046. www.sciencemag.org.

[37] I.E. Markó, A. Gautier, J.-L. Mutonkole, R. Dumeunier, A. Ates, C.J. Urch, S.M. Brown, Neutral, non-racemising, catalytic aerobic oxidation of alcohols, J. Organomet. Chem. 624 (2001) 344–347. https://doi.org/10.1016/S0022-328X(01)00681-7.

[38] A. Dijksman, I.W.C.E. Arends, R.A. Sheldon, Cu(II)-nitroxyl radicals as catalytic galactose oxidase mimics, Org. Biomol. Chem. 1 (2003) 3232–3237. https://doi.org/10.1039/b305941c.

[39] P. Gamez, I.W.C.E. Arends, J. Reedijk, R.A. Sheldon, Copper(ii)-catalysed aerobic oxidation of primary alcohols to aldehydes, Chem. Commun. 3 (2003) 2414–2415. https://doi.org/10.1039/b308668b.

[40] N.J. Hill, J.M. Hoover, S.S. Stahl, Aerobic alcohol oxidation using a copper(I)/TEMPO catalyst system: A green, catalytic oxidation reaction for the undergraduate organic chemistry laboratory, J. Chem. Educ. 90 (2013) 102–105. https://doi.org/10.1021/ed300368q.

[41] J.M. Hoover, J.E. Steves, S.S. Stahl, Copper(I)/tempo-catalyzed aerobic oxidation of primary alcohols to aldehydes with ambient air, Nat. Protoc. 7 (2012) 1161–1166. https://doi.org/10.1038/nprot.2012.057.

[42] J.M. Hoover, S.S. Stahl, Highly practical copper(I)/TEMPO catalyst system for chemoselective aerobic oxidation of primary alcohols, J. Am. Chem. Soc. 133 (2011) 16901–16910. https://doi.org/10.1021/ja206230h.

[43] J.M. Hoover, B.L. Ryland, S.S. Stahl, Copper/TEMPO-catalyzed aerobic alcohol oxidation: Mechanistic assessment of different catalyst systems, ACS Catal. 3 (2013) 2599–2605. https://doi.org/10.1021/cs400689a.

[44] B.L. Ryland, S.D. McCann, T.C. Brunold, S.S. Stahl, Mechanism of alcohol oxidation mediated by copper(II) and nitroxyl radicals, J. Am. Chem. Soc. 136 (2014) 12166–12173. https://doi.org/10.1021/ja5070137.

[45] J.M. Hoover, B.L. Ryland, S.S. Stahl, Mechanism of copper(I)/TEMPO-catalyzed aerobic alcohol oxidation, J. Am. Chem. Soc. 135 (2013) 2357–2367. https://doi.org/10.1021/ja3117203.

[46] J.E. Steves, S.S. Stahl, Copper(I)/ABNO-catalyzed aerobic alcohol oxidation: Alleviating steric and electronic constraints of Cu/TEMPO catalyst systems, J. Am. Chem. Soc. 135 (2013) 15742–15745. https://doi.org/10.1021/ja409241h.

[47] J.F. Greene, J.M. Hoover, D.S. Mannel, T.W. Root, S.S. Stahl, Continuous-flow aerobic oxidation of primary alcohols with a copper(I)/TEMPO catalyst, Org. Process. Res. Dev. 17 (2013) 1247–1251. https://doi.org/10.1021/op400207f.

[48] N.G. Anderson, Practical use of continuous processing in developing and scaling up laboratory processes, Org. Process. Res. Dev. 5 (2001) 613–621. https://doi.org/10.1021/op0100605.

[49] J.E. Steves, Y. Preger, J.R. Martinelli, C.J. Welch, T.W. Root, J.M. Hawkins, S.S. Stahl, Process Development of CuI/ABNO/NMI-Catalyzed Aerobic Alcohol Oxidation, Org. Process Res. Dev. 19 (2015) 1548–1553. https://doi.org/10.1021/acs.oprd.5b00179.

[50] C. Wiles, P. Watts, Continuous flow reactors: A perspective, Green Chem. 14 (2012) 38–54. https://doi.org/10.1039/c1gc16022b.

[51] X. Ye, M.D. Johnson, T. Diao, M.H. Yates, S.S. Stahl, Development of safe and scalable continuous-flow methods for palladium-catalyzed aerobic oxidation reactions, Green Chem. 12 (2010) 1180–1186. https://doi.org/10.1039/c0gc00106f.

[52] J.F. Greene, Y. Preger, S.S. Stahl, T.W. Root, PTFE-Membrane Flow Reactor for Aerobic Oxidation Reactions and Its Application to Alcohol Oxidation, Org. Process. Res. Dev. 19 (2015) 858–864. https://doi.org/10.1021/acs.oprd.5b00125.

[53] X. Xie, S.S. Stahl, Efficient and Selective Cu/Nitroxyl-Catalyzed Methods for Aerobic Oxidative Lactonization of Diols, J. Am. Chem. Soc. 137 (2015) 3767–3770. https://doi.org/10.1021/jacs.5b01036.

[54] S. Aıt-Mohand, J. Muzart, Palladium-catalyzed oxidative cyclization of 1,4-and 1,5-diols in 1,2-dichloroethane, J. Mol. Catal. A Chem. 129 (1998) 135–139.

[55] E.M. Huber, M. Basler, R. Schwab, W. Heinemeyer, C.J. Kirk, M. Groettrup, M. Groll, Immuno- and constitutive proteasome crystal structures reveal differences in substrate and inhibitor specificity, Cell. 148 (2012) 727–738. https://doi.org/10.1016/j.cell.2011.12.030.

[56] W.L. Holland, P.E. Scherer, Ronning after the adiponectin receptors, Science (1979). 342 (2013) 1460–1461. https://doi.org/10.1126/science.1249077.

[57] P.E. Piszel, A. Vasilopoulos, S.S. Stahl, Oxidative Amide Coupling from Functionally Diverse Alcohols and Amines Using Aerobic Copper/Nitroxyl Catalysis, Angew. Chem. Int. Ed. 58 (2019) 12211–12215. https://doi.org/10.1002/anie.201906130.

[58] K.C. Miles, S.S. Stahl, Practical Aerobic Alcohol Oxidation with Cu/Nitroxyl and Nitroxyl/NOx Catalyst System, Aldrichimica Acta. 48 (2015) 8–10. www.sigmaaldrich.com.

[59] Y. Seki, K. Oisaki, M. Kanai, Chemoselective aerobic oxidation catalyzed by a metal/stable organoradical redox conjugate, Tetrahedron Lett. 55 (2014) 3738–3746. https://doi.org/10.1016/j.tetlet.2014.05.085.

[60] K. Warm, G. Tripodi, E. Andris, S. Mebs, U. Kuhlmann, H. Dau, P. Hildebrandt, J. Roithová, K. Ray, Spektroskopische Charakterisierung eines reaktiven [Cu 2 (μ-OH) 2] 2+ Intermediates in Cu/TEMPO-katalysierten aeroben Alkoholoxidationen , Angewandte Chemie. 133 (2021) 23201–23208. https://doi.org/10.1002/ange.202108442.

[61] F. Wang, C. Chen, A continuing legend: The Brookhart-type α-diimine nickel and palladium catalysts, Polym. Chem. 10 (2019) 2354–2369. https://doi.org/10.1039/c9py00226j.

[62] R. Ziessel, Schiff-based bipyridine ligands. Unusual coordination features and mesomorphic behaviour, Coord. Chem. Rev. (2001) 195–223. www.elsevier.com/locate/ccr.

[63] E.C. Constable, C.E. Housecroft, The early years of 2,2′-bipyridine — A ligand in its own lifetime, Molecules. 24 (2019). https://doi.org/10.3390/molecules24213951.

[64] A. Dhakshinamoorthy, A.M. Asiri, H. Garcia, Metal-organic frameworks catalyzed C-C and C-heteroatom coupling reactions, Chem. Soc. Rev. 44 (2015) 1922–1947. https://doi.org/10.1039/c4cs00254g.

[65] N. Alvarez, L.F.S. Mendes, M.G. Kramer, M.H. Torre, A.J. Costa-Filho, J. Ellena, G. Facchin, Development of copper(II)-diimine-iminodiacetate mixed ligand complexes as potential antitumor agents, Inorganica Chim. Acta. 483 (2018) 61–70. https://doi.org/10.1016/j.ica.2018.07.052.

[66] J. Bernauer, J. Pölker, A. Jacobi von Wangelin, Redox-active BIAN-based Diimine Ligands in Metal-Catalyzed Small Molecule Syntheses**, ChemCatChem. 14 (2022). https://doi.org/10.1002/cctc.202101182.

[67] C. Espinoza-Hicks, P. Montoya, R. Bautista, H.A. Jiménez-Vázquez, L.M. Rodríguez-Valdez, A.A. Camacho-Dávila, F.P. Cossío, F. Delgado, J. Tamariz, Synthesis of exo-Imidazolidin-2-one Dienes, Their Isomerization, and Selectivity in Diels-Alder Cycloadditions, J. Org. Chem. 83 (2018) 5347–5364. https://doi.org/10.1021/acs.joc.7b02344.

[68] X. Jia, H. Liu, Y. Hu, Q. Dai, J. Bi, C. Bai, X. Zhang, Highly active and cis-1,4 selective polymerization of 1,3-butadiene catalyzed by cobalt(II) complexes bearing α-diimine ligands, Cuihua Xuebao/Chinese J. Catal. 34 (2013) 1560–1569. https://doi.org/10.1016/S1872-2067(12)60625-1.

[69] X. Jia, H. Liu, Y. Hu, Q. Dai, J. Bi, C. Bai, X. Zhang, Highly active and cis-1,4 selective polymerization of 1,3-butadiene catalyzed by cobalt(II) complexes bearing α-diimine ligands, Cuihua Xuebao/Chinese J. Catal. 34 (2013) 1560–1569. https://doi.org/10.1016/S1872-2067(12)60625-1.

[70] J.M. Kliegman, R.K. Barnes, Glyoxal Derivatives. Reaction of Glyoxal with Aromatic Primary Amines, J. Org Chem. 85 (1970) 3140–3143. https://pubs.acs.org/sharingguidelines.

[71] M.N. Pinto, I. Chakraborty, J. Jimenez, K. Murphy, J. Wenger, P.K. Mascharak, Therapeutic Potential of Two Visible Light Responsive Luminescent photoCORMs: Enhanced Cellular Internalization Driven by Lipophilicity, Inorg. Chem. 58 (2019) 14522–14531. https://doi.org/10.1021/acs.inorgchem.9b02121.

[72] A. Peppas, E. Papadaki, G. Schnakenburg, V. Magrioti, A.I. Philippopoulos, Heteroleptic copper(I) complexes incorporating sterically demanding diazabutadiene ligands (DABs). Synthesis, spectroscopic characterization and solid state structural analysis, Polyhedron. 171 (2019) 412–422. https://doi.org/10.1016/j.poly.2019.07.033.

[73] C. Chen, F.S. Liu, M. Szostak, BIAN-NHC Ligands in Transition-Metal-Catalysis: A Perfect Union of Sterically Encumbered, Electronically Tunable N-Heterocyclic Carbenes?, Chem. Eur. J. 27 (2021) 4478–4499. https://doi.org/10.1002/chem.202003923.

[74] V. Rosa, H. Laronha, C.S.B. Gomes, C.M. Cordas, J. Brinco, F. Freitas, M.D.R. Gomes da Silva, T. Avilés, Aerobic oxidation of benzylic alcohols catalysed by new (aryl-BIAN)copper(I) complexes: Their synthesis and structural characterization, Appl. Organomet. Chem. 37 (2023) e7193. https://doi.org/10.1002/aoc.7193.

[75] G.S. Day, B. Pan, D.L. Kellenberger, B.M. Foxman, C.M. Thomas, Guilty as charged: Non-innocent behavior by a pincer ligand featuring a central cationic phosphenium donor, Chem. Comm. 47 (2011) 3634–3636. https://doi.org/10.1039/c0cc05739h.

[76] L. Jafarpour, E.D. Stevens, S.P. Nolan, A sterically demanding nucleophilic carbene: 1,3-bis(2,6-diisopropylphenyl)imidazol-2-ylidene). Thermochemistry and catalytic application in olefin metathesis, J. Organomet. Chem. 606 (2000). www.elsevier.nl/locate/jorganchem.

[77] C.R. Groom, I.J. Bruno, M.P. Lightfoot, S.C. Ward, The Cambridge Structural Database, Acta Crystallogr. B Struct. Sci. Cryst. Eng. Mater. 72 (2016) 171–179. https://doi.org/10.1107/S2052520616003954.

[78] M.G. Tay, Y.Y. Chia, S.H.C. Kuan, T.P. Phan, The formation of dinuclear trichloro-bridged and mononuclear ruthenium complexes from the reactions of dichlorotris(p-tolylphosphine)ruthenium(II) with diazabutadiene ligands, Transit. Met. Chem. 44 (2019) 293–301. https://doi.org/10.1007/s11243-018-00293-0.

[79] F. Wang, R. Tanaka, Q. Li, Y. Nakayama, T. Shiono, Chain-Walking Polymerization of Linear Internal Octenes Catalyzed by α-Diimine Nickel Complexes, Organometallics. 37 (2018) 1358–1367. https://doi.org/10.1021/acs.organomet.8b00042.

[80] R.J. Angelic, Inorganic Syntheses, Wiley, 1990. https://doi.org/10.1002/9780470132555.

A

ANNEXES

A.1 Ligands spectra

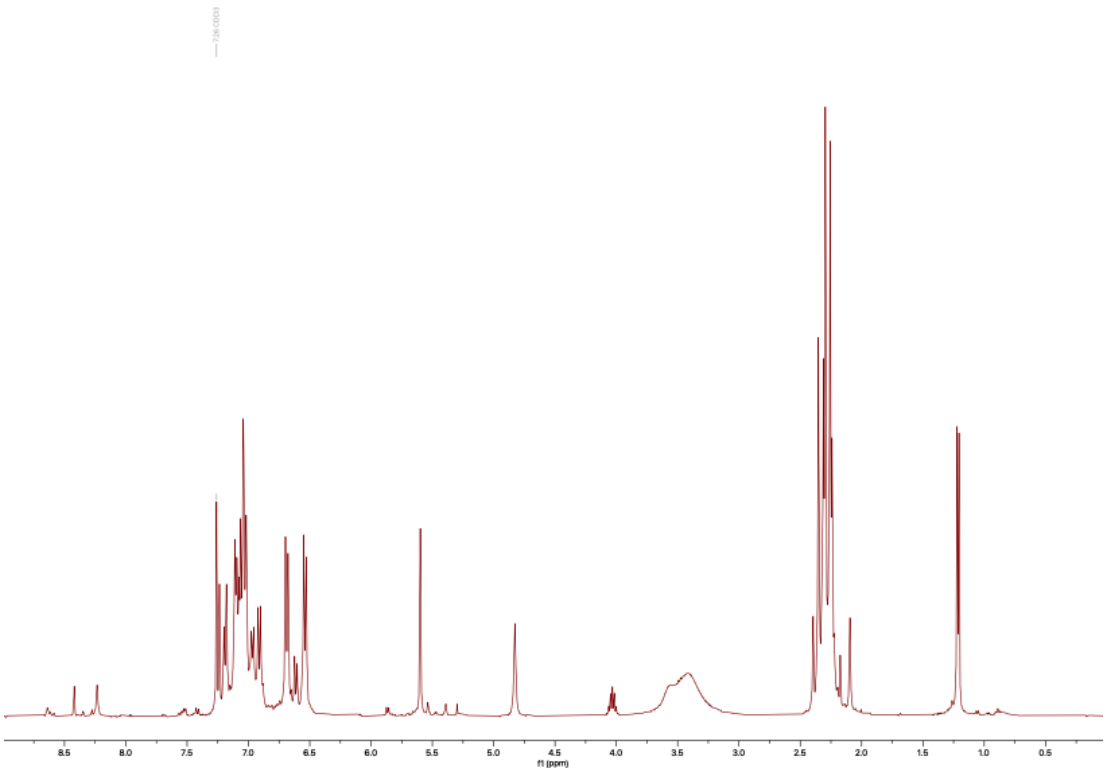

Figure A.1. ^{1}H NMR in $CDCl_3$ obtained from the dark brown oil proposed to be the polymer formed during the reaction

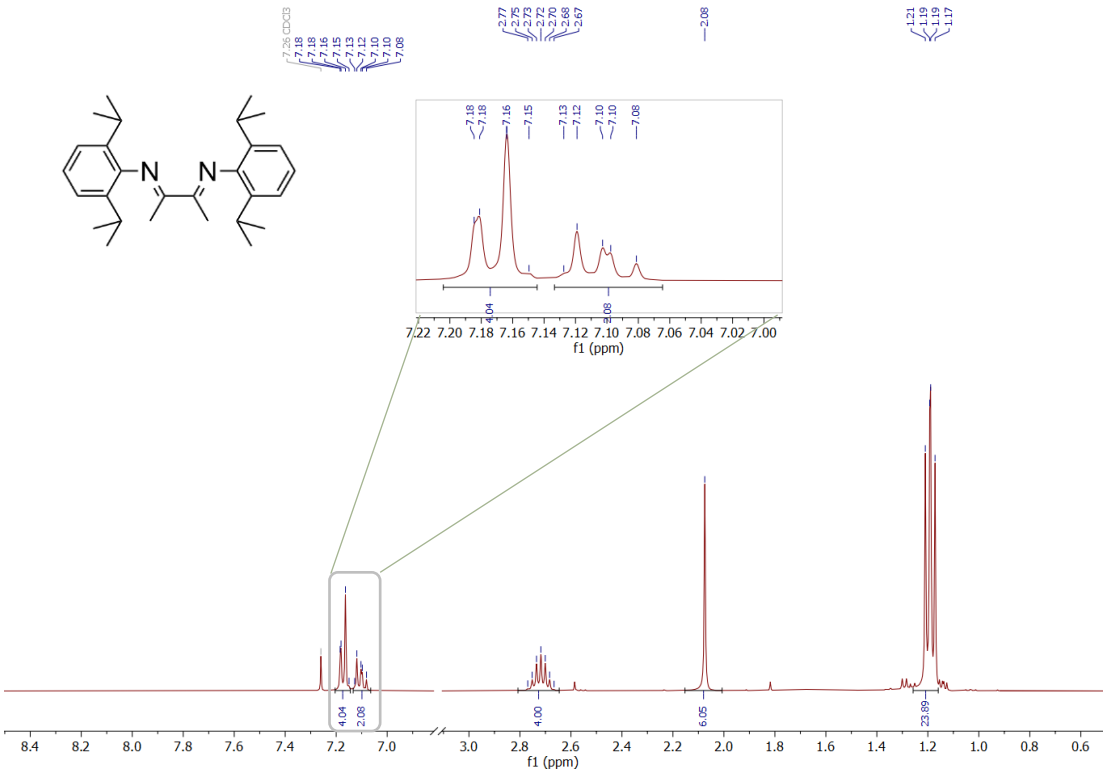

Figure A.2. ^{1}H NMR in $CDCl_3$ of the synthesised **R1** ligand.

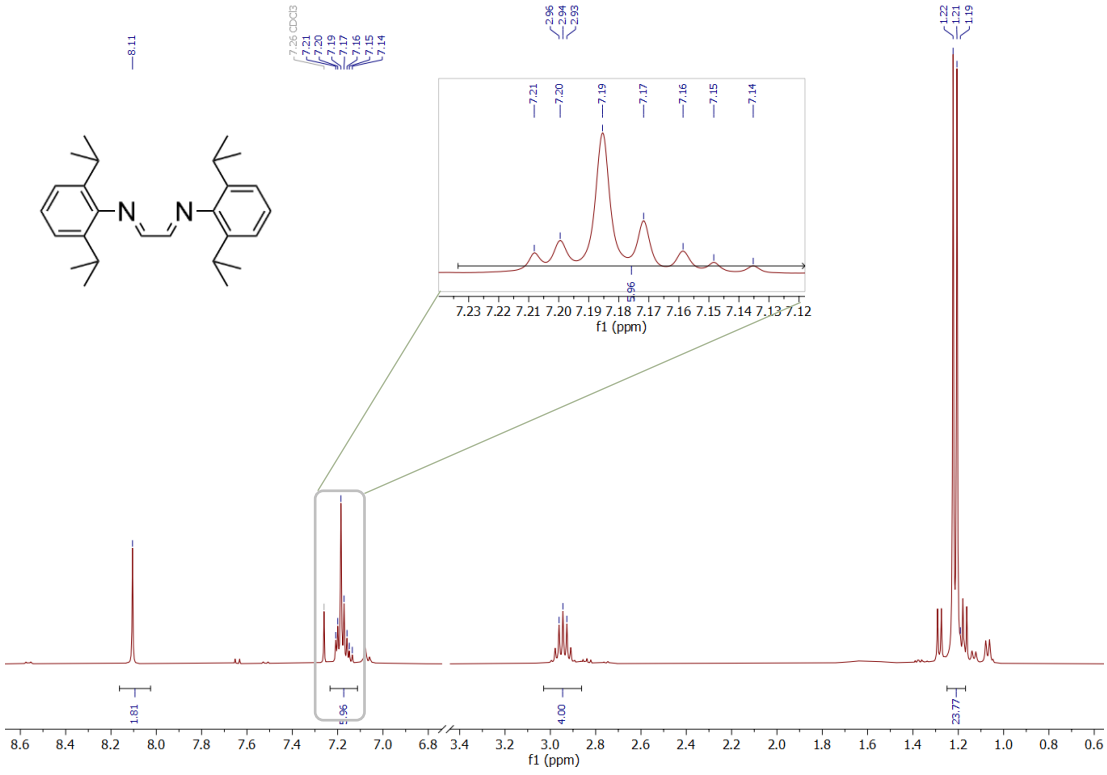

Figure A.3. ^{1}H NMR spectrum in $CDCl_3$ of the synthesised **R2** ligand.

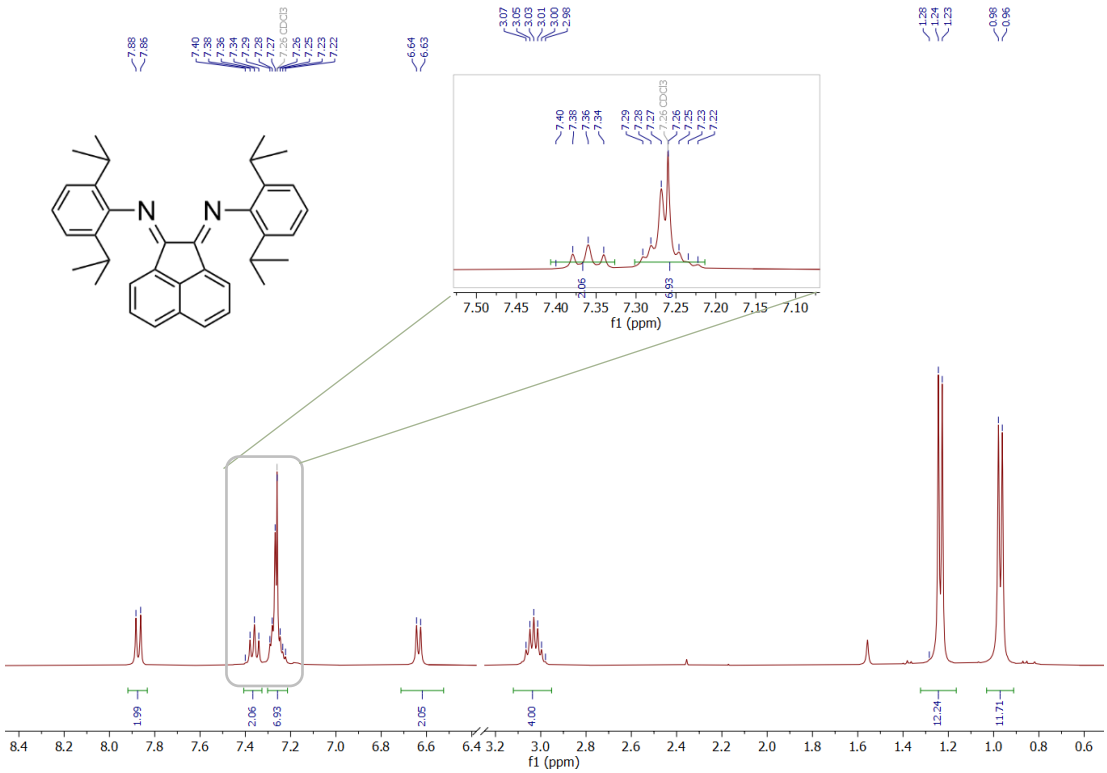

Figure A.4. ^{1}H NMR in $CDCl_3$ of the synthesised **R3** ligand.

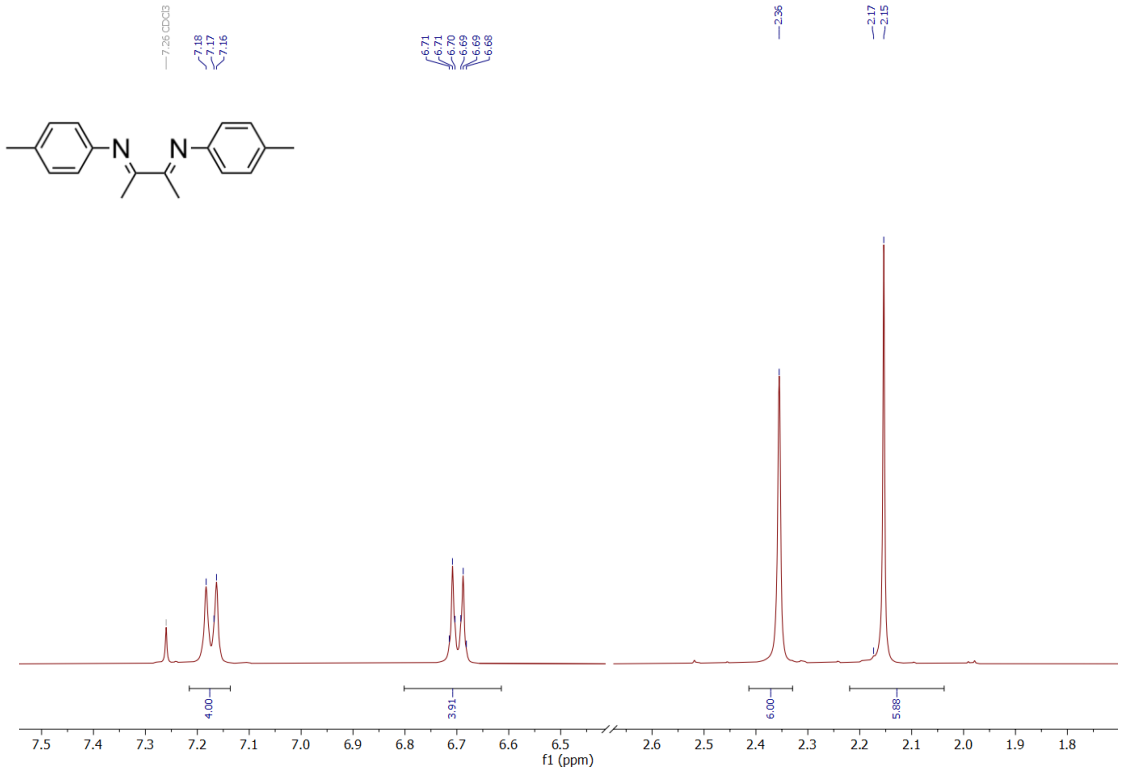

Figure A.5. ^{1}H NMR spectrum in $CDCl_3$ of the synthesised **R4** ligand.

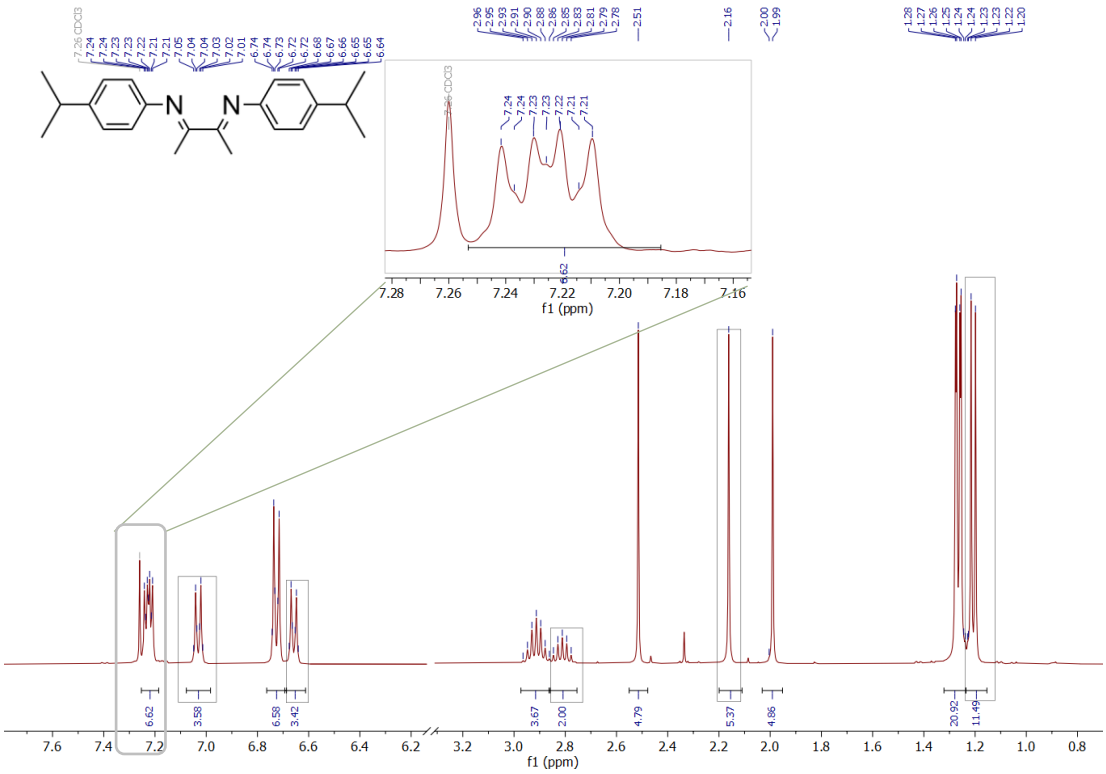

Figure A.6. ^{1}H NMR spectrum in $CDCl_3$ of the synthesised **R5** ligand.

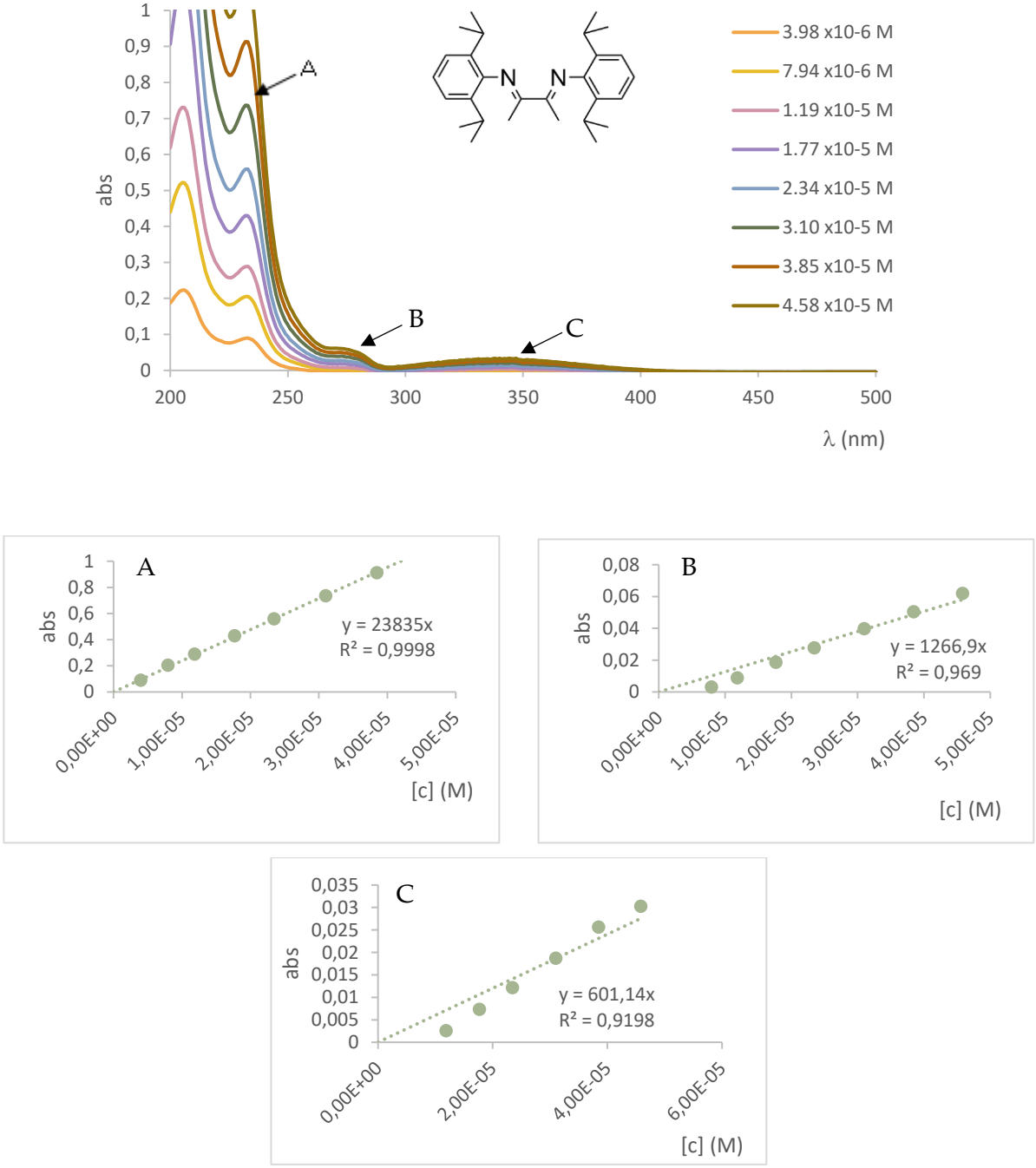

Figure A.7. UV/Vis spectrum in MeCN of the synthesised **R1** ligand. **A**- molar extinction coefficient for the transition at 233 nm. **B**- molar extinction coefficient for the transition at 267 nm. **C**- molar extinction coefficient for the transition at 348 nm.

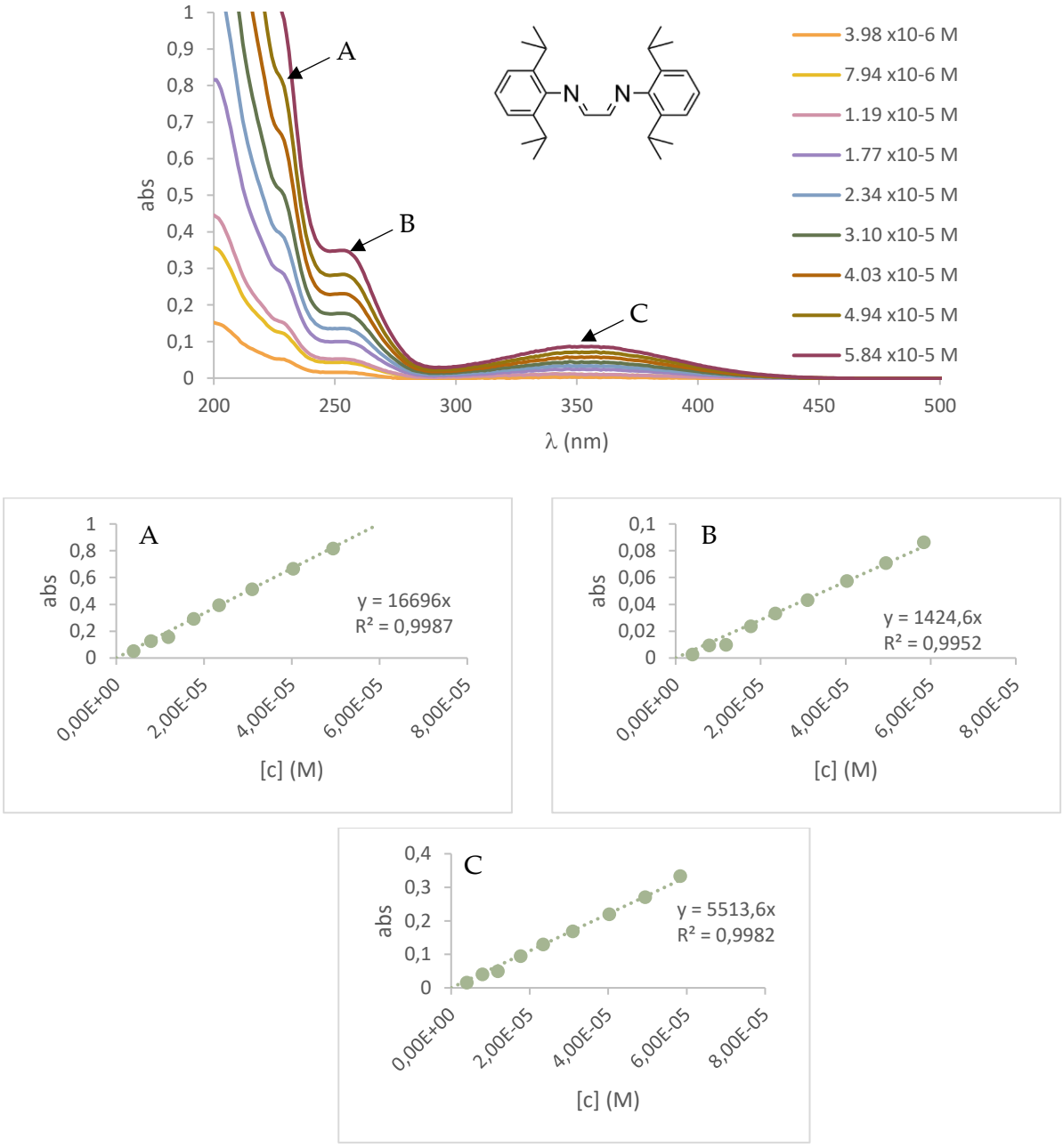

Figure A.8. UV/Vis spectrum in MeCN of the synthesised **R2** ligand. A- molar extinction coefficient for the transition at 228 nm. **B**- molar extinction coefficient for the transition at 258 nm. **C**- molar extinction coefficient for the transition at 354 nm.

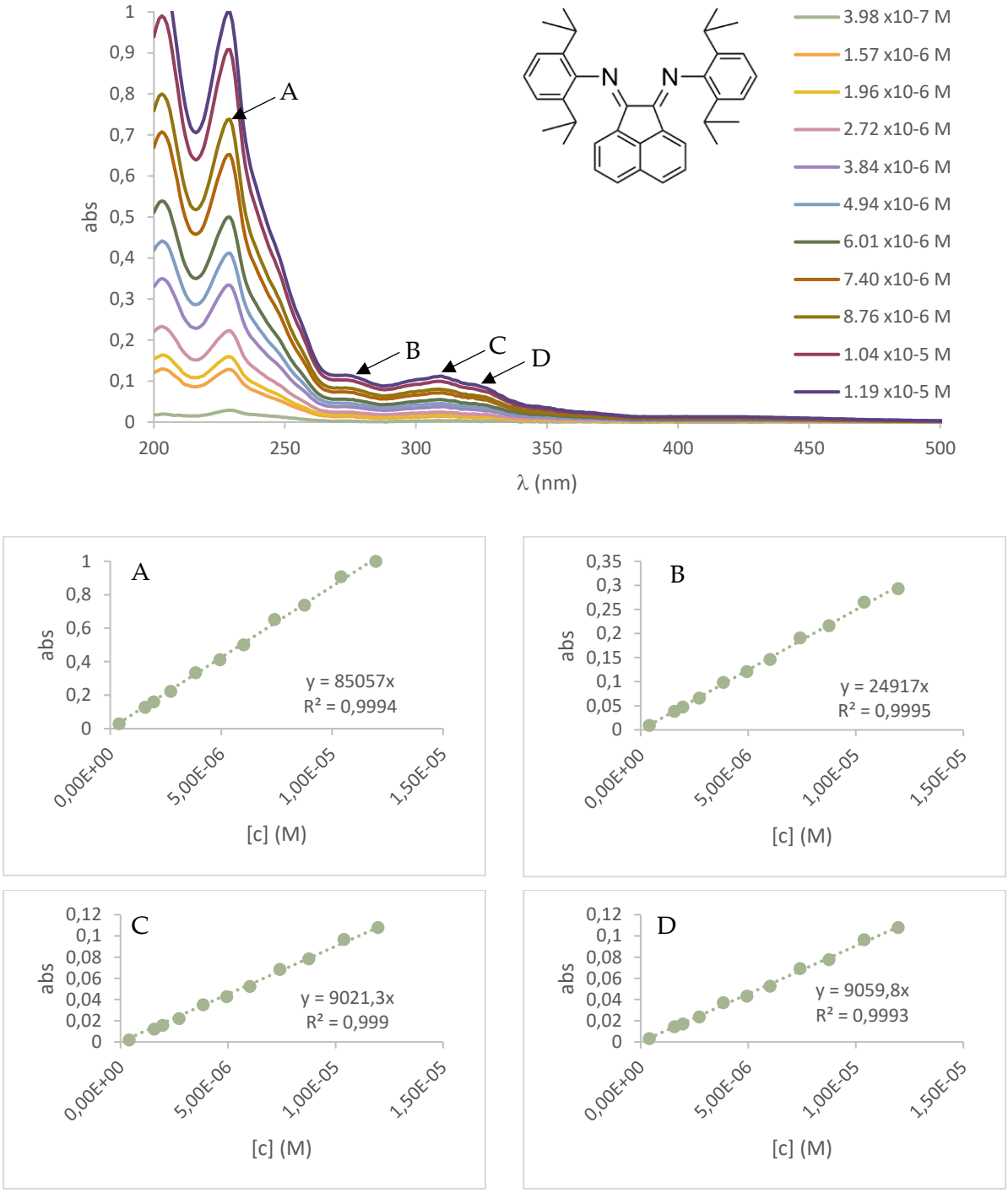

Figure A.9. UV/Vis spectrum in MeCN of the synthesised **R3** ligand. **A**- molar extinction coefficient for the transition at 229 nm. **B**- molar extinction coefficient for the transition at 253 nm. **C**- molar extinction coefficient for the transition at 278nm. **D**- molar extinction coefficient for the transition at 312 nm.

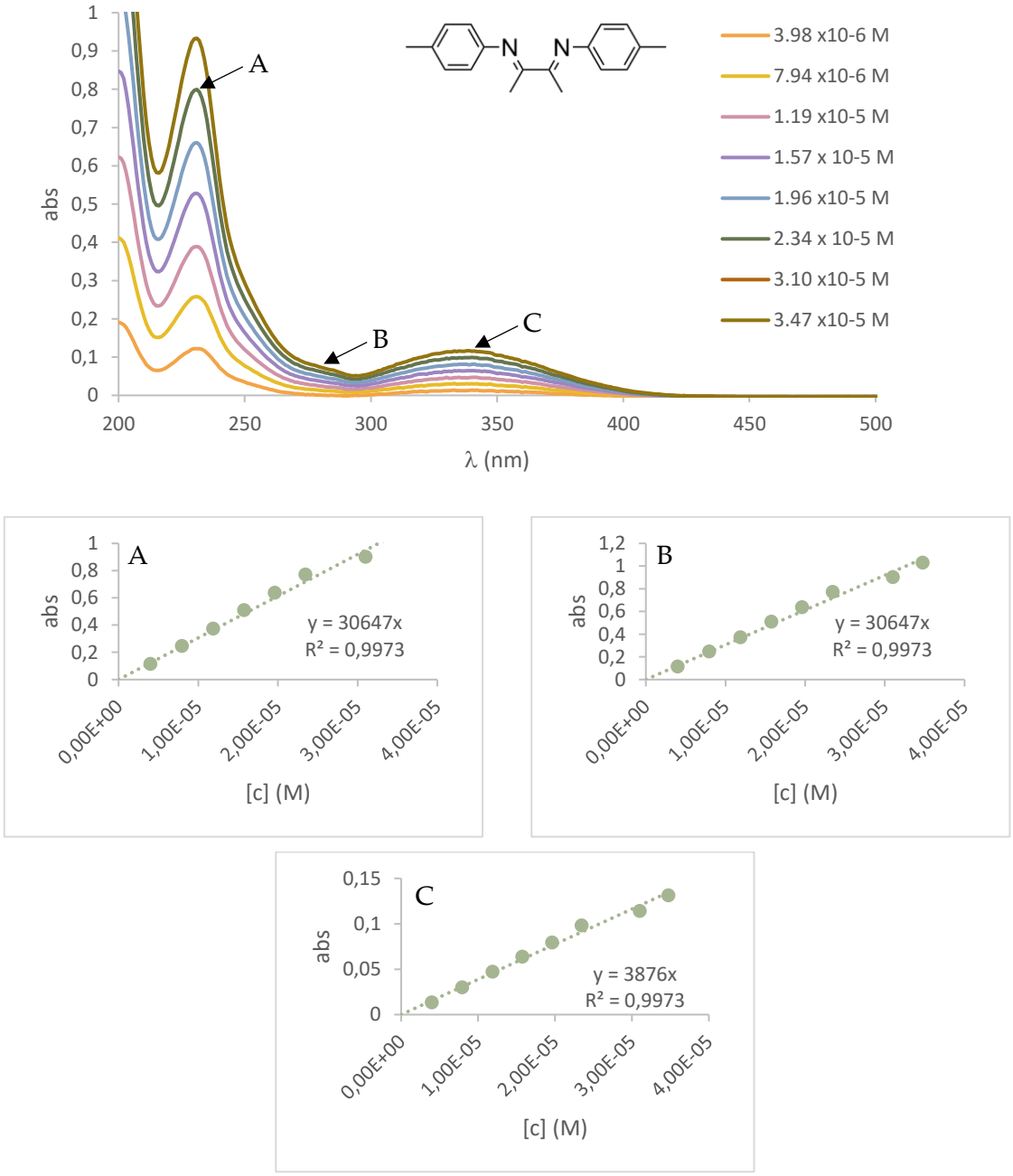

Figure A.10. UV/Vis spectrum in MeCN of the synthesised **R4** ligand. **A**- molar extinction coefficient for the transition at 228 nm. **B**- molar extinction coefficient for the transition at 284 nm. **C**- molar extinction coefficient for the transition at 278nm. **D**- molar extinction coefficient for the transition at 342 nm.

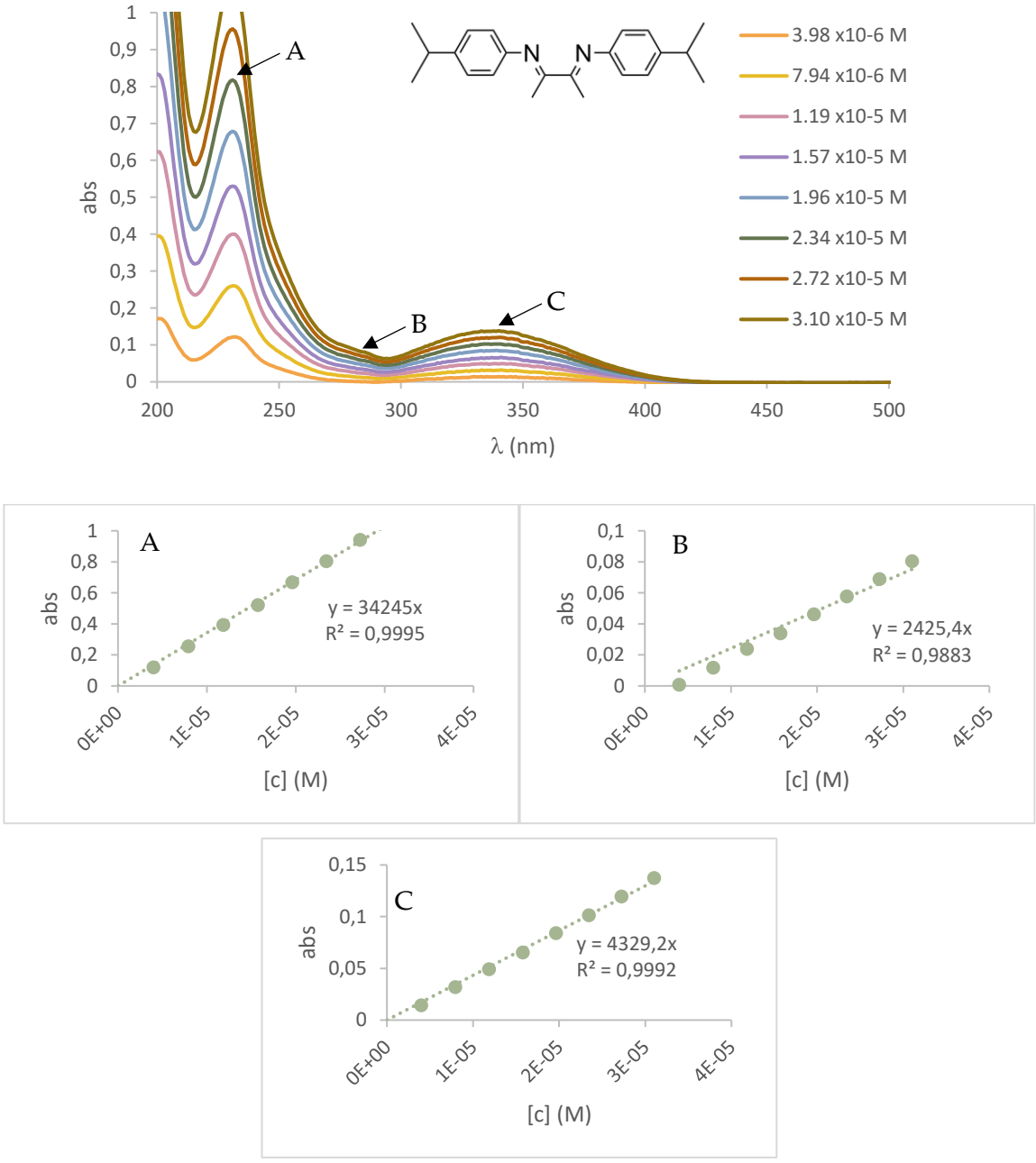

Figure A.11. UV/Vis spectrum in MeCN of the synthesised ligand **R5**. **A**- molar extinction coefficient for the transition at 229 nm. **B**- molar extinction coefficient for the transition at 285 nm. **C**- molar extinction coefficient for the transition at 342 nm.

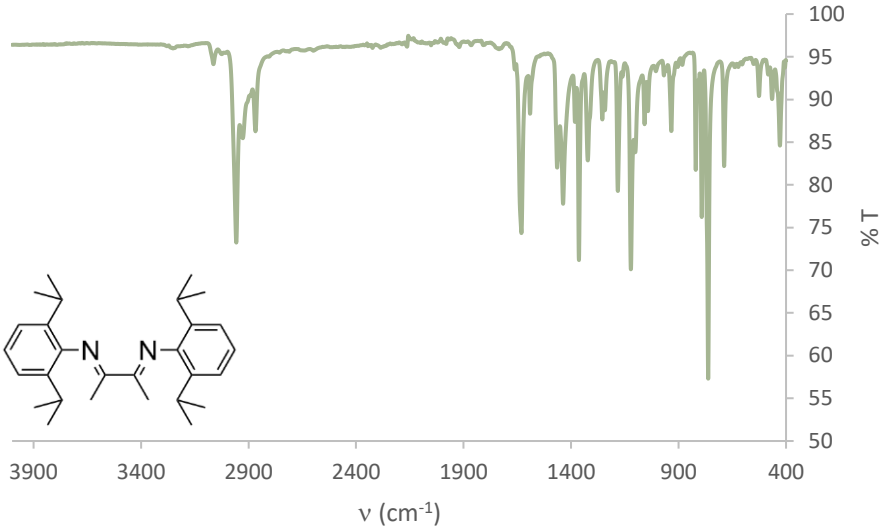

Figure A.12. IR spectrum obtained for the **R1** ligand.

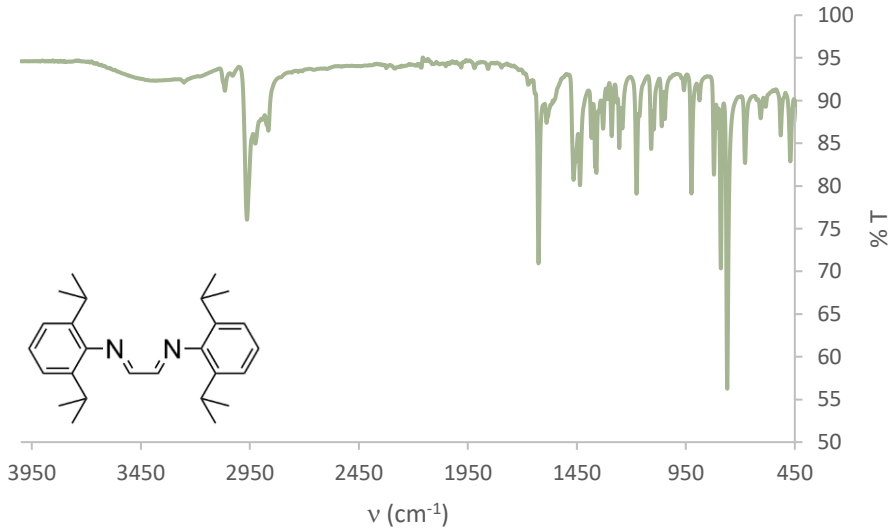

Figure A.13. IR spectrum obtained for the synthesised **R2** ligand.

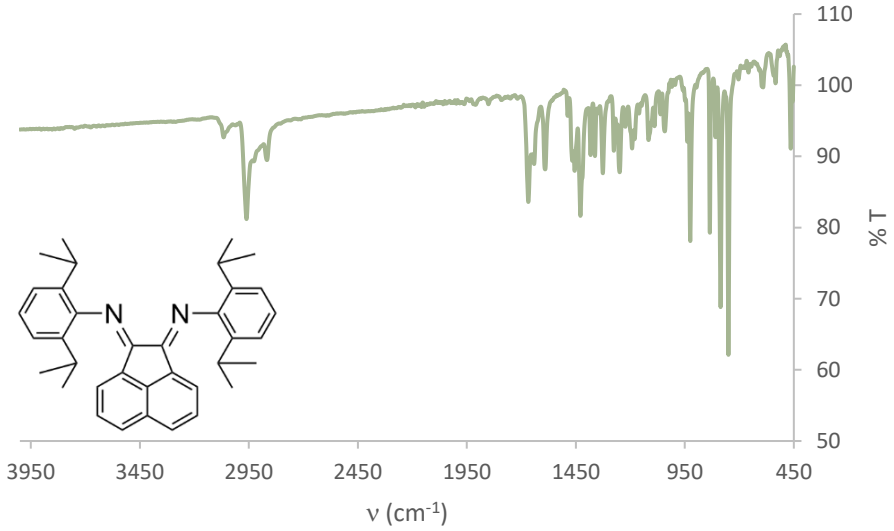

Figure A.14. IR spectrum obtained for the synthesised **R3** ligand.

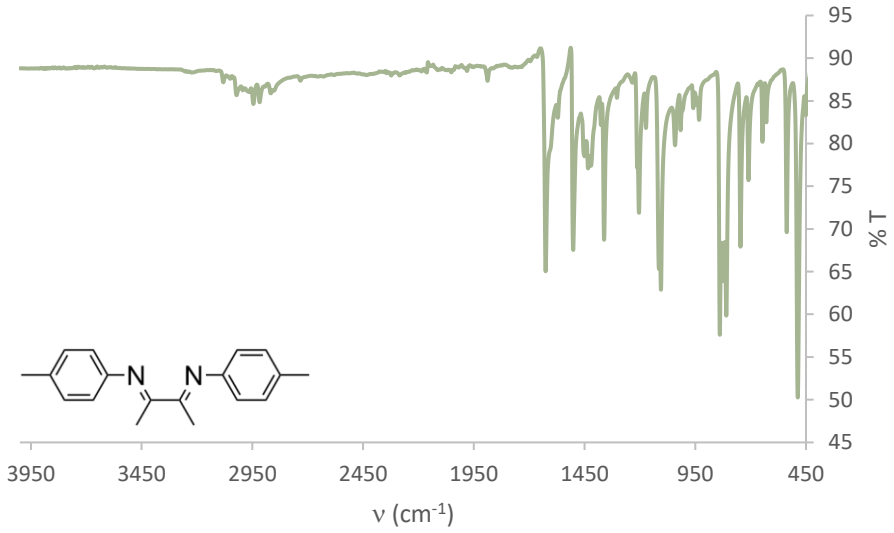

Figure A.15. IR spectrum obtained for the synthesised **R4** ligand.

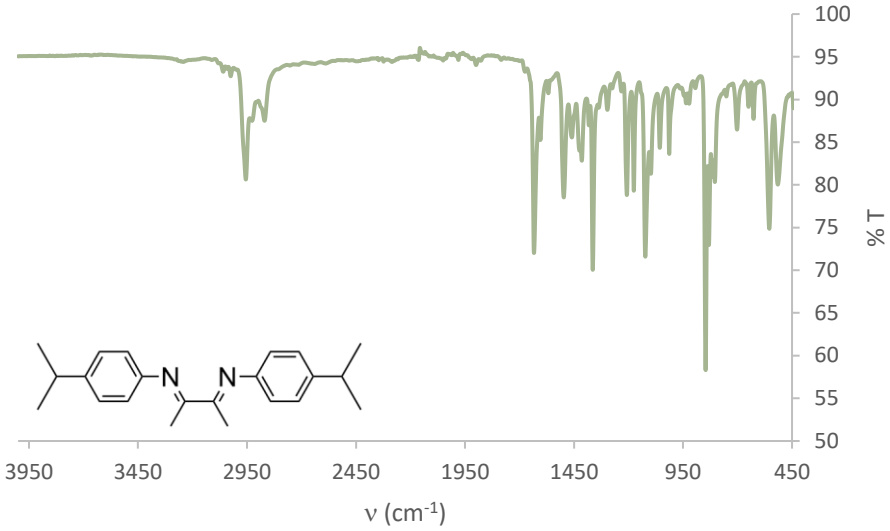

Figure A.16. IR spectrum obtained for the synthesised **R5** ligand.

A.2 Complexes spectra

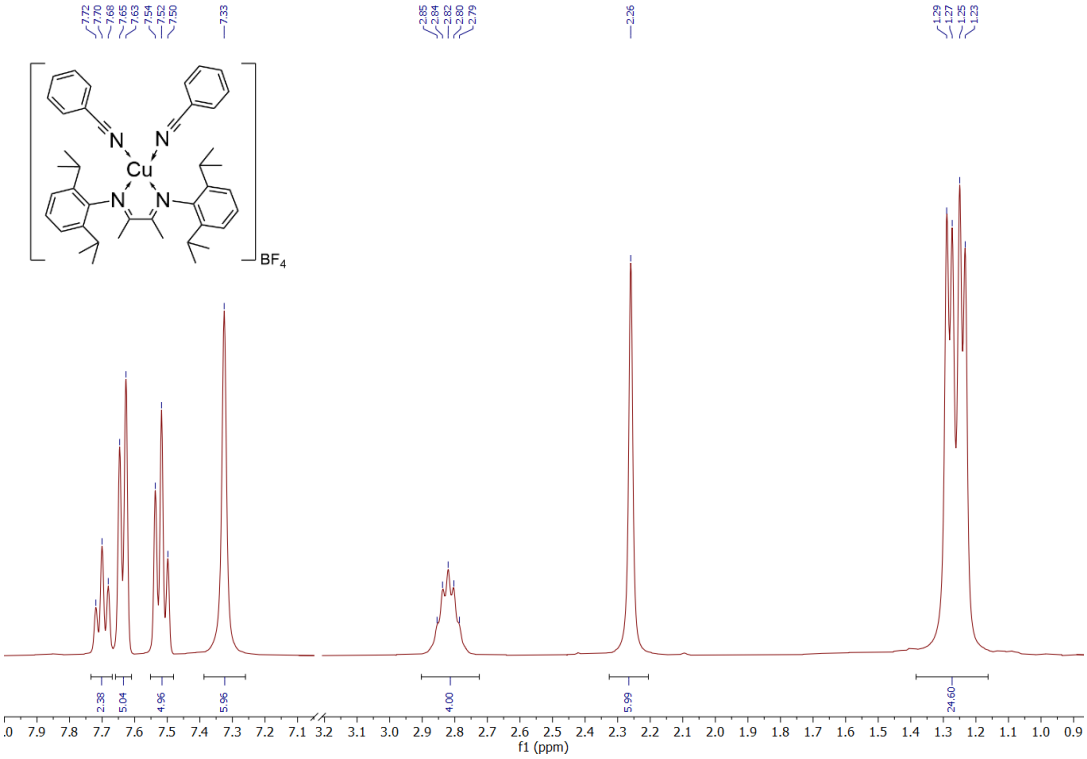

Figure A.17. ^{1}H NMR spectrum in CD_2Cl_2 of **C1** complex.

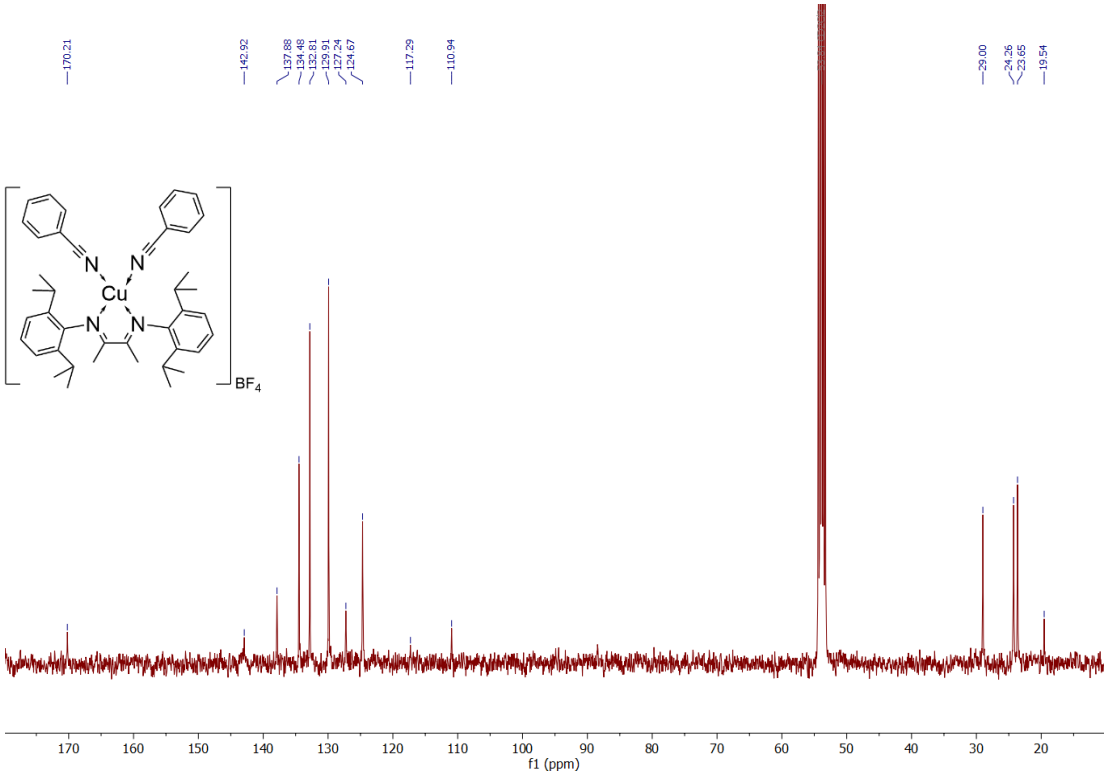

Figure A.18. ^{13}C NMR spectrum in CD_2Cl_2 of the **C1** complex.

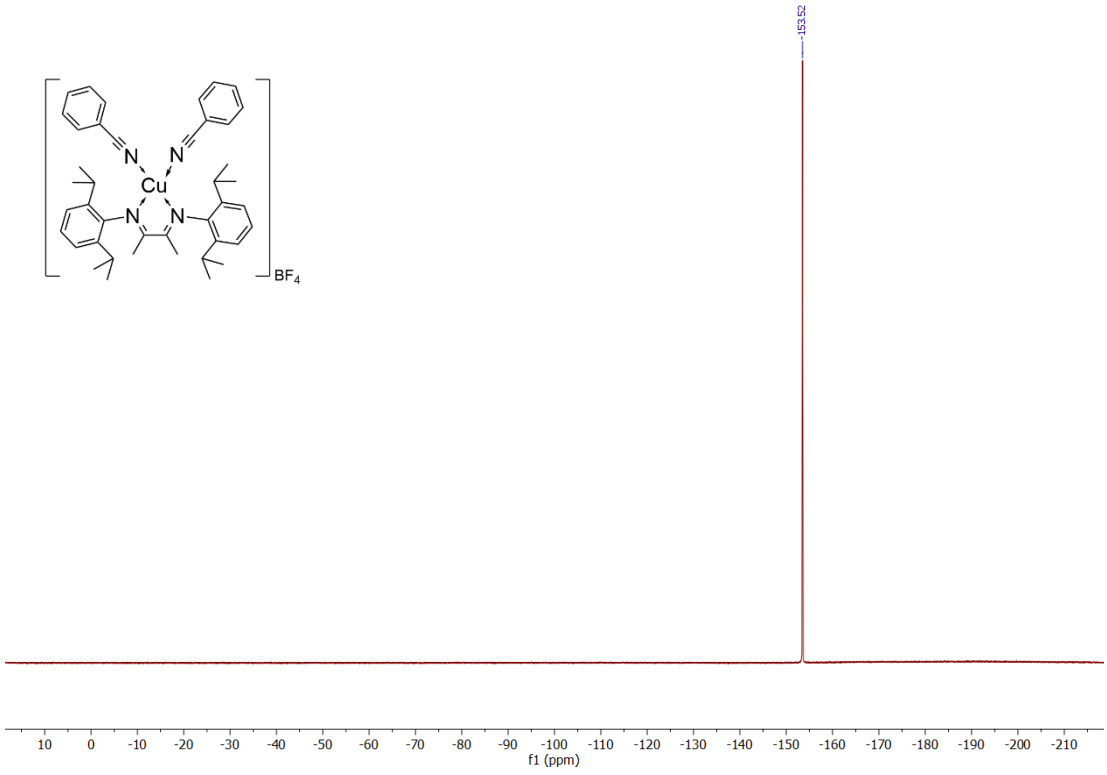

Figure A.19. ^{19}F NMR spectrum in CD_2Cl_2 of the **C1** complex.

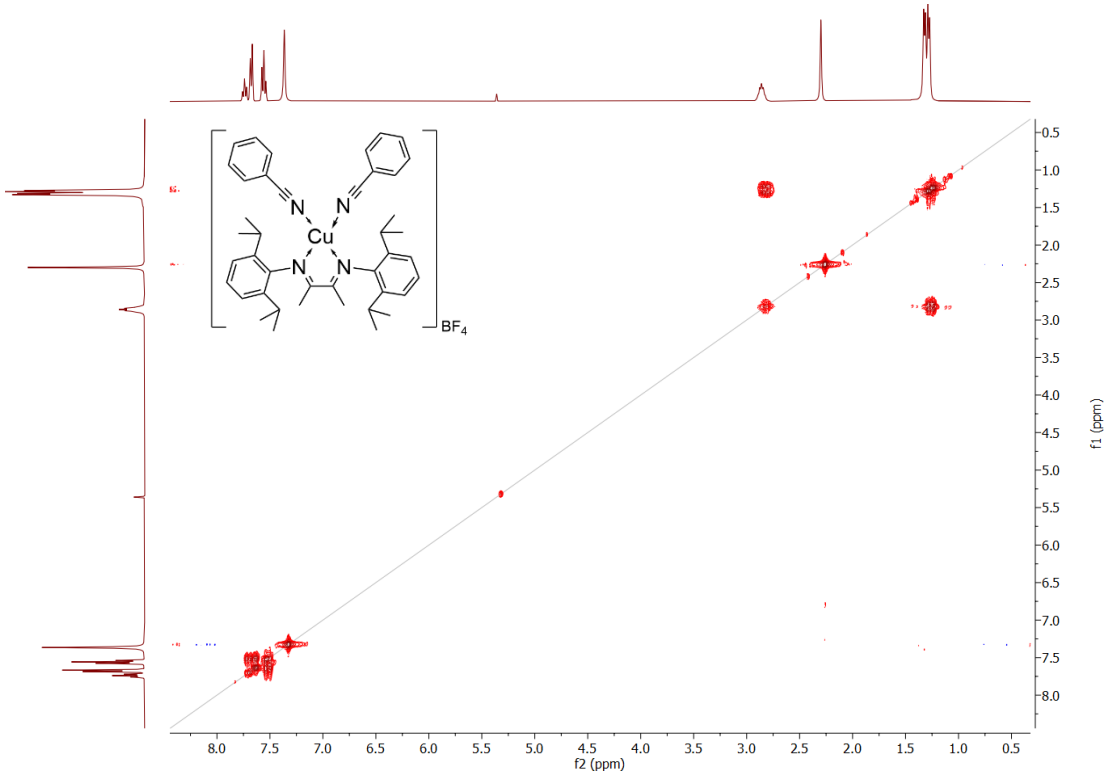

Figure A.20. COSY spectrum in CD_2Cl_2 of **C1** complex.

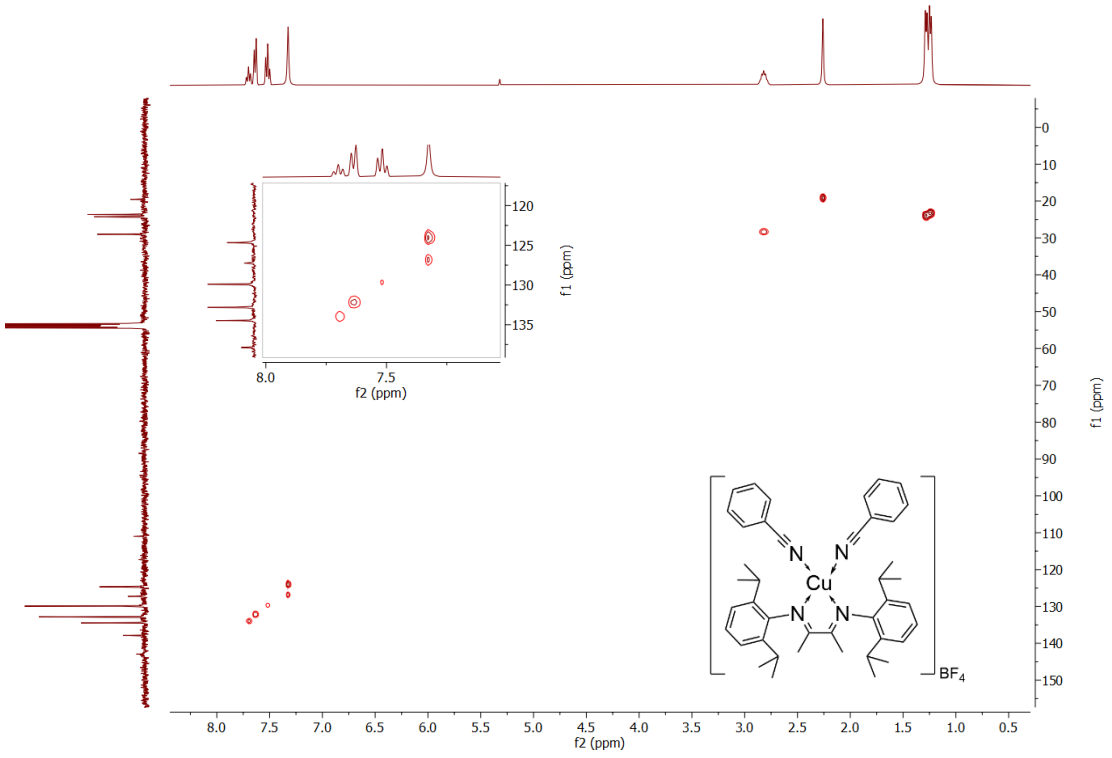

Figure A.21. HSQC spectrum in CD_2Cl_2 of **C1** complex.

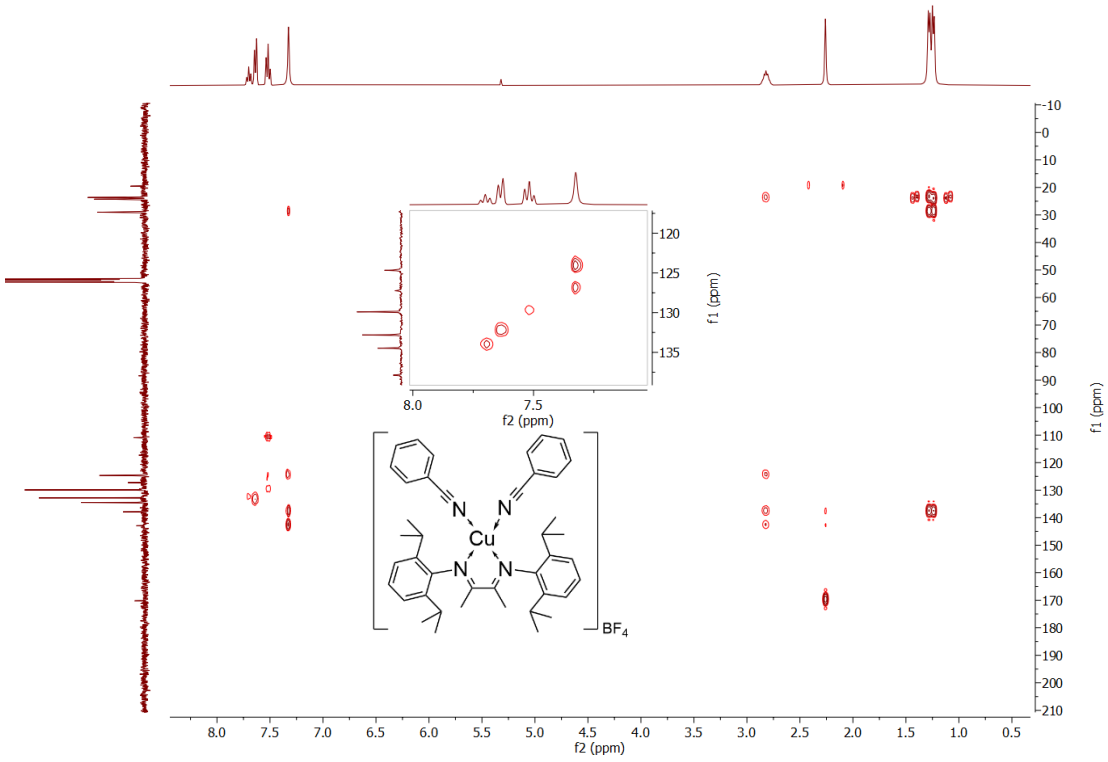

Figure A.22. HMBC spectrum in CD_2Cl_2 of **C1** complex.

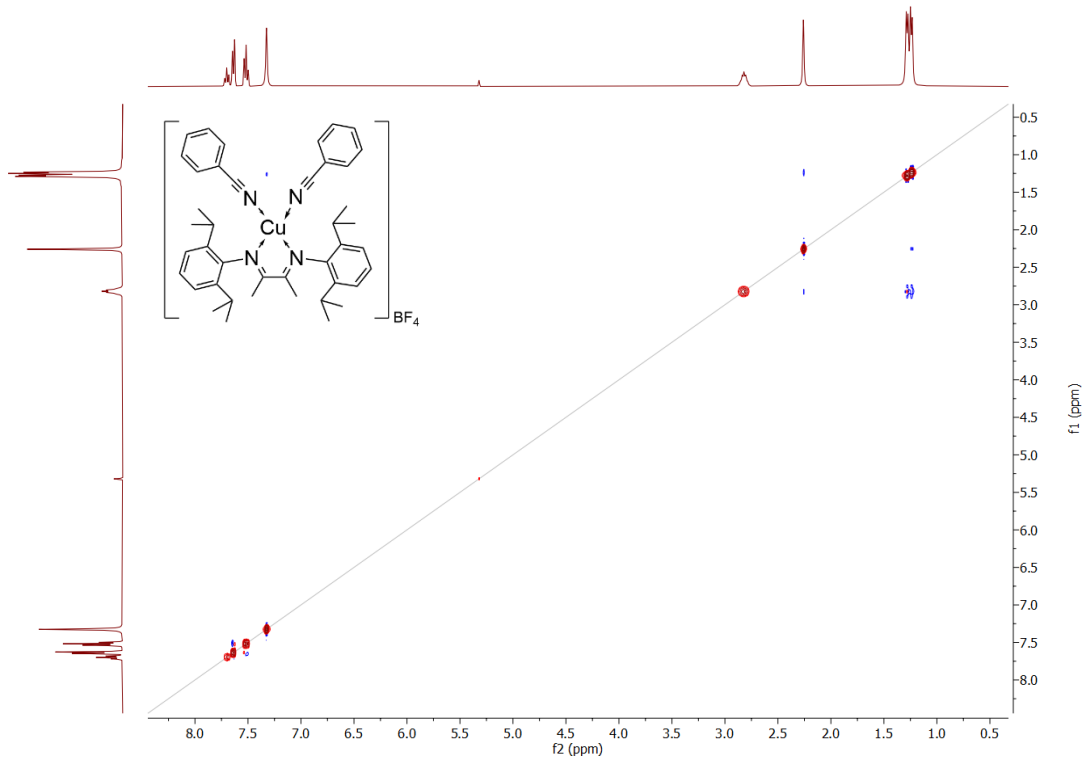

Figure A.23. NOESY spectrum in CD_2Cl_2 of **C1** complex.

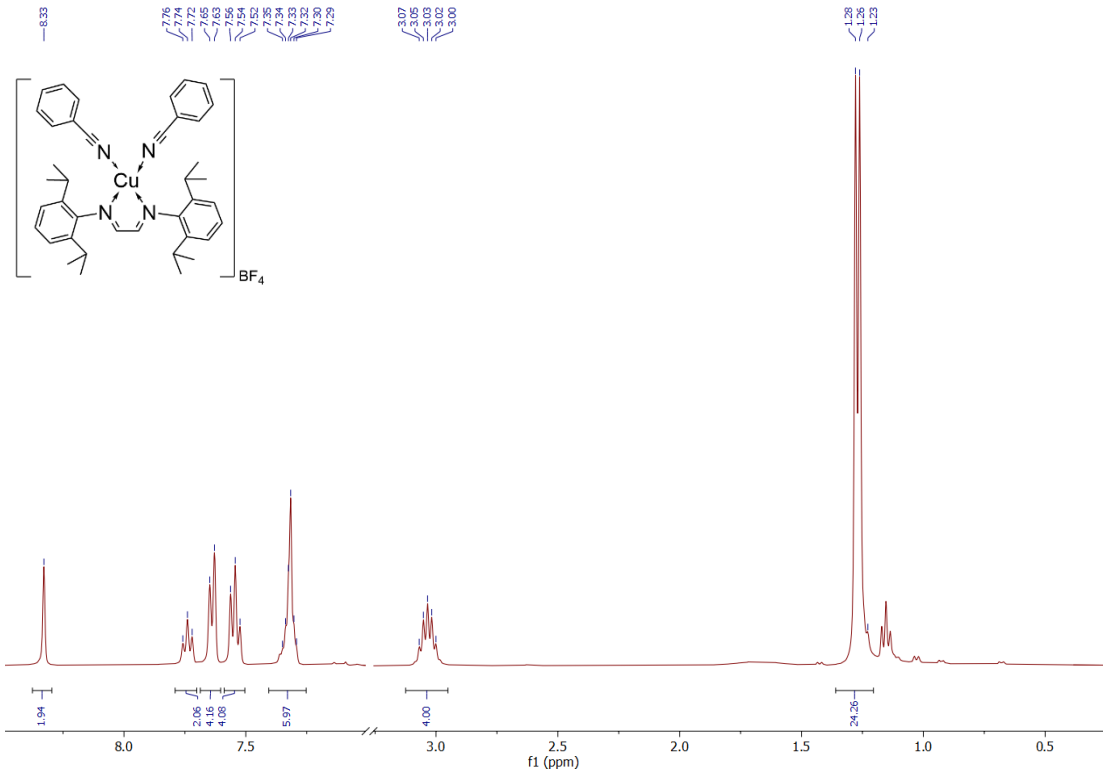

Figure A.24. ^{1}H NMR spectrum in CD_2Cl_2 of **C2** complex.

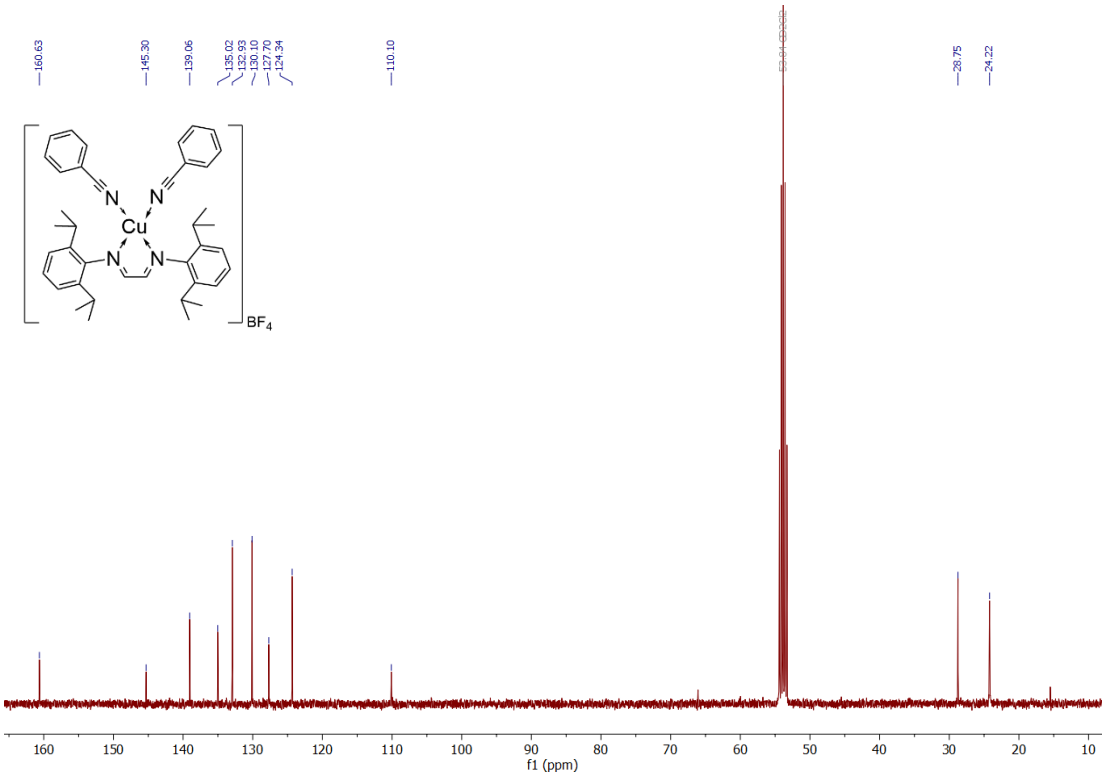

Figure A.25. ^{13}C NMR spectrum in CD_2Cl_2 of **C2** complex.

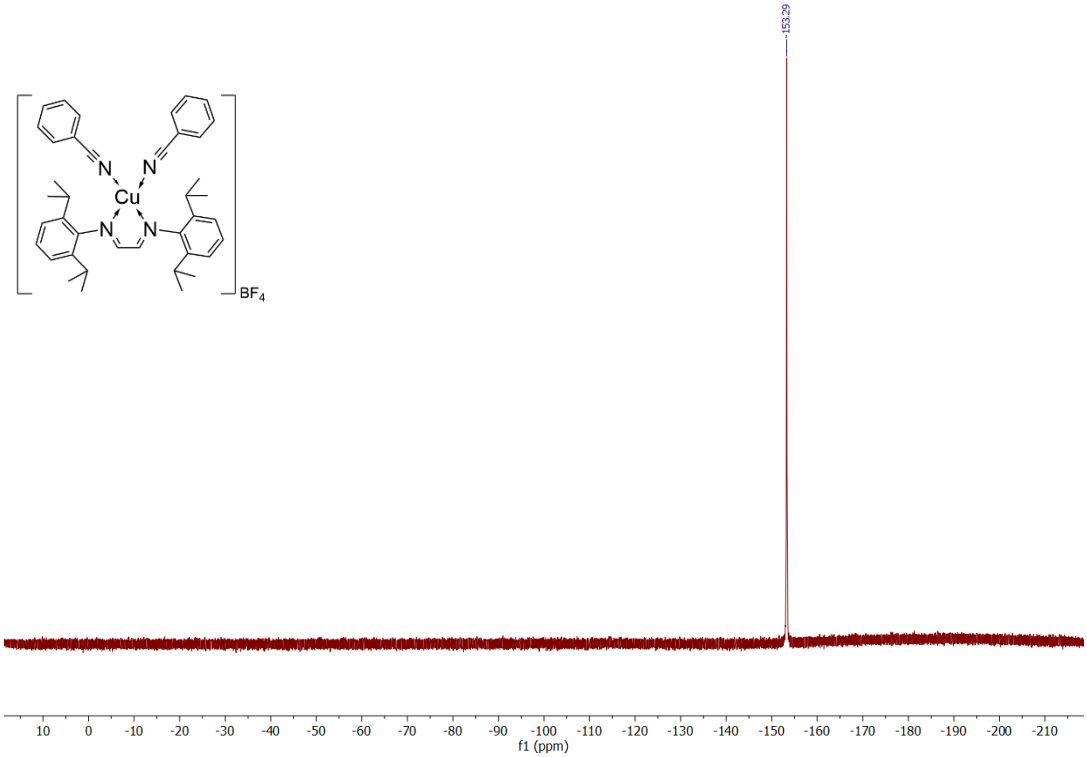

Figure A.26. ^{19}F NMR spectrum in CD_2Cl_2 of the **C2** complex.

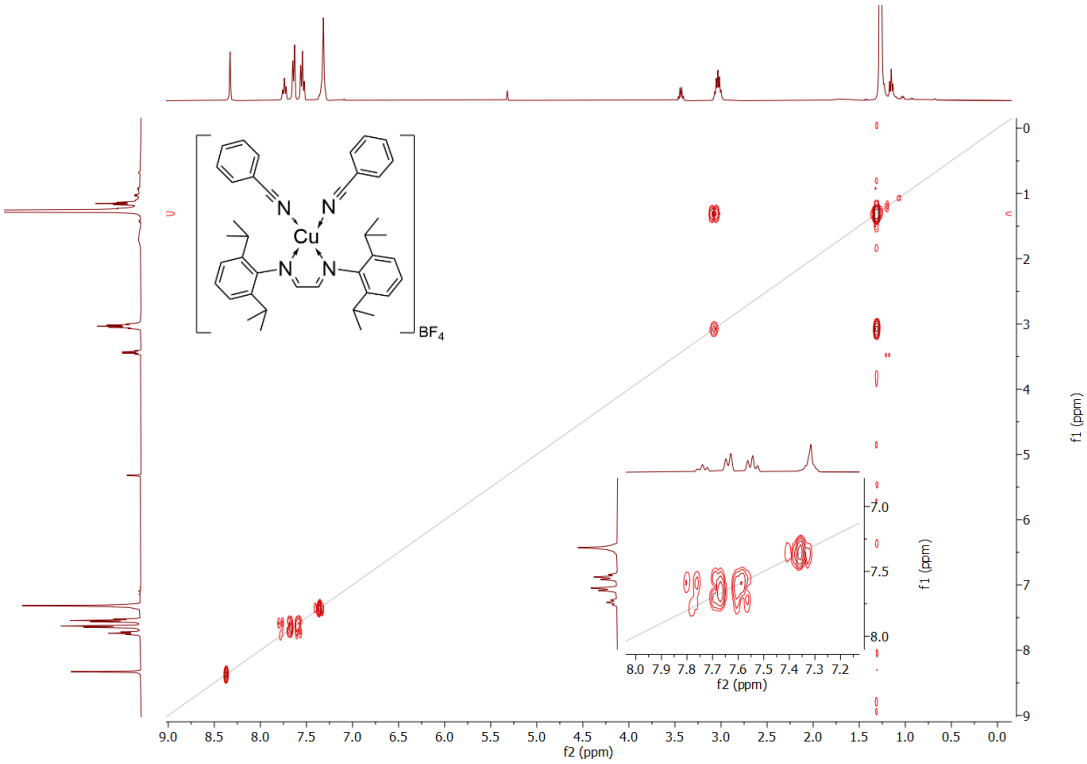

Figure A.27. COSY spectrum in CD_2Cl_2 of the **C2** complex.

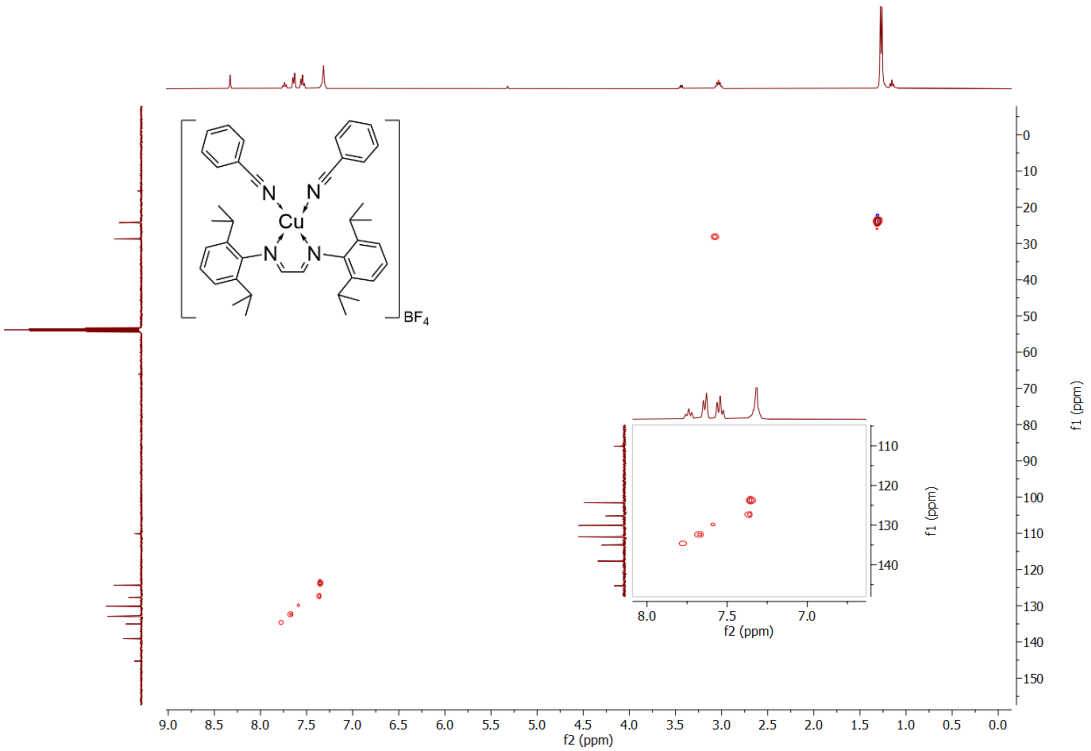

Figure A.28. HSQC spectrum in CD_2Cl_2 of the **C2** complex.

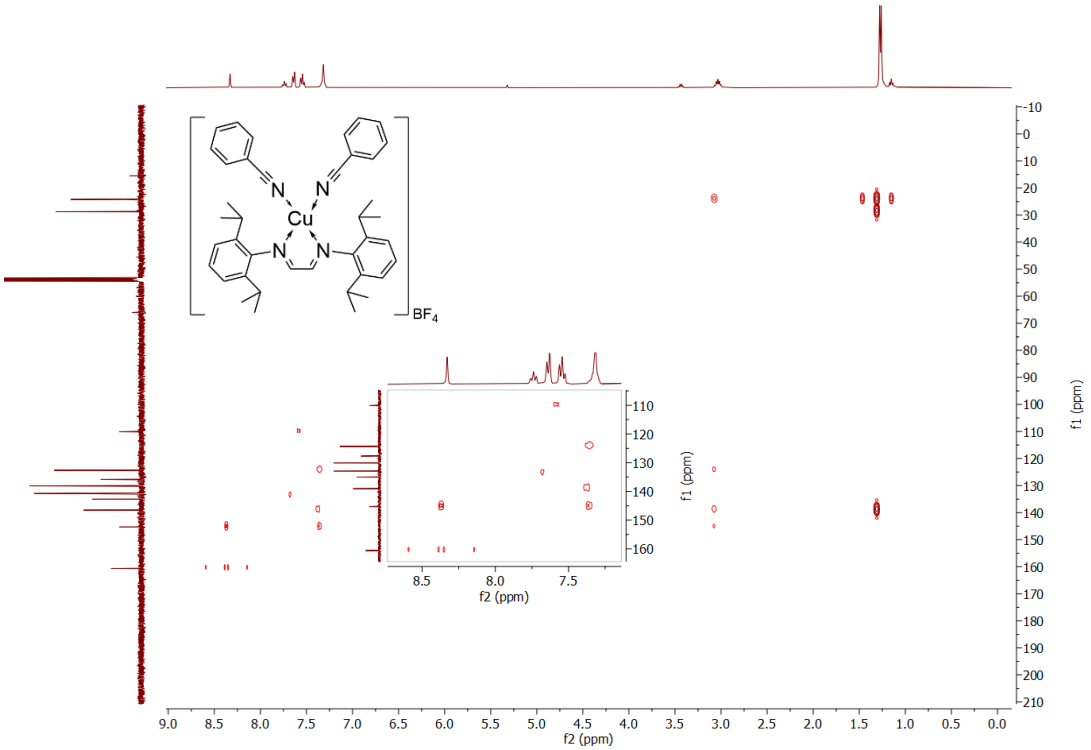

Figure A.29. HMBC spectrum in CD_2Cl_2 of the **C2** complex.

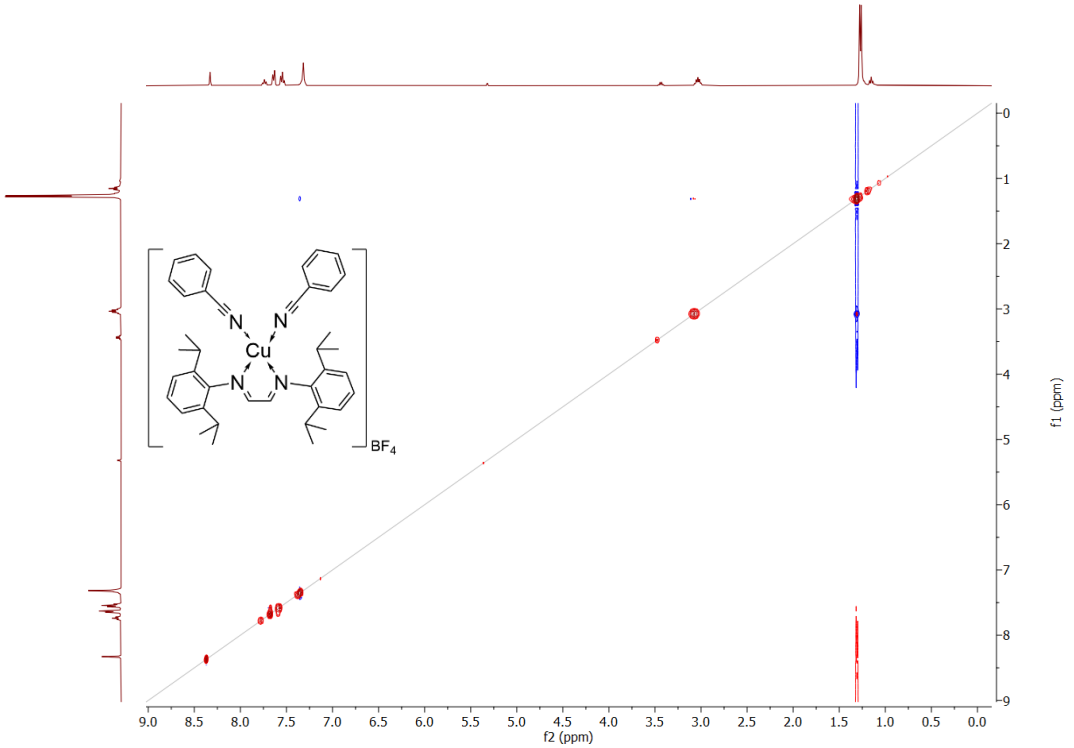

Figure A.30. NOESY spectrum in CD_2Cl_2 of the **C2** complex.

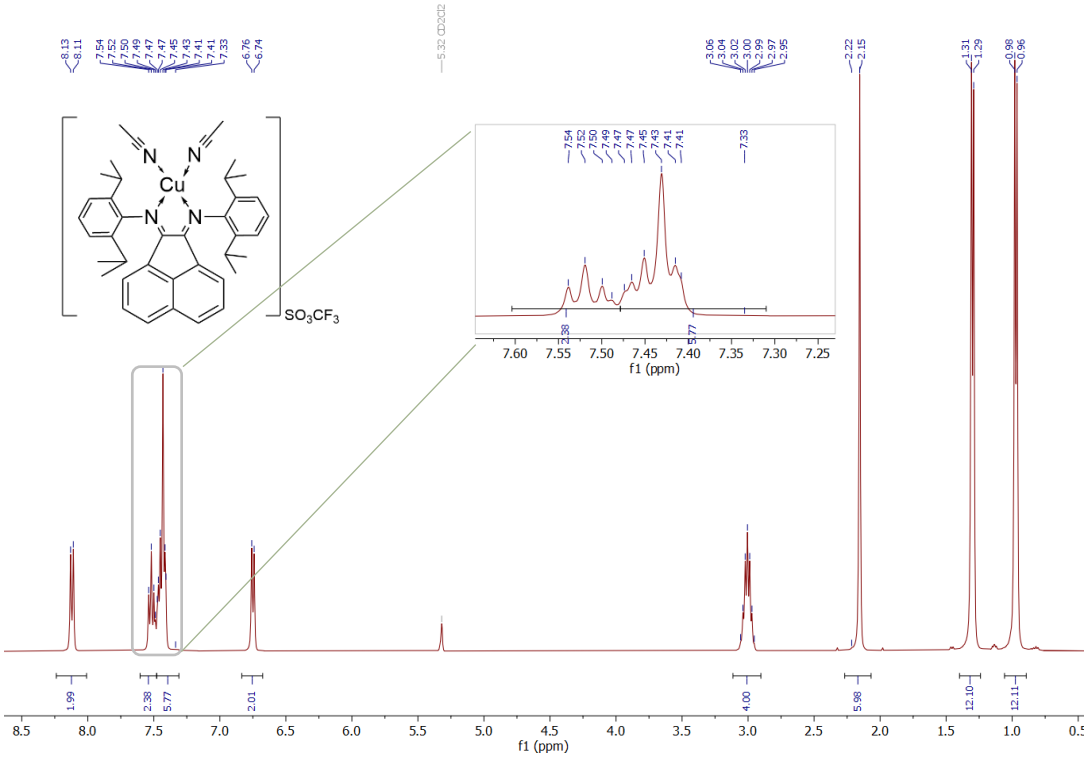

Figure A.31. ^1H NMR spectrum in CD_2Cl_2 of the **C3** complex.

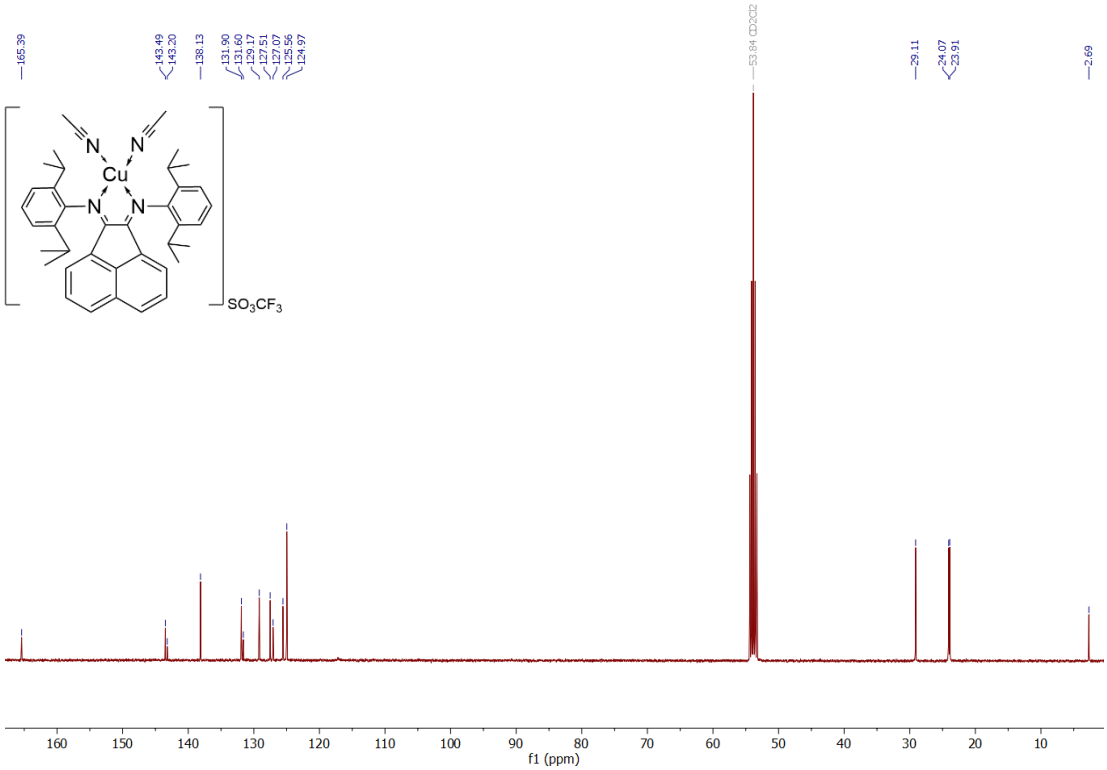

Figure A.32. ^{13}C NMR spectrum in CD_2Cl_2 of the **C3** complex.

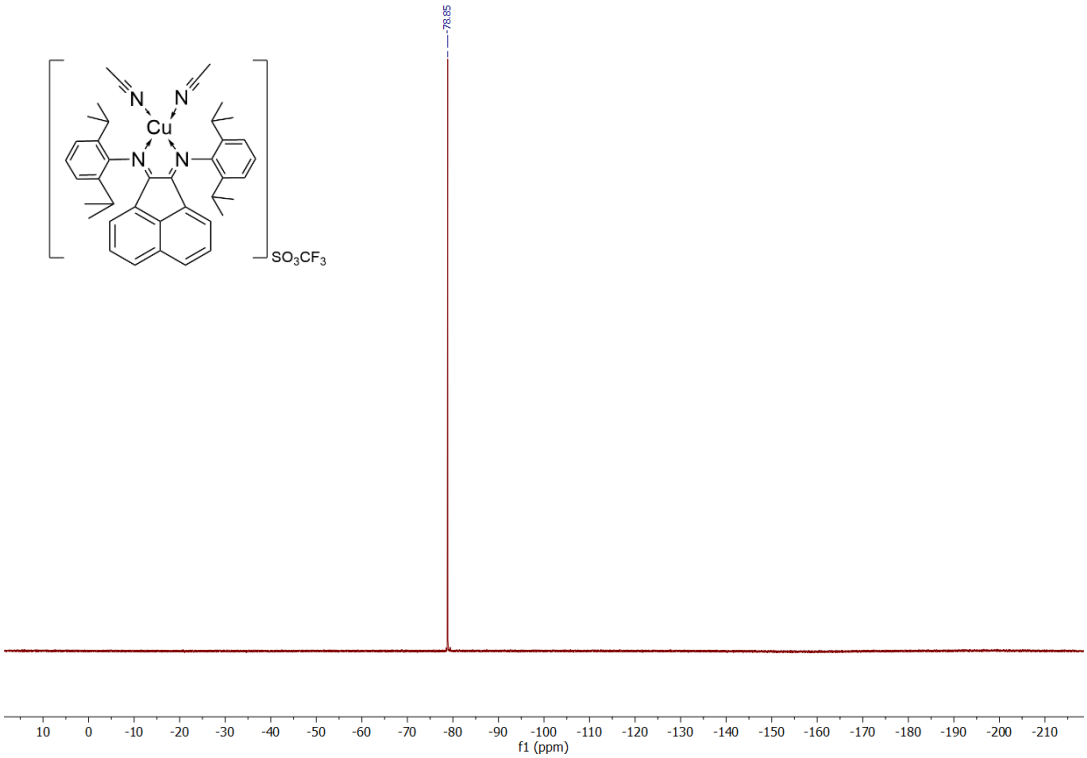

Figure A.33. ^{19}F NMR spectrum in CD_2Cl_2 of the **C3** complex.

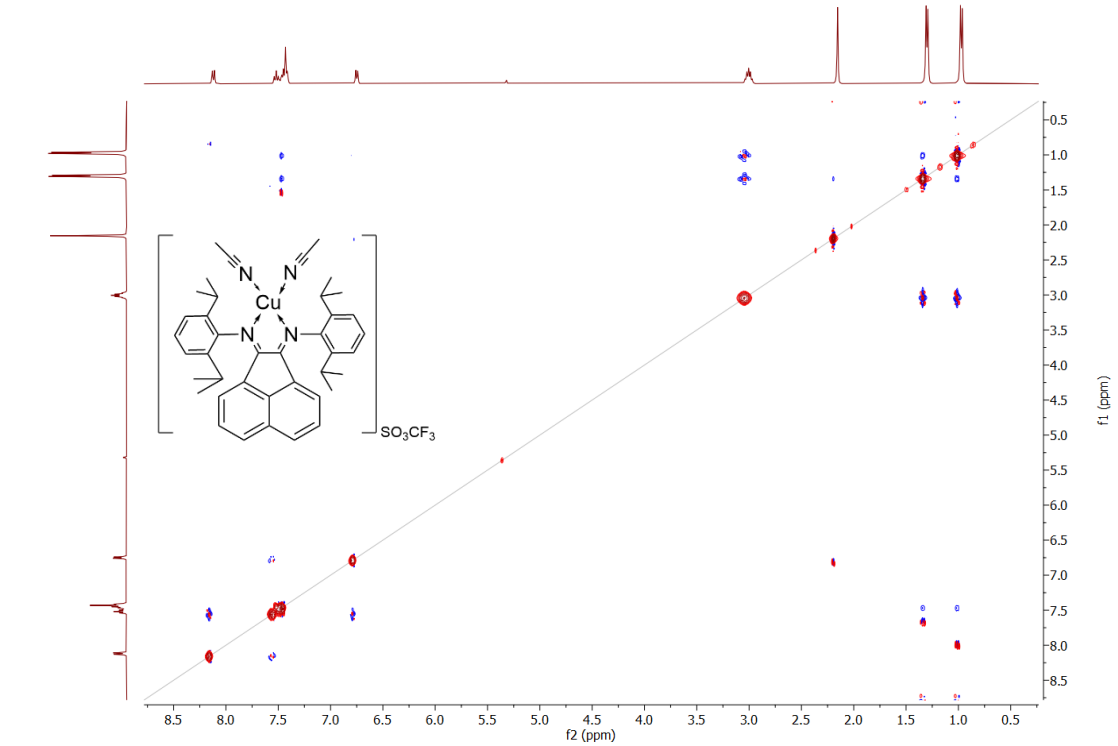

Figure A.34. COSY spectrum in CD_2Cl_2 of the **C3** complex.

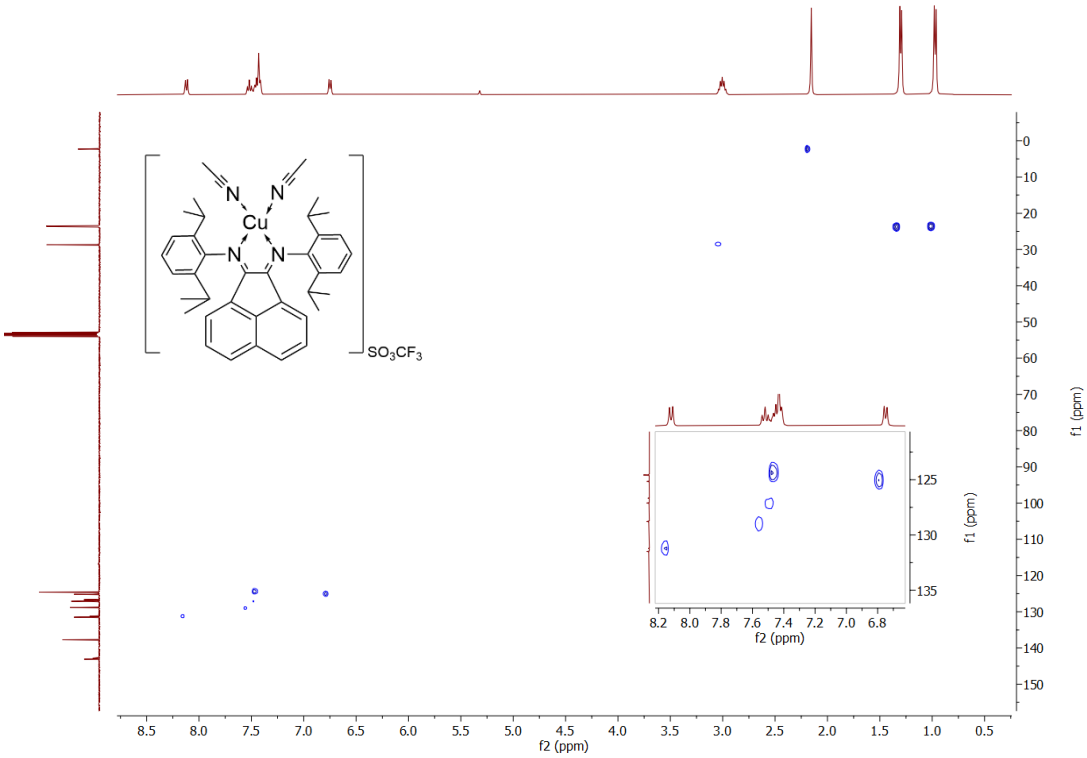

Figure A.35. HSQC spectrum in CD_2Cl_2 of the **C3** complex.

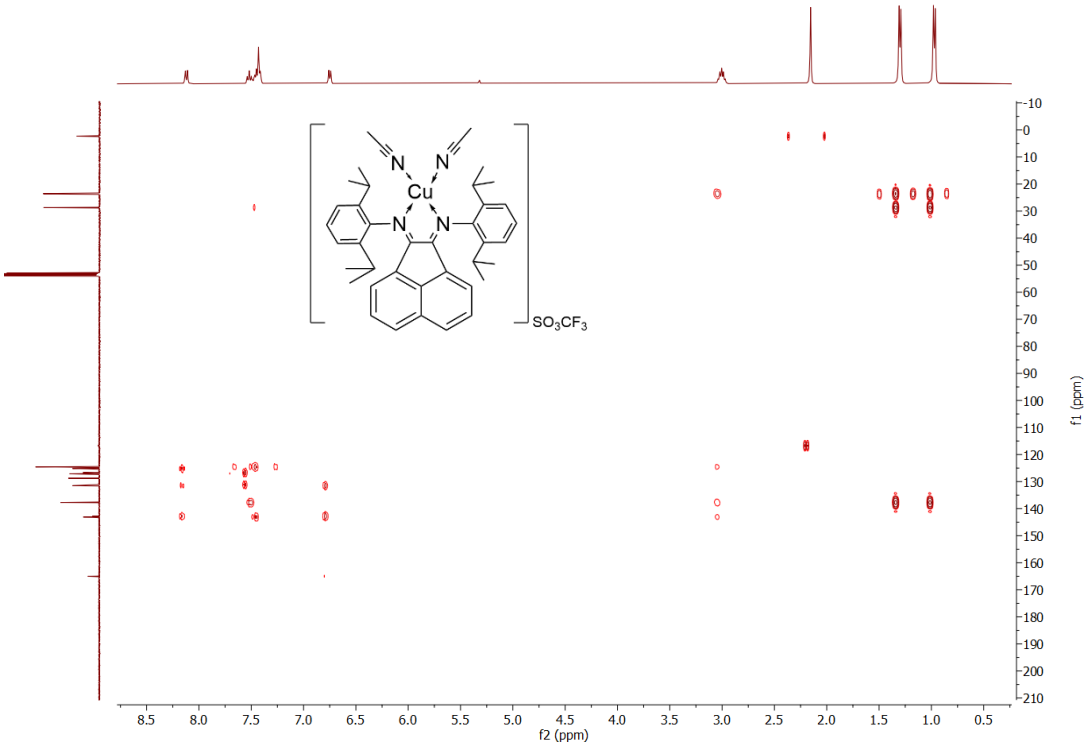

Figure A.36. HMBC spectrum in CD_2Cl_2 of the **C3** complex.

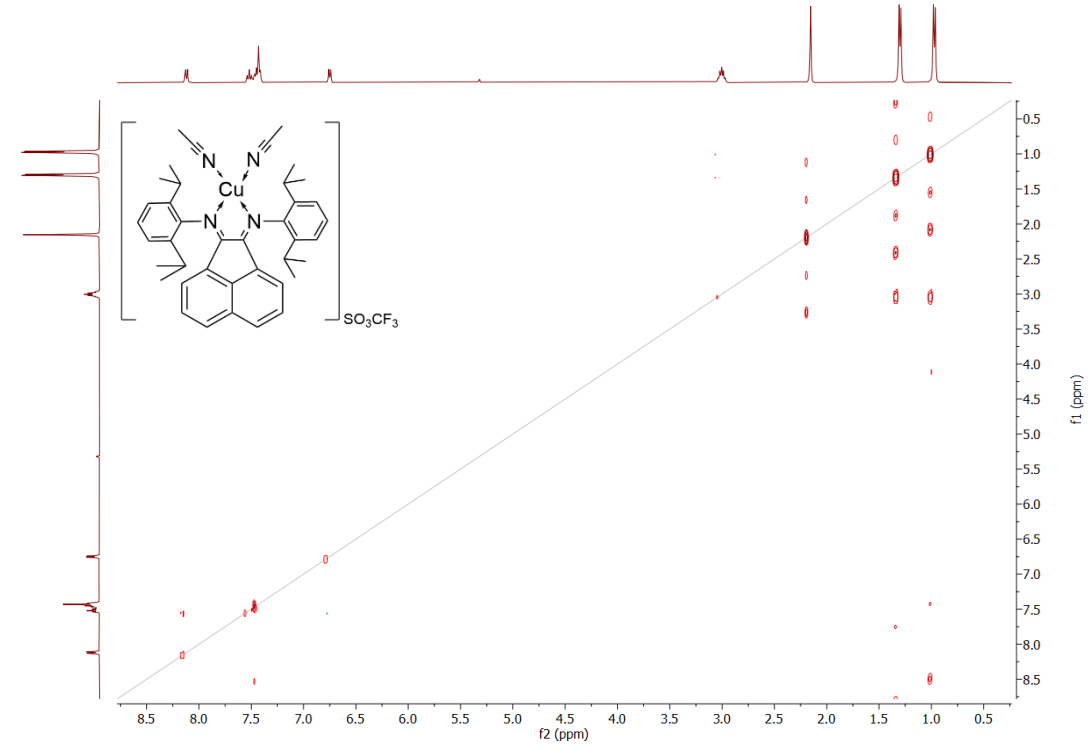

Figure A.37. NOESY spectrum in CD_2Cl_2 of the **C3** complex.

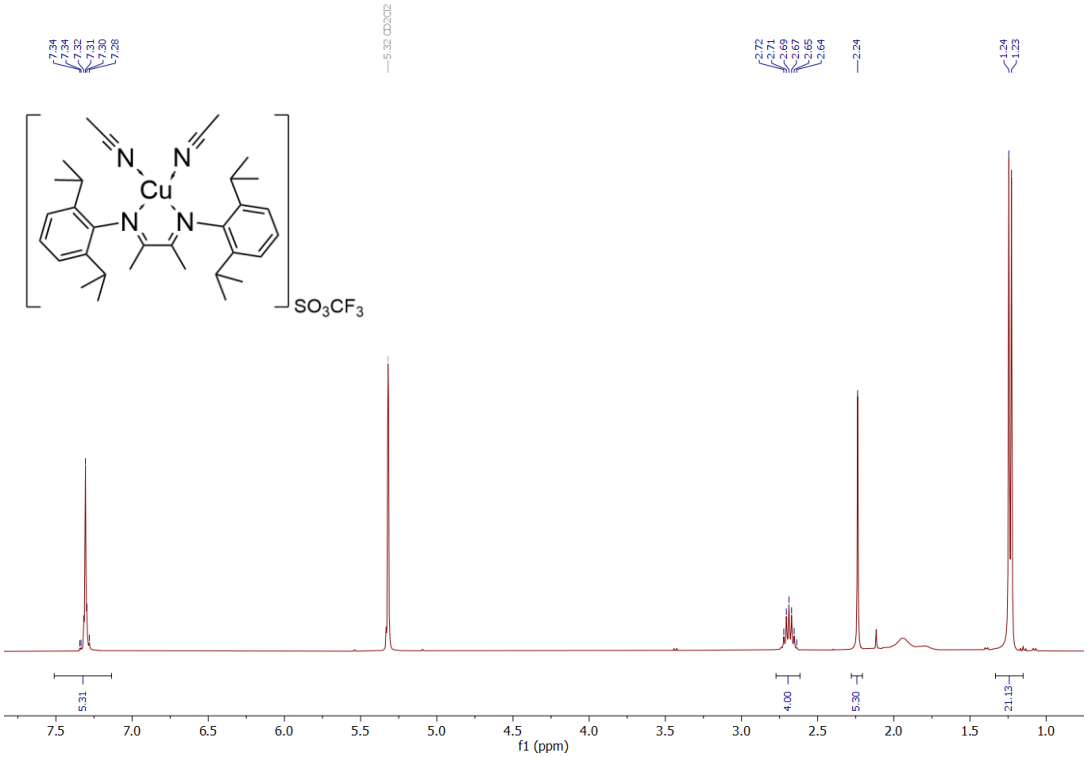

Figure A.38. ^{1}H NMR spectrum in CD_2Cl_2 of the **C4** complex.

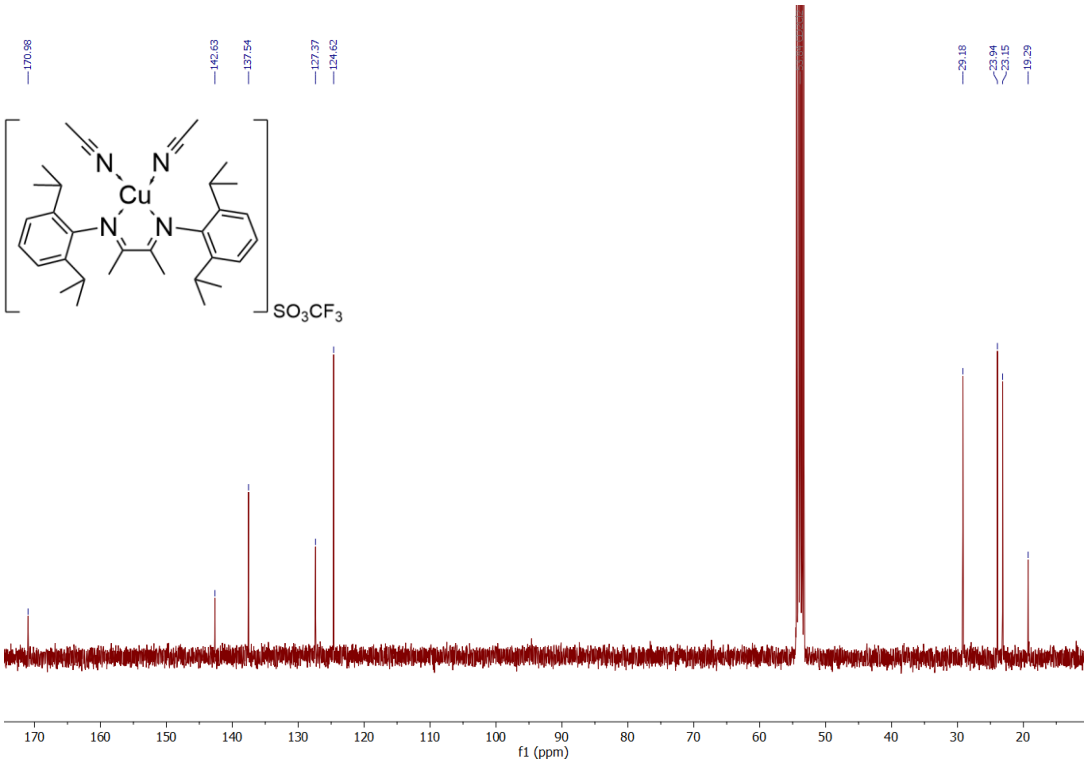

Figure A.39. ^{13}C NMR spectrum in CD_2Cl_2 of the **C4** complex.

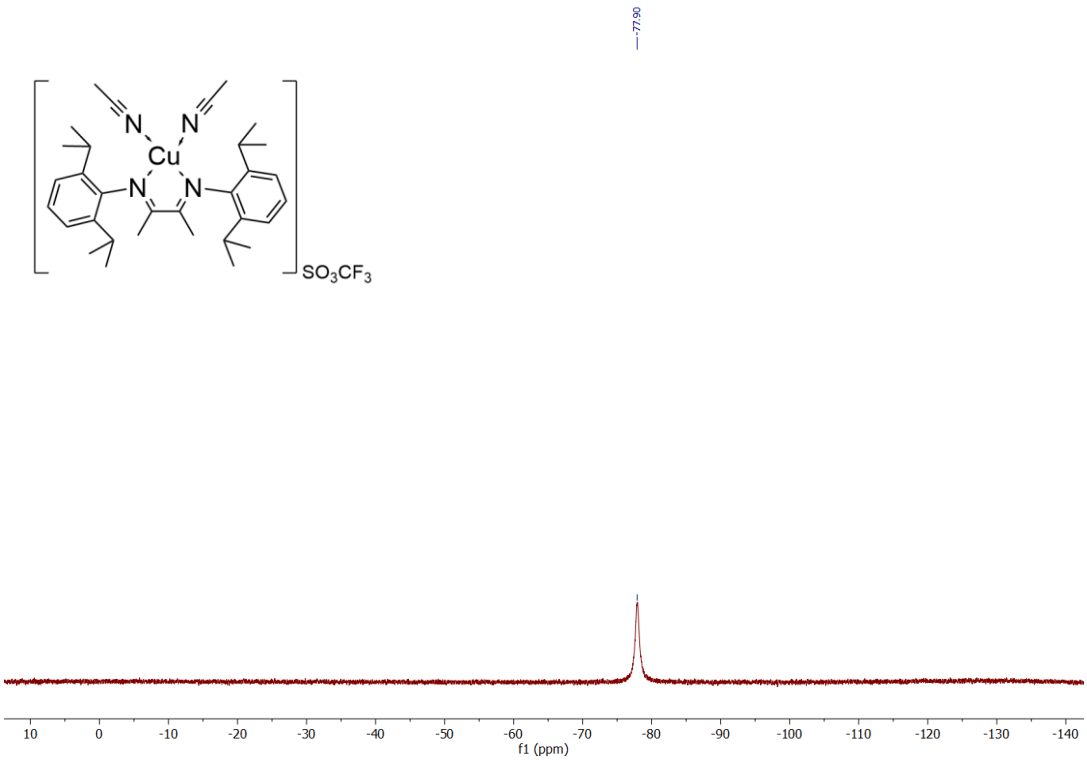

Figure A.40. ^{19}F NMR spectrum in CD_2Cl_2 of the **C4** complex.

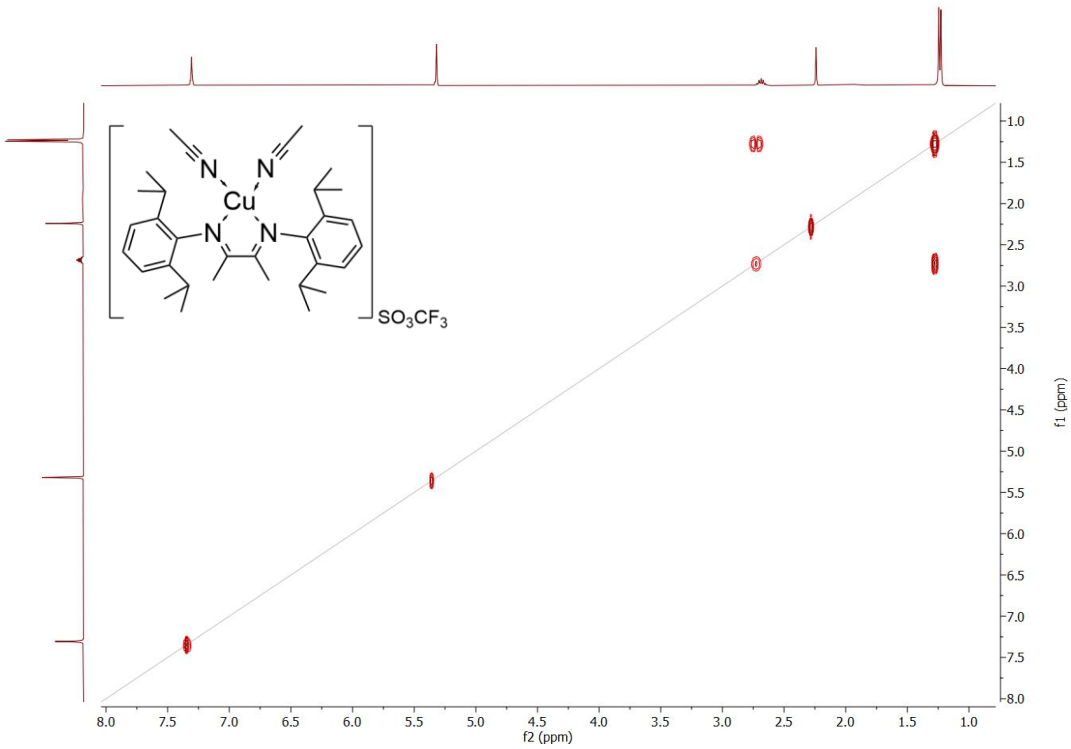

Figure A.41. COSY spectrum in CD_2Cl_2 of the **C4** complex.

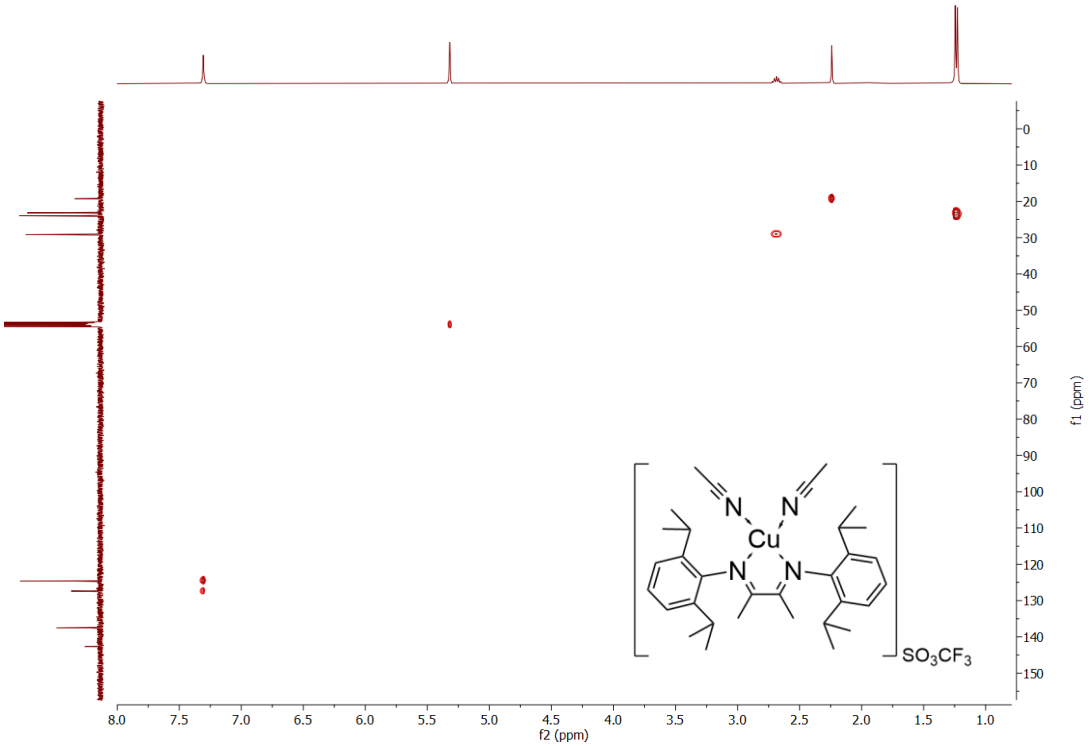

Figure A.42. HSQC spectrum in CD_2Cl_2 of the **C4** complex.

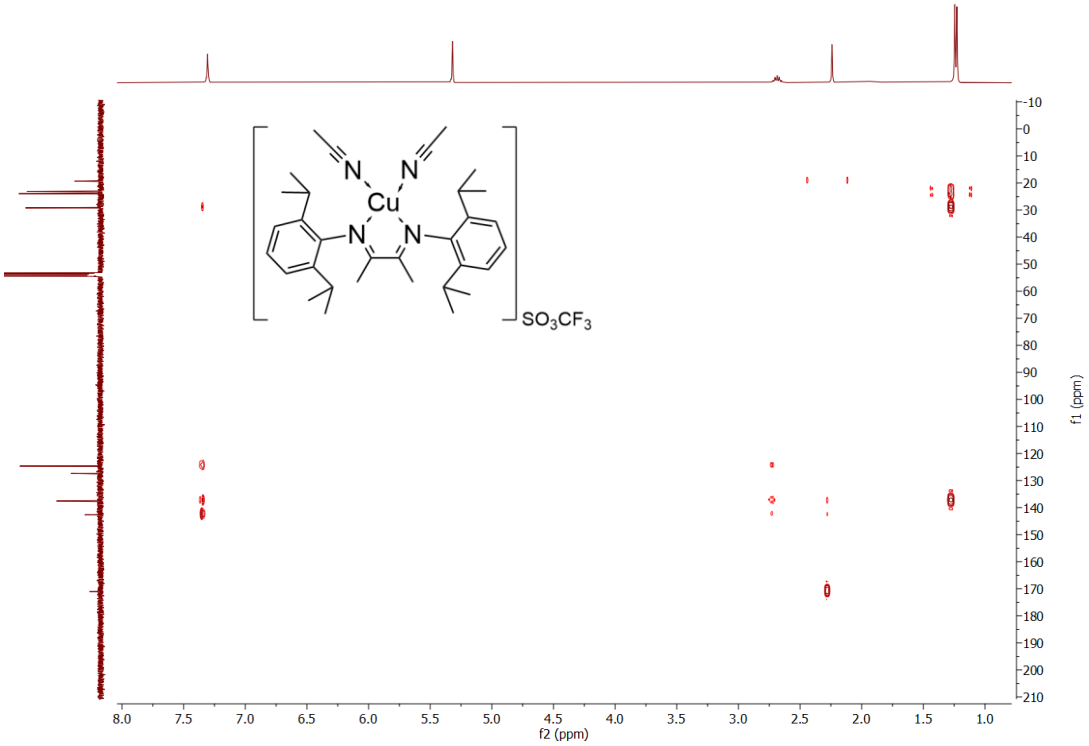

Figure A.43. HMBC spectrum in CD_2Cl_2 of the **C4** complex.

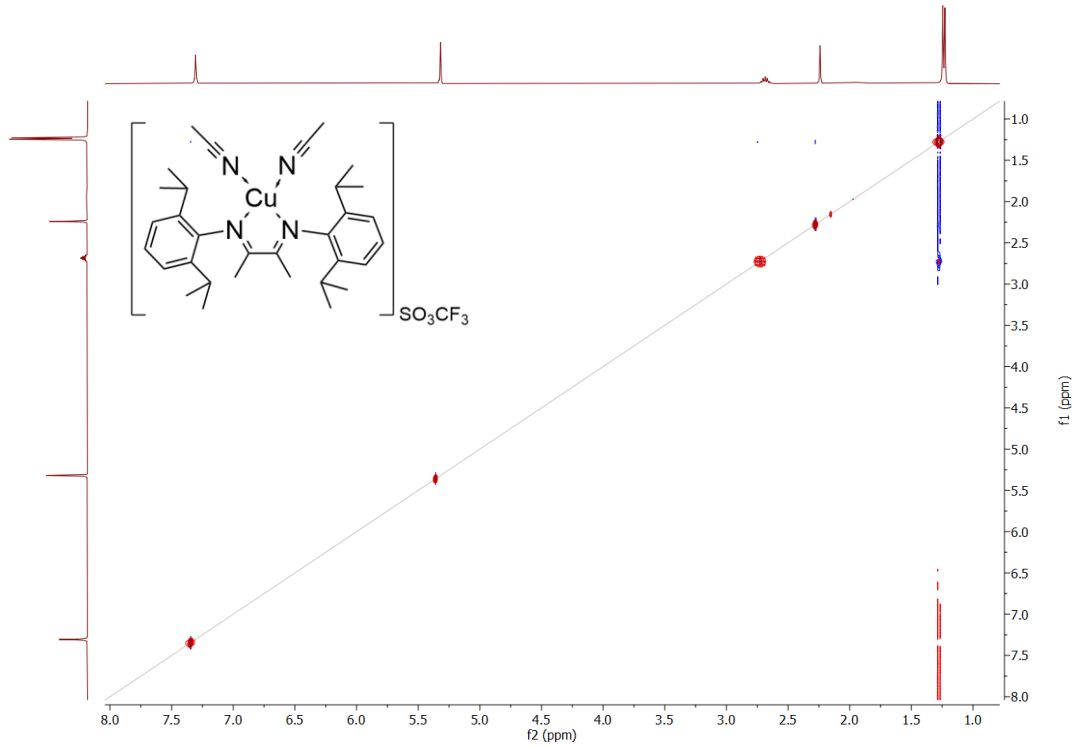

Figure A.44. NOESY spectrum in CD_2Cl_2 of the **C4** complex.

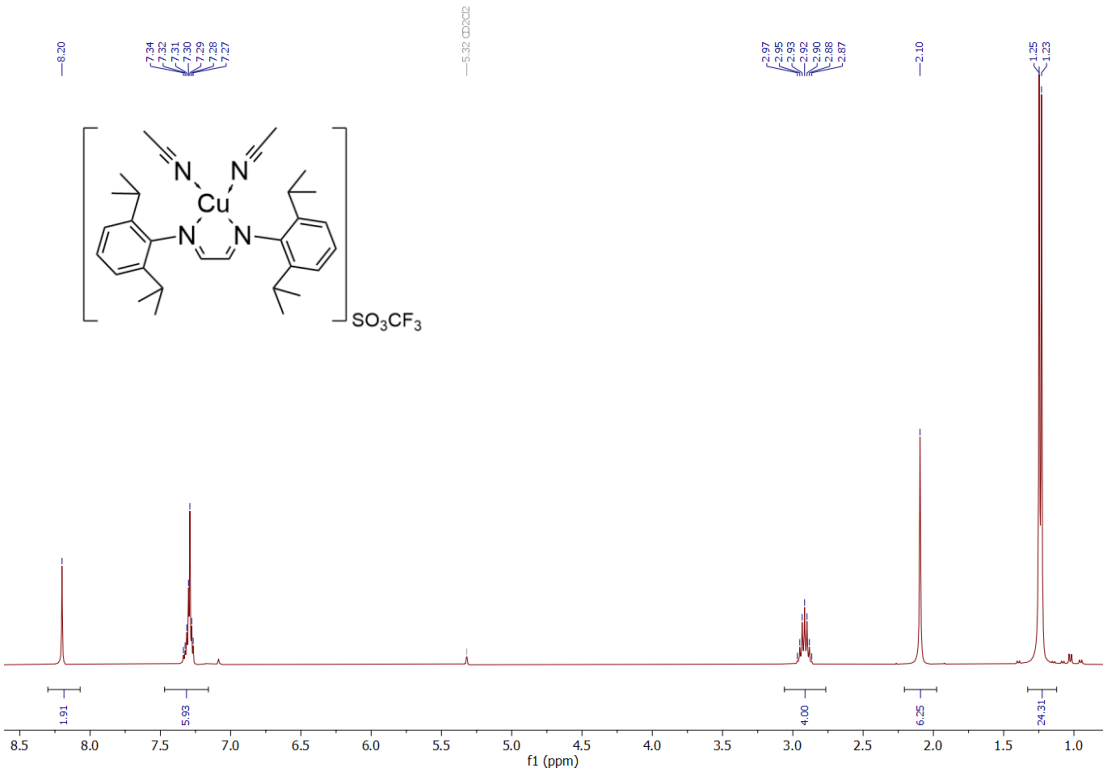

Figure A.45. ^1H NMR spectrum in CD_2Cl_2 of the **C5** complex.

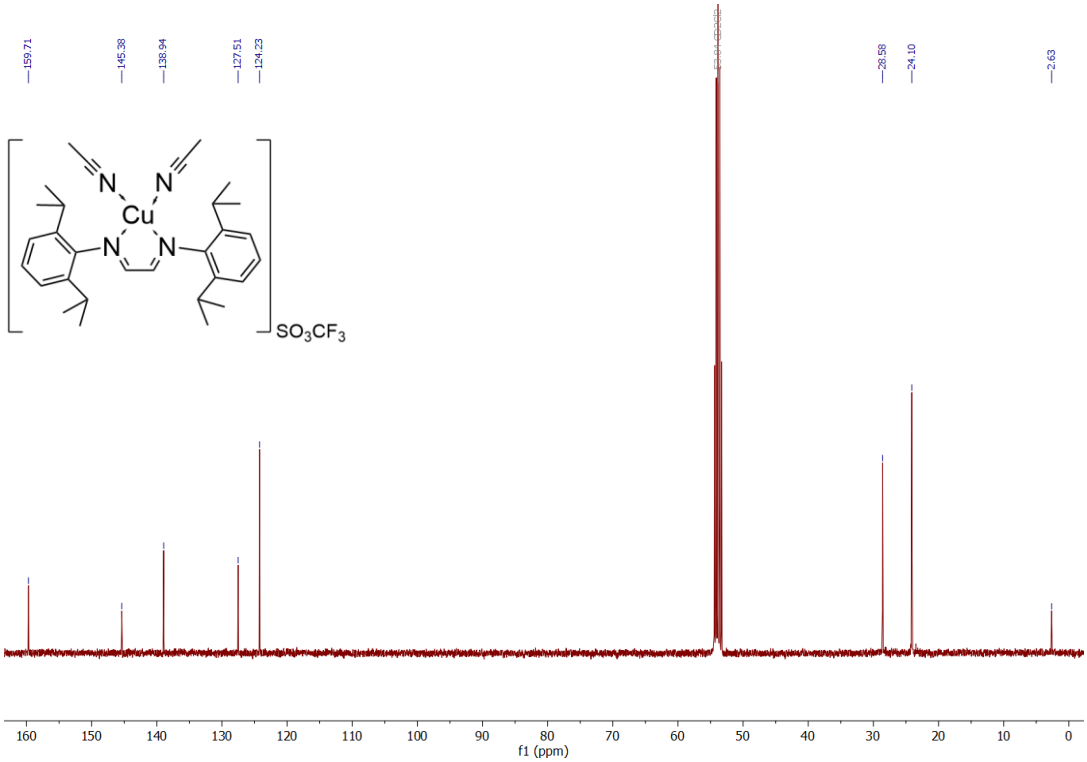

Figure A.46. ^{13}C NMR spectrum in CD_2Cl_2 of the **C5** complex.

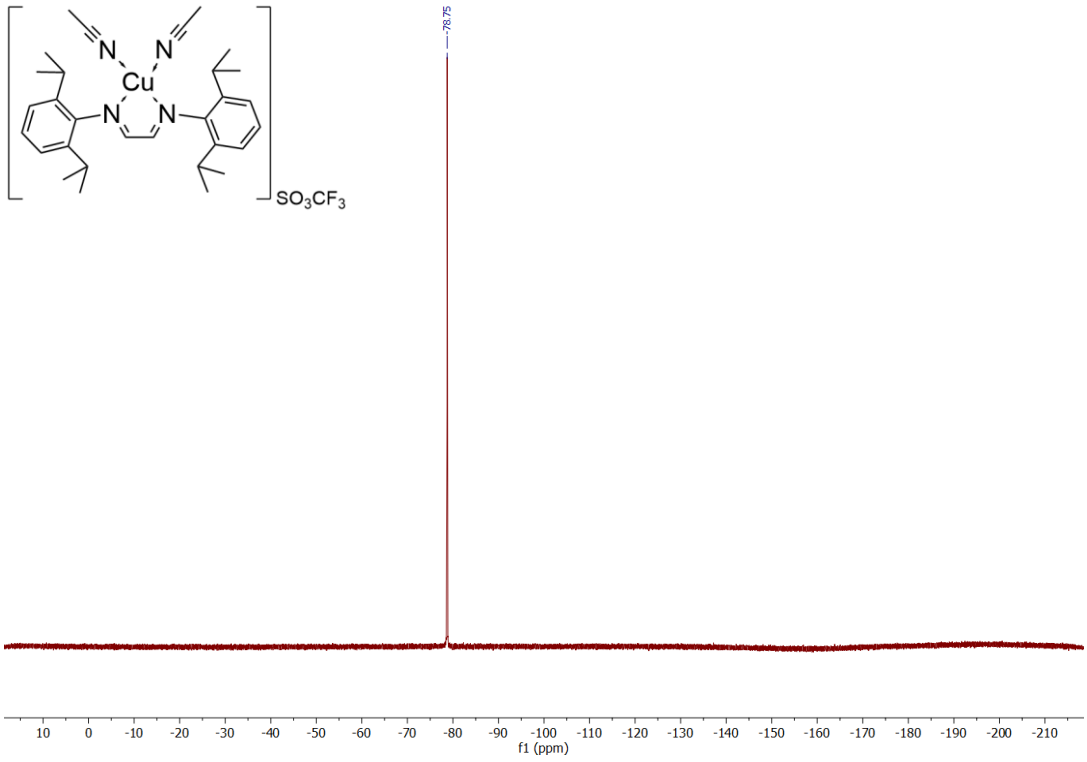

Figure A.47. ^{19}F NMR spectrum in CD_2Cl_2 of the **C5** complex.

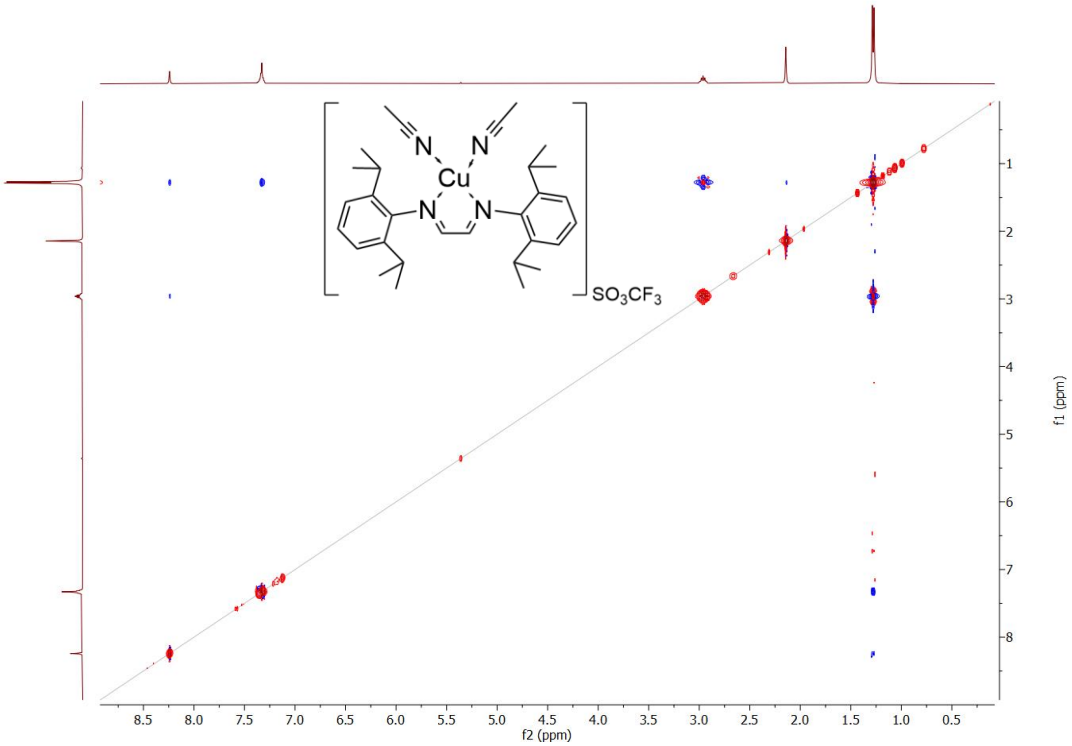

Figure A.48. COSY spectrum in CD_2Cl_2 of the **C5** complex.

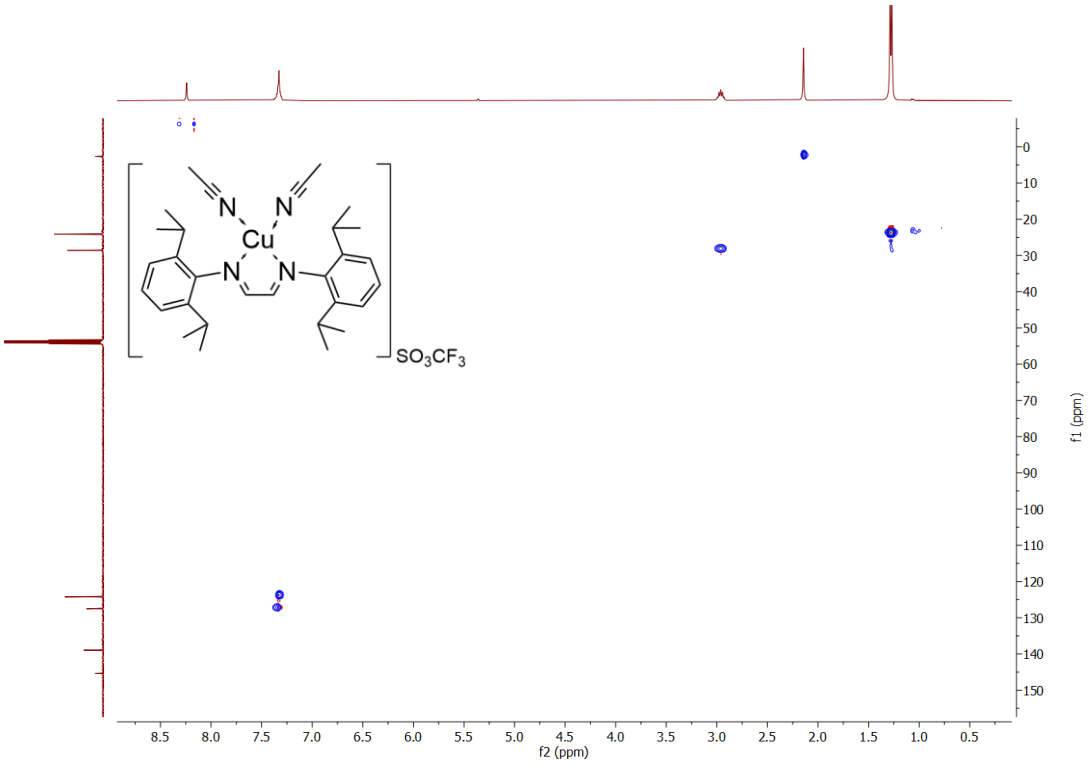

Figure A.49. HSQC spectrum in CD_2Cl_2 of the **C5** complex.

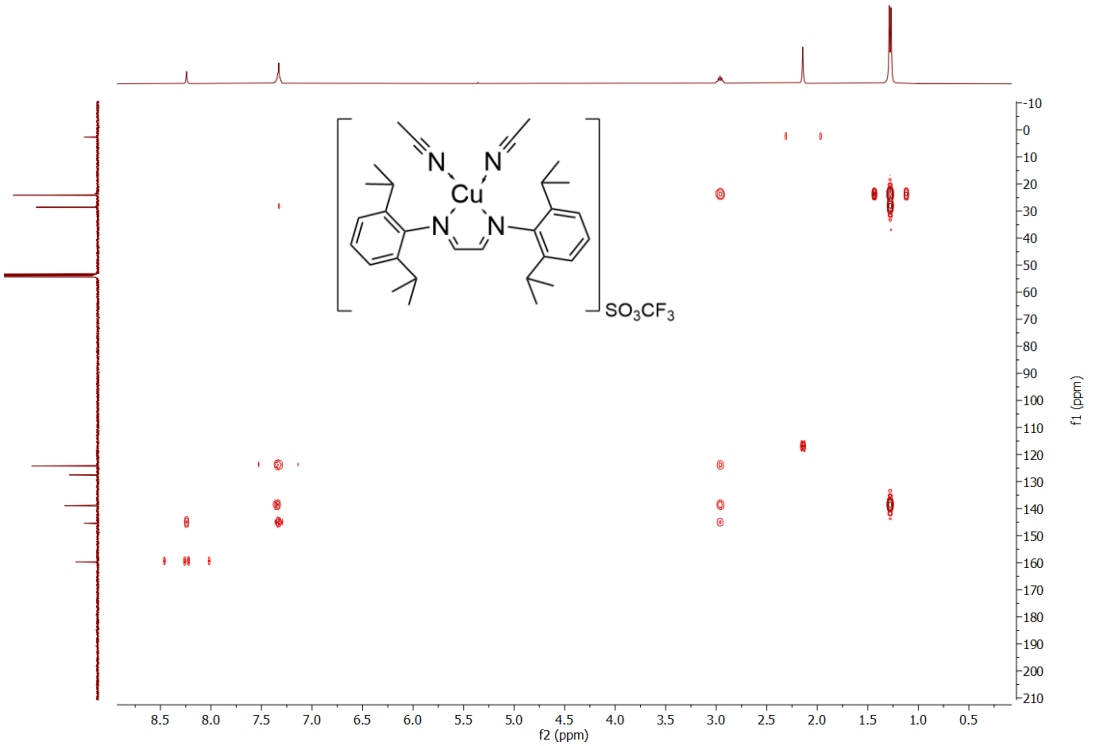

Figure A.50. HMBC spectrum in CD_2Cl_2 of the **C5** complex.

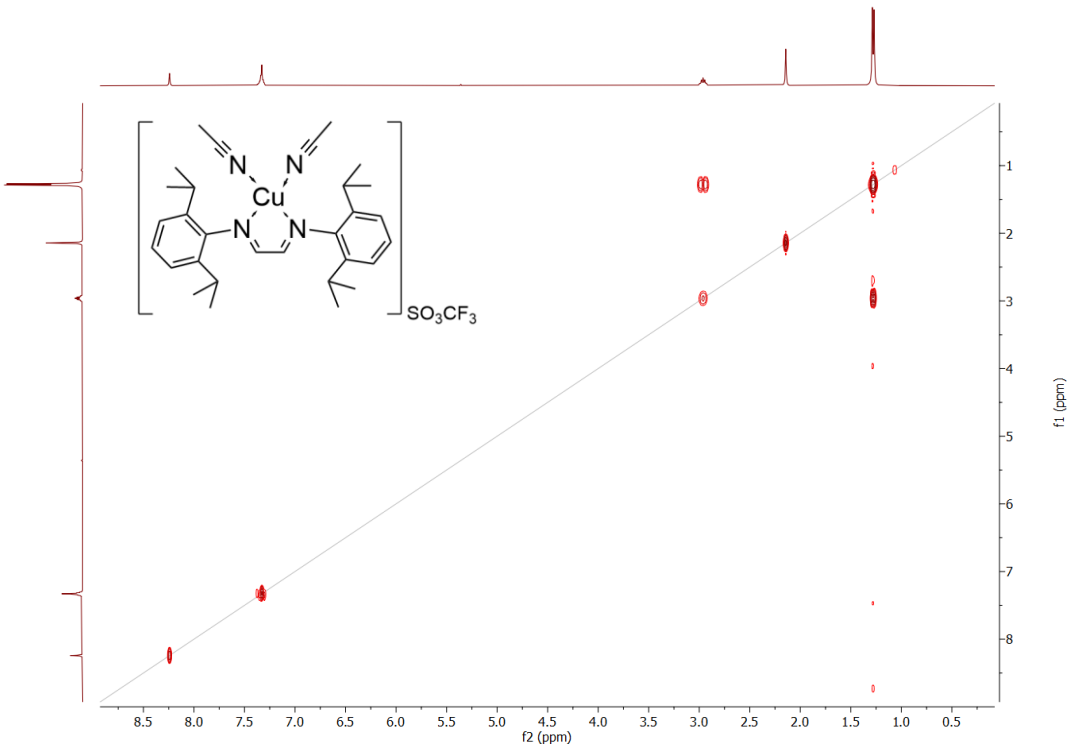

Figure A.51. NOESY spectrum in CD_2Cl_2 of the **C5** complex.

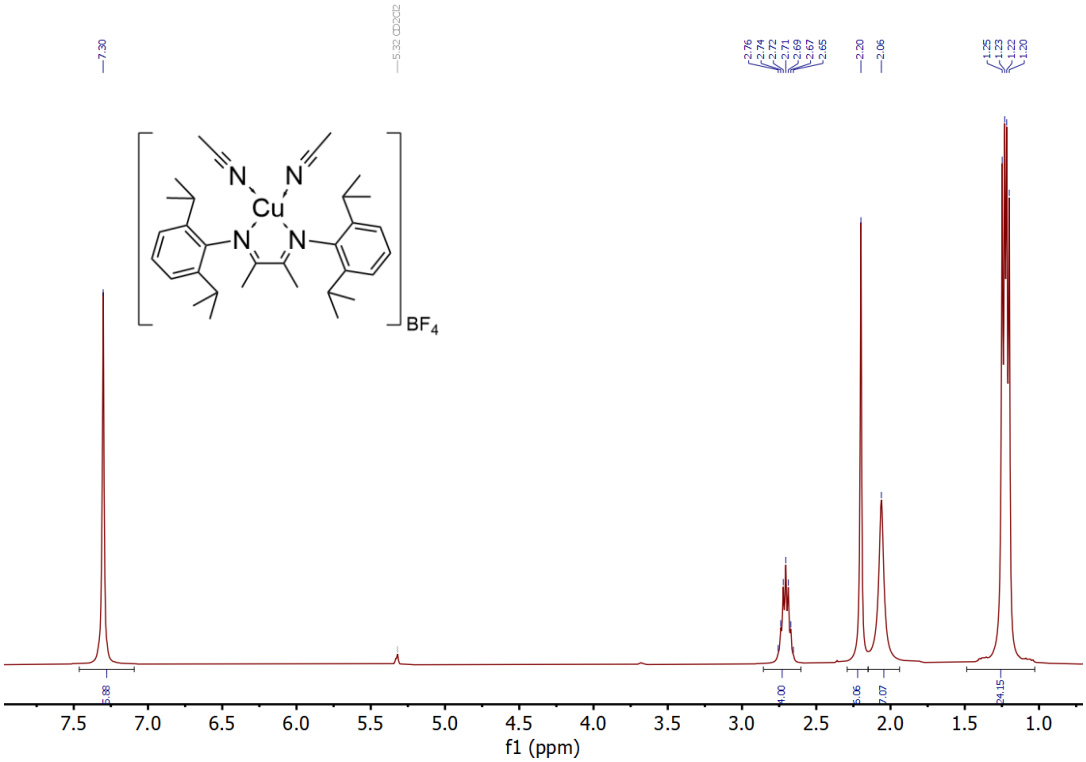

Figure A.52. ^{1}H NMR spectrum in CD_2Cl_2 of **C6** complex.

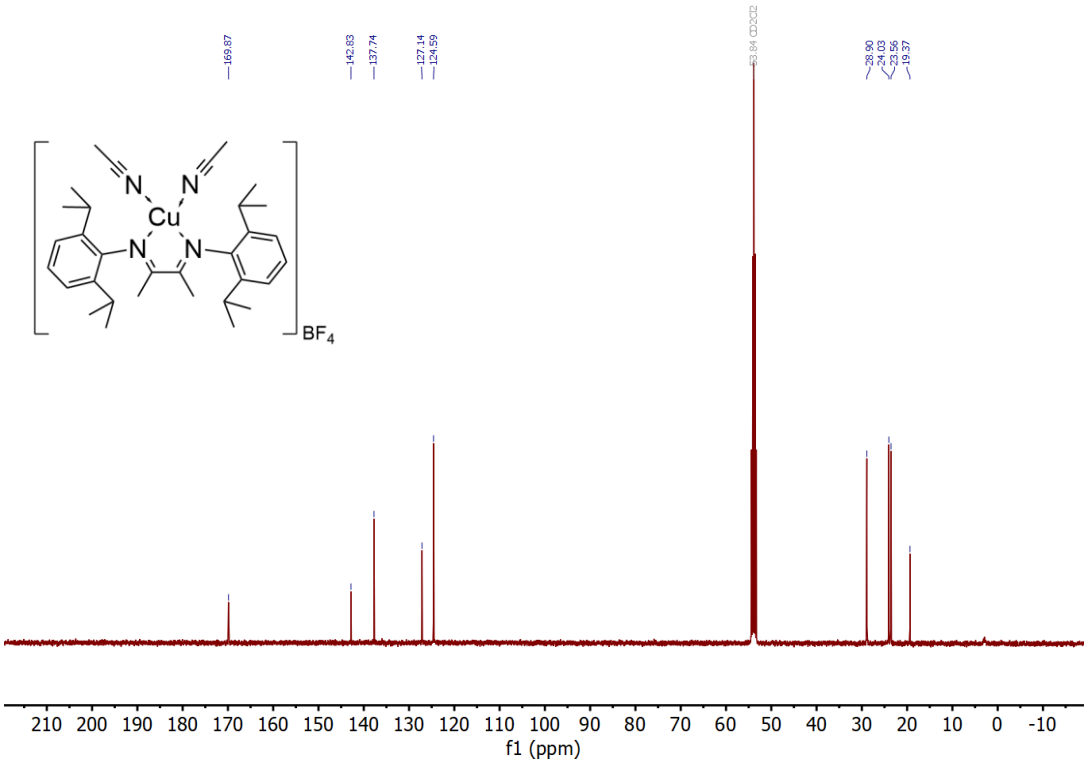

Figure A.53. ^{13}C NMR spectrum in CD_2Cl_2 of the **C6** complex.

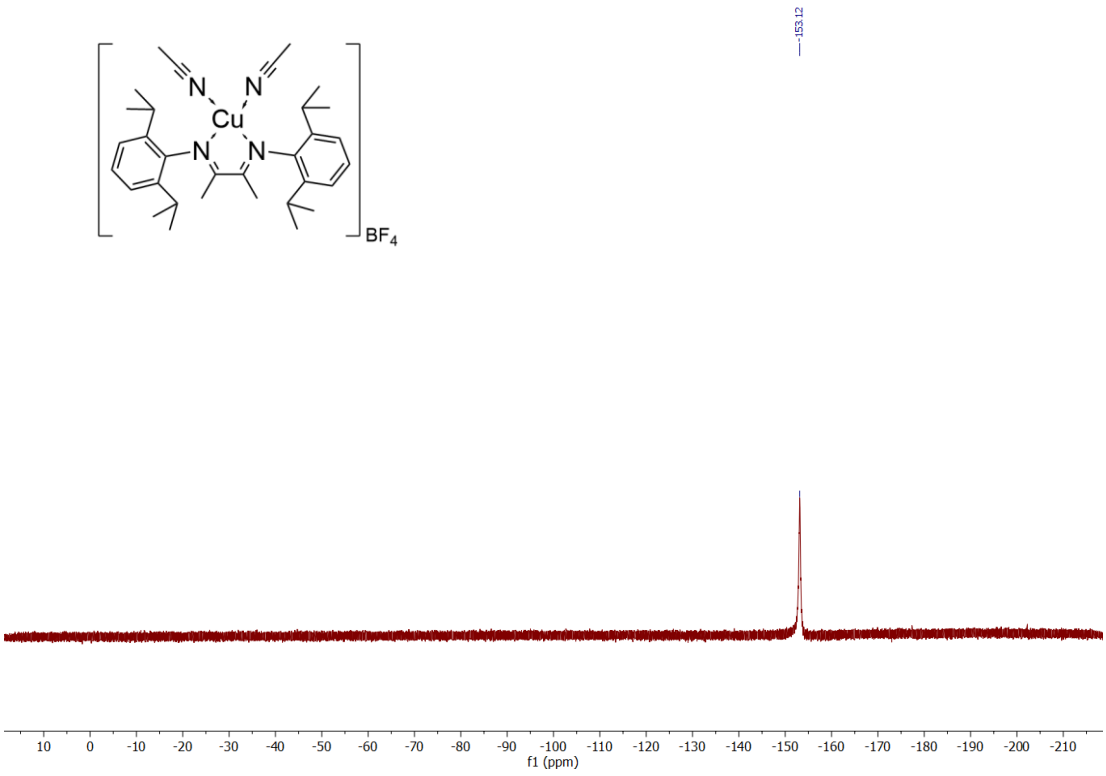

Figure A.54. ^{19}F NMR spectrum in CD_2Cl_2 of the synthesised **C6** complex.

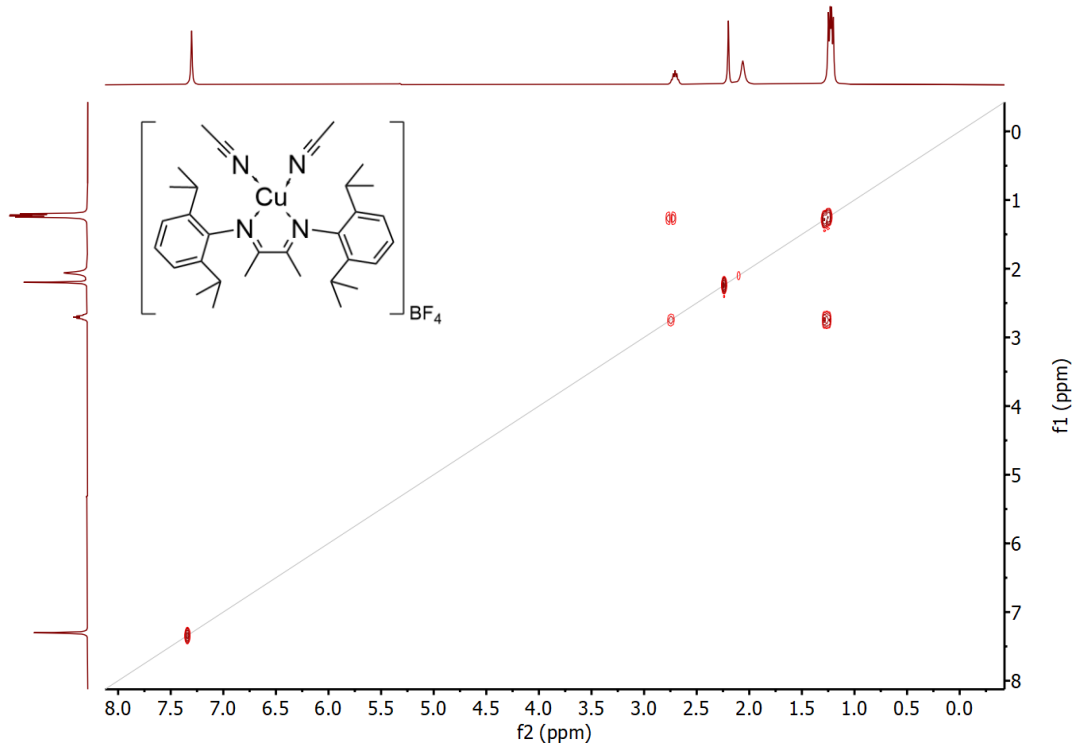

Figure A.55. COSY spectrum in CD_2Cl_2 of the **C6** complex.

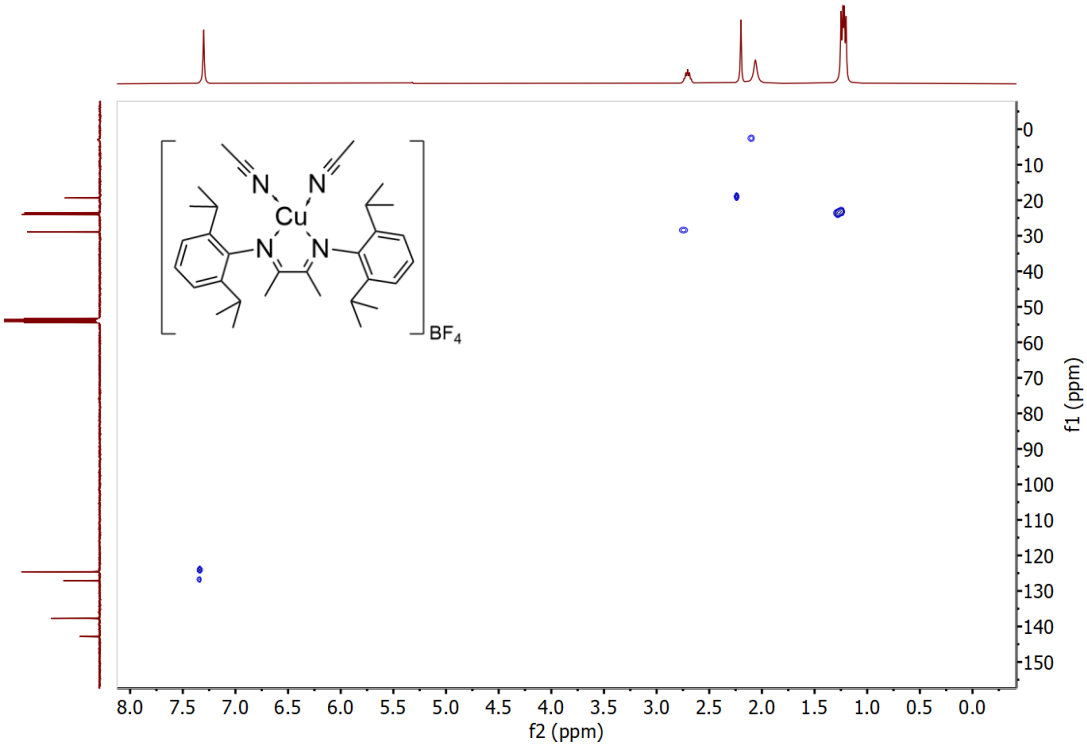

Figure A.56. HSQC spectrum in CD_2Cl_2 of the **C6** complex.

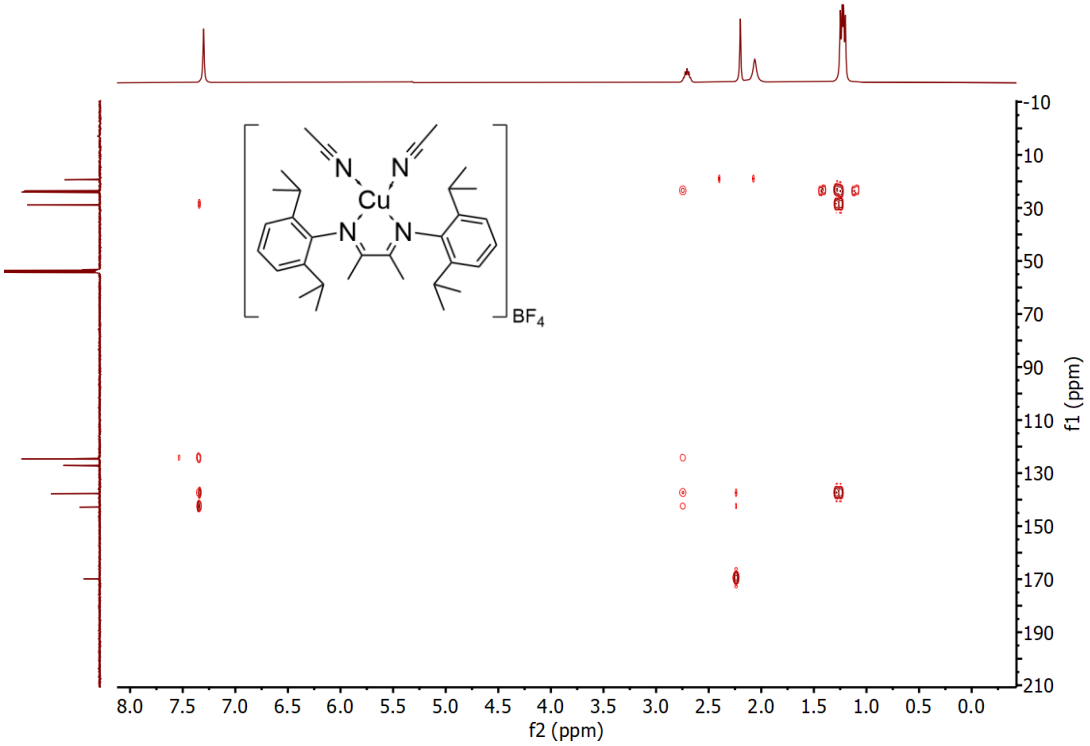

Figure A.57. HMBC spectrum in CD_2Cl_2 of the **C6** complex.

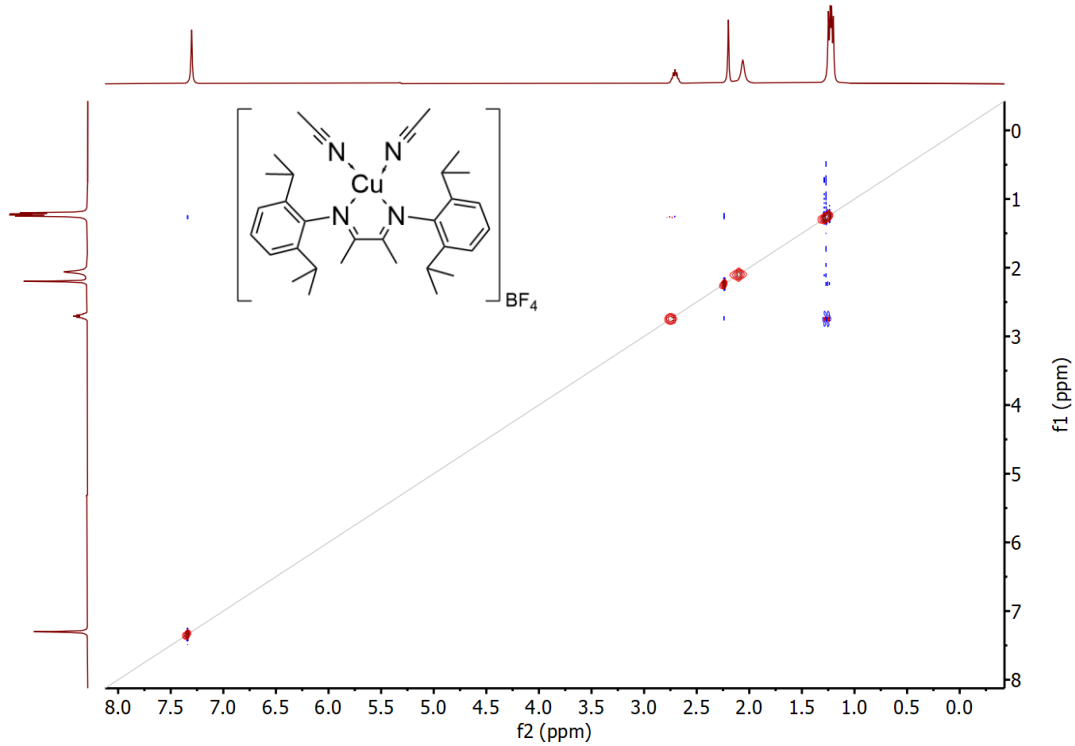

Figure A.58. NOESY spectrum in CD_2Cl_2 of the **C6** complex.

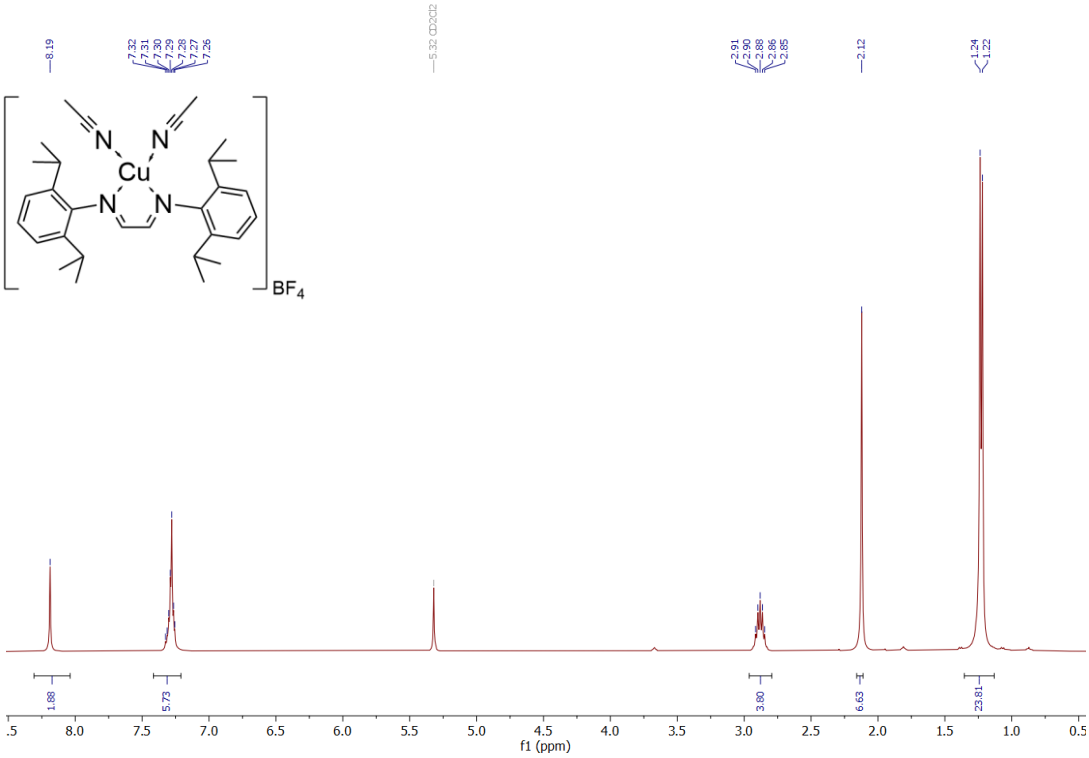

Figure A.59.^{1}H NMR spectrum in CD_2Cl_2 of the **C7** complex.

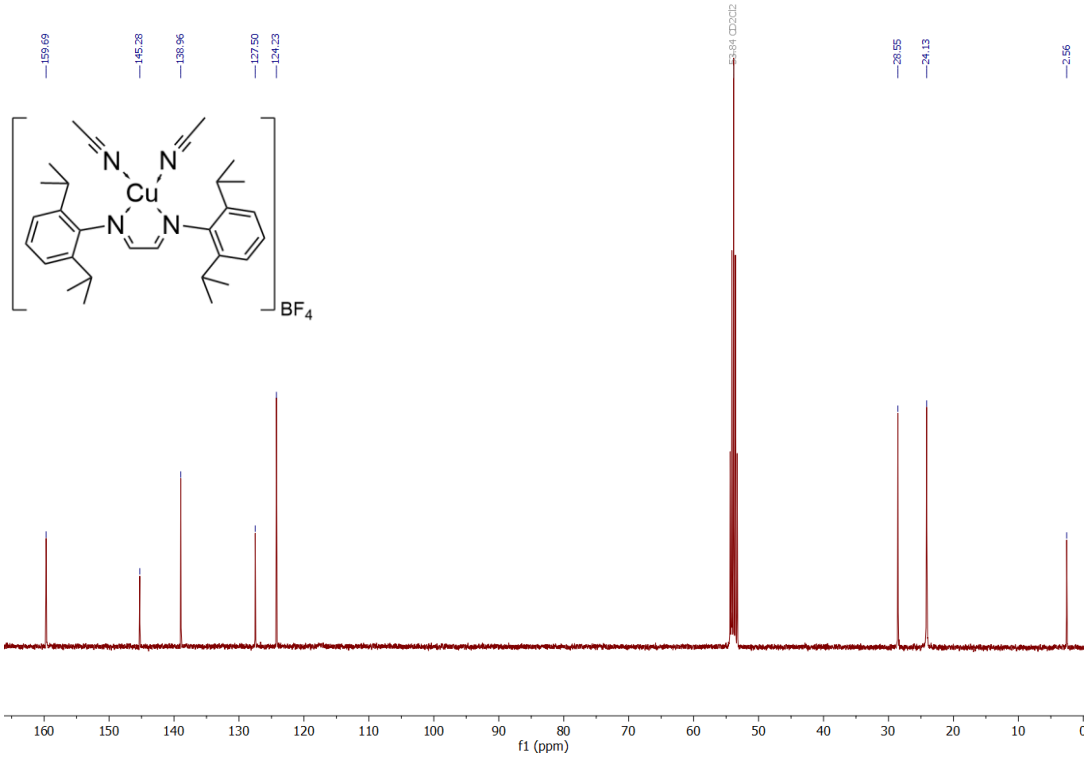

Figure A.60. ^{13}C NMR spectrum in CD_2Cl_2 of the **C7** complex.

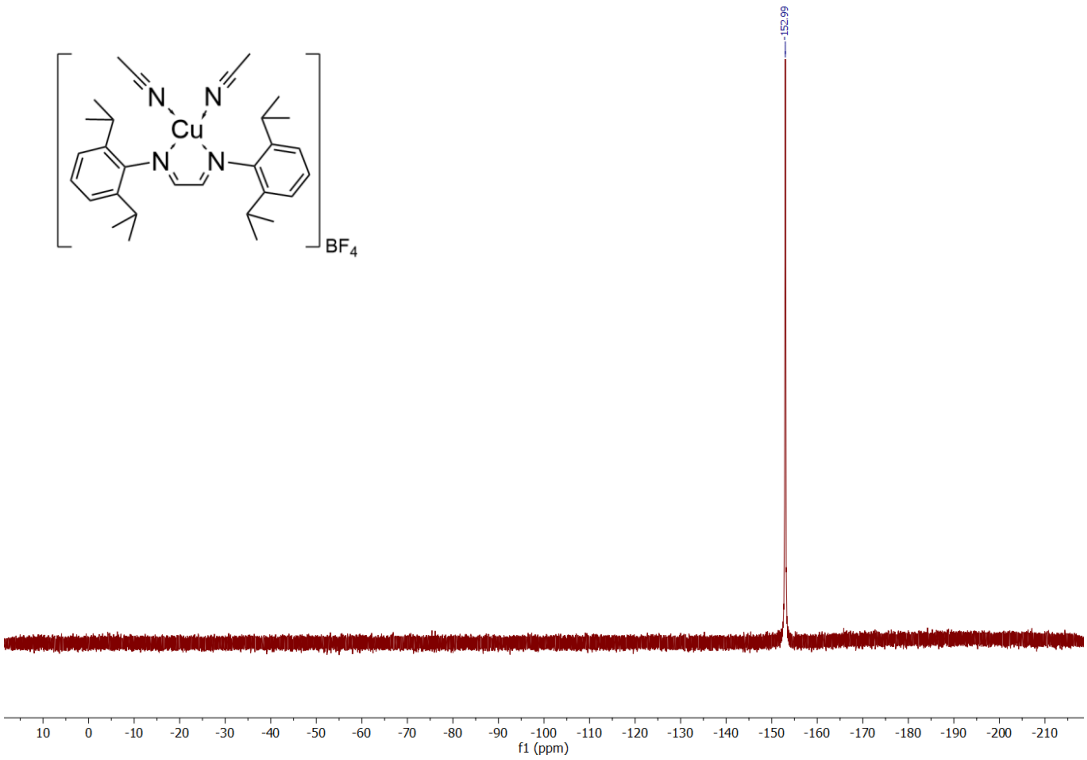

Figure A.61. ^{19}F NMR spectrum in CD_2Cl_2 of the **C7** complex.

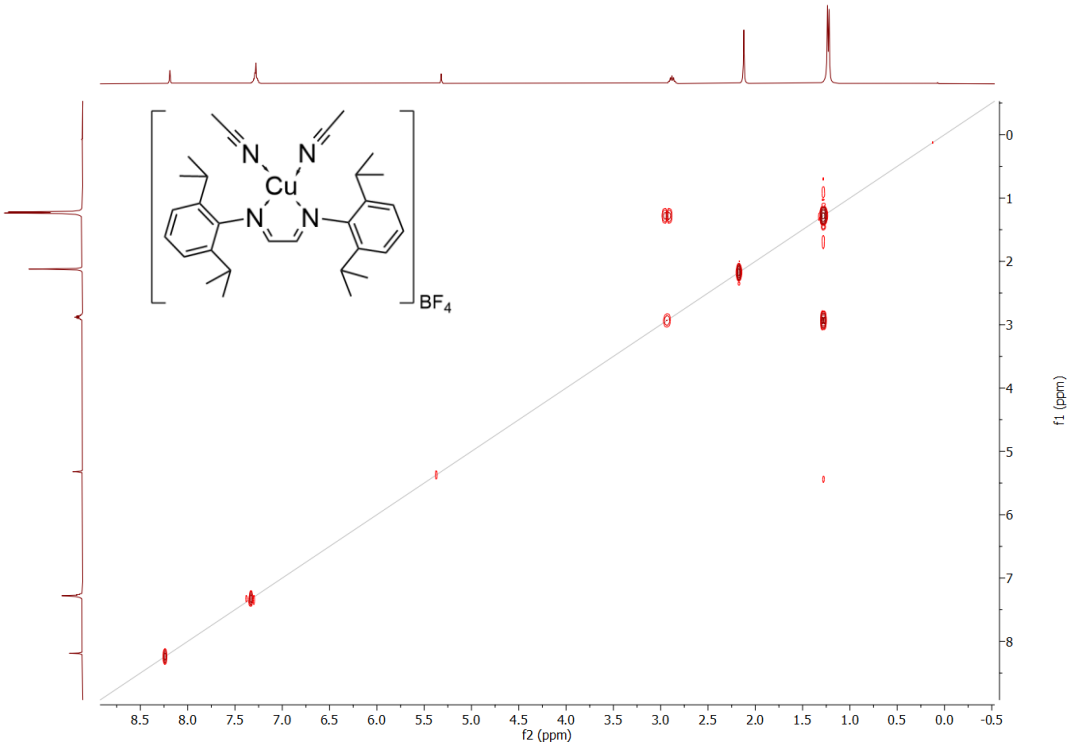

Figure A.62. COSY spectrum in CD_2Cl_2 of the **C7** complex.

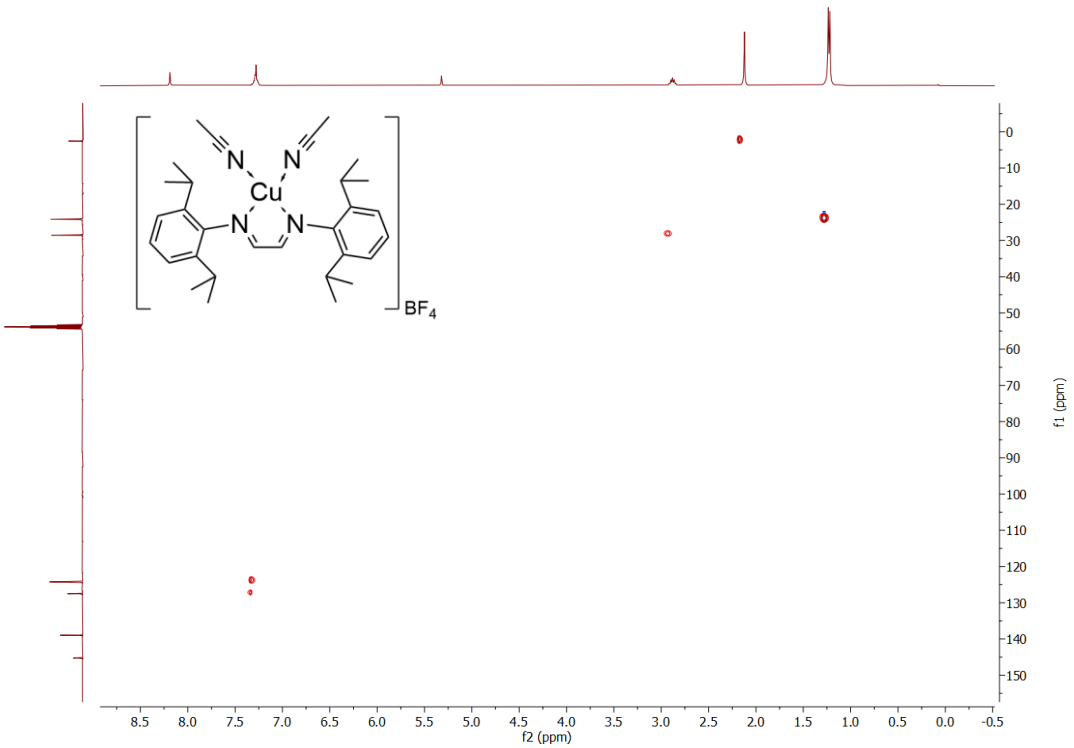

Figure A.63. HSQC spectrum in CD_2Cl_2 of the **C7** complex.

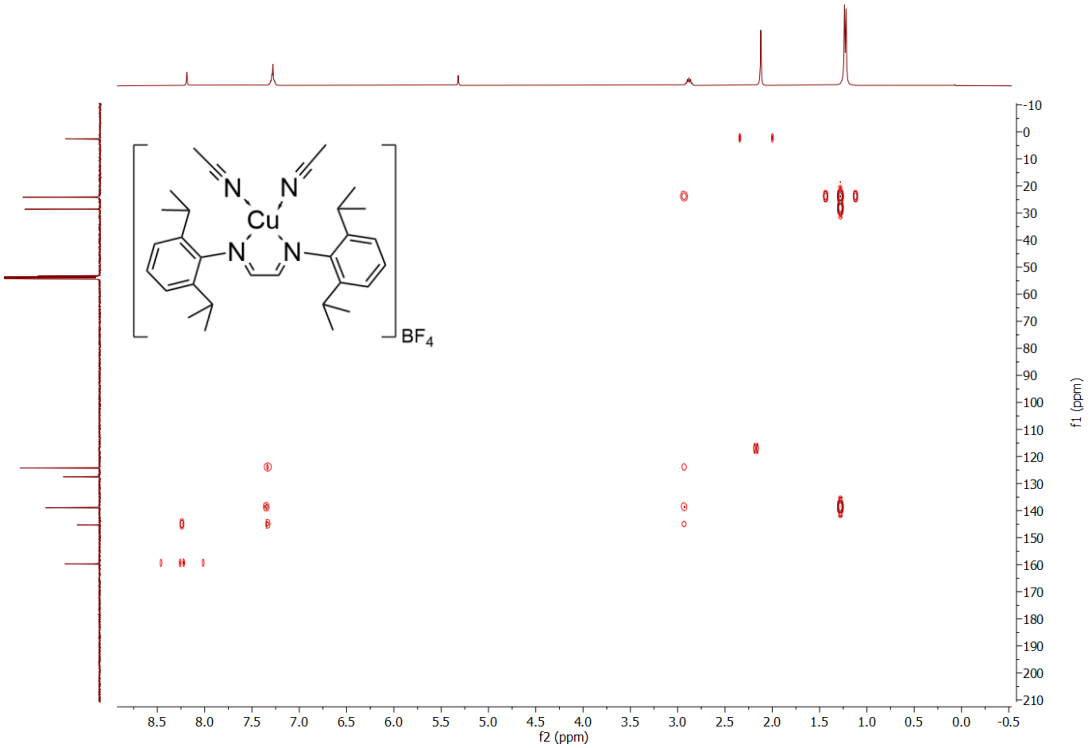

Figure A.64. HMBC spectrum in CD_2Cl_2 of the **C7** complex.

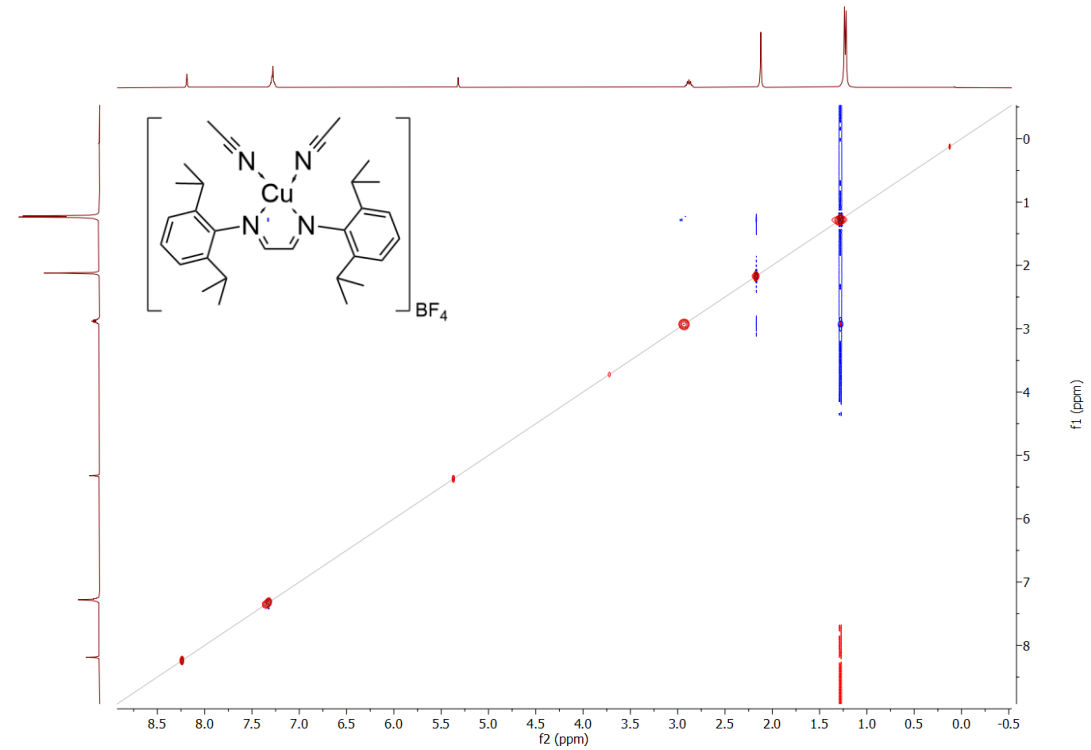

Figure A.65. NOESY spectrum in CD_2Cl_2 of the **C7** complex.

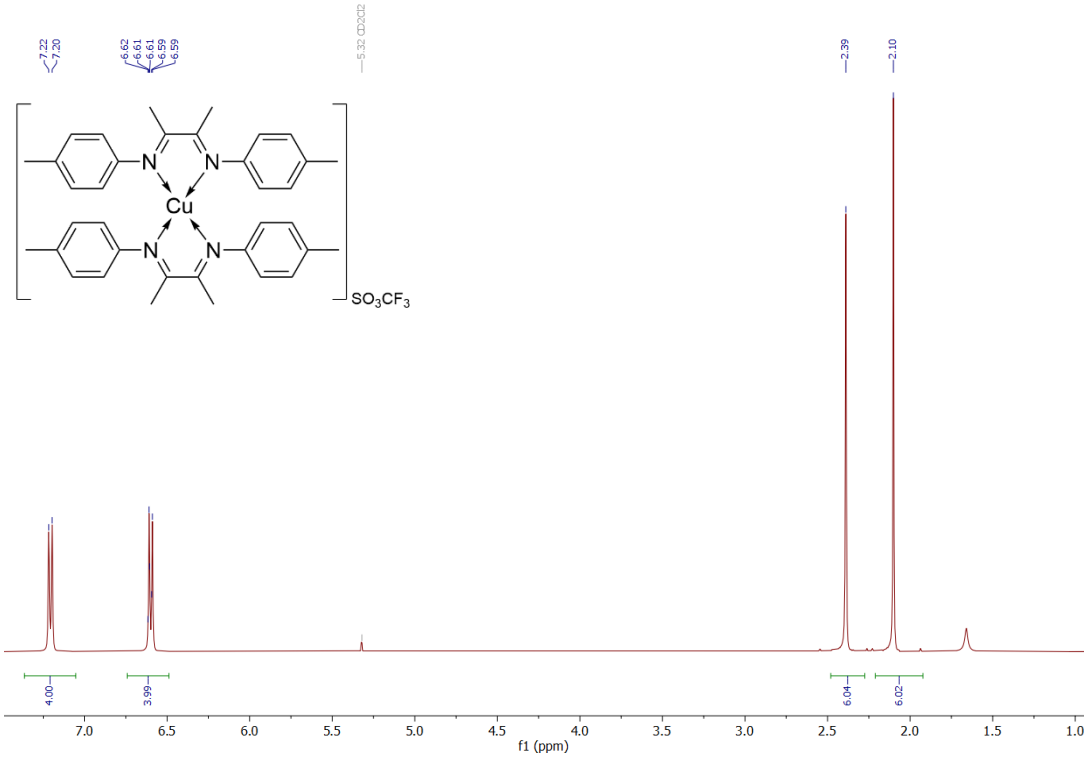

Figure A.66. ^{1}H NMR spectrum in CD_2Cl_2 of the **C8** complex.

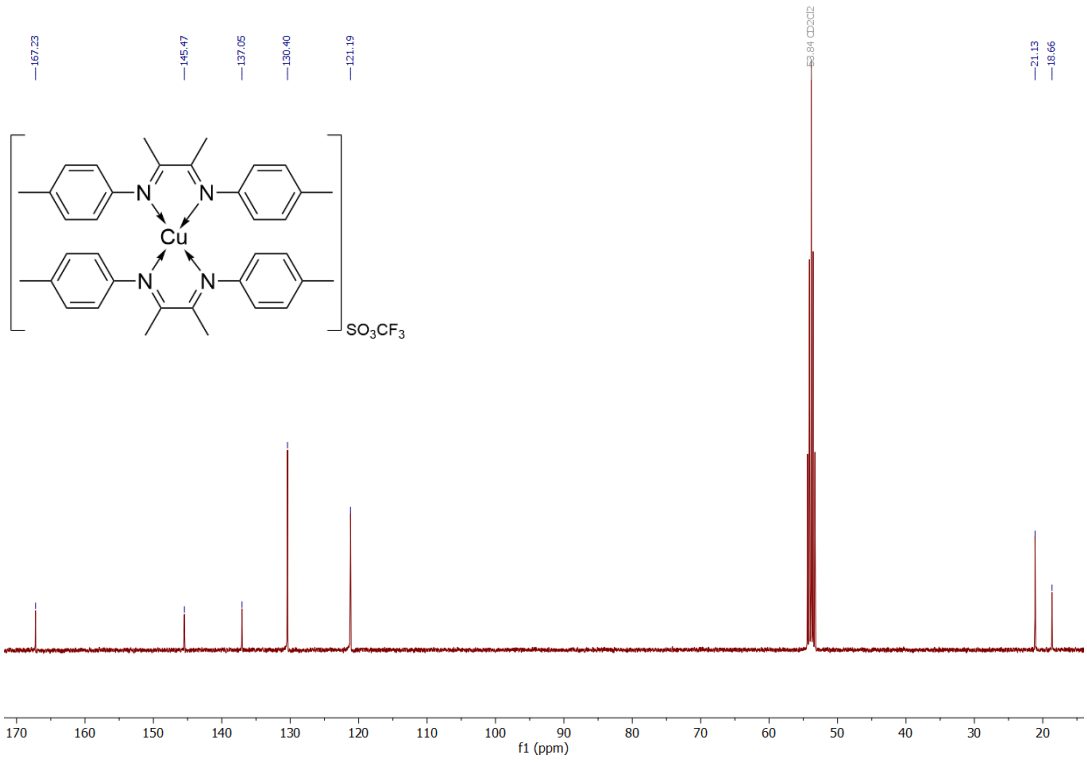

Figure A.67. ^{13}C NMR spectrum in CD_2Cl_2 of the **C8** complex.

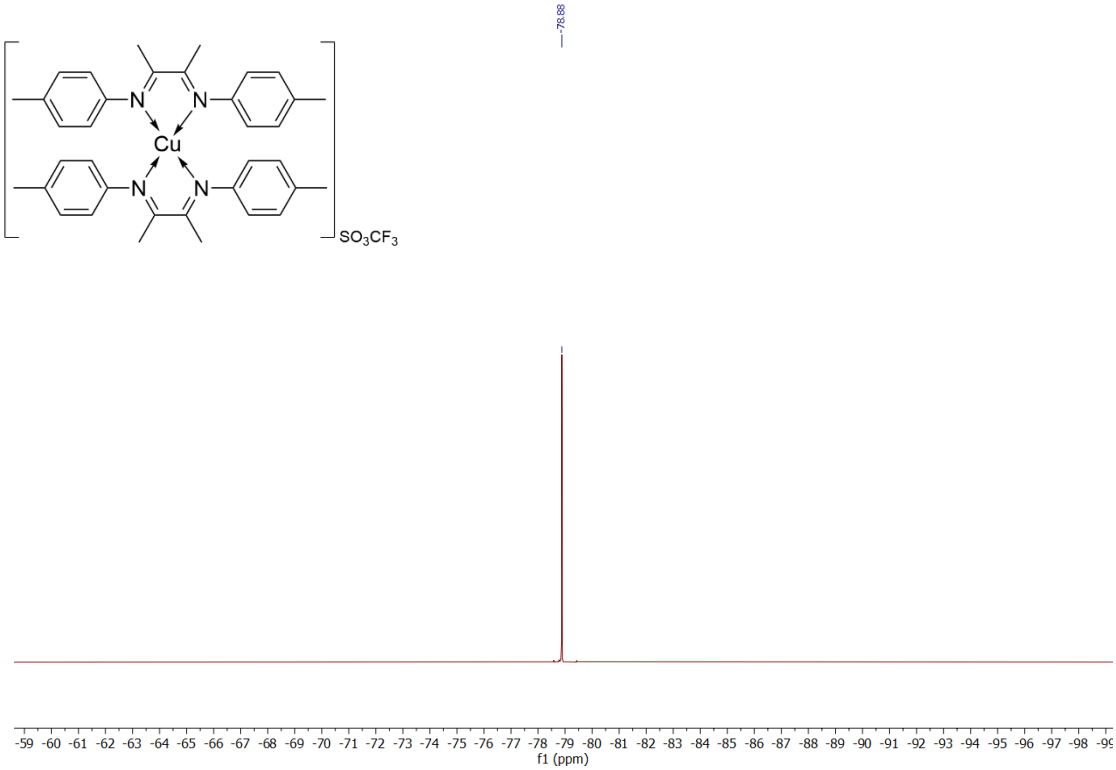

Figure A.68. ^{19}F NMR spectrum in CD_2Cl_2 of the **C8** complex.

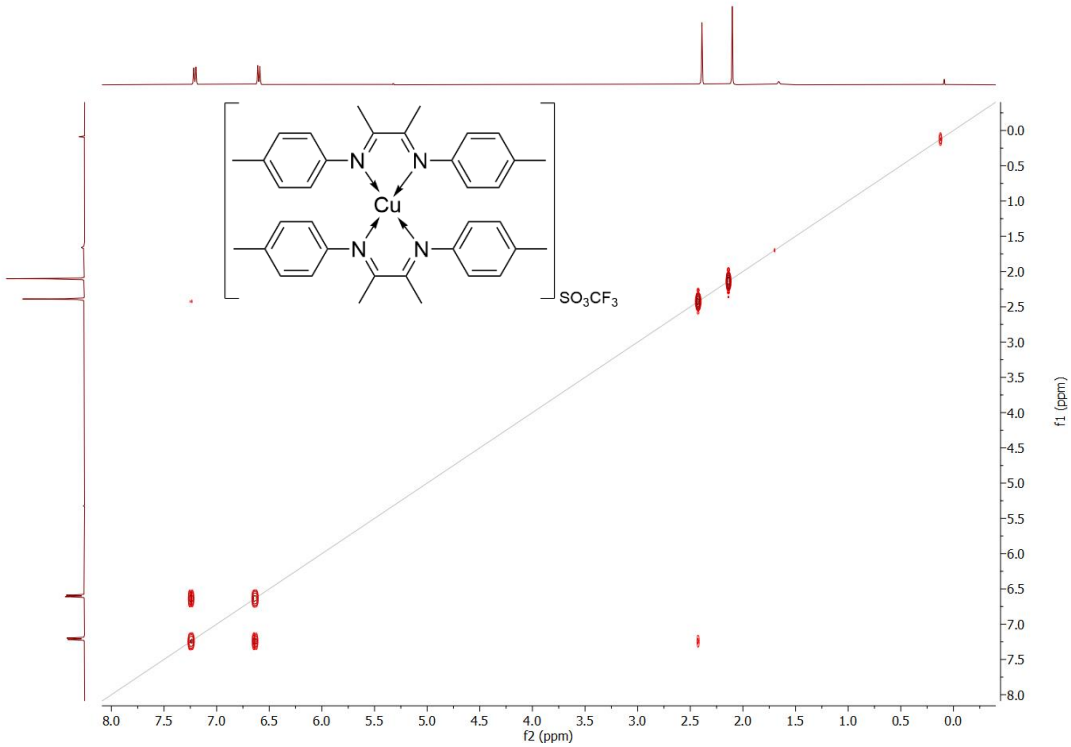

Figure A.69. COSY spectrum in CD_2Cl_2 of the **C8** complex.

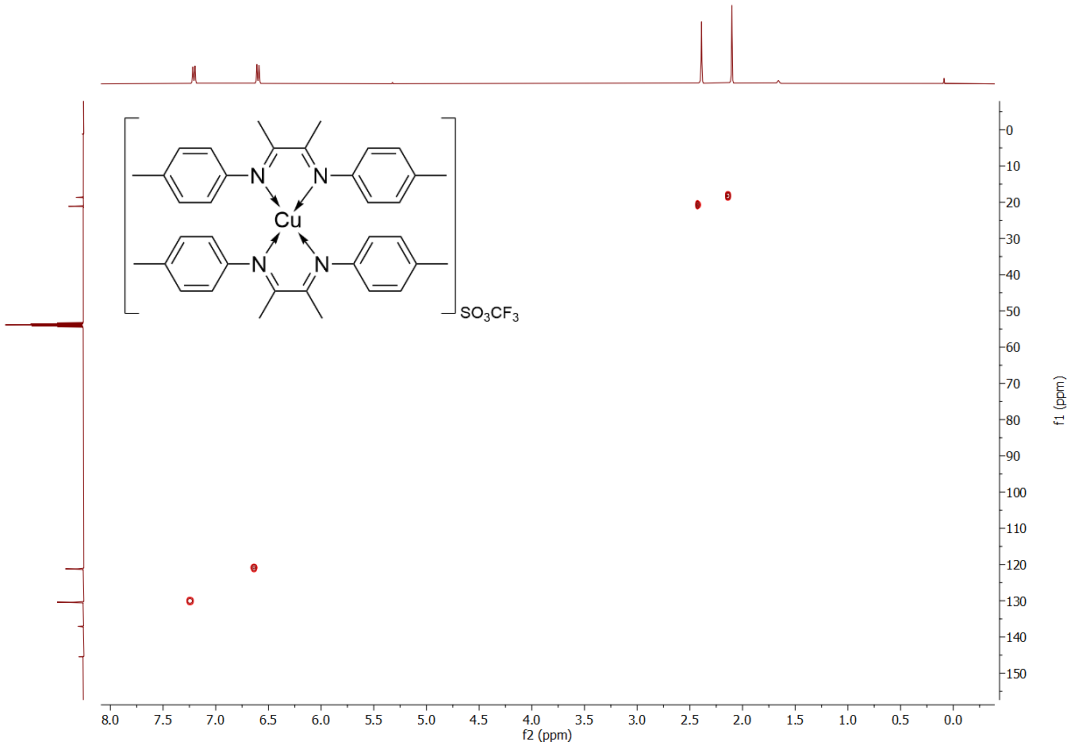

Figure A.70. HSQC spectrum in CD_2Cl_2 of the **C8** complex.

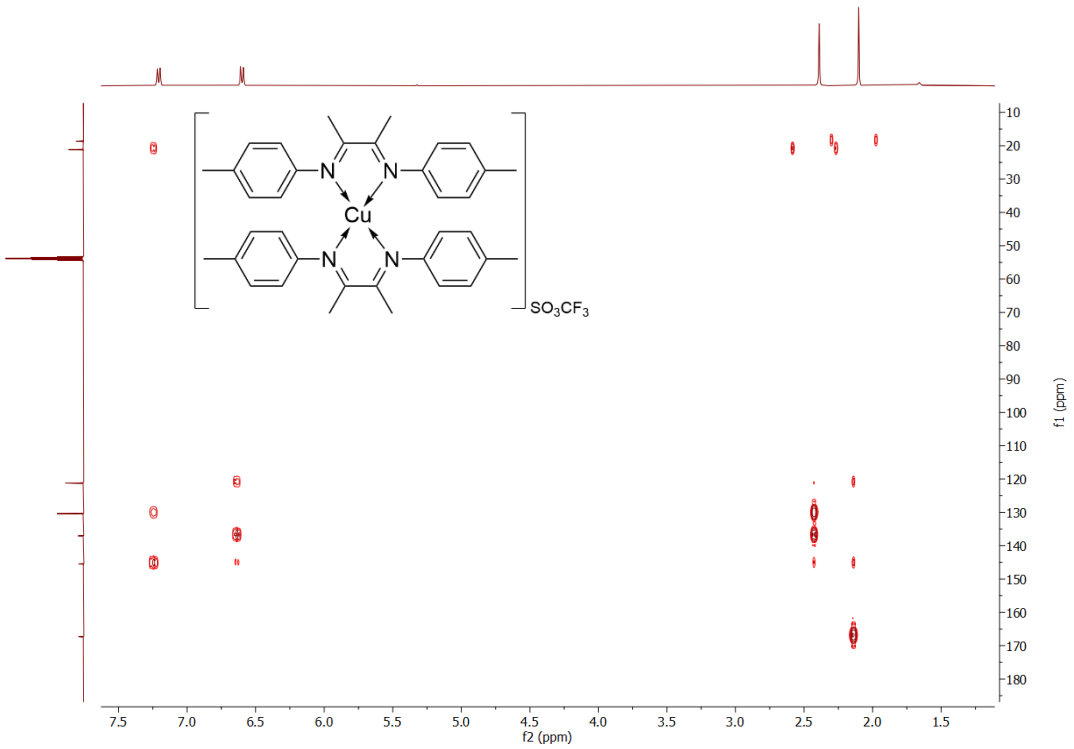

Figure A. 71. HMBC spectrum in CD_2Cl_2 of the **C8** complex.

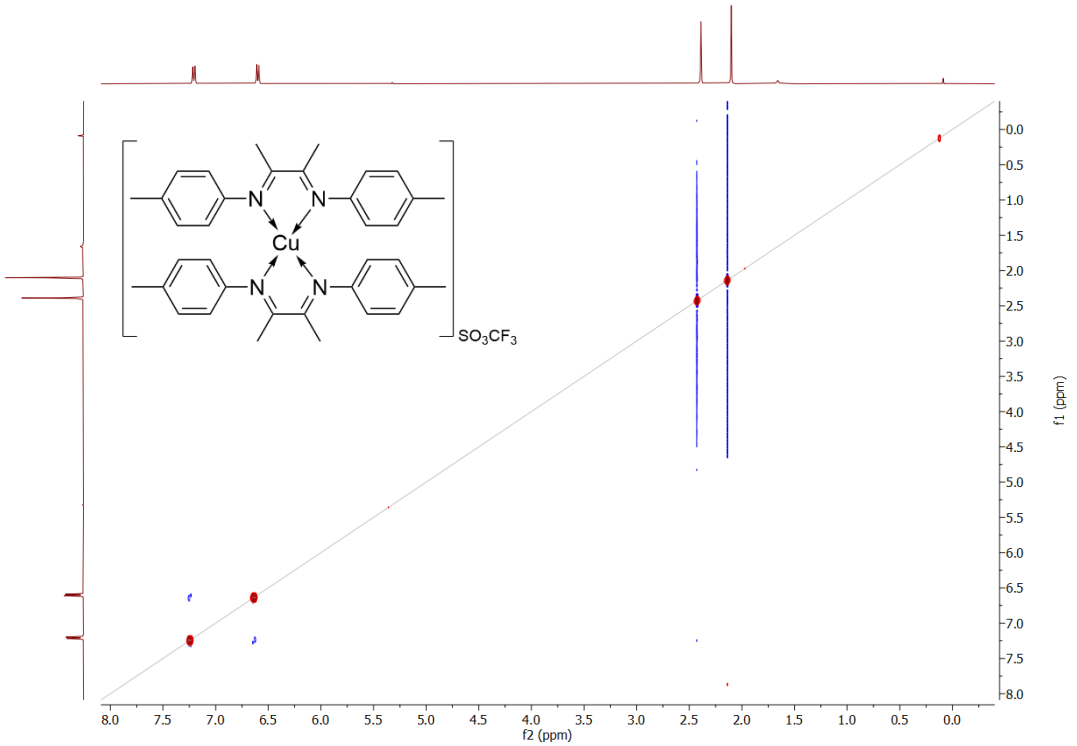

Figure A. 72. NOESY spectrum in CD_2Cl_2 of the **C8** complex.

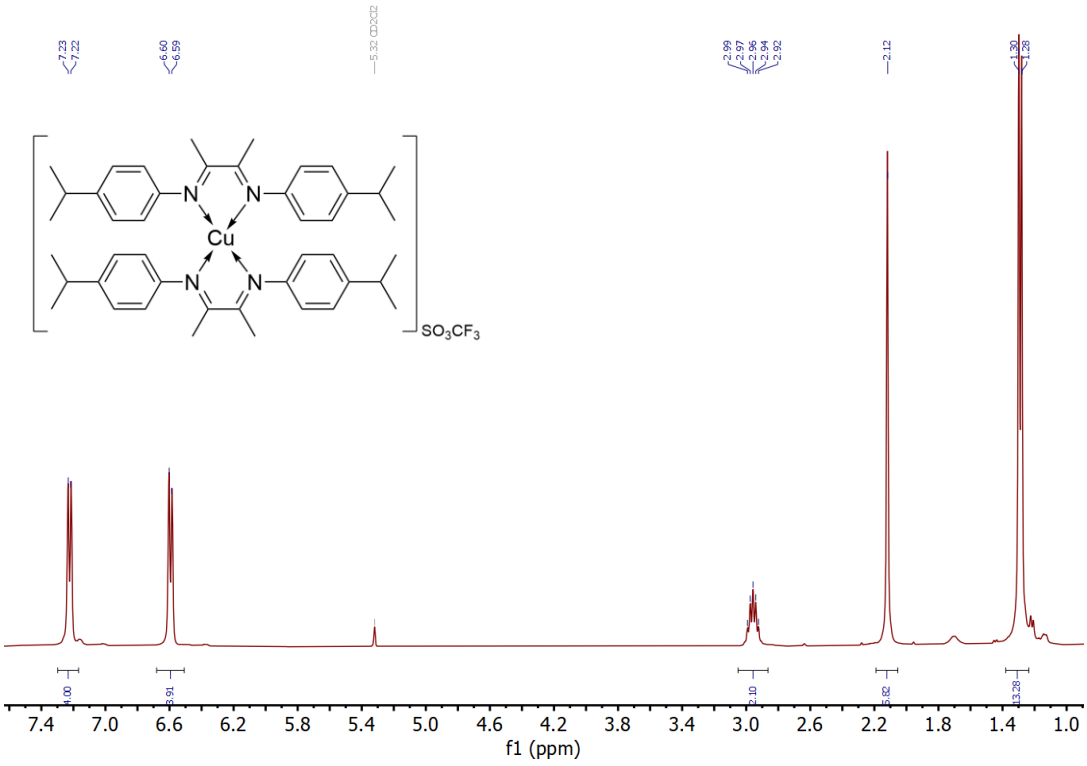

Figure A.73. ^1H NMR spectrum in CD_2Cl_2 of the **C9** complex.

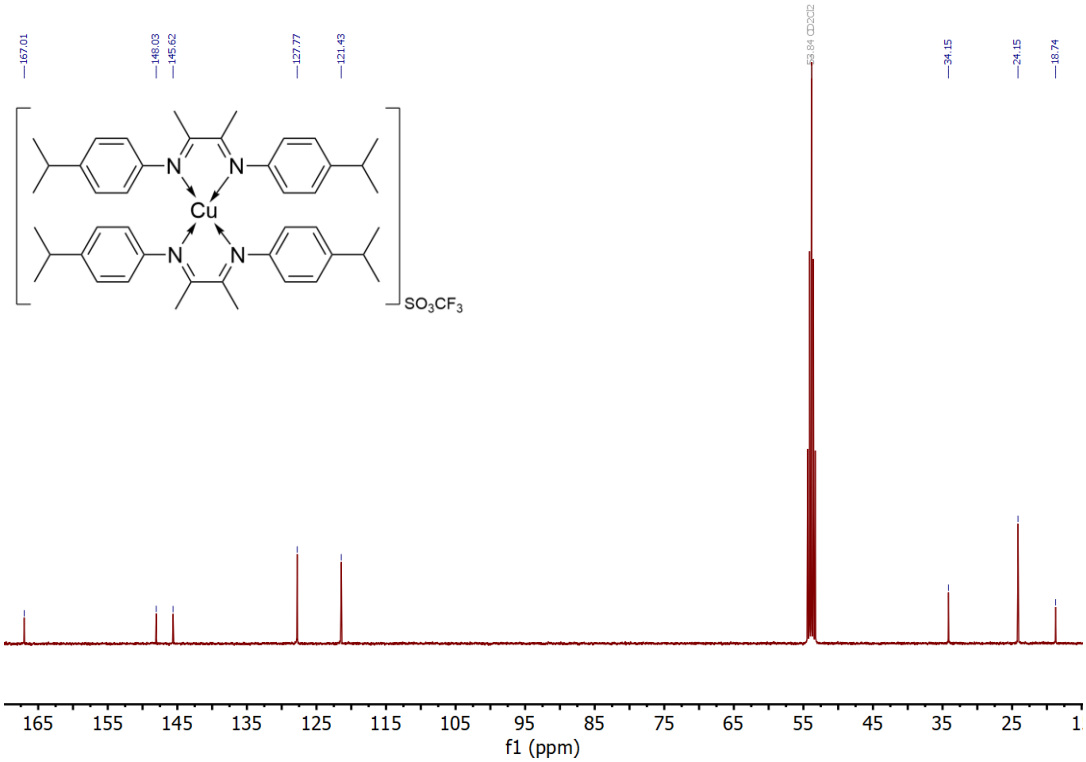

Figure A.74. ^{13}C NMR spectrum in CD_2Cl_2 of the **C9** complex.

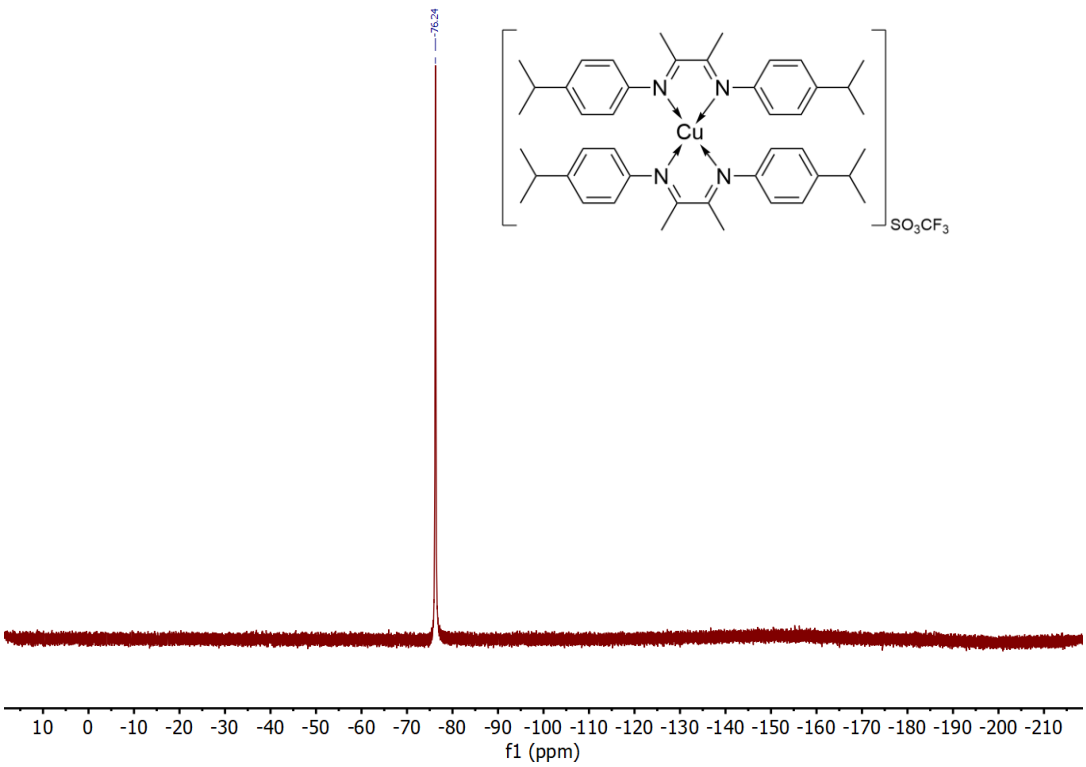

Figure A. 75. ^{19}F NMR spectrum in CD_2Cl_2 of the **C9** complex.

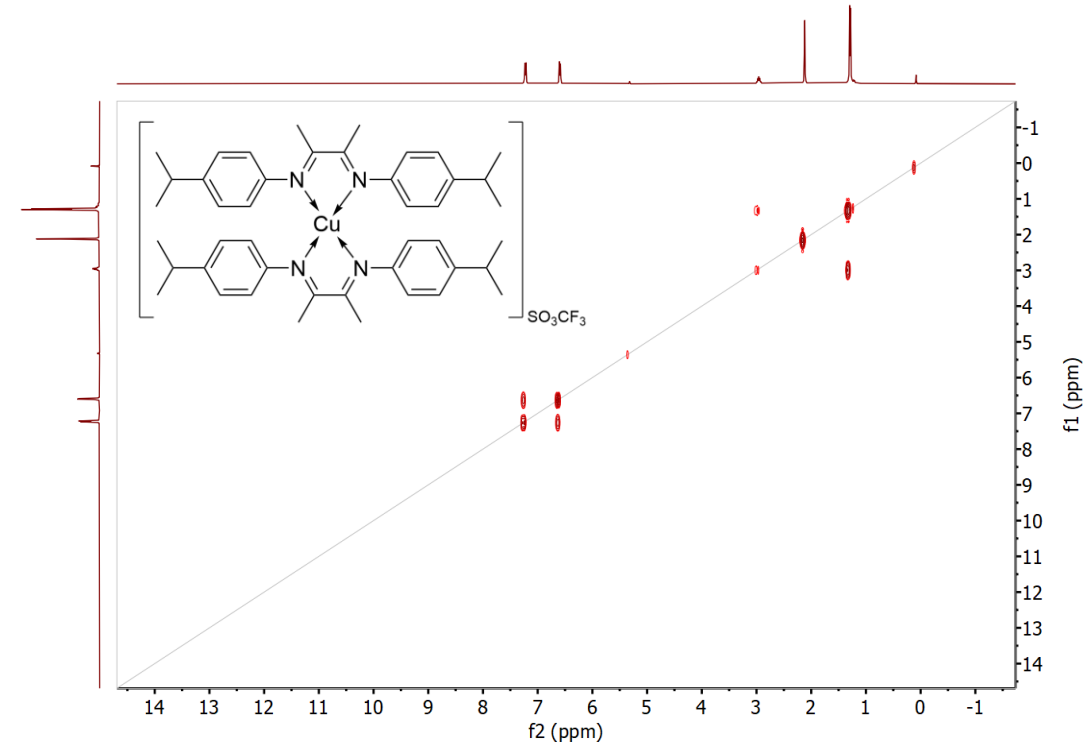

Figure A.76. COSY spectrum in CD_2Cl_2 of the **C9** complex.

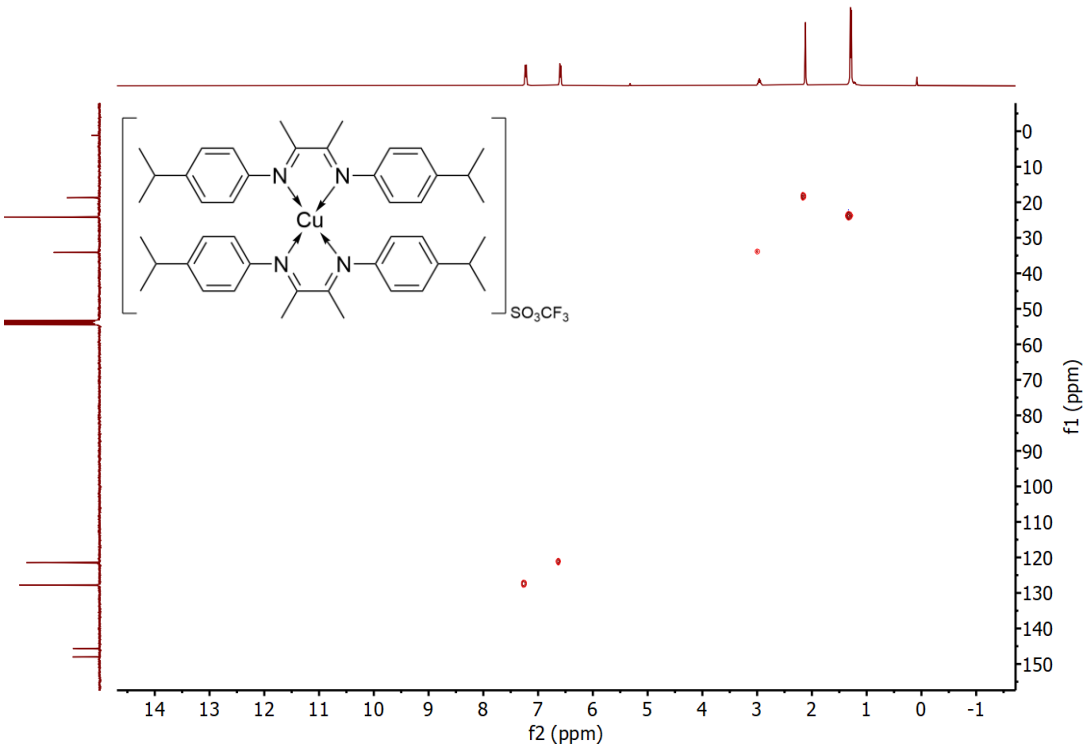

Figure A.77. HSQC spectrum in CD_2Cl_2 of the **C9** complex.

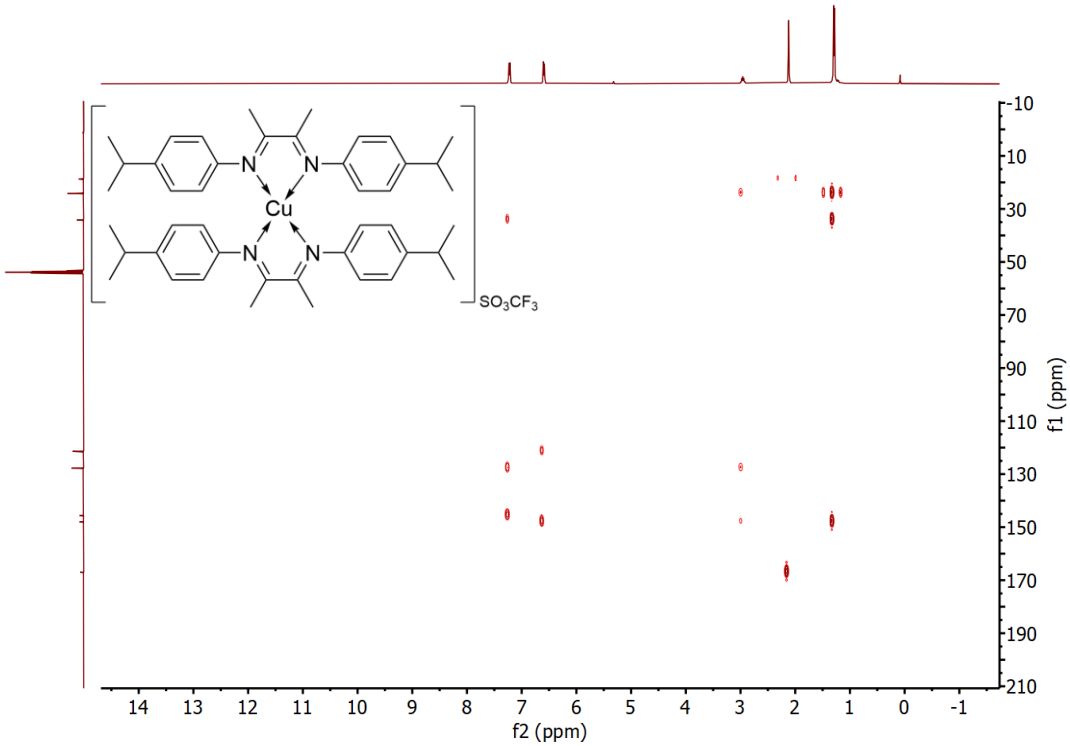

Figure A.78. HMBC spectrum in CD_2Cl_2 of the **C9** complex.

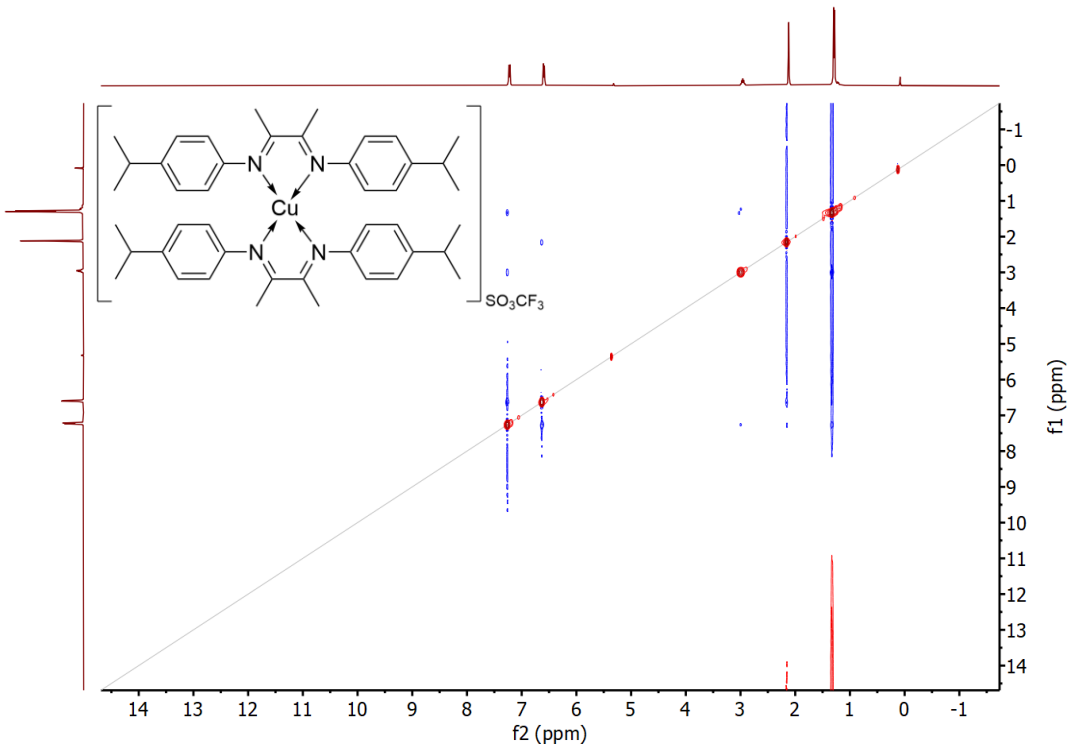

Figure A.79. NOESY spectrum in CD_2Cl_2 of the **C9** complex.

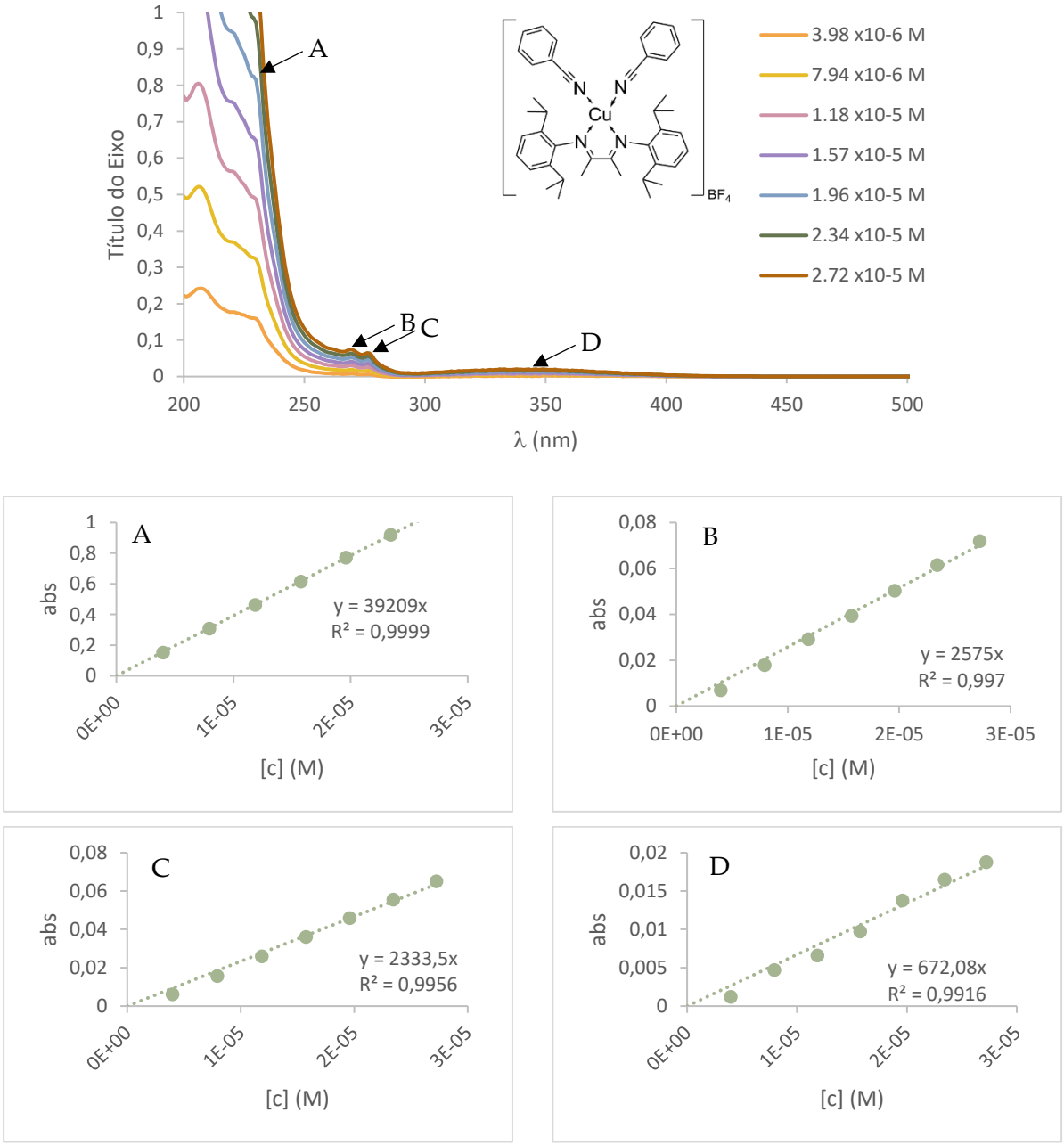

Figure A.80. UV/Vis spectrum in MeCN of the synthesised **C1** complex. **A**- molar extinction coefficient for the transition at 231 nm. **B**- molar extinction coefficient for the transition at 268 nm. **C**- molar extinction coefficient for the transition at 276 nm. **D**- molar extinction coefficient for the transition at 347 nm.

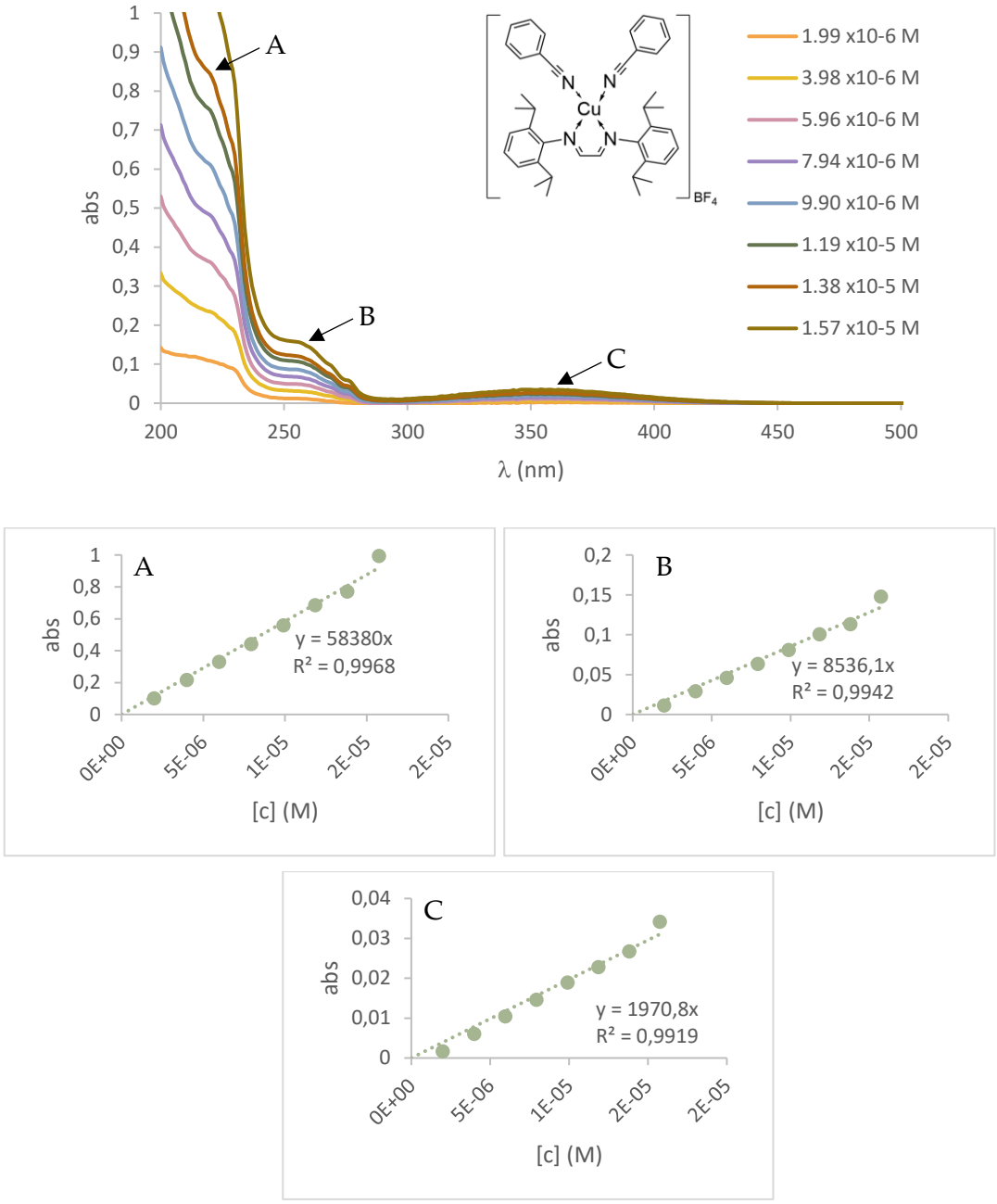

Figure A.81. UV/Vis spectrum in MeCN of the synthesised **C2** complex. **A**- molar extinction coefficient for the transition at 224 nm. **B**- molar extinction coefficient for the transition at 276 nm. **C**- molar extinction coefficient for the transition at 356 nm.

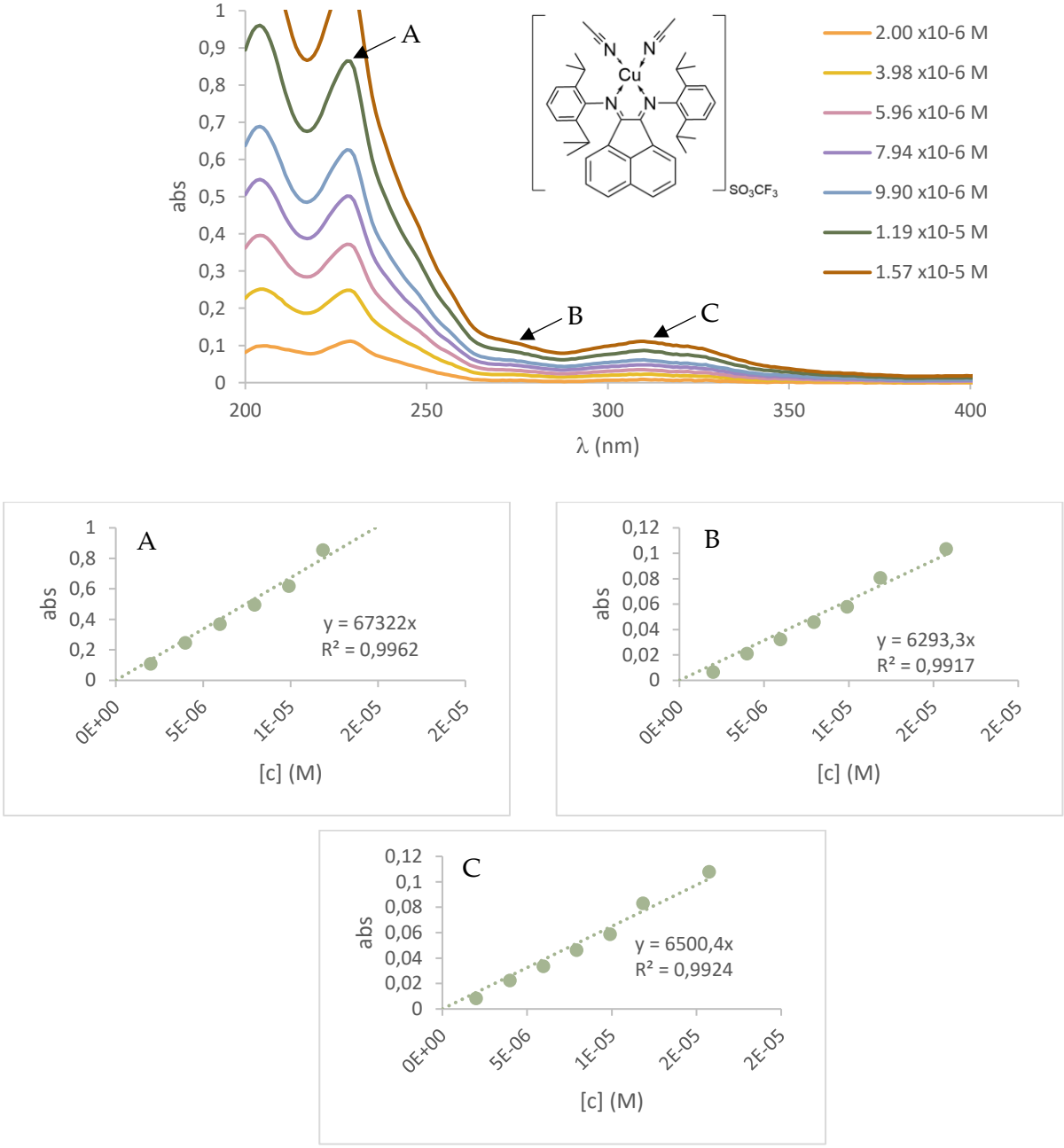

Figure A.82. UV/Vis spectrum in MeCN of the synthesised **C3** complex. **A**- molar extinction coefficient for the transition at 227 nm. **B**- molar extinction coefficient for the transition at 276 nm. **C**- molar extinction coefficient for the transition at 313 nm.

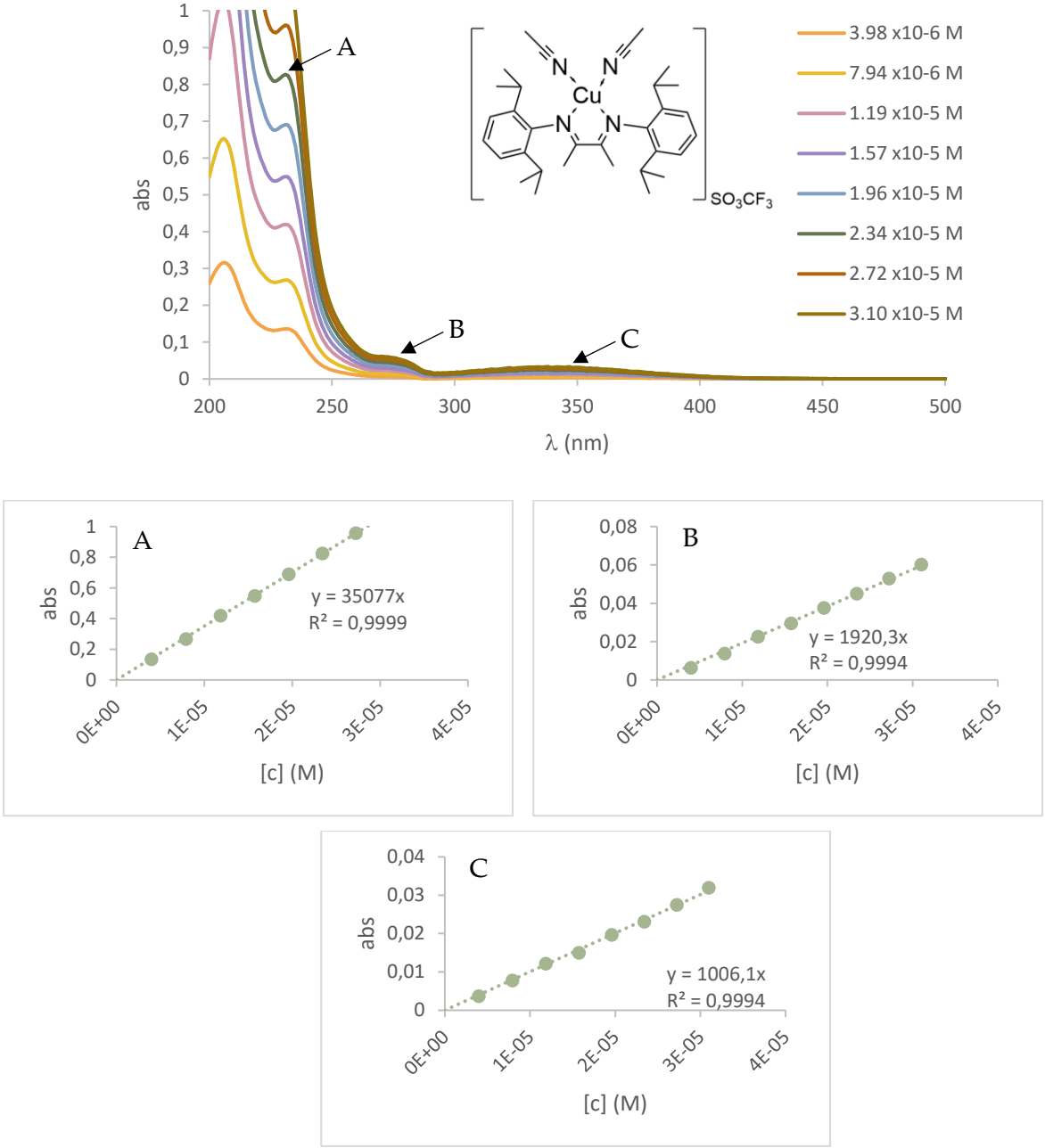

Figure A.83. UV/Vis spectrum in MeCN of the synthesised **C4** complex. **A**- molar extinction coefficient for the transition at 230 nm. **B**- molar extinction coefficient for the transition at 273 nm. **C**- molar extinction coefficient for the transition at 343 nm.

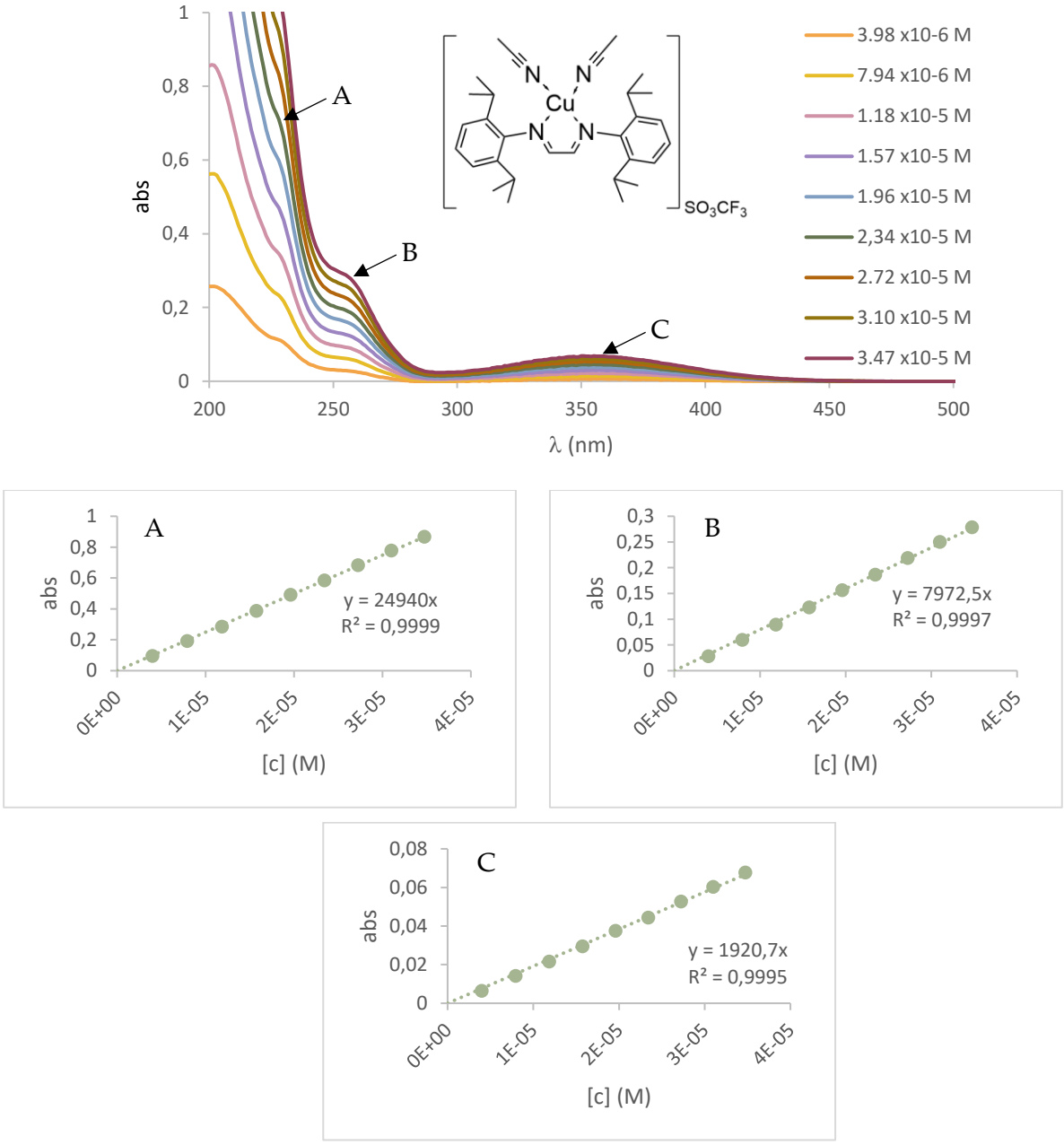

Figure A.84. UV/Vis spectrum in MeCN of the synthesised **C5** complex. **A**- molar extinction coefficient for the transition at 232 nm. **B**- molar extinction coefficient for the transition at 257 nm. **C**- molar extinction coefficient for the transition at 359 nm.

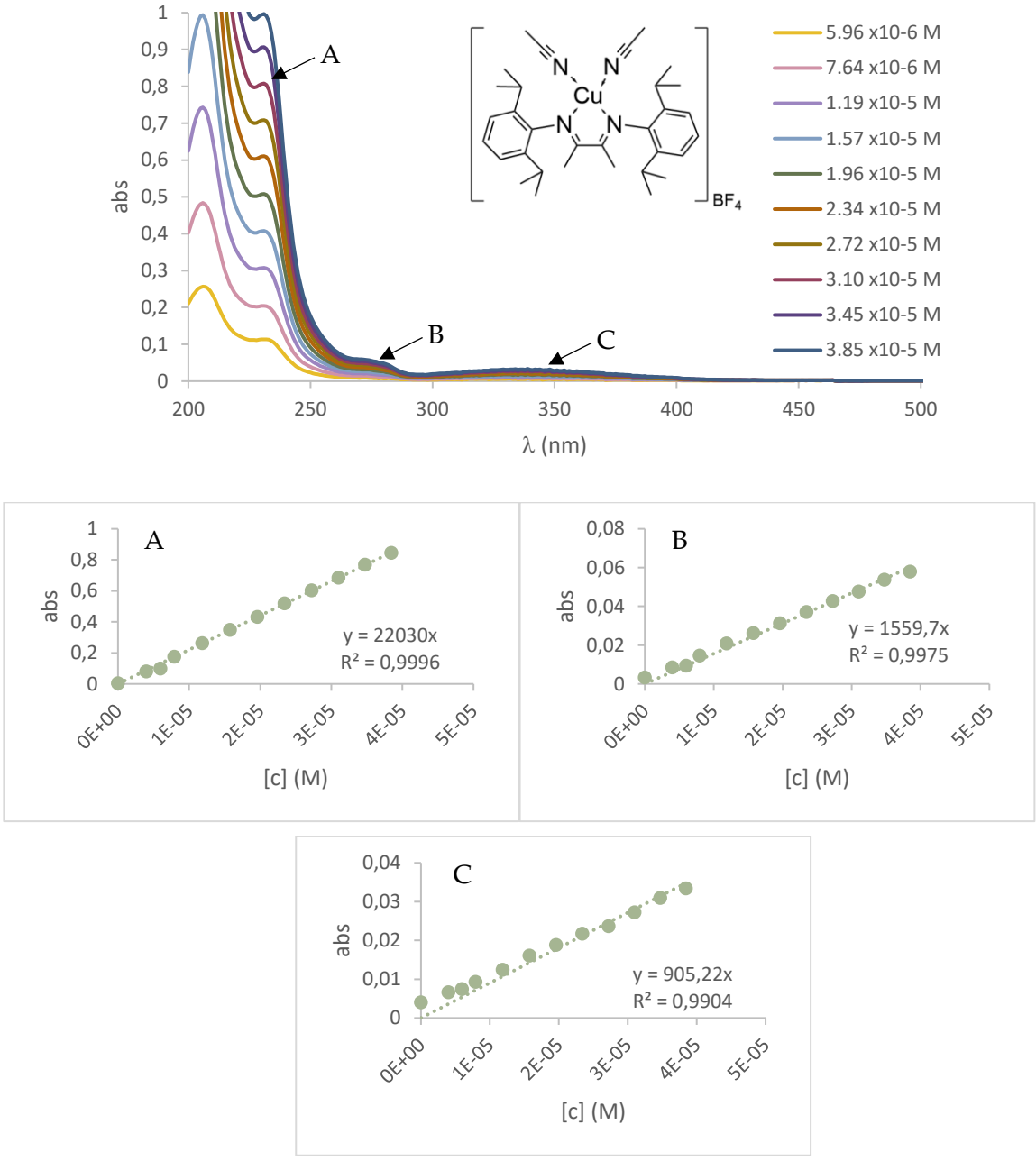

Figure A.85. UV/Vis spectrum in MeCN of the synthesised **C6** complex. **A**- molar extinction coefficient for the transition at 236 nm. **B**- molar extinction coefficient for the transition at 273 nm. **C**- molar extinction coefficient for the transition at 339 nm.

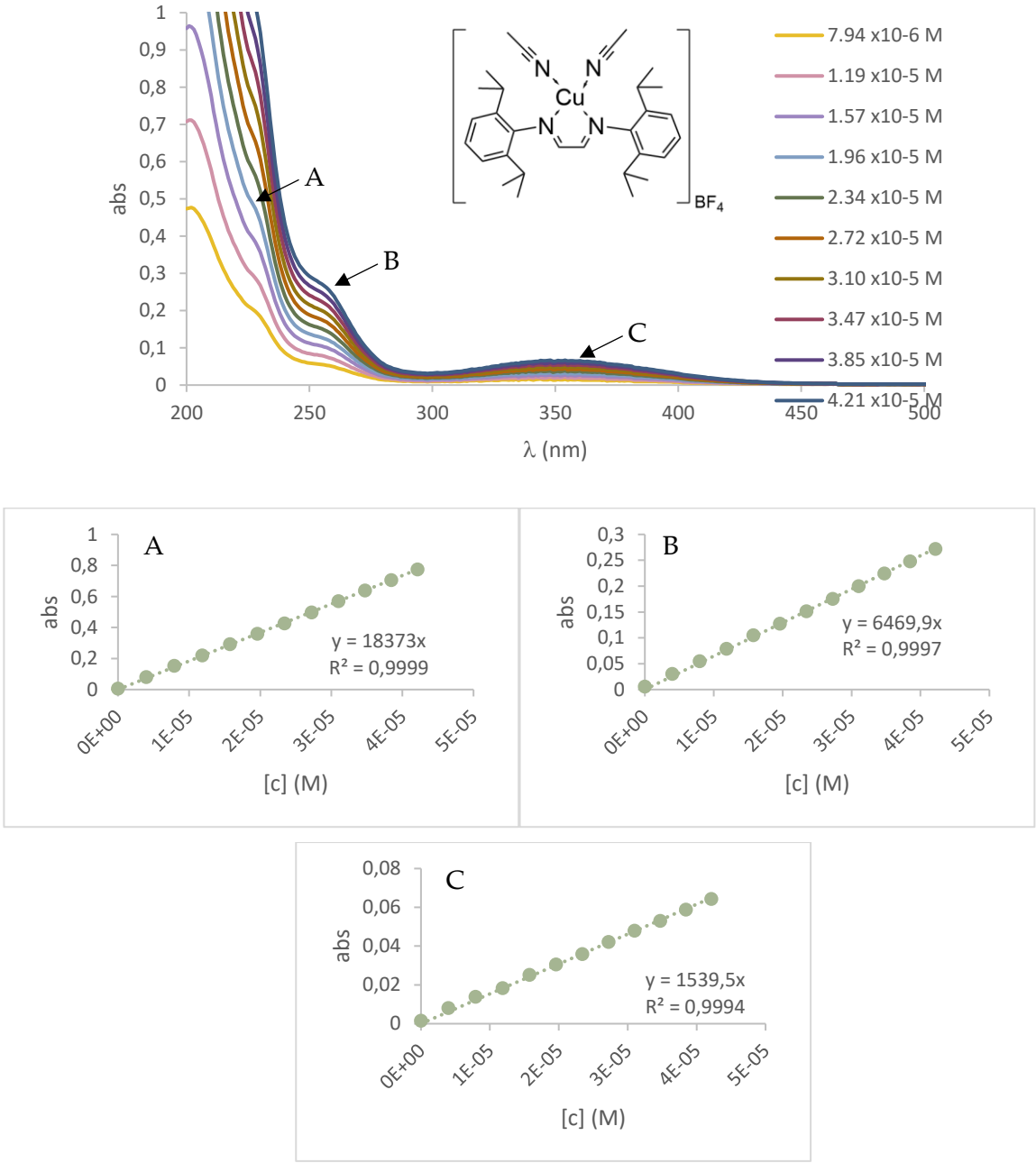

Figure A. 86. UV/Vis spectrum in MeCN of the synthesised **C7** complex. **A**- molar extinction coefficient for the transition at 233 nm. **B**- molar extinction coefficient for the transition at 255 nm. **C**- molar extinction coefficient for the transition at 358 nm.

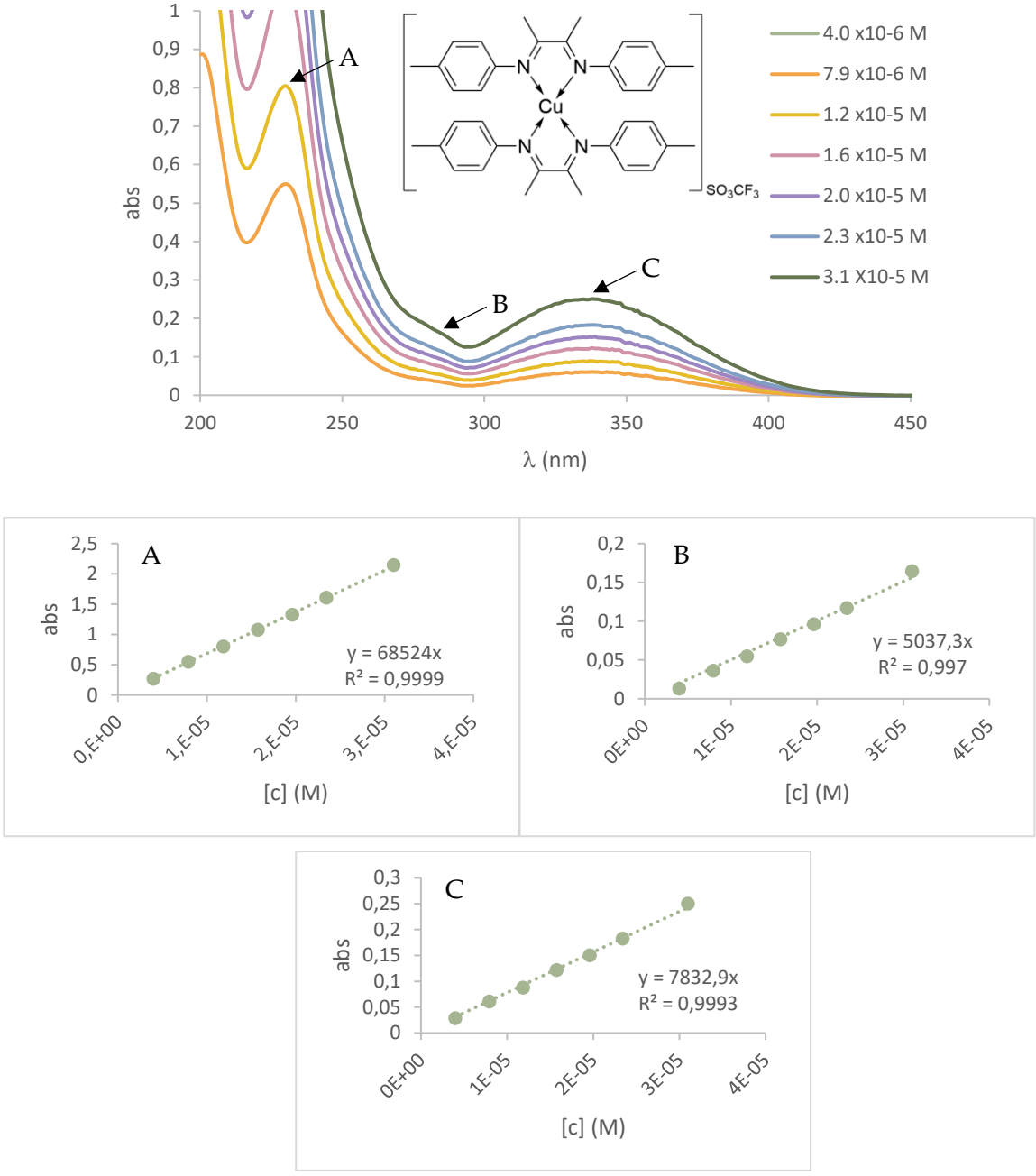

Figure A.87. UV/Vis spectrum in MeCN of the synthesised **C8** complex. **A**- molar extinction coefficient for the transition at 229 nm. **B**- molar extinction coefficient for the transition at 284 nm. **C**- molar extinction coefficient for the transition at 340 nm.

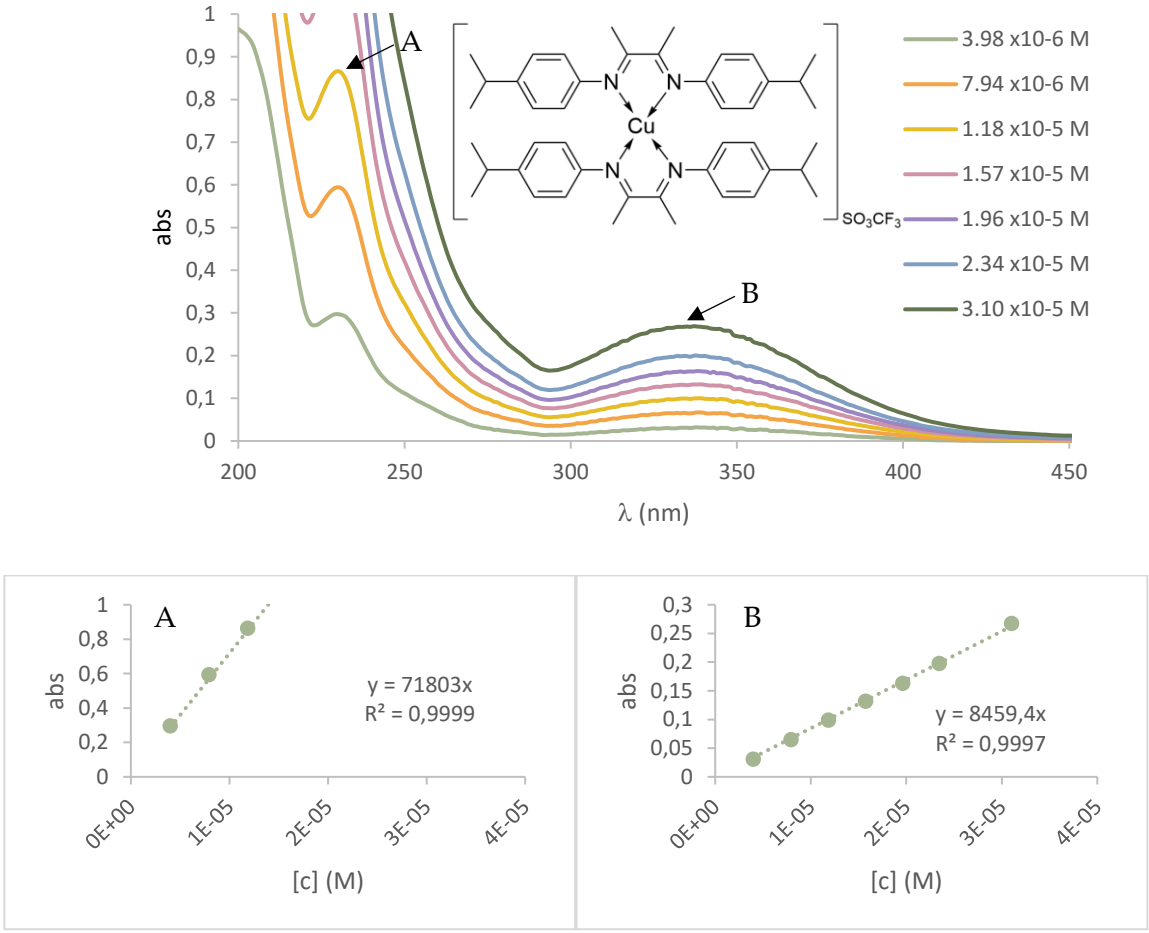

Figure A.88. UV/Vis spectrum in MeCN of the synthesised **C9** complex. **A**- molar extinction coefficient for the transition at 231 nm. **B**- molar extinction coefficient for the transition at 336 nm.

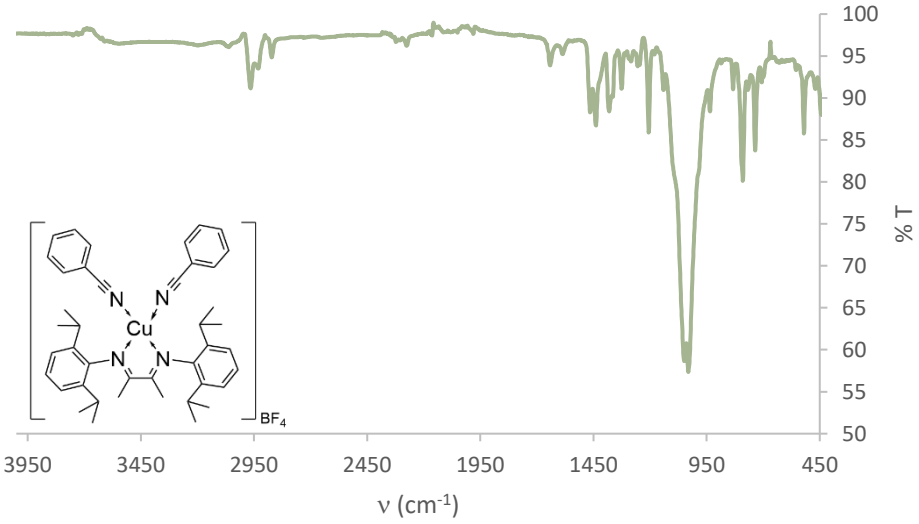

Figure A.89. IR spectrum of the synthesised **C1** complex.

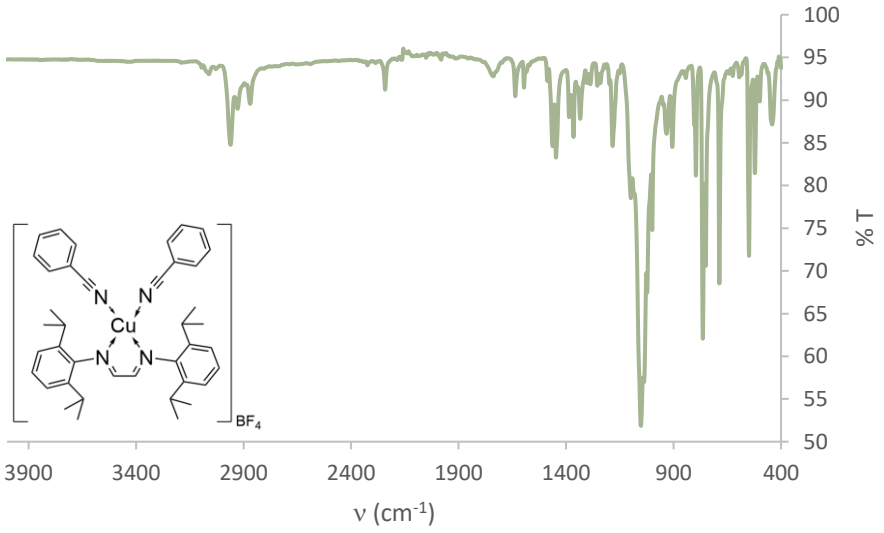

Figure A.90. IR spectrum of the synthesised **C2** complex.

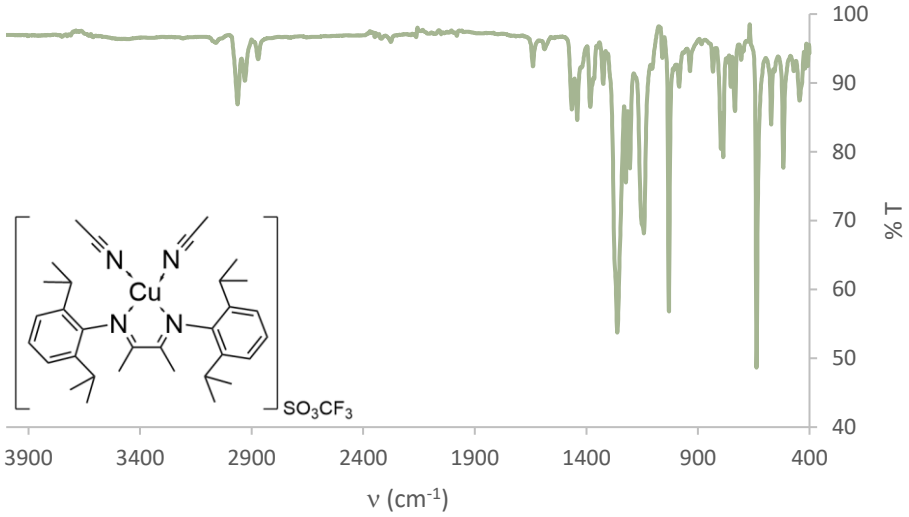

Figure A.91. IR of the synthesised **C4** complex.

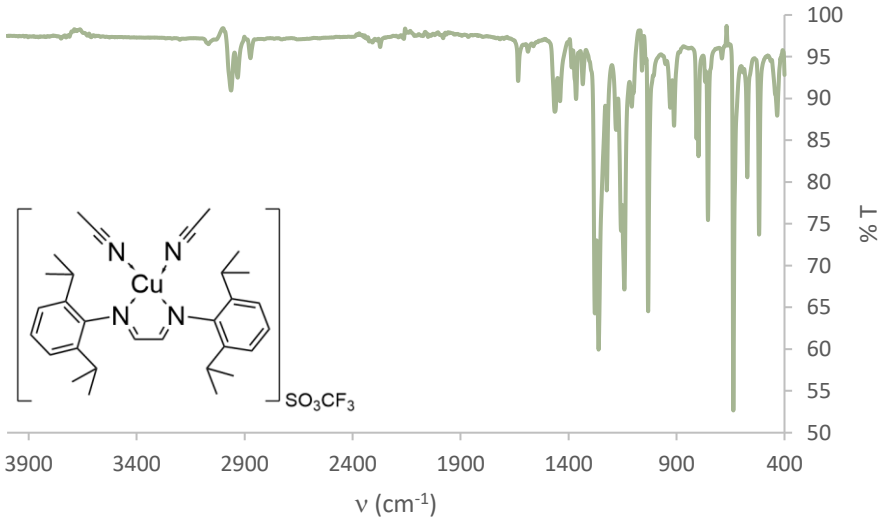

Figure A.92. IR spectrum of the synthesised **C5** complex.

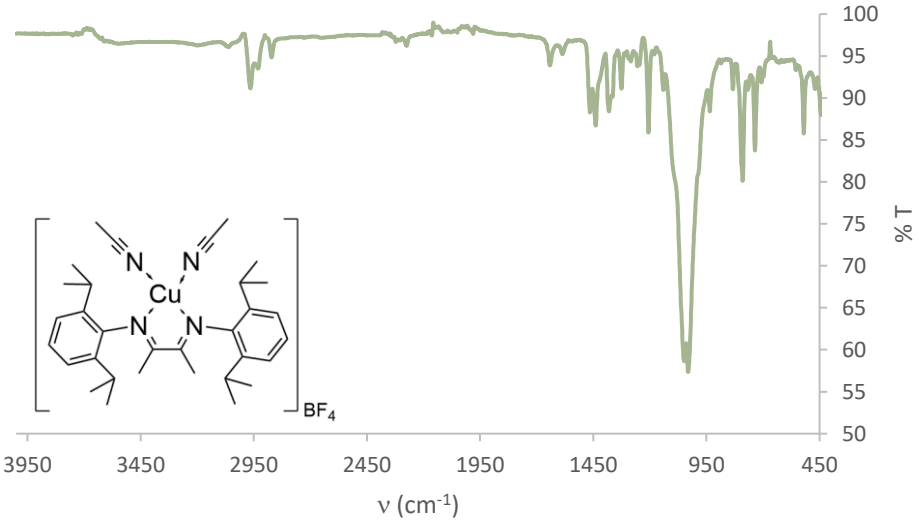

Figure A.93. IR spectrum of the synthesised **C6** complex.

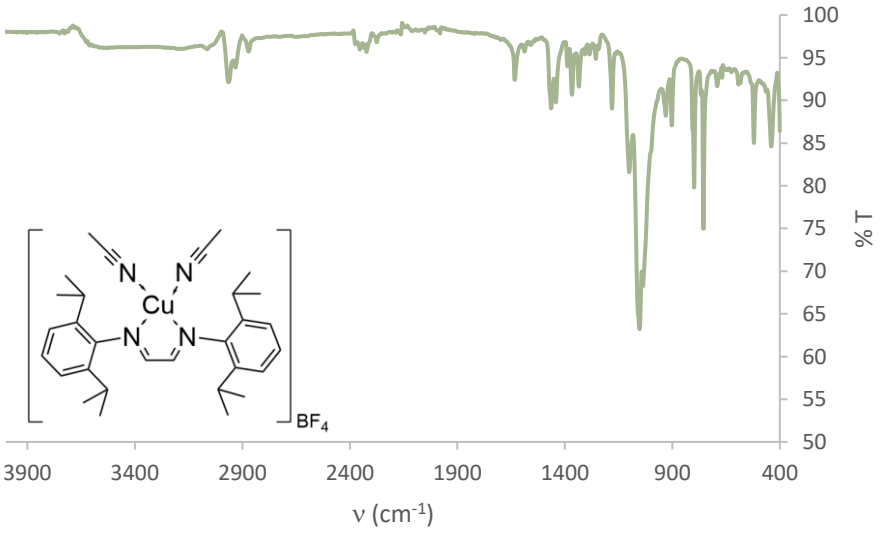

Figure A.94. IR spectrum of the synthesised **C7** complex.

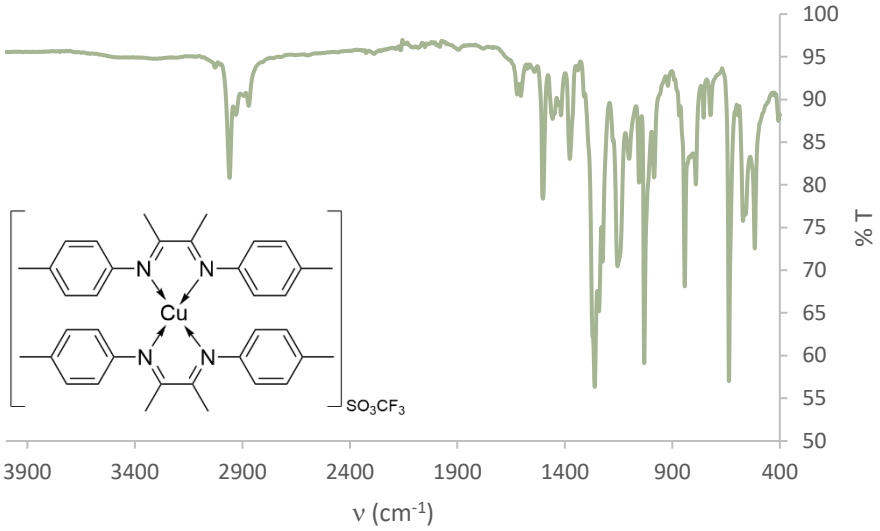

Figure A.95. IR spectrum of the synthesised **C8** complex.

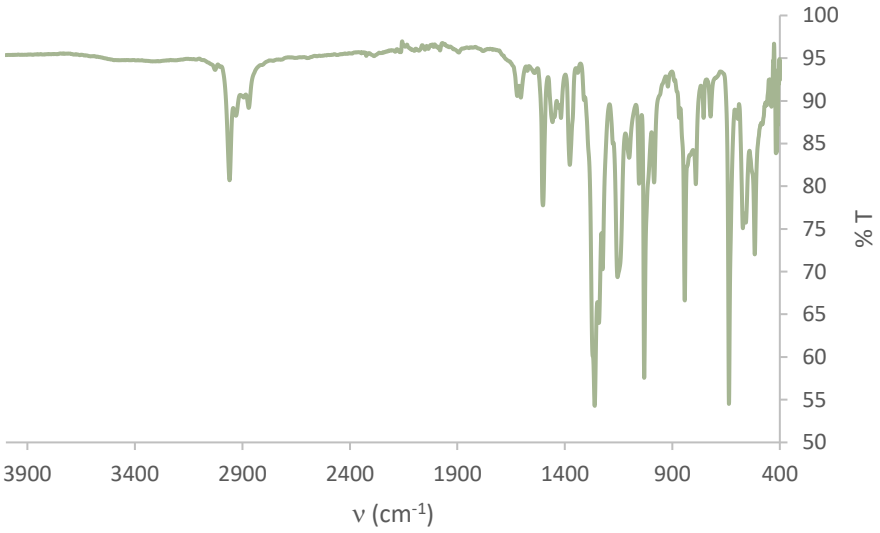

Figure A.96. IR spectrum of the synthesised **C9** complex.

A.3 Catalytic studies

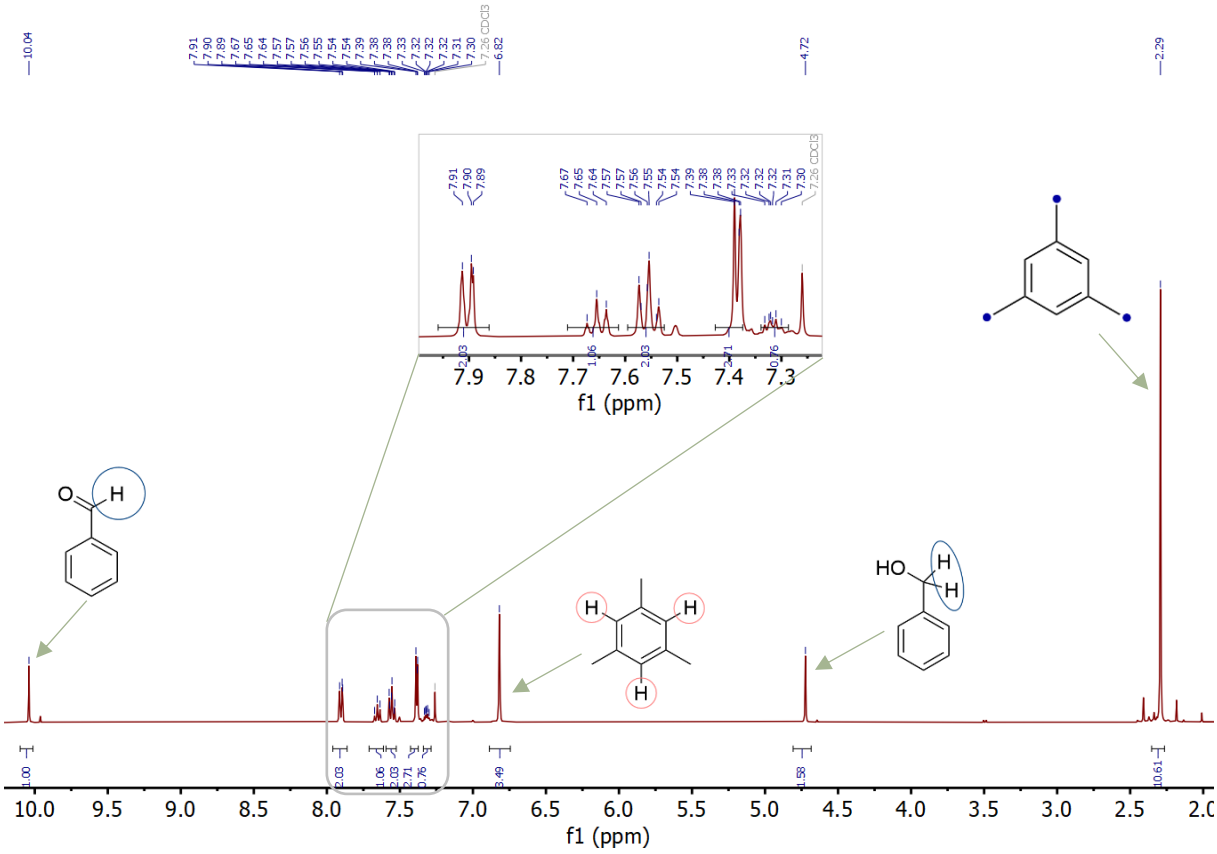

Figure A.97. ^{1}H NMR obtained for the catalytic studies with internal standard (mesitylene).

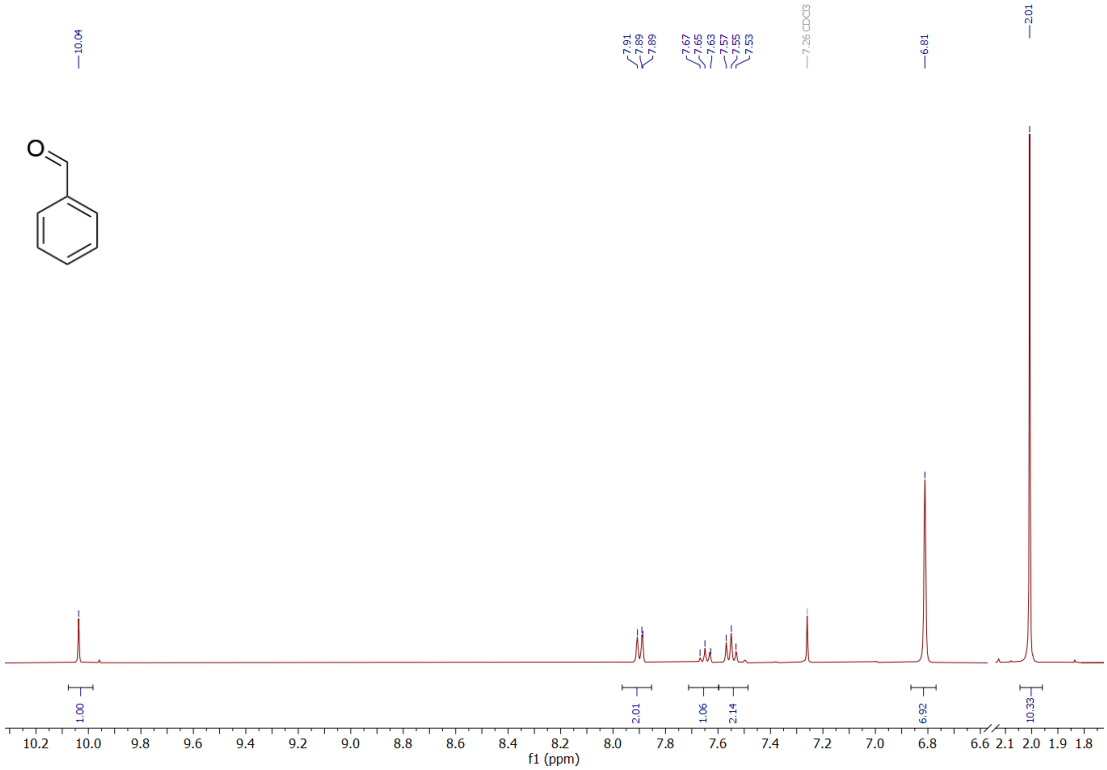

Figure A.98. ^{1}H NMR spectrum of the obtained benzaldehyde.

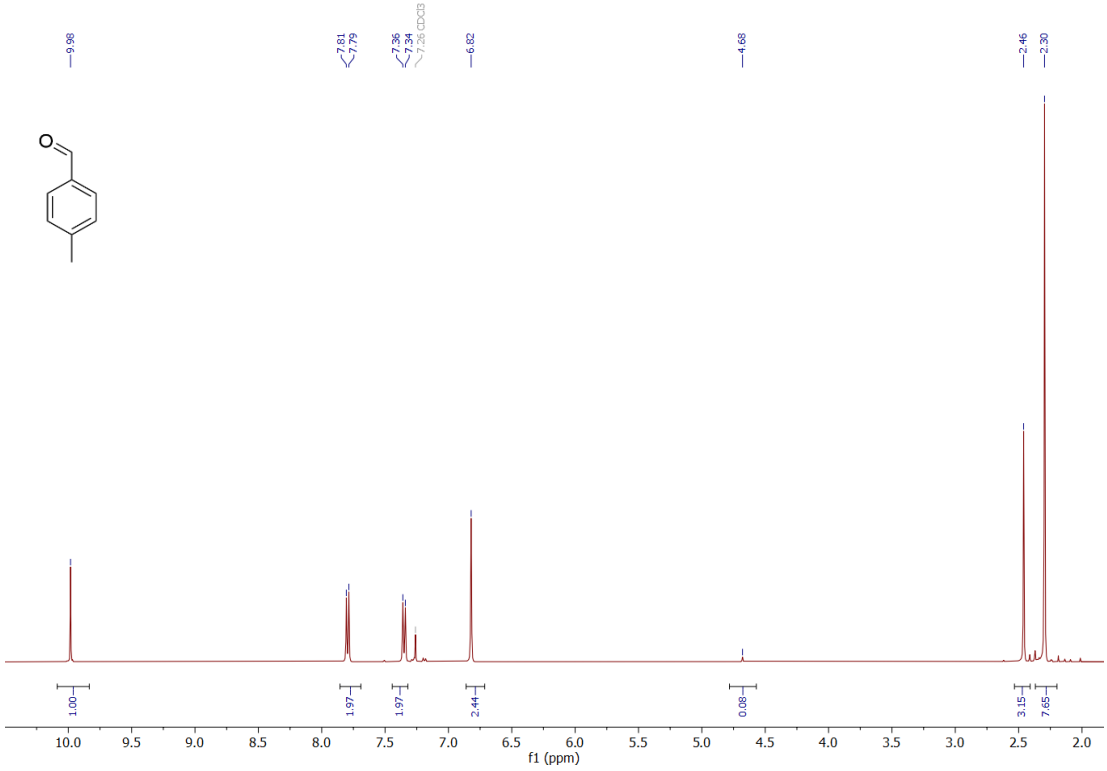

Figure A.99. ^{1}H NMR spectrum of the obtained *p*-methylbenzaldehyde.

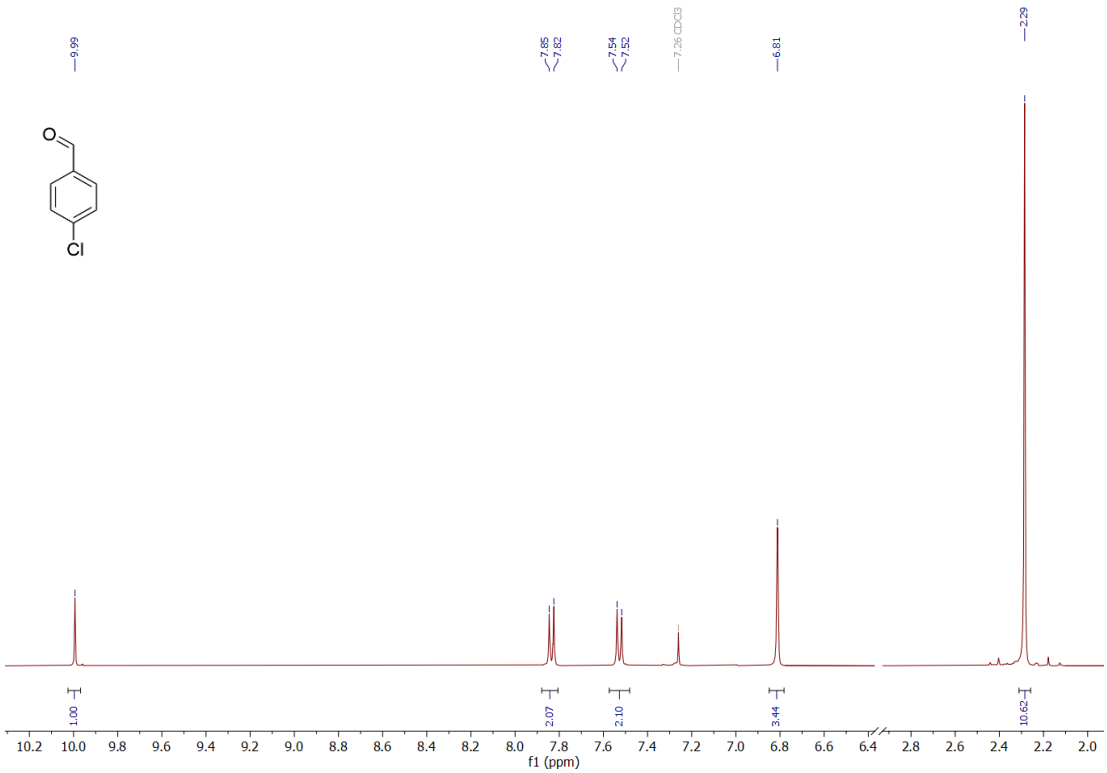

Figure A.100. [1]H NMR spectrum of the obtained *p*-chlorobenzaldehyde.

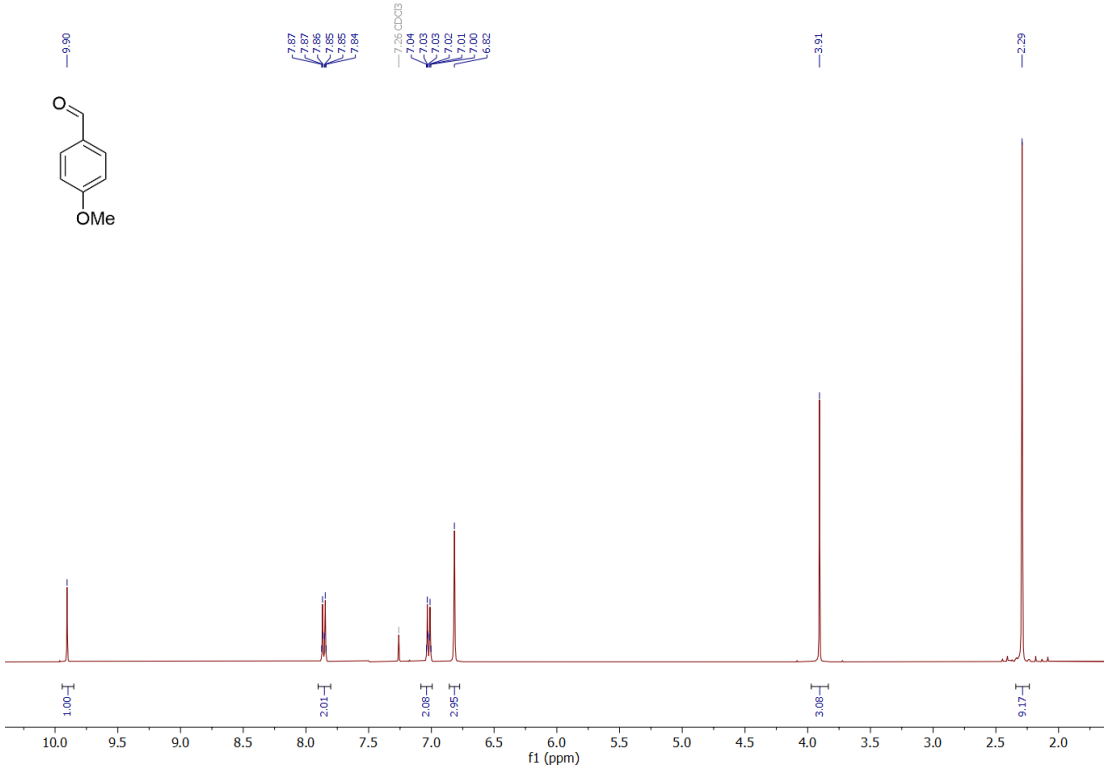

Figure A.101. [1]H NMR of the obtained *p*-methoxybenzaldehyde.

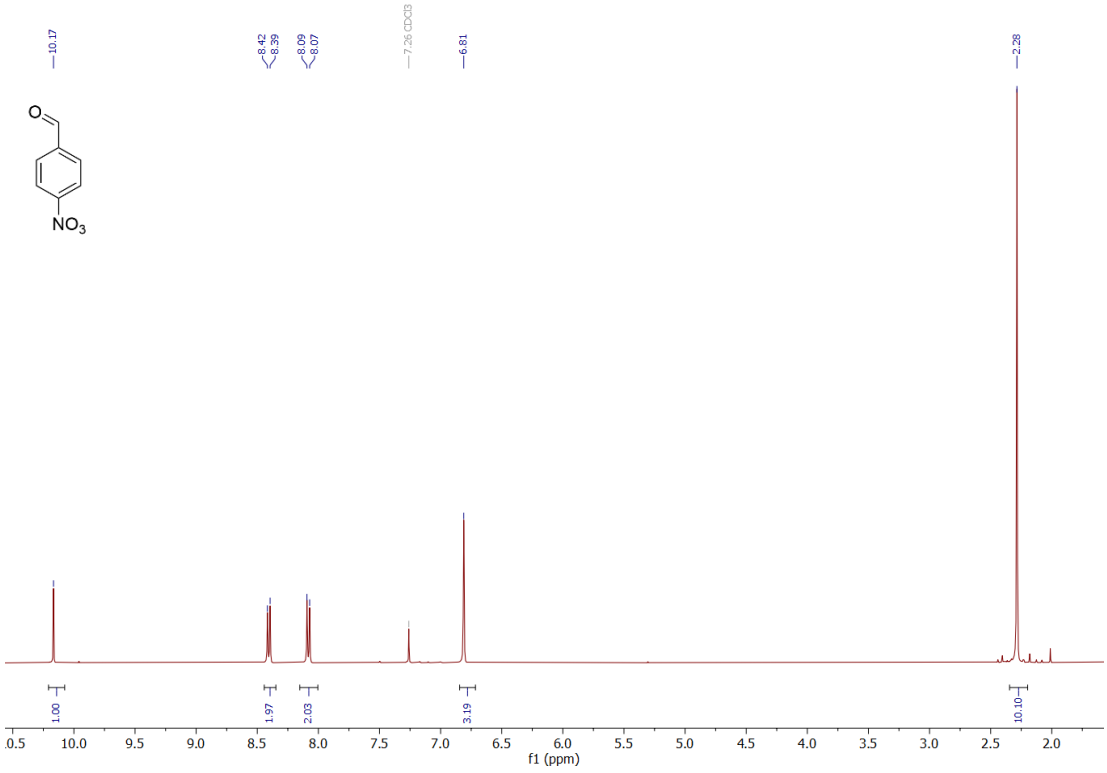

Figure A.102. [1]H NMR spectrum of the obtained *p*-nitrobenzaldehyde.

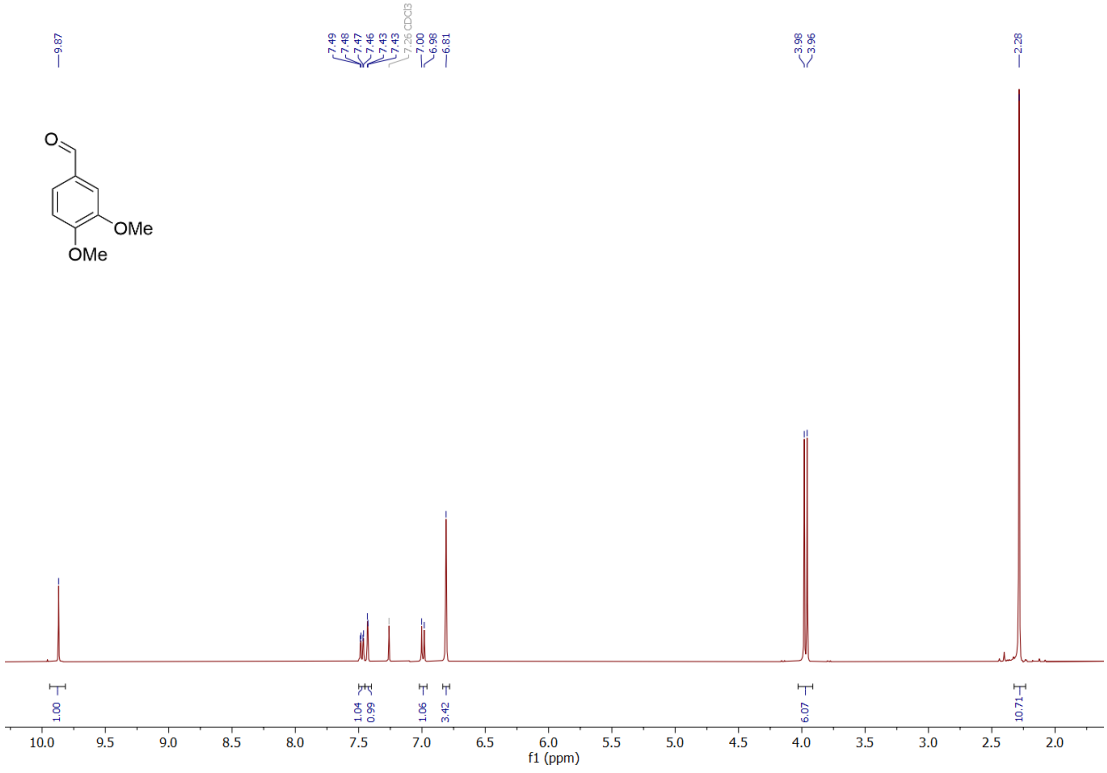

Figure A.103. [1]H NMR spectrum of the obtained *m,p*-dimethoxybenzaldehyde.

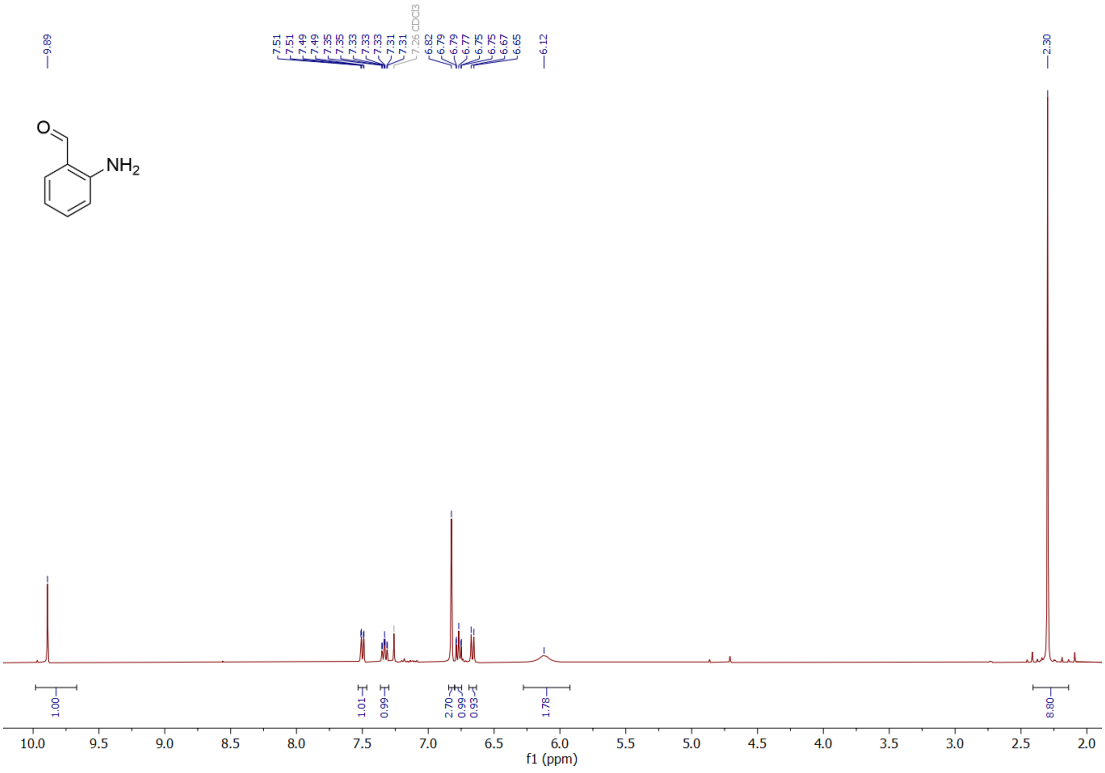

Figure A.104. [1]H NMR spectrum of the obtained *o*-aminobenzaldehyde.

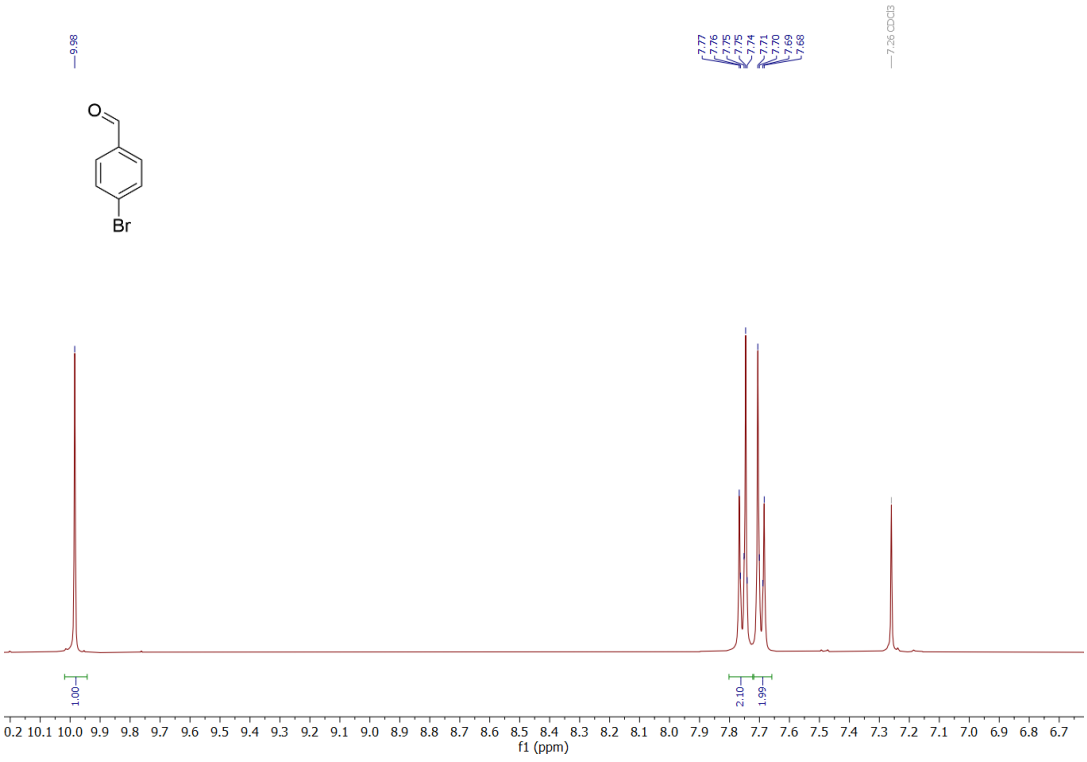

Figure A.105. [1]H NMR spectrum of the obtained *p*-bromobenzaldehyde.

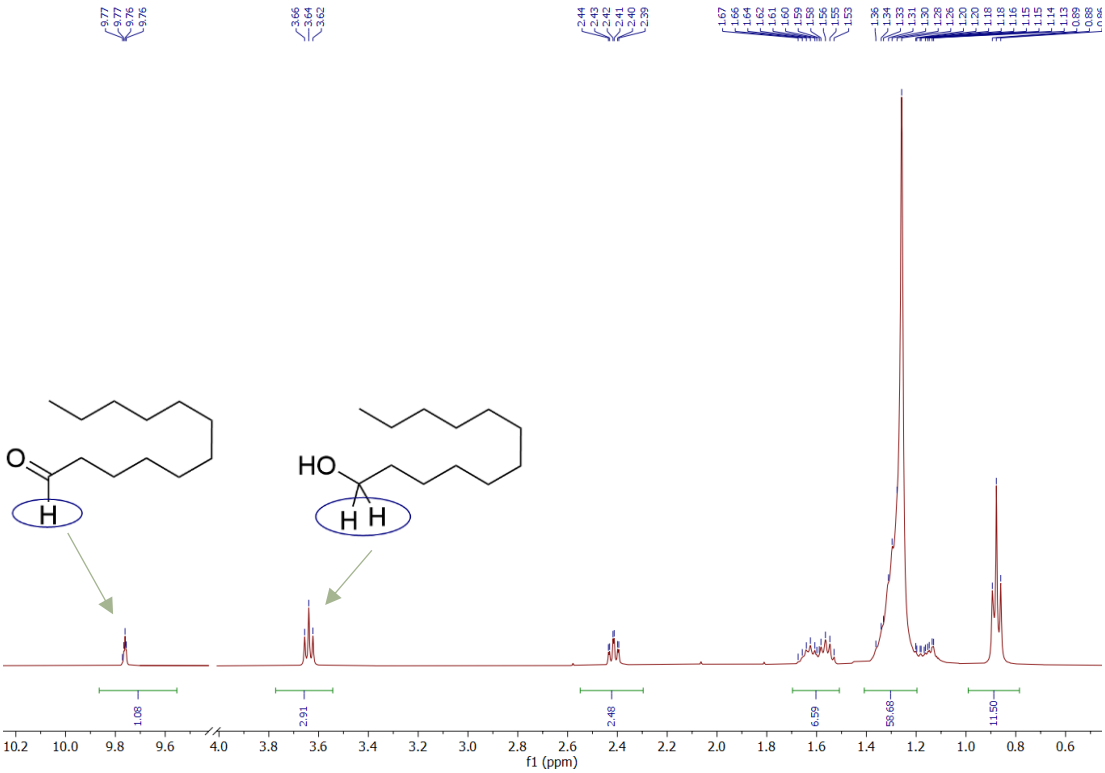

Figure A.106. ^{1}H NMR spectrum of the obtained mixture of dodecanol and dodecanal.

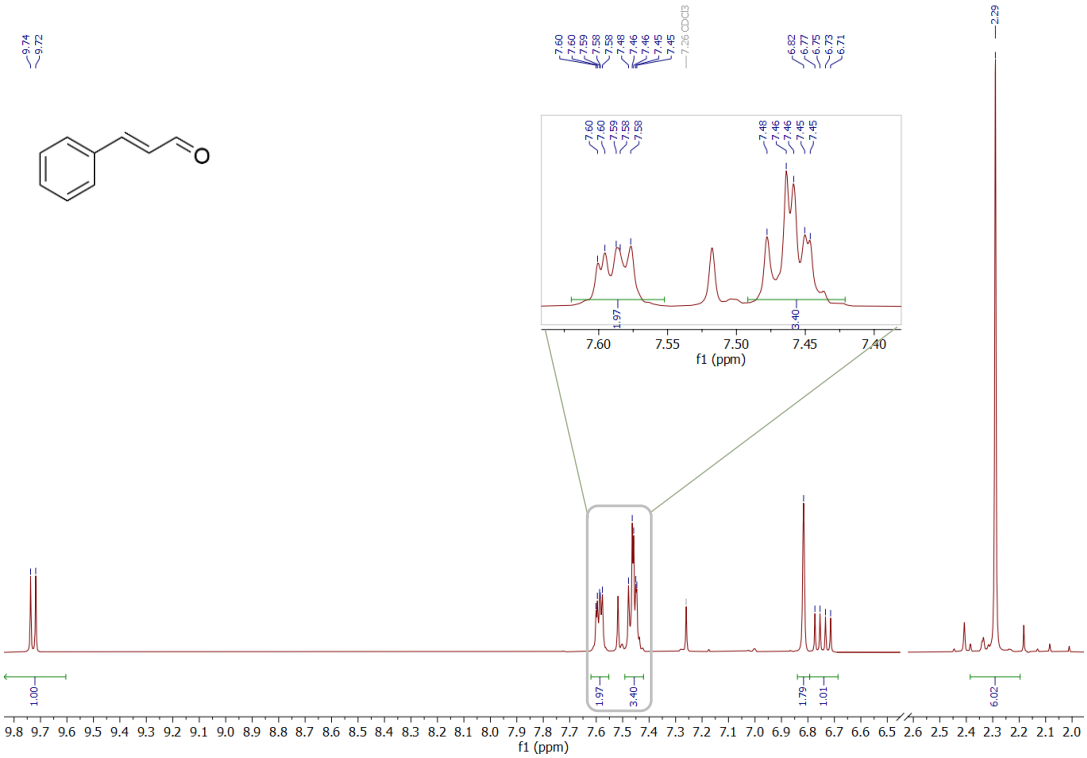

Figure A.107. ^{1}H NMR spectrum of the obtained cinnaldehyde.